Ragnar Torvanger Igland

Reliability analysis of pipelines during laying, considering ultimate strength under combined loads

NTNU Trondheim
Norges teknisk-naturvitenskapelige universitet

Doktor ingeniøravhandling 1997:80
Institutt for marine konstruksjoner

MTA-rapport 1997:118

Reliability Analysis of Pipelines during Laying, Considering Ultimate Strength under Combined Loads

A Thesis Submitted in Partial Fulfilment of the
Requirements for the Degree of "Doktor Ingeniør"

by

Ragnar Torvanger Igland

Department of Marine Structures
Faculty of Marine Technology
The Norwegian University of Science and Technology
7034 Trondheim, Norway

Trondheim, August 1997

Dedicated to
Ingrid Ellen
for
her support and encouragement
and to Odd Eirik and Brynhild for their special inspiration

Abstract

Offshore pipelines are a part of the infrastructure of offshore oil/gas field. Pipelines seem to be the most suitable long term solution for transporting fluids when the offshore hydrocarbon exploration and production activities expand into deep water. The design and construction of pipeline system shall be such as to ensure that no single failure during installation or operation shall lead to human fatalities, serious environmental consequences or unacceptable economic losses. Installation is one of the most severe condition for pipeline design. Buckling and collapse are the most important failure modes for laying condition. The pipeline will experience a combination of loads and load effects: pressure, tension and bending during laying. This work has two main objectives. The first one is to study the ultimate strength of pipelines under combined loads. The second objective of the work is to apply reliability theory to achieve a more uniform and consistent safety level for design criteria for pipelines with different geometry and load conditions during laying. The collapse strength calculation, parametric studies and the subsequent reliability calculations are performed for pipeline laid in North Sea condition.

The ultimate collapse of thick tubes ($15<D_o/t<35$) under combined external pressure, tension and bending loads are studied applying the finite element method. Nonlinear effects of large deformations, effects of initial ovality, residual stress, strain-hardening, yield anisotropy and loading paths were accounted for in the analysis. Extensive comparisons between the analysis and laboratory tests, demonstrate that the analysis can accurately predict the collapse behaviour of thick tubes under combined external pressure, tension and bending loads. A series of parametric study on collapse of thick tubes was carried out. A set of interaction equations is proposed accounting for major factors affecting collapse envelopes. Extensive comparisons with the present finite element analysis results confirm the suitability of the proposed equations.

The presence of the concrete is neglected in laying analysis. However, because of the discontinuity in the concrete coating, occurrence of strain concentrations at the field joints arise during bending

of the pipe. Finite element analyses for the bending of pipelines including concrete coating are performed. The effects of concrete coating thickness, diameter to thickness ratio, shear strength of the corrosion coating and reinforcement in longitudinal and hoop direction were accounted for in the analysis. Comparisons between the analysis and laboratory tests, demonstrate that the analysis can predict the strain concentration in the field joints, defined as maximum strain in joint / nominal global strain. Simple formulae are proposed to account for major factors affecting strain concentration. A strain concentration factor is found to vary in the range of 1.1 to 1.6.

Finite element analyses of the load effects in the pipelines under ultimate sea state for S-lay operations are studied. The effects of uncertainties for yield stress, mass, stiffness of the stinger, transfer function and peak period for the wave spectrum were accounted for in the analysis. The maximum load effects are found for overbend and sagbend and is presented using response surfaces. The response surfaces are established in two ways, first using a nominal case and complementary experiments where only one of the parameters has been varied. Second using randomizing of the variables and calculate the load effect for several sets of experiments. In the present investigation four response-surface-models have been explored; multiplicative model, linear plane, polynomial without interaction and polynomial including interaction between the variables. The linear and polynomial model without interaction overestimate the load effect compared to the polynomial model with interaction between the variables. Use of the polynomial model with interaction between the variables is found to give a good prediction of the actual load effects. The drawback using this model is the large number of experiments required for establishing the response surface. Use of the multiplicative model is found to give good prediction of the actual load effects, given that extraction of response is done *within* the range of points defining the response surface, no coupling effects are included in this approach.

Structural reliability methods provide a measure of safety, based on the uncertainties in load effect and resistance. In applying structural reliability analysis to make decisions, measure of uncertainty, method of reliability and a target level need to be established. Herein, a combination of design point calculation and important sampling procedure is used when calculating the probability of failure. The study includes calibration of safety factors for design format. The most important random variable is the model uncertainty for bending capacity and the uncertainty of the load effect has minor importance for the probability of failure. The system effect is taken into account considering a high correlation between the resistance from one element to another, the effect on the usage factor for bending capacity is less than 5% compared to independent resistance. Considering the probability of failure for the total laying period, the safety factor for environmental load effect should be increased compared to considering the failure of a element during a 3 hour period.

Acknowledgements

This study has been carried out under the supervision of Professor Torgeir Moan. His advice, guidance and support are gratefully acknowledged.

Special thanks and appreciation are extended to Dr. Yong Bai and Mr. Geir Endal for their cooperation in the course of the work. Thanks are also extended to colleagues at SINTEF: Mr. Philippe Maincon, Mr. Kjell M Lund, Dr. Guoyang Jiao and Dr. Daniel Karunakaran for valuable discussions and encouragement throughout the course of the work.

I am thankful to Professor Segen Farid Estefen and Dr. Torbjørn Sotberg for their participation as member of the thesis committee.

I gratefully appreciate Ms Randi Sve for her help in typing and Ms Guri Berge for preparing figures and the presentation material.

A part of the work has been done within the projects : "Limit States for Tendon and Production Riser Bodies. Numerical Data Basis" and "SUPERB". Their contribution and support in this work are gratefully acknowledged.

This study was made possible by a scholarship from the Norwegian Research Council and the support is sincerely appreciated. I am also greatly indebted to the Faculty of Marine Technology at the Norwegian University of Science and Technology, and SINTEF Civil and Environmental Engineering, Structural Engineering, for their financial support.

Last but not least, I wish to thank my wife Ingrid Ellen and our children Odd Eirik and Brynhild for their patience and support during the long working days.

Table of Contents

Notations

All symbols are defined when they first appear in the text. Some symbols may have different meanings in different chapter and these are clearly defined when used. The most common symbols are listed below :

Abbreviations

API	- American Petroleum Institute
ALS	- Accidental Limit States
CTOD	- Crack Tip Opening Displacement
DOF	- Degree of Freedom
FE	- Finite Element
FOB	- Failure in OverBend
FORM	- First-Order Reliability Method
FLS	- Fatigue Limit States
FSB	- Failure in SagBend
LF	- Low Frequency
LRFD	- Load and Resistance Factor Design
HF	- High Frequency
PLS	- Progressive Limit State
RAO	- Response Amplitude Operator
RS	- Response Surface
SLS	- Serviceability Limit States
SMYS	- Specified Minimum Yield Strength
SORM	- Second-Order Reliability Method
ULS	- Ultimate Limit States
X52	- Material grade, yield strength = 52 ksi = 358 MPa

X65 - Material grade, yield strength = 65 ksi = 448 MPA
X77 - Material grade, yield strength = 77 ksi = 530 MPA
3-D - Three Dimensional

Subscript

0 - yield or mean
θ - circumferential
r - radial or residual
c - characteristic
co - collapse
E - environmental or elastic
F - functional
nom - nominal
x - longitudinal

Superscript

M - moment
P - pressure
T - tension

Mathematical Symbols

α - unit normal vector
$\mathbf{X}$ - random variable vector
$\cup$ - union
$\prod$ - product
$\sum$ - sum
$f_x(x)$ - marginal probability density function of x
$F_x(x)$ - cumulative distribution function of x
$f_{xy}(x,y)$ - joint probability density function of x and y
$f_{x|y}(x|y)$ - conditional probability density function of x given y
g(x) - limit state function in physical space
g(u) - limit state function in standard normal space
P( ) - probability
CoV - Coefficient of Variation = standard deviation / mean
ϕ ( ) - Standard normal density function
Φ( ) - Standard normal distribution function

Roman Symbols

A	- cross section, $= \pi D_0 t$
C	- strain concentration
C_i	- coefficient *i* in predicted equation
CT	- concrete thickness
D_0	- mean tube diameter = D - t
E	- Young's modulus
g	- acceleration of gravity
H_S	- significant wave height
m	- number of parameters
M	- applied collapse moment
M_{co}	- maximum bending moment capacity
$M_{co,c}$	- characteristic maximum bending moment capacity
$M_{F,C}$	- characteristic maximum functional moment
$M_{E,C}$	- characteristic maximum environmental moment
M_0	- plastic moment, $= D_0^{\,2} t \sigma_0$
N	- number of experiments or observations
N_c	- number of coefficients
N_E	- number of elements
n	- strain-hardening parameter of material
P_f	- probability of failure
P	- applied collapse pressure
P_{co}	- collapse under pure pressure
$P_{co,c}$	- characteristic collapse pressure
P_E	- linear buckling pressure, $P_E = 2E(t/D_0)^3/(1-\nu^2)$
P_0	- yield pressure, $P_0 = 2\sigma_0 t/D_0$
P_0^*	- modified yield pressure accounting for the effect of axial load
q_M	- ratio of characteristic dynamic to static moment (load level) = $M_{E,c}/M_{F,c}$
q_T	- ratio of tension to collapse tension = $T_c/T_{co,c}$
q_P	- ratio of external pressure to collapse pressure = $P_o/P_{co,c}$
q_ε	- ratio of characteristic dynamic to static strain (load level)= $\varepsilon_{E,c}/\varepsilon_{F,c}$
r	- response (load effect)
$\boldsymbol{R}^I$	- inertia force vector
$\boldsymbol{R}^D$	- damping force vector
$\boldsymbol{R}^S$	- internal structural reaction force vector
$\boldsymbol{R}^E$	- external force vector
$\boldsymbol{r},\dot{\boldsymbol{r}},\ddot{\boldsymbol{r}}$	- structural displacement, velocity and accelerations vectors
S	- anisotropy, $= \sigma_{\theta 0}/\sigma_{x0}$
t	- tube thickness

T - applied collapse tension
T_{co} - collapse tension
$T_{co,c}$ - characteristic collapse tension
T_0 - yield tension, $= \pi D_0 t \sigma_0$
T_P - peak period for wave spectrum
W - elastic section modulus,$= \pi/4D_0^2 t$
w - effective weight
X - model uncertainty parameter
X^{true} - value measured by laboratory tests
X^{pred} - value predicted by design equations
$X\varepsilon_{co}^{T}$ - normalized bending strain capacity $= \varepsilon_{co}^{T}/\varepsilon_{co,c}^{T}$
X_E - normalized dynamic strain load effect $= \varepsilon_E/\varepsilon_{E,c}$ or $M_E/M_{E,c}$
X_F - normalized static strain load effect $= \varepsilon_F/\varepsilon_{F,c}$ or $M_F/M_{F,c}$
X_I - normalized strain intensification factor
X_m^{ε} - model uncertainty for critical bending strain
X_m^{T} - model uncertainty collapse tension
X_{mass} - linear mass / nominal mass
X_m - normalized moment $= M/M_c$
X_{mco} - normalized moment capacity $= M_{co}/M_{co,c}$
X_{mco}^{P} - normalized moment capacity $= M_{co}^{P} / M_{co,c}^{P}$
X_P - normalized external overpressure load effect $= P/P_c$
X_{Pco} - normalized collapse pressure capacity $= P_{co}/P_{co,c}$
X_{RAO} - RAO/ nominal RAO
X_{stiff} - stinger stiffness/nominal value
X_σ - normalized yield strength $= \sigma/SMYS$
X_T - normalized load effect, tension,$= T/T_c$
X_{Tco} - normalized collapse tension capacity $= T_{co}/T_{co,c}$
X_{Tco}^{P} - normalized collapse tension capacity $= T_{co}^{P} / T_{co,c}^{P}$
X_t - normalized wall thickness $= t/t_{nom}$
X_{Tp} - Tp/ nominal Tp

Greek Symbols

α_i^2 - important factor
β - reliability index
γ_E - environmental load coefficient
γ_F - functional load coefficient
γ_R - resistance coefficient
δ - skewness

δ_0 - imperfection amplitude, $\delta_0 = (D_{max}-D_{min})/(D_{max}+D_{min})$

ε_{co} - collapse extreme fibre strain under pure bending

$\varepsilon_{co,c}$ - characteristic maximum strain capacity

$\varepsilon_{F,c}$ - characteristic maximum functional (static) strain load effect

$\varepsilon_{E,c}$ - characteristic maximum environmental (dynamic) strain load effect

ε_0 - yield strain , = 0.005

ε_F - flow strain , = 0.02

η_e - usage factor, bending strain

η_M - usage factor, bending moment

η_P - usage factor, pressure

η_T - usage factor, tension

κ - curvature, kurtosis

κ_{co} - collapse curvature under pure bending

κ_0 - t/D_0^2

λ - tube slenderness

μ - mean value

ν - Poisson's ratio

π - 3.1415927

ρ - correlation coefficient, mass density

σ - standard deviation

σ_0 - yield stress of material, $\varepsilon = 0.005$

σ_θ - circumferential stress

σ_p - proportional limit stress of material, $\varepsilon = 0.0012$, 0.0016 and 0.0020 for X52, X65 and X77 respectively.

τ - shear strength

ω - angle frequency

1 INTRODUCTION

1.1 Rational

Offshore pipelines are a part of the infrastructure of offshore oil/gas field. Pipelines seem to be the most suitable long term solution for transporting fluids when the offshore hydrocarbon exploration and production activities expand into deep water. Pipelines include the whole range of pipelines: from in-field flowlines to large inter-continental export pipeline. The total number of pipelines in the North Sea listed to the end of 1993 is 930, amounting 17 245 km, Robertson et al (1995). Including fields from offshore Brazil, the Gulf of Mexico and the Middle-East Asia, the length of pipeline will be several times more.

The design and construction of pipeline system shall be such as to ensure that no single failure during installation or operation shall lead to human fatalities, serious environmental consequences or unacceptable economic losses.

Installation is one of the most severe condition for pipeline design. Buckling and collapse are the most important failure modes for laying condition. The pipeline will experience a combination of loads and load effects: pressure, tension and bending during laying. Assessment of buckling and collapse are important tasks in the design of pipeline during laying.

Capacity of the pipeline

The capacity of the pipeline, for the basic failure modes and some of the load combinations have been assessed by several authors :

Early studies on the collapse behaviour of thick tubes under external pressure were well outlined

by Timoshenko and Gere (1961). Due to increasing needs in offshore engineering, careful experimental and analytical investigations have been carried out, e.g. Tokimasa and Tanaka (1986), Yeh and Kyriakides (1986, 1988). An extensive survey of literature has been presented in their papers. Using FEM approach, Tokimasa and Tanaka (1986) investigated the effects of initial ovality, residual stress and strain hardening. They finally derived a set of formulae to predict the collapse strength of tubes under external pressure. It was claimed that the circumferential residual stress greatly reduced the collapse strength. However, according to Yeh and Kyriakides (1986), the effect of residual stress seems to be very small. Due to that the opinion differ, hence it is necessary to study the residual stress effect more systematically for various D_0/t ratios and material properties. It should be noted that the initial ovality amplitude in the test specimens is relatively small. To interpret the test data for code development, it is necessary to know how much the collapse strength would be reduced when the initial ovality amplitude is increased.

The type of instability for a tube under pure bending depend on the D_0/t ratio and the material properties of the tube. Brazier (1927) solved a limit load type of instability of long elastic tubes in pure bending due to ovalization of the cross-section. The solution was extended by Ades (1957) for long elastic-plastic tubes in pure bending by assuming that the cross-section ovalized always into an elliptical form. For thinner tubes (larger D_0/t values), a bifurcation buckling (local shell buckling) occurs, Timoshenko and Gere (1961). However, the D_0/t value which separates the limit load instability and the bifurcation buckling depends on the material properties of the tubes. Experiments conducted by Kyriakides and Ju (1992) and Corona and Kyriakides (1988) show this D_0/t value for typical pipeline material is around 35 to 40. Therefore in the present study, only the limit type of instability is considered.

In recent years, the understanding of collapse behaviour of thick tubes under bending load was further extended to the case including pressure. The state-of-art as well as literature review could be found from de Winter et al (1985), Corona and Kyriakides (1988) and Ju and Kyriakides (1991). It was shown by Corona and Kyriakides (1988) that the limit load type of instability could be numerically predicted provided the geometric and material parameters and loading path were known. They presented the sensitivity of pressure-curvature envelopes to D_0/t, initial ovality, yield anisotropy and hardening parameters and loading paths.

Tension tearing rupture of material is a rare, but a basic failure mode for the pipeline. During the last 30 years, many fracture mechanics criteria have been developed to predict the material resistance, including both brittle fracture and tension tearing rupture (ductile fracture). Example of the criteria is the CTOD design curve (see e.g. Andersen 1990). The major parameters governing the fracture are defect size and fracture toughness. However, it should be emphasized that the CTOD design curve applies to the localized strain near weld defects, and not to the strain from beam-column theory. On the other hand, for pipelines with surface flaws or through-wall flaws, systematic investigations on tensile failure criteria have been carried out by e.g. Wilkowski and

Eiber (1981). The tensile failure is estimated using a flow stress concept. Several relationships between flow stress σ_f, yield stress σ_0 and ultimate stress σ_u, have been proposed by Wilkowski and Eiber (1981).

Some of the earliest experiments to establish a criterion for combined external pressure and tension loads were carried out by Edwards et al in 1939. Recent experimental investigations were presented by Kyogoku et al (1981), Tamano et al (1982). Babcock and Madhavan (1987) conducted a number of small scale tests and presented a systematic analysis considering the effects of initial ovality, yield anisotropy and strain hardening. They showed that for tubes with small initial ovalities changing the loading paths had very little effect on the tension-pressure collapse envelope unless tension load was dominant. However, for tubes with relatively large initial ovalities this conclusion should be further confirmed, e.g. by numerical simulation.

For the collapse behaviour of thick tubes under combined tension and bending and combined pressure, tension and bending loads, there is no laboratory test data available. Therefore it is necessary to study the combination using numerical simulations.

Load effect and strain concentration of pipeline during laying

During S-laying installation of offshore pipelines, the pipe is exposed to plastic strains when the pipe passes over a stinger exceeding a certain curvature. Generally the presence of the concrete is neglected in laying analysis. However, because of the discontinuity in the concrete coating, several additional problems arise (Konuk, 1984). The most important of which is the occurrence of strain concentrations at the field joints during bending of the pipe. During the last decades several experimental investigations have been carried out in order to better understand the behaviour of concrete coated pipelines in pure bending (Jirsa et al. (1969), Mogbo et al. (1971), Archer and Adams (1983), Akten et al. (1985), Lund et al. (1993)). The results of these studies can be summarized as follows: The pipeline is discontinuously coated with concrete, which introduces strain concentrations at the field joints. Small shear strength in the anti-corrosion layer implies weak bond between the steel pipe and the concrete coating. Bending of the pipeline implies sliding between the steel and the concrete. The shear strength of the corrosion layer is dependent on the type material used. The true shear strength increases considerably if sliding is prevented. The strain concentrations at the field joints are dependent on the temperature and the time it takes to deform the pipe since the anti-corrosion material is visco-elastic. The problem is difficult to model analytically, especially when the strains in the field joint enters the nonlinear area.

Design of pipelines

Design scenarios for pipeline under laying operation are the combination of functional and environmental loads. In the traditional design, the relevant design loads are defined as deterministic

quantities. In reality, these loads are random variables and will result in large uncertainties in the load effects. In addition, incomplete knowledge of design conditions and idealised structure modelling in design will all lead to uncertainties. Hence, probabilistic methods should be applied in modelling the various load and response quantities.

Furthermore, pipeline failure modes are different for different design scenario and lead to different consequences of failure. To achieve a cost beneficial design, design levels should be based on the consequences of failure which balance the safety and the costs. A deterministic design is unable to achieve this goal, but rational reliability based design can match the requirement.

The assessment of the installation is currently carried out by making reference to a maximum allowable strain at the stinger equal to about 0.2% and a maximum allowable stress at the sagbend equal to about 0.72 of the yield stress, see DnV (1981). The criteria are applied both when laying in deep water and in shallow water. In reality when laying in the shallow water the critical section is the sagbend and its behaviour can be significantly affected by environmental loading. This imply that the stress criterion is the limiting one (load controlled). When laying on deep water the environmental load effect are of minor importance and the critical section is the pipe on the stinger. For this scenario the limiting strain value of 0.2% may be too conservative with respect to strain capacity.

Structural Reliability Analysis

A rational step forward in the assessment of offshore pipeline design is the application of reliability methods as a basis for the limit state design concept. Within the reliability theory a number of methods applied to marine structures are used. *Quantitative Risk Analysis* is concerned with the estimation of overall risk to human health and safety and the environment. *Structural Reliability Analysis* is concerned with the estimation of the failure probability of a structure considering normal uncertainties, without accounting for the gross error due to human incapability. Structural reliability theory provides a probability based method for supporting the decision making.

Structural reliability methods consider structural analysis models in conjunction with available information of the involved variables and their associated uncertainties. The reliability predicted by structural reliability methods is not an objective physical property of the pipeline itself in the given operational and environmental condition, but rather a nominal measure of the reliability for a given physical and probabilistic modelling and an applied analysis procedure.

SUPERB (1996) presents the state of the art concerning with limit state design of pipelines. With respect to the laying situation and reference unit is the study limited and a further study is necessary.

Response surface

The response surface technique has been used for many purposes during the last decades, e.g. calculate nonlinear dynamic response of offshore platforms, the assessment of the reliability of nuclear power stations.

As all reliability methods are based on repeated evaluation of the failure function, a large number of load effect predictions are required. An integrated load effect prediction would require a large number of time consuming analyses. Response surfaces are therefore introduced in the reliability assessment in order to have an efficient and accurate prediction of load effects. The response surface is a parameterization of the response in terms of the basic random parameters. The points which define the response surface are characteristic load effect values obtained for variations in the uncertain parameters. The response surface forms an n-dimensional space in which Monte Carlo and Important Sampling simulation can be performed to obtain load effects using interpolation/extrapolation. Also, it is important that the response surface provides an accurate prediction of the response in the neighbourhood of the design point, Bucher and Bourgund (1990).

1.2 Purpose of the present work

This work has two main objectives. The first one is to study the ultimate strength of pipelines under combined loads. The load effects include pressure, tension, bending loads as well as their combination. After validating the FEM approach, a parametric study is carried out to investigate collapse behaviour and interaction envelopes for tubes under combined loading.

The second objective of the work is to apply reliability theory to achieve a more uniform and consistent safety level for design criteria for pipelines with different geometry and load conditions during laying. The finding from the first part of the work will form the basis for the reliability study.

The collapse strength calculation, parametric studies and the subsequent reliability calculations are performed for pipeline laid in North Sea condition.

1.3 Organization and presentation of the work

The work is organized in four parts, basic concepts, capacity of tubes under combined loads, load effect during laying and reliability analysis.

The basic concepts for the work is presented in Chapter 2. Chapter 3 contains interaction envelopes for capacity of tubes under combined loads, the data basis for the equations is enclosed in Appendix A. Chapter 4 and 5 relate to load effect during laying of pipeline. Chapter 6 contains limit states and calibration of design codes for pipelines under displacement and load controlled conditions.

Chapter 2 gives a brief overview of structural reliability theory, and provides a description of various methods for component reliability analysis used in this study. It also emphasis on reliability based calibration of partial coefficients in design equations for a specific failure mode. Response surfaces are introduced in the reliability assessment in order to have an efficient and accurate prediction of load effects. The procedure used to determine the response surface parameters is described. A pipeline during laying will experience a combined load effect due to bending and tension and pressure-tension-bending, the method proposed for treating load combination during laying is presented. For design purposes, it is essential to know not only the maximum response, but also the extreme response which is a value that is not expected to occur more than once in the period considered. An overview of distributions and how to calculate the extreme value is presented.

Ultimate strength of tubes is affected by the geometry of the tube, the material properties and the load path considered. Chapter 3 is devoted to the problems concerning ultimate collapse behaviour of thick tubes under external pressure, tension and bending loads and their combination. A set of design interaction equations are derived, based on parametric studies. The design equations are compared with existing design codes and test results. The data base from the FE-analysis is enclosed in Appendix A.

Offshore pipelines are usually coated with concrete in order to counteract buoyancy and ensure on-bottom stability of the pipeline. Generally the presence of the concrete is neglected in laying analyses. However, because of the discontinuity in the concrete coating, occurrence of strain concentration at the field joints during bending of the pipe. Chapter 4 is concerned with a numerical model which is applied to establish an equation which expresses the strain concentration for a pipeline being bent over the stinger during laying.

S-lay is applied to lay the vast majority of large diameter (larger than 16 in) pipelines e.g. in the North Sea. The S-lay method is considered in Chapter 5. The mechanics of loading and the uncertainties related to lay operations will be discussed. The procedure used to determine the points which define the response surface is described.

The structural reliability method is used to calibrate code in Chapter 6, considering structural analysis models in conjunction with available information of the involved variables and their associated uncertainties. Design formats for displacement and load controlled design conditions are outlined. Calibration of design codes where the effect of series system and weather window are described.

2 BASIC CONCEPTS

2.1 General remarks

Reliability theory has become a design tool with the objective of achieving a more uniform and consistent reliability within marine structures. Chapter 2.2 gives a brief review of structural reliability theory, and provides descriptions of various methods for component reliability analysis used in this study.

In Chapter 2.3 emphasis is placed on reliability based calibration of partial coefficients in design equations for a specific failure mode. The process of an entire code calibration in which a code may be calibrated by a formal process of explicit optimization is briefly considered.

As all reliability methods are based on repeated evaluation of the failure function, a large number of load effect predictions are required. An integrated load effect prediction would require a large number of time consuming FE-analyses as each characteristic load effect corresponds to a representative extreme value found from a 3-hour period. Response surfaces are therefore introduced in the reliability assessment in order to have an efficient and accurate prediction of load effects. The points which define the response surface are characteristic load effect values obtained for variations in the uncertain parameters. The procedure used to determine these values is described in Chapter 2.4.

A pipeline during laying will experience a combined load effect for a given loading. The most important load combination process during laying is bending and tension. The combination pressure-tension-bending is not of interest since the pressure for practical purposes is considered as deterministic at a specified location of the pipeline. The simplest method to treat linear combination of loads modelled is, e.g. Ferry-Borges method and Turkstra's rule. Chapter 2.5

propose the method used for load combination during laying.

For design purposes, it is essential to know not only the maximum response, but also the extreme response which is a value that is not expected to occur more than once in the period considered. Chapter 2.6 gives an overview of distributions and how to calculate the extreme value.

2.2 Reliability analysis

The central objective for a pipeline design is to achieve an accepted reliability for the total pipeline both from a safety and economic point of view, and the goal for the structural reliability analysis is then to document that this reliability is achieved.

The objective of a reliability analysis is to calculate the probability of failure. This probability represents a realistic measure of the safety of the actual structure. A practical application of structural reliability analysis typically involves the following steps (see e.g. Melchers (1987)):

- *Failure modes and limit state functions*
  All significant modes of failure have to be identified. Examples of failure modes for laying operations are yielding, buckling, excessive ovalization and fatigue.

  Failure mode criteria are to be modelled in accordance with the state-of-the-art within the field. The limit state functions are functions of the basic variables which govern the behaviour of the pipeline and represent the failure modes.

- *Probabilistic modelling*
  To identify all physical variables, incorporation of all relevant sources of uncertainties in the analysis. Typically the physical variables are material properties, seabed geometry and characteristics of external or functional loads and load effects.

  The effect of measurement and statistical uncertainty due to a state of imperfect knowledge must be quantified.

  The model uncertainties should be quantified by the bias and random variability in the model. An adequate assessment may be based on theoretical considerations, refined analyses, field or laboratory measurements or simply based on experience /standardization.

  For all variables a probability distribution must be assigned based on engineering judgment and experience from similar types of problems, physical knowledge, analytical results or distribution fitted to available observations of the uncertain quantities.

- *Method for calculating failure probability*
  The failure probability may be calculated by analytical methods or simulation techniques, see overview in e.g. Melchers (1987). Further, for more involved limit state functions a response surface technique may be applied.

- *Target safety level*
  Establish a target reliability level for the problem based on the consequence of failure and safety class and consistent with reliability method used, see e.g. Sotberg et al (1997).

- *Perform the calculations*
  Perform the calculations based on the probabilistic method and uncertainty measures used for all failure limit states.

- *Evaluation of the results*
  An evaluation of the reliability analysis must be performed in order to assure that the design point is reasonable. Further it must be assured that it is not in conflict with obvious physical knowledge or limitations and that it is within the validity range of the applied physical and probabilistic model. The important factors are calculated, which are applied to focus attention on the most important variables.

  Based on established design practice or assessment based on consequences and class of failure, a comparison with the target value is performed.

2.2.1 Failure modes and limit state functions

All significant modes of failure have to be identified and corresponding limit state criteria have to be established. For offshore pipeline the limit-states may be categorized as:

- Serviceability Limit-State (SLS) in which the pipeline is considered to perform its design function satisfactorily and remain in service. Failure modes are yielding, ovalization, ratcheting and loss of concrete.
- Ultimate Limit-State (ULS) in which the pipeline must remain intact, but not necessarily be able to operate. Failure modes are bursting, unstable fracture and plastic collapse, buckling and collapse and tensile rupture.
- Fatigue Limit-State (FLS) results from excessive fatigue crack growth or damage accumulation under cyclic loading.
- Accidental Limit-State (ALS) correspond to ultimate failure of the pipeline due to accidental loads and/or local damage with loss of structural integrity and rupture.

From the limit state categories previously presented, the ultimate limit state is the most severe limit state for laying and is considering in this work.

ULS

The *ultimate limit state* defines the maximum load carrying capacity includes the following limit states:

Bursting: rupture of the pipe wall due to, e.g., excessive internal pressure, corrosion, etc.
Fracture: unstable fracture and/or plastic collapse of defects under tensile loading
Buckling: loss of equilibrium/stability under compressive loading
Collapse: exceed the limit load-carrying capacity

The installation of pipelines in offshore locations can induce rather severe loads to the structure. The lines are usually installed empty and must have the capacity to withstand the ambient external pressure as well as the bending and tension loads induced by the lay process. As a result, optimally designed pipelines are critical to buckling (collapse). Buckling and collapse may be consider as the same failure mode, but will depend on the pipeline diameter, wall thickness, material properties and presence of initial geometric imperfections.

Typical offshore pipelines have D_0/t ratios ranging between 80 - 15. They are usually made from steel with yield strength ranging between 276 - 448 MPa and an initial ovality less than 0.5 %.

Collapse of pipes under external pressure buckles from the uniform circular to the uniform oval configuration. Due to interaction of ovaling and yielding, the pipeline experience a limit pressure type of instability. The presence of even small initial imperfections has been shown to significantly reduce the collapse pressure.

Pure bending induces ovalization to the cross-section of the tube. This nonlinear effect, coupled with the plastic material characteristics, lead to a limit load type of instability (moment maximum). For thinner pipes, a bifurcation type of instability can precede the limit load. This takes form of wrinkles of the compressed side of the pipe. However, deformation soon localizes and results in the development of one sharp 'kink' in the pipe and a total collapse of the structure (local buckling). For thicker pipes, the bifurcation occurs in the plastic range and is followed again by a limit load instability. For D_0/t ratios below 35-40 the limit load type of instability is reached before bifurcation, which imply that most of the pipeline will be considered under this instability type.

The most severe failure mode during installation is buckling and collapse, where the two load effects, the bending of the pipeline in the presence of external pressure, interact strongly through the ovalization of the cross-section.

2.2.2 Probabilistic modelling

The objective of the probabilistic modelling is to develop models which embody its salient features. The aim is to focus on the significant items including treatment of variability and uncertainty that will contribute to the probability of structural failure.

Types of Uncertainties

A structural reliability analysis demand that all relevant uncertainties related to the limit state considered shall be assessed and documented. The uncertainties to be considered are represented by modelling the basic variables as random variables in order to reflect the current knowledge of the variables and analysis models applied.

Uncertainties associated with an engineering problem may be divided into two main groups: inherent uncertainty and uncertainty due to inadequate knowledge.

Physical uncertainty is an inherent uncertainty while the statistical and the model uncertainties belong to uncertainties due to inadequate knowledge. Inherent uncertainty is a natural randomness of a quantity which by definition can not be altered by human activity while the other uncertainties represents insufficient knowledge or errors which can be corrected by improved measurements and models, or from increased data sets.

Uncertainties related to gross errors are normally not covered within the framework of structural reliability and should be considered by other means, i.e. organisational reliability analysis.

Physical Uncertainty

Physical uncertainty, also known as inherent or intrinsic uncertainty is a natural randomness of a quantity such as variability in current, uncertainty in yield stress etc. It may be divided into two categories, whether it can be affected by human activities or not. Examples on the first category is the uncertainty related to the strength of steel or a tolerance on a geometric quantity. These uncertainties may be reduced by use of more advanced production or quality control systems. An example of an uncertainty which can not be changed is the natural variability of an environmental load estimated from a very large representative data set. This distinction is important when economic aspects are considered.

Statistical Uncertainty

Statistical uncertainty is due to a limited amount of information such as a limited number of observations which causes uncertainty in the estimation of statistical parameters. Statistical uncertainty may further occur due to negligence of systematic variations of the observed variables e.g. from long term climate variations or by neglecting correlations.

Special care must be taken for cases based on a small amount of data. The statistical uncertainty is a function of the type of distribution fitted, the type of estimation technique applied, the value of the distribution parameters and the amount of underlying data.

For independent distributed samples the standard deviation of the moment estimators are given by e.g. (Kendall and Stuart, 1977) :

$$s_\mu = \sigma/\sqrt{N}, \quad s_\sigma = \sigma\sqrt{\frac{\kappa-1}{4N}}, \quad s_\delta = \sqrt{6/N}, \quad s_\kappa = \sqrt{24/N} \tag{2.1}$$

where μ, σ, δ, κ and N are defined as mean, standard deviation, skewness, kurtosis and number of observations, respectively. The estimate of statistical uncertainties of skewness and kurtosis are valid for normal parent.

Model Uncertainty

Model uncertainty is uncertainty due to imperfections and idealizations made in the applied physical and probabilistic models, and reflects a general confidence in the applied model to describe "real life". It may further account for unknown effects of other variables and their interaction which are not included in the model.

Model uncertainties in a physical model for representation of load or resistance quantities can be represented by stochastic factors each defined as the ratio, (or alternatively the difference), between the true "real life" quantity and the quantity described by the model. A mean value not equal to 1.0 (or alternatively 0.0) expresses a bias in the models prediction of reality while the coefficient of variation expresses the corresponding scatter of the prediction.

An adequate assessment of the model uncertainty may be available from sets of laboratory or field measurements, physical arguments, refined analyses or simply from engineering judgment. However, subjective choices of the distribution of a model uncertainty will often be necessary.

Distribution of Variables

The probability distribution for a random variable represents the uncertainty of the variable. The results of a reliability analysis may be very sensitive to the tail behaviour of the probability distribution applied, implying that a proper procedure for the choice of distribution is required.

The process of establishing a probability distribution for a stochastic variable, consists of *choice of distribution model, estimation of distribution parameters* and *verification of fitted distributions*.

Choice of Distribution Model

In order to describe the statistical nature of load, load effects, material properties, geometrical parameters and capacities a probability distribution function must be assumed. Often there is no theoretical preference when it comes to deciding on probabilistic models. The Normal distributions is recommended applied for load variables and Lognormal distributions is applied for resistance variable when no detailed information is available.

Deviations from the above default distributions must be well documented on the basis of physical reasoning of the nature. The underlying generation mechanism has to be examined in order to evaluate whether it may be considered an approximation to a well known stochastic experiment, i.e.

- the limiting additive mechanism (central limit theorem) leads to a *Gaussian* distribution
- the multiplicative mechanism leads to the *Log-normal* distribution as a product of independent identically distributed variables
- asymptotic maximum and extreme values (type I, II and III extreme value distributions) i.e. distribution for the smallest or largest values, see e.g. (Gumbel, 1958)

Hence, based on experience from similar types of problems, physical reasoning or analytical results, a set of possible distributions may be selected.

Methods for Estimating Distribution Parameters

A frequently applied technique for estimating distribution parameters is *Method of Moments*. The method of moments can be applied to evaluate distribution parameters by assigning analytical moments to the sample moments. Usually estimates for the four moments estimators are applied, where μ is the mean value, σ is the standard deviation, δ is the coefficient of skewness and κ is the coefficient of kurtosis. For small data sets, following estimates may be applied :

Mean value:

$$\mu = \frac{1}{N}\sum_{i=1}^{N} x_i \tag{2.2}$$

Standard deviation:

$$\sigma^2 = \frac{1}{(N-1)}\sum_{i=1}^{N}(x_i-\mu)^2 \tag{2.3}$$

Coefficient of skewness:

$$\delta = \left(\frac{1}{N}\sum_{i=1}^{N}(x_i-\mu)^3\right) /\sigma^3 \tag{2.4}$$

Coefficient of kurtosis:

$$\kappa = \left(\frac{1}{N}\sum_{i=1}^{N}(x_i-\mu)^4\right) /\sigma^4 \tag{2.5}$$

where N is the number of observations.

Other applied techniques for estimating distribution parameters are *Graphical Procedure*, *Maximum Likelihood Estimation Technique* and *Bayes Estimation*. see e.g Ang & Tang (1975).

Verification of Fitted Distributions

The final stage in the selection process of a distribution with fitted parameters is the model verification. The adequacy of a fitted model can be indicated by subjective judgement or by objective methods.

A subjective judgement based on a probability plot is often the most accepted approach. Such a verification may be performed by plotting both the empirical and the fitted distribution function in a quantile plot or in a plot constructed so that the fitted model appear as a straight line. The verification can the be focused on the important part of the distribution, (left tail, right tail or central part of the distribution).

The most commonly adopted objective methods (Ang &Tang, 1975) are *Kolmogorov-Smirnov test and* χ^2 *test*

Joint Description of Variables

In a reliability analysis all significant variables should be considered. In case the involved variables are independent, the joint description (i.e. the joint distribution) of the variables is obtained as the

product of the marginal distribution. If a sufficient amount of data is available, the mutual dependency among the random variables may be accounted for by using conditional distributions. Hence, the joint distribution of two random variables may be written

$$f_{X,Y}(x,y) = f_{Y|X}(y|x) f_X(x)$$

Otherwise, the mutual dependency may be included in the analysis as a multidimensional model, or to provide the marginal distributions and the coefficient of correlation between the variables.

2.2.3 Methods for calculating failure probability

General

The selection of a method depend on the objective of the analysis, the number and type of random variables involved, the computational cost of evaluating the failure function for a given realization of the variable vector, the mathematical properties of the limit state function and the reliability level of interest.

Reliability methods are often categorized into four levels of increasing complexity, see for instance Thoft-Cristiansen and Baker (1982), Madsen et.al (1986) and Melchers (1987). Briefly, the level I methods are associated with the code level methods where each uncertain parameter is represented by a characteristic value ; the level II methods are the second moment methods where each uncertain parameter is represented by two values, commonly taken as the mean and the variance, supplemented with a measure of correlation between the parameters; the level III methods, which are adopted herein, employ failure probability as the reliability measure, and require knowledge of the joint distribution of all uncertain parameters; and finally, the level IV methods, which also incorporate engineering economic analysis under uncertainty in order to optimize the structure with respect cost and utility.

For time-independent stochastic variables P_f is defined by

$$P_f = \int_{g(x)<0} f_x(x)dx \qquad (2.7)$$

where $\mathbf{x}$ is a vector of stochastic variables, $f_{\mathbf{X}}(\mathbf{x})$ is the joint probability density function and $g(\mathbf{x})$ is the failure or limit state function where $g(\mathbf{x})<0$ signifies failure. The function $g(\mathbf{x})$ may represent a single failure cause, i.e., single event function, or a system representation of several failure modes.

Analytically Based Methods - FORM/SORM

Analytical methods consists of a first order reliability method (FORM) and a second order reliability method (SORM), (see e.g. Madsen et al 1986). The advantage of the analytical methods is that they do usually not require excessively large computer time. The drawback is that they do not give exact

results for the sought probability, but only approximations which may not always be sufficiently accurate. Further, a requirement for the analysis, is that the failure function is twice continuously differentiable in the vicinity of the design point. Figure 2.1 present a schematic illustration of FORM and SORM.

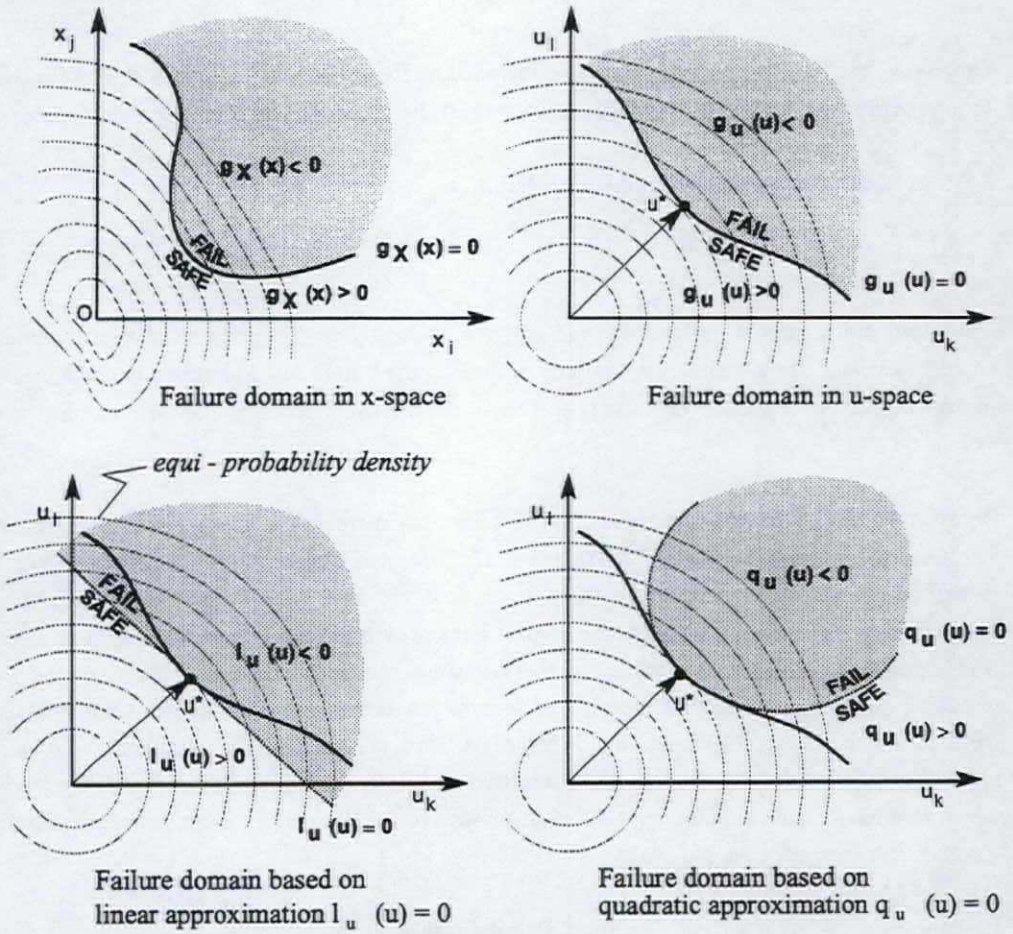

Figure 2.1 Schematic illustration of FORM and SORM

The general procedure for FORM basically consists of the following steps (see e.g. Madsen et al 1986 for more details).

The first step is to transform the basic variable **X** into independent standard normal variables **U**, i.e. identify a transformation **T** such that $\mathbf{U} = \mathbf{T}(\mathbf{X})$. For correlated variables, the Rosenblatt transformation has been suggested by Hohenbichler and Rackwitz (1981). In the standard normal space, the failure domain is expressed by $[g(\mathbf{U}) < 0]$, where $g(\mathbf{U}) = g(\mathbf{T}^{-1}\mathbf{X})$.

The second step is to find the design point $\mathbf{u}^*$, which is the point on the surface [g(U)=0], where the probability density in the standard normal space is largest. At the design point a tangent to the surface has to be found. In FORM the tangent is chosen as a linear approximation. The design point is found by a minimisation procedure with one constraint

$$\min |\boldsymbol{u}| \; ; \; g(\boldsymbol{u}) = 0 \tag{2.8}$$

The design point is expressed by a vector given as:

$$\boldsymbol{u}^* = \beta \boldsymbol{\alpha}^* \tag{2.9}$$

Where β is the distance from the origin to the design point, which is referred as the reliability index, and $\alpha^*$is a unit normal vector to the limit state surface.

The last step is to estimate the failure probability using the tangent plane as approximation of the failure surface as :

$$P_f = \Phi(-\beta) \tag{2.10}$$

SORM is similar except for the Taylor expansion of the failure function about the design point, which include a quadratic approximation of the failure surface.

Simulation techniques

The multi-dimensional failure probability integral in Eq. 2.7 can be calculated by Monte Carlo simulation technique. The basic Monte Carlo simulation and Monte Carlo simulation with importance sampling may be classified as zero-one indicator-based simulations, while directional simulation and axis-orthogonal simulation belong to the class of conditional expectation methods.

The *basic Monte-Carlo simulation method* samples from the joint distribution $f_{\mathbf{x}}(\mathbf{x})$, and the indicator function $I(\mathbf{x})$, defined as $I(\mathbf{x})=1$ if $g(\mathbf{x}) \leq 0$ and $I(\mathbf{x})=0$ if $g(\mathbf{x}) > 0$, is evaluated at each sample point. An unbiased estimator for the failure probability is then given by the sample mean

$$\hat{P}_f = \frac{1}{N} \sum_{j=1}^{N} I(\boldsymbol{x}_j) \tag{2.11}$$

The advantage of the method is that it makes use of point values of the g-function only, and that the g-function and the distributions do not require any analytical properties. Further, the method gives solutions which converge towards exact results when sufficient number of simulations are carried out. The disadvantage is the computational time for small probabilities.

Improved efficiency of simulations can be obtained by using known information about the problem through variance reduction techniques (Rubinstein, 1981). The purpose of the variance reduction techniques is to reduce the variance of the estimated output variable by using the same execution

time and storage requirements without disturbing its expected value (Ayyub and Haldar, 1984).

Important sampling is probably the most commonly used variance-reduction technique developed so far, and it can be shown to be extremely efficient. In importance sampling the sample points are concentrated in parts of the region that are most important, i.e., in the neighbourhood of the design point (Bourgund and Bucher, 1986). When applying importance sampling technique, the probability of failure is expressed as

$$\hat{P}_f = \frac{1}{N}\sum_{j=1}^{N} I(\boldsymbol{x}_j)\left(\frac{f_x(\boldsymbol{x}_j)}{h_x(\boldsymbol{x}_j)}\right) \tag{2.12}$$

where

$f_x(\mathbf{x}_j)$ the actual joint probability of problem

$h_x(\mathbf{x}_j)$ the new sampling density

The expression in parenthesis in Eq. 2.12, plays the role of a weight function. Figure 2.2 shows the important sampling for the basic variables x_1 and x_2.

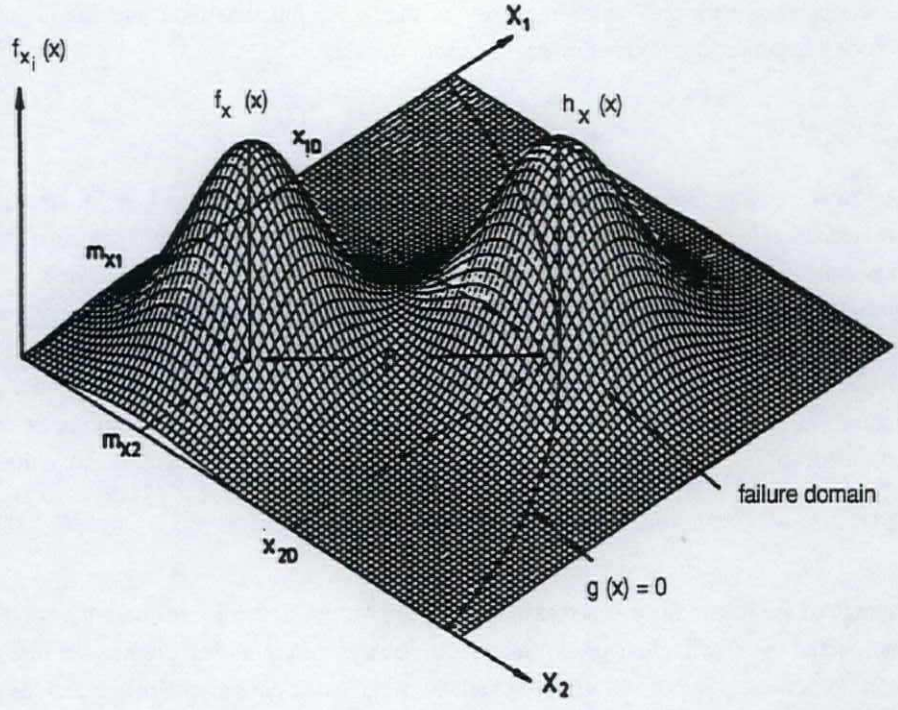

Figure 2.2 Schematic presentation of Important Sampling

Reference Units

When dealing with reliability analysis of structures, an appropriate acceptable safety (or reliability) level should be selected. This is referred to as a target reliability level. Required minimal reliability levels only make sense together with a specification of a reference period.

The reference period should reflect the nature of the failure and it is generally accepted that an annual target failure probability apply when human life is at stake, while lifetime target failure probabilities is a rational choice if the consequence is mainly material cost. The following reference periods are adopted:

- Temporary condition (installation, as-laid, testing, etc): the target failure probability should relate to the total time period relevant before the pipeline is commissioned.
- In-service conditions: annual period should be used for all limit states apart from the fatigue limit state where the lifetime period from the start of the installation process to the expiration of the pipeline design period should be used.

Installation is a temporary condition. The failure probability of a pipeline during laying could relate to the total time period relevant before the pipeline is commissioned. When doing the calibration of the design equations two circumstances have to be considered:

- During the design storm several pipeline elements pass the critical overbend and sagbend position, which implies a series system of pipe elements and including correlation between the elements. Hence, there is a relation between the time and space reference unit.
- Probability of failure for the laying period will depend on the weather window for the laying period and the load effect for the sea states.

The most relevant reference unit for lay operation is the actual period of laying operation. Then the effect of weather window can be taken into account. Herein, a three months summer season (June-August) is used as reference unit.

The probability of failure in the laying period will be

$$p_f = P[\bigcup_{Hs_i=1}^{Hs_{max}} \bigcup_{N_{Hs}=1}^{N_{Hs_i}} FOB \cup FSB] \tag{2.13}$$

where Hs_{max} is the maximum allowable significant wave height for operation, $N_{Hs,i}$ is the number of sea-states with significant wave height H_{Si} for the laying period. FOB is event describing failure at the overbend. These events and the analogous ones for the sagbend (FSB) may be expressed by

definition of the failure functions $g_{OB}(*)$ and $g_{SB}(*)$ by

$$\begin{aligned} FOB &= \bigcup_{i=1}^{N_{Es,i}} g_{OB}(\boldsymbol{x}_i) \le 0 \\ FSB &= \bigcup_{i=1}^{N_{Es,i}} g_{SB}(\boldsymbol{x}_i) \le 0 \end{aligned} \tag{2.14}$$

where $N_{E,si}$ is the number of elements passing overbend/sagbend during sea states (i).

Eq. 2.13 is first consider for one pipe element in $N_{Hs,i}$ sea-states of the same intensity (H_S) in the laying period. Then the effect of different sea-states (Hs) is assessed. Finally, the fact that a series of pipe elements will pass over the sagbend/overbend in a given sea-state is considered.

Consider then first Eq. 2.13 for the failure function g(x) given by an interaction between moment, tension and pressure, but when one of the components is dominant, the relation between resistance and load effect will be approximately linear. In this case, the probability of failure in N_{Hs} time periods with a sea-state intensity H_S may be expressed as

$$\begin{aligned} p_f &= P[\bigcup_{i=1}^{N_{Hs}} g(\boldsymbol{x}) \le 0] \\ &\approx P[(R-S_1 \le 0) \cup (R-S_2 \le 0) \cup \ .....] \\ &= 1-P[(R-S_1 \ge 0) \cap (R-S_2 \ge 0) \cap \ .....] \\ &= 1-\int_0^{\infty} P[(R-S_1 \ge 0 \,|R=r) \cap (R-S_2 \ge 0 \,|R=r) \cap \ .....]\, f_R(r)\, dr \end{aligned} \tag{2.15}$$

where R is resistance and S is load effect. For independent S_i and $r - S_i > 0 \Rightarrow S_i < r$ and $P[S_1 < r] \cdot P[S_2 < r] \cdot P[....]$, the probability of failure will be

$$\begin{aligned} p_f &= 1-\int_0^{\infty} F_{S_i}(r)^N\, f_R(r)\, dr \\ &= P[R-S^{max} \le 0] \\ \textit{where} \quad S^{max} &= \max_{N_{Hs_i}} [S_i] \end{aligned} \tag{2.16}$$

If the S_i is equal to a sum of a static (constant) and a dynamic load effect, the failure probability becomes

$$p_f = P[(R-(S_{static_1}+S_{dyn_1})\leq 0)\cup(R-(S_{static_2}+S_{dyn_2})\leq 0)\cup \ldots\ldots] = P[(R-(S_{static}+S_{dyn}{}^{max})\leq 0)] \quad (2.17)$$

Note, this super position is dependent of the level of the static load effect.

When all the allowable sea states for operation are considered and Eq. 2.16 is recognized, the probability of failure will be

$$p_{f\ layingperiod} = P\left[\bigcup_{Hs}^{Hs_{max}}\left[\bigcup_{i}^{N_{Hs_i}}[R-S_i\leq 0]\right]\right] \approx P\left[\bigcup_{Hs}^{Hs_{max}}[R-S_i^{max}\leq 0]\right] \quad (2.18)$$

when discrete values of H_S: H_{S1}= 1m, H_{S2}= 2m, H_{S3}= 3m, and $H_{S,max}$ are considered and $H_{S,max}$ is the maximum operational sea state, $N_{Hs,i}$ is the number of sea-states with significant wave height H_{Si} for the laying period. $N_{Hs,i}$ can be found from a scatter diagram, see Table 2.2.

Eq. 2.18 is a union of probability of failure for several sea states. The bounds for a union of events will be

$$P[F_i] < P[\bigcup_{i=1}^{N} F_i] \leq N\cdot P[F_i] \quad (2.19)$$

where the left hand side of the inequality is a system with full correlation between the failure elements F_i, while the right hand side of the inequality is a system without correlation between the elements.

So far, the failure of one pipe element has been considered. In reality, a number ($N_{Es,i}$) of pipe elements pass over the overbend/sagbend in a given sea-state of duration 3 hours. The failure probability will then be governed by the minimum of (R-S) for the series system in time and space, recognizing that R varies from element to element and S_E varies over time and, hence from element to element. A conservative approach would then be to take

$$\min(R-S) = R^{\min} - S^{\max} \quad (2.20)$$

Rather, due to the high correlation of relevant resistance variables and the static loading between elements, the following approximation is used in the present work

$$\min_{elements_i}(R-S) \approx R_i - S^{\max} \quad (2.21)$$

where R_i is the resistance of a single element.

In summary, the probability of failure will be

$$P_f \approx \max_{Hs_i \le Hs_{max}} P[R-(S_{F_i}+S_{E_i}^{max})\le 0] \tag{2.22}$$

where R is calculated using random values for the resistance and an extreme value is used for S^{max}.

When considering the entire laying period all relevant sea state conditions for the laying operation have to be considered. The load effect is divided in two parts, functional and environmental load effects; $S_j = S_{Fj} + S_{Ej}$. S_{Fj} will be constant for all the H_S in the laying period while the environmental load effect, S_{Ej} will vary over time and is dependent of the distribution of the maximum load effect. For the dynamic load effect, the expected largest maximum of N independent Weibull distributed maxima is given by

$$\mu_{max}{}^{W} = \mu + \alpha\left([\ln N]^{\frac{1}{\lambda}} + \frac{0.5772}{\lambda}[\ln N]^{\frac{1-\lambda}{\lambda}} \right) \tag{2.23}$$

where μ, α and λ are location, scale and shape factor for the Weibull distribution. A simplification can be used for a narrow banded Gaussian process where the mean value for the process is zero and the maximum follow a Rayleigh distribution, as :

$$\mu_{max}{}^{R} = \sigma\left[\sqrt{2\ln N} + \frac{0.5772}{\sqrt{2\ln N}}\right] \tag{2.24}$$

where σ is the standard deviation of the process.

For the entire period the dynamic load effect (S_{Ej}) will be scaled (k_j) using the number of H_S for the laying period and for instance Eq. 2.23 and Eq. 2.24 for the expected maximum load effect.

$$k_j = \frac{E[S_{E_j}(N_{Hs_i} \cdot N_{max}^{3hours})]}{E[S_{E_j}(N_{max}^{3hours})]} \tag{2.25}$$

By considering for instance the scaling constant k_j for different occurrences of H_S for the laying period, k_j is shown in Table 2.1. The number of maximum response for three hour is 1300, using an average upcrossing period (T_Z) equal to 8.3 sec. $N_{Hs,i}$ is found from scatter diagram in Table 2.2.

Table 2.1 Scaling factor for maximum dynamic response for a laying period

Hs (m)	N_{Hsi}	Weibull, Eq. 2.23 shape factor			Rayleigh Eq. 2.24
		1.4	1.6	1.8	
1	267	1.473	1.403	1.351	1.324
2	298	1.482	1.411	1.358	1.330
3	130	1.416	1.356	1.310	1.287
4	31	1.296	1.255	1.224	1.207

Table 2.2 Scatter diagram for 6 hourly sea states defined by significant wave height, H_s and the spectral peak period.
Summer condition (June-August), the data represent the distribution of sea states for the North Sea during a 39 year period

Hs (m)	Spectral peak period (s)																	Sum
	1	2	3	4	5	6	7	8	9	10	11	12	13	14	15	16	17	18	
1	13	26	63	207	628	692	1137	854	788	461	216	100	17	10	2	1		1	5212
2					17	266	1253	1626	1149	683	470	254	75	19					5816
3							87	573	826	504	267	184	64	20	6	1	1	1	2534
4								11	166	172	137	70	17	18	11	1			603
5									2	43	38	35	11	1	1				131
6											13	10	7	6					36
7											1	5	4	5	1				16
8												2	1						3
9														1					1
Sum	13	26	63	207	645	958	2477	3064	2931	1863	1142	660	196	80	21	3	1	2	14352

2.2.4 Target reliability levels

When dealing with reliability analysis of structures, an appropriate acceptable safety (or reliability) level should be selected. This is referred to as a target reliability level. Required minimal reliability levels only make sense together with a specification of a reference period.

Target Safety Level

Target safety levels for offshore pipelines are determined on the basis of consequences of failure, offshore pipeline failure data, and implied safety levels in acceptable codes. More specifically, target safety levels should depend upon

- consequences of failure, e.g. the risk of human safety, environmental damage and economic consequences
- pipeline location, i.e., near or off platform
- pipeline content, i.e., oil or gas
- pipeline conditions, i.e., in-service, non-operation or installation
- nature of failure e.g. pipeline limit state, SLS, FLS, ULS or PLS; and type of limit state within these classes

In addition the target level should depend on reliability approach which is applied.

The evaluation of the consequence of failure comprises an evaluation with regard to human injury, environmental impact, economical loss and company or industry reputation. The target failure probability may be established by

- Calculating the inherent failure probability (p_f) in existing code(s), and choosing the target as the mean or any other characteristic values of the inherent p_f-based on the uncertainties known at the time when the existing code was established.
- Relating the target p_f for pipelines to the target level for similar structures.
- Comparing the target p_f with experienced accident/failure rates.

It should be observed that structural reliability deals with normal uncertainties in loads and resistances and is applied to calculate failure probability relating to the component failure modes (SLS, ULS, FLS).

Implied target level in the acceptable codes

The reliability based calibration of codes for pipelines and other structures should be centred around current design. This means that existing codes should be the basis for improving the code, e.g. by

harmonizing the reliability level in the codes. The implied reliability level in existing codes then represents a reference reliability level. However, it is reasonable to establish this reference target level by using usage factors, and uncertainty measures existing at the time the current code was introduced. Centring the reliability based calibration of ULS, FLS and SLS criteria around current design also means that the failure probability (reliability) should primarily be referred to each joint; not the system.

Some initial calculations of implied failure probabilities of existing codes have been made for local buckling according to BS 8010 (1993). The implied probability of buckling and collapse due to pressure, tension and bending is determined using uncertainties associated with the pipeline technology applied when current criteria were introduced. The interaction is relevant for pipeline during laying in load controlled condition. The load levels for bending moment, pressure and axial tension vary in the range 0.55-0.89, 0.1-0.4 and 0.1-0.4, respectively. The interaction pressure-tension-bending is normalized, Eq. 2.26, and important sampling is used for calculating the probability of failure.

$$g(x) = 1.0 - \left(\frac{X_M \cdot ((1. - q_p)^{(1+300\,t/D)^{-1}} - q_T)}{X_{Mco}} + \frac{X_T \cdot q_T}{X_{Tco}} \right)^{(1+300\,t/D)} - \frac{X_p \cdot q_p}{X_{Pco}} \qquad (2.26)$$

Uncertainty measures for the buckling limit state are given in Table 2.3

Table 2.3 Uncertainty measures for local buckling limit state

			Old Technology		New Technology	
Variable		Distribution	Bias	CoV (%)	Bias	CoV (%)
X_t	t/t_{nom}	LogNormal	1.01	6.8	1.04	2
X_σ	σ/SMYS	LogNormal	1.14	8	1.08	4
X_{Mco}	$M_{co}/M_{co,c}$	$X_t X_\sigma$				
X_{Tco}	$T_{co}/T_{co,c}$	X_σ				
X_{Pco}	$P_{co}/P_{co,c}$	Normal	1.1	10	1.1	10
X_M	M/M_c	Normal	1.0	5	1.0	5
X_T	T/T_c	Normal	1.04	4	1.04	4
X_P	P/P_c	Normal	1.0	3	1.0	3

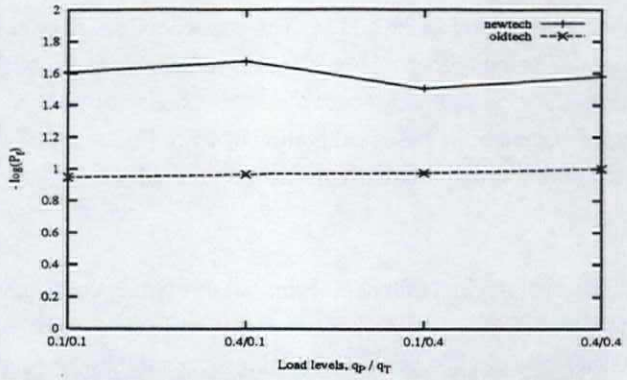

Figure 2.3 Probability of failure for different loadlevels, new and old technology

Figure 2.3 presents the reliability results implied by the past and the new technology. It is seen that the failure probability is in the order of 10^{-1} to 10^{-2} per elements. The load levels for pressure (q_p) and axial load (q_T) vary in the range 0.1 to 0.4. Taken into account the effect of union of elements and corresponding correlation and the consider the laying process as a return period, the target level in order of 10^{-2} will be reasonable but on the restrictive side.

Similar initial calculations of implied failure probabilities of existing codes have been made in the SUPERB project, Jiao and Moan (1994). Existing codes only have explicit design criteria for yielding. Hence, the implied probability of hoop yielding due to pressure containment is determined using uncertainties associated with the pipeline technology applied when current yield criteria were introduced. The annual probabilities corresponding to utilization factors of 0.72 and 0.60 are approximately 10^{-4} and 10^{-7}, respectively. Yielding of a strain hardening material is not necessarily an ultimate limit state, i.e. between SLS and ULS. The implied failure probability may, hence, be considered to be somewhere between SLS and ULS.

For the combined load combination, a von Mises equivalent stress design check typically applies in most codes to control yielding. The new ISO-96 draft code for pipelines allow a stress level of 1.0 SMYS for construction and 0.90 SMYS for operation. The implied probability of exceeding the yielding point in this case is in the order of $P_f = 10^{-1}$ to 10^{-2} dependent on the actual load combination, Mørk et al (1997).

For temporary conditions a low safety level (10^{-1}-10^{-2}) is acceptable for yielding while a higher safety level (10^{-2}-10^{-3}) is required for operational conditions.

Explicit safety level in acceptable codes

Certain target safety levels for civil and offshore structures have been well defined, specified or recommended by relevant authorities or institutions. These existing safety levels may constitute a basis for determining rational target safety levels for offshore pipelines.

For design of components in civil engineering structures, the target failure probability for the serviceability limit state is of the order 10^{-1} to 10^{-2}. The target failure probability for ULS is in the range of 10^{-3} to 10^{-7} per year, NKB (1978). DnV (1992) recommends the range 10^{-3} to 10^{-6} for structures which can not be compared with existing and well established structures. With reference to offshore platforms, CSA (1987) specified the target annual probability from 10^{-1} to 10^{-5}. This range is in good agreement with implied safety levels in NPD (1990) as shown in Moan (1988).

Hence, the existing target annual failure probability for ULS is found in the range of 10^{-3} to 10^{-7}, depending upon the consequences of failure.

Failure data

Experienced failure rate should be considered when setting target safety levels for pipelines. The main causes of offshore pipeline failure are due to material fault or construction, external damage or mechanical failure of ancillary equipment. The failure causes depend on location, pipeline size, content, pipe age and preventional work.

The experienced pipeline accident rate for the safety zone and midline regions is 10^{-3} and 10^{-4} per km per year, respectively, Robertson et al (1995), and are primarily due to gross fabrication and operational errors. The target level for ULS is normally taken to be 1-10% of the experienced accident/failure rate.

To summarize, a range of recommended target failure probability level as a function of the limit state category, pipeline condition and failure class is given in Table 2.4, Sotberg et al (1997). Note, the target level is valid when using the same reliability method as Sotberg et al (1997).

Table 2.4 Target failure probabilities

Limit State Category	Temporary Conditions[1)] Low Safety Class	In-Service Conditions[2)]	
		Off Platform zone, Normal Safety Class	Near Platform zone, High Safety Class
SLS	10^{-1}- 10^{-2}	10^{-2}- 10^{-3}	10^{-2}- 10^{-3}
ULS	10^{-2}- 10^{-3}	10^{-3}- 10^{-4}	10^{-4}- 10^{-5}

1) unit: per relevant period per element for all limit states.
2) unit: per year for SLS, ULS. The target probabilities given in the table for SLS/ULS apply per element for instance if all elements in a 1 km pipeline are fully correlated.

The target probability level for some limit states may be higher than the generic level given for SLS, ULS, FLS and PLS in Table 2.4. For SLS, the target levels recommended in the Table may be on the restrictive side. The difference between target safety levels for the near platform zone and those for the off platform zone may be further increased to reflect considerably different consequences of failure.

It is well known that the failure probability is sensitive to the assumption of distributions of loads and resistances. A target level can only be rationally defined when the reliability method, including probabilistic models for loads and resistances, are defined. The target levels given up to now, and partially quoted above, have not been properly referred to a given reliability methodology.

2.2.5 Calculation of failure probability

The failure probability may be calculated by analytical methods or simulation techniques. Further, for more complex limit state functions a response surface technique may be applied to establish the link between e.g. the deterministic structural analysis and the reliability calculations. Herein, a combination of design point calculation and important sampling procedure is used when calculating the probability of failure.

2.2.6 Evaluation of the results

An evaluation of the reliability analysis must be performed in order to assure that the design point is reasonable and the target failure probability level is not exceeded.

Design Point.

The main purpose of a post-evaluation of the reliability analysis is to evaluate whether the design point is reasonable, based on engineering judgment and experience from similar types of problems and that it is not in conflict with obvious physical knowledge or limitations. First, it has to be checked that the obtained design point from the reliability analysis is a global solution to the optimization problem that is considered and not a local minimum. Further, the results from the reliability analysis also have to be assessed by verifying that the design point coordinates corresponds to physically realizable outcomes of the stochastic variables. If a response surface technique is applied it must be verified that the response surface performs satisfactorily in the neighbourhood of the design point.

An important result of reliability calculations is information about the sensitivity of the design point and hence the reliability to variations of parameters or changes in the stochastic behaviour of the variables. This information can be used as a decision tool by providing measures of where to most efficiently allocate resources to increase the reliability of the pipeline. Also the reliability of a modified design can in some cases be determined without any re-analysis.

The *parametric sensitivity factor* is defined as $\partial\beta/\partial\theta$, where θ may be a parameter in the limit state function or a parameter of the distributions of the basic variables. It follows that the updated reliability caused by a change $\Delta\theta$ in the parameter θ can be approximated by

$$\beta(\theta + \Delta\theta) \approx \beta(\theta) + \frac{\partial\beta(\theta)}{\partial\theta}\Delta\theta \qquad (2.27)$$

The *importance factor* which can be interpreted as a relative measure of the significance of the uncertainty of a basic variable (or a group of variables) for the problem considered.
Let α_i, Eq. 2.9, denote the *i*th component of the normalized gradient vector to the failure surface in the design point, then the quantity α_i^2 is denoted as *importance factor*. The importance factors can then be applied to focus attention on the most important variables.

Probabilistic design check

The reliability analysis can be used to verify that such a target reliability is achieved for a structural element or the entire pipeline. The probabilistic design check can be performed using the following design format

$$P_{f,calculated} \leq P_{f,target} \qquad (2.28)$$

where $P_{f,calculated}$ is the calculated probability of failure from the reliability analysis and $P_{f,target}$ is a target value that should be fulfilled for a design to be accepted. It should be noted that a requirement of Eq. 2.28 is only relevant if the underlying probabilistic modelling are equivalent. Required minimal reliability levels only make sense together with a specification of a reference period.

2.3 Load and Resistance Factor Design

2.3.1 General

In the present section emphasis will be on reliability based calibration of partial coefficients in design equations for a specific failure mode. The process of an entire code calibration in which a code may be calibrated by a formal process of explicit optimization is only briefly considered.

With a reliability method available, a set of partial safety factors (or safety coefficients) can be determined which will result in designs with a prescribed target reliability. In general, the first step

is to estimate the reliability of a set of initial designs. Then the designs are modified and the reliability calculation is repeated until the target reliability is met. Based on the relationships between the characteristic values of the design variables and the corresponding values in the design point, a set of calibrated partial safety factors for a given failure mode may be obtained.

2.3.2 Design equation

The objective is to establish a simple and practical design format capable of providing a uniform reliability level for a large parameter variation and wide range of design scenarios. The selected design equation should preferably resemble the impact of the most important variables in the limit state function. A general design equation may be given as, cf. ISO (1995)

$$g(\boldsymbol{S}_d, \boldsymbol{R}_d, \boldsymbol{a}_d, \boldsymbol{\Theta}_d, \boldsymbol{C}, \delta) \geq 0 \tag{2.29}$$

where

- $\mathbf{S}_d$ is a vector of design load values determined from $S_{d,i} = S_{c,i}\,\gamma_{s,i}$. Index c indicates a characteristic value, index d indicates a design value and $\gamma_{s,i}$ is the partial safety factor related to load component number i.
- $\mathbf{R}_d$ is a vector of design capacities determined from $R_{d,i} = R_{c,i}/\gamma_{R,i}$ where $\gamma_{R,i}$ is the partial safety factor related to the capacity or strength component number i.
- $\mathbf{a}_d$ is a vector of design values of geometrical quantities determined from $a_{d,i} = a_{c,i} \pm \Delta a_i$ where Δa_i are additive geometrical quantities.
- $\boldsymbol{\Theta}_d$ is a vector of design values of the model uncertainties not implemented in the load and capacity variables.
- $\mathbf{C}$ is a vector of serviceability constraints, e.g. damage detectability demands.
- δ is a vector of coefficients accounting for the importance of the pipeline or pipeline element, i.e accounting for the reliability level required e.g related to a given safety zone.

Normally a Load and Resistance Factored Design (LRFD) format can be utilized in the form

$$\gamma_E S_{C_E} + \gamma_F S_{C_F} \leq \frac{R_c}{\gamma_R} \tag{2.30}$$

where S_C is the characteristic load effect with subscript E and F referring to the environmental and functional load respectively. R_C is the characteristic resistance or material property for the considered failure mode and γ_E, γ_F and γ_R are calibrated safety factors. In some cases it may be convenient to further distinguish between environmental loads arising from different load phenomena or between loads with different magnitude and frequency content.

2.3.3 Characteristic values

The characteristic values are reference values to be used in the design process. In general, a characteristic value should be specified as a quantile of the respective probability distribution, or equivalently as a value with a prescribed probability of being exceeded, DNVC (1992). In case of time dependent material properties or for environmental conditions where the load effect causes alteration to the material leading to a reduction in the structural safety over time, the characteristic values used for design must include such alterations and degradations.

Material and Capacity Variables

Characteristic structural resistance is to be determined on the basis of reliable data and appropriate statistical techniques based on recognized methods for testing.

For *steel* the characteristic value of strength (or resistance) is normally to be based on the 5th or the 95th percentile of the test result, whichever is the most unfavourable. The characteristic fatigue strength (or resistance) is normally to be based on the 2.5th percentile of the test results. The data set should if possible be confined to a specific mill or as a second choice be estimated from relevant mills with comparable production quality levels.

The characteristic properties of soil are to be determined for all deposits of importance. The characteristic properties of the different deposits are normally to be taken as conservatively assessed mean values based on the results from in-situ tests and laboratory tests. Further, stiffness properties should refer to mean values.

Load and Load Effect Variables

The characteristic values for load and load effect variables are normally to be determined as a load which causes load effects with a given probability of being exceeded. For time dependent load processes, characteristic values are to be given in the terms of return period values. For loads without a statistical representation, the characteristic value is the specified value which will define operational limitations for the pipeline.

The characteristic value of a *permanent load* is normally taken as the expected value. E.g. weight and residual lay tension.

The characteristic value of a *constant functional load* is the expected value of the load effect, e.g static load effect during lay operations. In the case of *a variable functional load* is the maximum (or minimum) specified value which produces the most unfavourable load effect in the pipeline element under consideration. Operational (difference-) pressure and temperature loads and shut-

down induced loads are examples belonging to this category.

The characteristic value of an *environmental load* or *load effect* is normally the maximum or minimum value (whichever is the most unfavourable) corresponding to a load effect with a prescribed probability of exceedance, or taken as the most probable extreme value, with a specified return period. For a pipeline under operation a 100 year return period (annual exceedance probability of 10^{-2}) is often applied. For temporary design conditions, the characteristic values may be based on specified values, where the probability of exceedance is according to season and the duration of the installation period.

The characteristic value of an *accidental load* is selected on the basis of a prescribed annual probability of being exceeded. This annual probability is taken to be equal to, or less than 10^{-4} unless some other probability of accedence can be justified.

Load Combinations

Load combinations of time dependent load effects must be considered both in the probabilistic modelling and in the design equation format. The following issues should be noted:

- The load effect shall be combined so that they produce the most unfavourable condition on the pipeline for the failure mode considered (e.g. the combination of functional and environmental load).
- Linear load combination may be simplified by a Turkstra approach, (Madsen et al., 1986)
- Load effects that are mutually exclusive should not enter together in the same combination.
- The effect of reduced likelihood for simultaneous occurrence of individual load effects may be accounted for by a reduction factor, Ψ_0, ref. (ISO,1995).

2.3.4 Calibration of partial safety factors

The partial safety factors in a Load and Resistance Factored Design (LRFD) (or Partial Factor Design, (ISO,1995)) equation, Eq. 2.30, may be calculated including the following items:

- Definition of the *scope* for the calibration comprising a definition of failure mode(s), type of pipeline, condition, content and location.
- Specification of *validity* range and *physical limitations* for the basic variables and scenarios.
- Establishment of a *design equation.*
- Specification of *characteristic values* for the variables, specified according to a detailed recipe.
- Estimation of a *trial set of partial safety factors* reflecting the most important uncertainty sources as determined by the reliability analysis.
- Establish a *set of representative design* cases utilizing the design equation with characteristic

values and partial safety factors in compliance with the scope.

- Estimate the *probability of failure* for the design cases from a Level III reliability analysis and evaluate against the target value.
- Select final partial safety factors associated to the *most "critical" test design* which in general is a conservative approach.

2.4 Response surfaces

2.4.1 General

The roots of response surface methodology (RSM) can be traced back to works in the early 1930s or beyond, however, it was not until 1951 that RSM was formally developed by G E P Box and K B Wilson, (Khuri and Cornell, 1987). RSM is a set of techniques that encompasses:

- Setting up a series of experiments that will yield adequate and reliable measurements of the response of interest.
- Determining a mathematical model that best fits the data collected from the design, by conducting appropriate tests of hypotheses concerning the model's parameter.
- Determining the optimal settings of the experimental factors that produce the maximum (or minimum) value of the response.

Various methods and techniques are used for modelling response surfaces, see e.g. Myers (1976), Khuri and Cornell (1987). The polynomial representation of a response surface is frequently used and is the similarity to the regression analysis of experiments. Polynomial models includes first-order and second-order response surface depending on the degree of the factors including in the mathematical model. A practical model, here called multiplicative model, consists of a central point and complementary experiments where one only of the parameters has been given a value different from the nominal one. For each variable, one may choose to have one or more complementary experiments.

Response surfaces are introduced in the reliability assessment in order to have an efficient and accurate prediction of load effects. The response surface forms an n-dimensional space in which Monte Carlo and Important Sampling simulation can be performed to obtain load effects using interpolation/extrapolation. It is important that the response surface provides an accurate prediction of the response in the neighbourhood of the design point, Bucher and Bourgund (1990).

The points which define the response surface are characteristic load effect values obtained for variations in the uncertain parameters. The procedure used to determine these values is described subsequently, where yield strength, mass, stinger stiffness, RAO and peak period will employ in the response surfaces. First-order, second-order polynomial models and multiplicative models are

described in the present context.

2.4.2 Response surface models

Multiplicative model

For a given set of response calculations, the response may be expressed as a function of various parameters of the structure and its loading. Various interpolation models can be chosen to build the response surface. The choice of this model depends on the shape of the experiment point set. An economical set of experiments consists of a central point (nominal case) and complementary experiments where one only of the parameters has been given a value different from the nominal one. For each variable, one may choose to have one or more complementary experiments. The obvious advantage of such an experiment set is to avoid the combinatory explosion that will occur as the number of parameters is taken larger.

For the multiplicative model the interpolation is taken in two steps. First interpolation is done for each parameter alone: $r_i = f(x_i)$. For this purpose, any interpolation method f(x) can be considered, as for example linear by interval interpolation, Lagrange polynomials or splines. Herein a linear interval interpolation is used $r_i = c_i\ (x_i - x_{i0})$, where c_i is found from the nominal case and the complimentary experiment. x_i (i = 1..m) is a set of parameter value for which an interpolation of the experimental result, r, is to be calculated and x_{i0} (i = 1..m) is the parameters for the nominal case. The vector for the central point is denoted by $\mathbf{x}^0$ and the corresponding result is denoted r^0. r^0 will be in the neighbourhood of the design point . Note that for all i: $r^0 = f(x_{i0})$.

The second step is combining the results from the one dimensional interpolations, to define a complete interpolation of the experiment set (the response surface). The multiplicative combination is expressed by :

$$r = r(x_{i0}) \prod_{i=1}^{m} \left(\frac{c_i \cdot (x_i - x_{i0})}{r(x_{i0})} \right) \qquad = r^0 \prod_{i=1}^{m} \left(\frac{r_i}{r^0} \right) \tag{2.31}$$

This method is preferred to a linear combination because the effect of each parameter on the result is multiplied with the effect of other parameters. An immediate observation however, is that such a response surface is not invariant for a shift of the zero of the results. Preferably, the points defining the response surface should represent 2-3 standard deviations (supplements and reductions) in the parameters in order to avoid extrapolation. To establish the multiplicative model (1+2*m) experiments is needed.

Polynomial models

When the combination of two or several parameters are taken into account the term response surface arise, since the set of points (r, **X**) define a hyper-surface in (m+1)-dimensional space. The hyper-surface may be modelled as a plane or higher order polynomials. The hyper-surface is made in the neighbourhood of the design point.

A set of experiments where the parameters have been given values from sampling of the uncertainty in accordance with the statistical properties for each parameter is the basis for modelling the hyper-surface.

Let x_i (i = 1..m) be a set of parameter value for which the response r, is to be calculated. The response r is here calculated in three ways, using a plane, a polynomial without interaction between the parameters and a polynomial including this interaction.

The simplest is a plane :

$$r = A_0 + A_1 \cdot x_1 + A_2 \cdot x_2 + A_3 \cdot x_3 + A_4 \cdot x_4 + A_5 \cdot x_5 \tag{2.32}$$

where r is the response surface results, A_0 is the coefficient of zeroth order and A_i are the first order coefficients. The plane model requires (m+1) experiments for estimating the coefficients.

Weighted sum of polynomials will take the nonlinear effect into account when the load effect is nonlinear for different parameters. There is defined two polynomials of second order here, first the response r is found by a polynomial without interaction between the variables:

$$r = B_0 + B_1 \cdot x_1 + B_2 \cdot x_2 + B_3 \cdot x_3 + B_4 \cdot x_4 + B_5 \cdot x_5 + B_6 \cdot x_1^2 + B_7 \cdot x_2^2 + B_8 \cdot x_3^2 + B_9 \cdot x_4^2 + B_{10} \cdot x_5^2 \tag{2.33}$$

where B_0 is the coefficient of zeroth order and B_i (i = 1-5) are the first order coefficients and B_j (j = 6-10) are the second order coefficients. The required number of experiments is (1+2*m) for the polynomial model without interaction.

Next the response r is found by a response surface that contains the interaction between the parameters as:

$$\begin{aligned} r = {} & C_0 + C_1 \cdot x_1 + C_2 \cdot x_2 + C_3 \cdot x_3 + C_4 \cdot x_4 + C_5 \cdot x_5 \\ & + C_6 \cdot x_1 \cdot x_1 + C_7 \cdot x_1 \cdot x_2 + C_8 \cdot x_1 \cdot x_3 + C_9 \cdot x_1 \cdot x_4 + C_{10} \cdot x_1 \cdot x_5 \\ & + C_{11} \cdot x_2 \cdot x_2 + C_{12} \cdot x_2 \cdot x_3 + C_{13} \cdot x_2 \cdot x_4 + C_{14} \cdot x_2 \cdot x_5 + C_{15} \cdot x_3 \cdot x_3 \\ & + C_{16} \cdot x_3 \cdot x_4 + C_{17} \cdot x_3 \cdot x_5 + C_{18} \cdot x_4 \cdot x_4 + C_{19} \cdot x_4 \cdot x_5 + C_{20} \cdot x_5 \cdot x_5 \end{aligned} \tag{2.34}$$

where in this case C_0 is the coefficient of zeroth order and C_i (i = 1-5) are the first order coefficients and C_j (j = 6-20) are the second order coefficients. When a polynomial model including interaction between the variables is used, the number of required experiments is (1+m+m*(m+1)/2).

The coefficients C_i, i = 0,1,2...N_c in Eq. 2.32 - Eq. 2.34, are calculated based on least square fit from experimental data. $\mathbf{C}^* = \mathbf{X}^{-1}\mathbf{L}$, where $\mathbf{C}^*$ includes C_0 and C_i, i=1,2. $\mathbf{X}$ is a $N \cdot N_c$ matrix where X_i, i=1,2...N_c, contains the values of the variables or interaction between variables. $\mathbf{L}$ is the load effect vector, where L_i, i=1,2....N, is the load effect for the set of experiment , $N>N_c$. N is the number of experiments and N_c is the number of coefficients.

2.5 Load combinations

A pipeline during laying will experience a load combination, e.g. pressure-tension-bending, bending-tension. During the laying process, a cross section of the pipe will experience a time history for moment, tension and pressure. The maxima and extreme response of the load effect quantities have marginal distributions but may be correlated. The combination of the load effects is an interaction between two or three response quantities. In the present context the combination of the maxima response will be discussed for the situation where one of the response quantities is dominant.

The most important load combination issue during laying is bending and tension. The combination pressure-tension-bending is not of interest since the pressure for practical purposes is considered as deterministic at a specified location of the pipeline. The load-combination is given as a nonlinear interaction of the load-combination, Eq. 3.21 or Eq. 3.23.

The simplest method to treat linear combination of loads modelled as stochastic process is, e.g. Ferry-Borges method, Ferry-Borges and Castenheta (1971) or deterministic process, e.g. Turkstra's rule, Turkstra (1970).

Turkstra's rule, Turkstra (1970), states that the maximum value of the sum of two independent random processes occurs when one of the processes has its maximum, that is

$$Y_{max} = \max\left[(maxY_1 + Y_2^*);(Y_1^* + maxY_2)\right] \tag{2.35}$$

in which Y_j^* is the-arbitrary-point-in-time value of Y_j . Typically, Y_j^* is taken as the mean value of Y_j. Although a simple and convenient rule for code calibration and sometime for other situations, Turkstra's rule may be a lower bound solution to load combination, and thus somewhat underestimate the maximum value, Melchers (1987).

For load effects that are uncorrelated and independent the same philosophy as Turkstra's rule, can

be used when one of the load effect is more significant than the other one. The error will be small when one of the load effect components is dominant.

Sagbend

The combination of pressure-tension-bending will occur at sagbend. The maximum bending moment will be located not far from the touchdown point for the pipeline. Where maximum bending moment is located the pressure will be approximately constant and equal to $\rho \cdot g \cdot z$, where ρ is the density of water, g is the gravity and z is the water depth.

Figure 2.4 shows the correlation between bending moment and tension for sagbend. The correlation seems to have a small negative trend. Assuming independence and in according to Turkstra's rule, the load combination max $[M/M_{co}]$ together with $E[\ T/T_{co}\ ]$ together with $E[\ P/P_{co}\ ]$ is the most severe situation. The max $[M/M_{co}]$ will dominate over $E[\ T/T_{co}]$ (about 0.01) in Eq 3.21. Therefore T/T_{co} and P/P_{co} are considered as deterministic, with a characteristic tension and pressure load effect equal to the mean value, in the present application.

Overbend

A combination of tension and bending moment is the most severe situation at the stinger. Figure 2.5 show no correlation between tension and bending curvature. According to Turkstra's rule, the load combination max $[\ \kappa/\kappa_{co}\ ]$ together with $E[\ T/T_{co}\ ]$ will dominate this situation. The max $[\kappa/\kappa_{co}]$ will dominate $E[\ T/T_{co}\ ]$(about 0.05) in Eq. 3.23. Therefore T/T_{co} is considered as deterministic with a characteristic value equal to the mean value, in the present application.

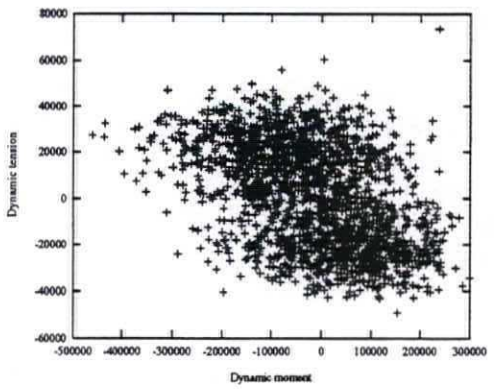

Figure 2.4 Correlation between moment and tension, sagbend

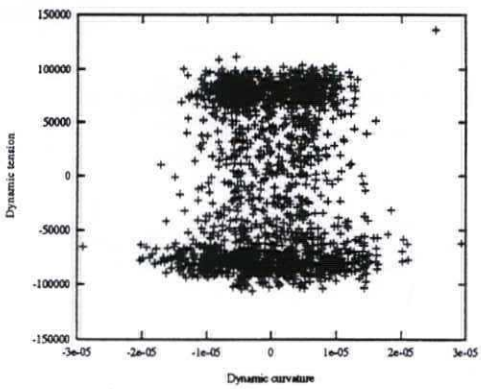

Figure 2.5 Correlation between curvature and tension, overbend

2.6 Extreme response

The entire laying process is laying of pipelines under different sea state conditions and will take 1-3 months. Time domain simulations are made for the laying process, where the maximum response are found for extreme sea state of a 3 hour period. This mean that the response is taken from the tail of a maximum distribution and a extreme value distribution has to be considered when using the response in reliability analysis.

A marine structure will in general be influenced by many types of nonlinearities, e.g. wave load, material properties. The wave loads on sender structures as pipeline, are usually calculated by the Morison's equation, where the drag term gives the most contribution to the non-linearity. However, the most important contribution to the non-linearity is the non-linear material property. The extreme response distribution has to be selected in a way that take care of the non-linearity that affect the pipeline response.

The extreme value distribution will be outlined in the subsequent section on the basis of a maxima distribution for a short term response history. A short-term response distribution will describe the situation for a 3-6 hour period. Several authors have described relevant distributions for fitting responses of nonlinear phenomena, Farnes (1990), Sødahl (1991). A short summary will be outlined here.

It is difficult to find an analytical distribution function for the non-linearity but it will be to choose a known model distribution that have a reasonable shape in the region that is of importance to the analysis. For extreme response distribution is the tail the most important region. Empirical methods are used for determination of response distributions. Distributions used for empirical fit to a sample need to have sufficient number of parameters to be flexible.

First it is noted that the best results are obtained by using only global maxima, i.e. largest maxima between zero crossings, Figure 2.6, in the sample statistics, Farnes and Moan(1993).

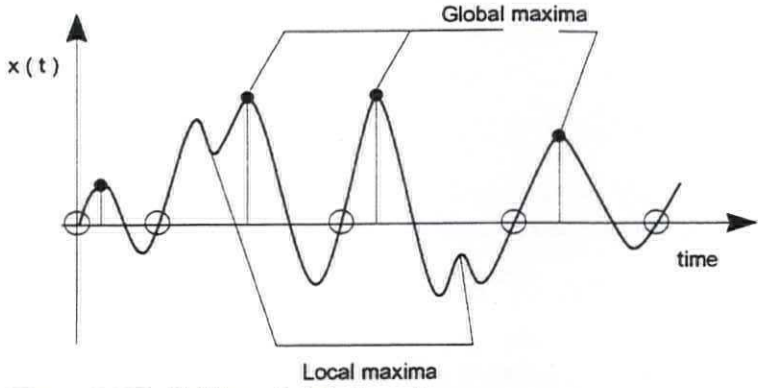

Figure 2.6 Definition of global maxima.

The Weibull, Gaussian, Rayleigh and Log-normal distributions are commonly used for modelling the distribution of individual response maxima. These distributions are examples of initial distributions with an exponentially decaying tail.

As an example for pipe laying a time series of response from the time-domain simulations are analysed and the statistical properties of the response maxima series are established. Two methods of point estimation that are popular among statisticans are the maximum likelihood method and the method of moment. In contrast to the method of moments, the maximum likelihood method provides a procedure for deriving the point estimator of the parameter directly. Based on experience, fitting of statistical moments is recommended. The sample distribution for the maxima series is found to give a good fit to the Weibull distribution, see Figure 2.7.

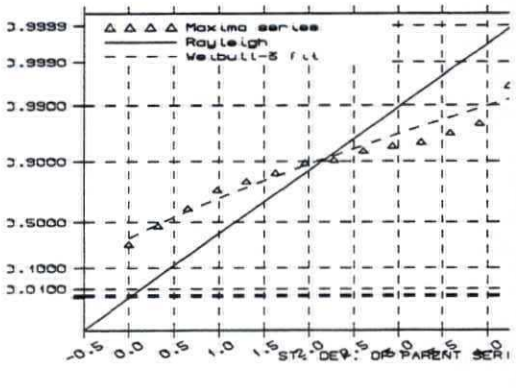

Figure 2.7 Comparison between maximum response and maximum distribution

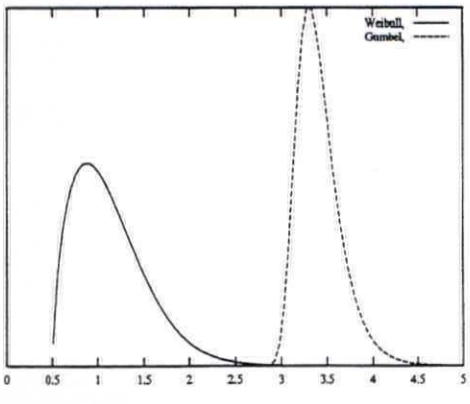

Figure 2.8 Weibull and Gumbel distribution

The exact extreme value distribution

The extreme value is defined as the largest of N individual maxima, expressed as :

$$X_e = \max\ (X_m^{\,1},\ X_m^{\,2},\ldots\ldots,\ X_m^{\,N}) \tag{2.36}$$

The exact extreme value distribution of N independent, identically distributed maxima is given by:

$$F_{x_e}(x_e) = \left[F_{x_m}(x_e)\right]^N \tag{2.37}$$

where F_{Xe} is the extreme value distribution and F_{Xm} is the maxima distribution (initial distribution).

The exact extreme value distribution will converge asymptotically to one of three limiting forms as m trends to infinity depending on the tail behaviour of the initial distribution. The limiting forms are commonly classified as type I, II and III asymptotic forms (Gumbel 1958).

The type I asymptotic form arises from initial distributions with an exponentially decaying tail. An exponentially decaying tail is the form $e^{-a(x)}$ where a(x) is an increasing function of x. The type I asymptotic form, also called the Gumbel distribution, which is given by :

$$F_{x_e}(x_e) = e^{-e^{-\alpha_e(x_e - u_e)}} \tag{2.38}$$

where u_e and α_e are location and scale parameters, respectively.

The Gumbel distribution will be the asymptotic extreme value distribution for largest individual response maximum. The location and scale parameters in the Gumbel distribution are found from the initial distribution by the following relations :

$$F_{X_m}(u_e) = 1 - \frac{1}{N} \tag{2.39}$$

$$\alpha_e = N f_{X_m}(u_e) \tag{2.40}$$

The Gumbel parameters follow from Eq. 2.39 and Eq. 2.40 :

$$u_e = u + \alpha[\ln(N)]^{\frac{1}{\lambda}} \tag{2.41}$$

$$\alpha_e = \frac{\lambda}{\alpha}[\ln(N)]^{\frac{\lambda-1}{\lambda}} \tag{2.42}$$

Where u, α and λ are location, scaling and shape parameters for Weibull distribution, the corresponding mean value and standard deviation for the extreme values can be outlined from the same Weibull parameters. As an example Figure 2.8 show the Weibull distribution using m =10000, u= 0.5, α = 0.7 and λ =1.6 and the corresponding Gumbel distribution based on the these parameters.

For description of the type II and III limiting forms, confer Gumbel (1958) and Ang and Tang (1984). It can be shown that the same connections between initial distributions and asymptotic forms hold for correlated stochastic variables provided that the correlation is "not too strong" (Leadbetter et. al. 1983).

3 CAPACITY OF TUBES UNDER COMBINED LOADS

3.1 General remarks

Thick tubes are widely used in deepwater pipelines, oil casing, tendons of tension-leg platforms and risers in offshore platforms. The high ambient pressure in deepwater requires use of tubular with lower diameter to thickness ratios D_0/t, normally between 10 to 40. Practically when a pipeline is pulled through a J-tube, some tension load exists due to pulling of pipelines, while large plastic curvature is applied together with high external pressure. This type of load combination also occurs in the sag bend of tubes in laying. In this situation, all of three loads are moderate. The combination of external pressure, tension and bending loads is also encountered in tendons of tension-leg platforms (TLPs).

The collapse behaviour of thick tubes are strongly influenced by D_0/t, material properties (yield stress and strain hardening parameters), and initial imperfections. Depending on loading situations, the collapse modes of thick tubes can be classified as:

Hoop collapse :	Collapse due to circumferential, elastic-plastic buckling of rings, defined as maximum pressure capacity of the tubes.
Bending collapse :	Collapse due to a combination of ovalization of the cross-section and yielding in the longitudinal direction of the tubes. The collapse is defined as maximum bending moment capacity point.
Tension collapse :	Collapse due to large tension load, defined as maximum tension capacity.

Combination of these failure modes, where the collapse is a combination of elastic-plastic buckling of rings, ovalisation of the cross-section and yielding in longitudinal direction of the tube.

The present study is devoted to the problems concerning collapse of thick tubes under external

pressure, tension and bending loads and their combinations. Since FEM approach has not been widely employed to this kind of problems, it is validated through a systematic comparison with results from experimental and other analytical investigations.

In this Chapter, the summary of this study will be outlined and the details are given in Appendix A. After validating the FEM approach, a parametric study is carried out to investigate collapse behaviour and interaction envelopes for the tubes under combined tension and pressure, combined pressure and bending, combined tension and bending as well as combined pressure, tension and bending loads.

A set of design interaction equations are derived, based on these parameter studies. The design equations are compared with existing design codes and test results. The data from the FE-analysis is enclosed in Appendix A. The interaction equations will form the basic for the reliability study in Chapter 6.

3.2 External pressure

3.2.1 General

Long, relatively thick-walled tubes under external pressure buckles from the circular to a uniformly oval configuration (hoop collapse). Due to the interaction of ovalization and yielding, the tubes experience a limit pressure type of instability. In a pressure controlled environment like that of a deepwater pipeline, this leads to a propagation collapse along the line.

Early studies on the collapse behaviour of thick tubes under external pressure were well outlined by Timoshenko and Gere (1961). Due to increasing needs in offshore engineering, careful experimental and analytical investigations have been carried out (e.g. Tokimasa and Tanaka (1986), Yeh and Kyriakides (1986, 1988). An extensive survey of literature has been presented in their papers. Using FEM approach, Tokimasa and Tanaka (1986) investigated the effects of initial ovality, residual stress and strain hardening. They finally derived a set of formulae to predict the collapse strength of tubes under external pressure. It was claimed that circumferential residual stress greatly reduced the collapse strength. However, according to Yeh and Kyriakides (1986), the effect of residual stress seems to be very small. Therefore it is necessary to study the residual stress effect more systematically for various D_0/t ratios and material properties. It should be noted that the initial ovality amplitude in the test specimens is relatively small, - normally less than 0.0015. In contrast, the allowable initial ovality amplitude in codes is about 0.005. To interpret the test data for the code development, there is a need to know how large the collapse strength would be reduced when the initial ovality amplitude is increased e.g. from 0.0015 to 0.005.

The FEM analysis procedure is validated through comparison with a series of full-scale experiments using X-42 and X-65 grade steel tubes, the details are found in Appendix A. Then, two problems which have not been resolved, were studied, namely:

- the effect of residual stress on the collapse pressure
- the effect of initial imperfection on the collapse pressure

The first problem is chosen because some researchers claimed that the residual stress greatly reduces the collapse strength while others showed that the effect is very small. In addition, formulae to predict collapse pressure are compared with the FEM results.

3.2.2 Effect of residual stress

Figure 3.1 show the effect of residual stress on the collapse pressure for typical pipe material X-52 and X-77. In the figure, P_{co}^{*} denotes collapse pressure of tubes free from residual stress. The collapse strength is linearly reduced with the increase of the amount of residual stress $\sigma_{\theta r}/\sigma_0$. However, the biggest reduction of the capacity for a residual stress $\sigma_{\theta r}/\sigma_0$ equal to 0.5, is less than 5 percent. This effect is basically in agreement with Yeh and Kyriakides (1986). However, even if the material is assumed to be elastic-perfectly-plastic as assumed by Tokimasa and Tanaka (1986), the large reduction has not been obtained. The reduction is almost zero when D_0/t is 15 for material X-52 and D_0/t is 35 for material X-77. This implies that in the fully plastic collapse region and fully elastic collapse region, there is no residual stress effect. Even in elastic-plastic collapse region, the effect of residual stress seems to be small and could normally be neglected.

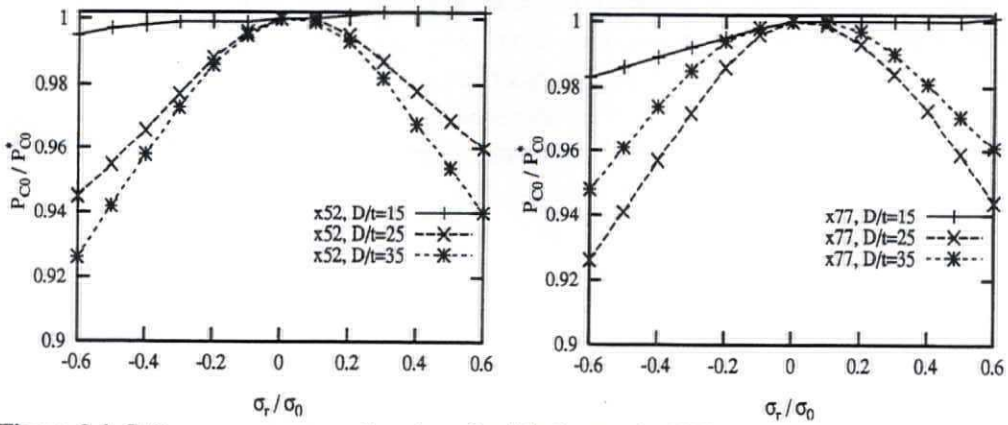

Figure 3.1 Collapse pressure as a function of residual stress for X52 and X77

3.2.3 Effect of initial ovality

The results for material X-52 and X-77 are presented in Figure 3.2. This shows how the collapse strength is reduced by varying the initial ovality between δ_0= 0.0015 and 0.005. The slenderness ratio λ is defined as

$$\lambda = (P_0/P_E)^{1/2} = (D_0/t)[\frac{(1-\nu^2)}{E}\sigma_0]^{1/2} \tag{3.1}$$

A typical tolerance level for the initial ovality magnitude δ_0 in design codes for tendons, risers and pipelines may be 0.005. For D_0/t in the range between 15 and 35, the difference between collapse pressure for imperfection amplitudes 0.0015 and 0.005 is about 15 percent.

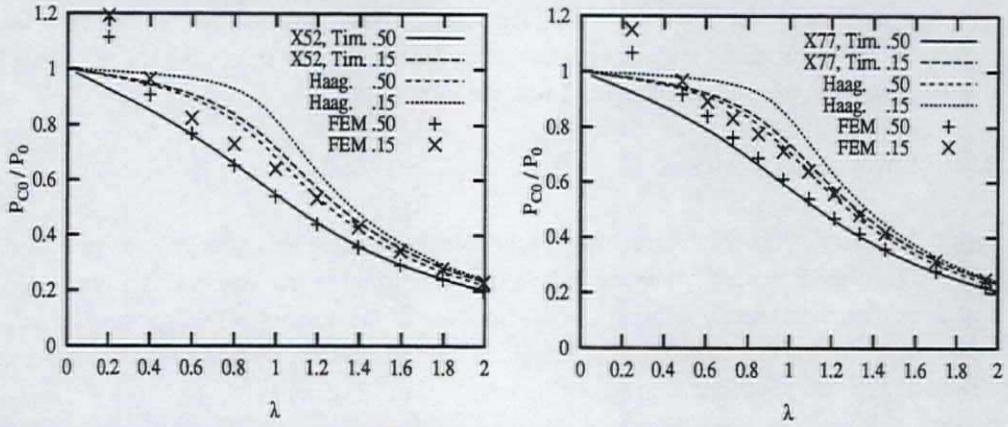

Figure 3.2 Critical pressure for X52 and X77

3.2.4 Comparison with collapse pressure formulae

By assuming that the tube has an initial ovality with symmetric cosine shape, Timoshenko and Gere (1961) derived the hoop compressive force and the hoop bending moment. Substituting the force and the moment into the initial yielding condition and the full yielding condition of the rectangle, the well-known Timoshenko formula and Haagsma and Schaap formula (Haagsma and Schaap 1981), respectively, are obtained. The Timoshenko formula is

$$(P_{co}-P_E)(P_{co}-P_0) = P_{co}P_E(3\delta_0 D_0/t) \tag{3.2}$$

The Haagsma and Schaap formula is

$$(P_{co}-P_E)(P_{co}^2-P_0^2) = P_{co}P_E P_0(2\delta_0 D_0/t) \tag{3.3}$$

Solving Eq. 3.2 or Eq. 3.3, the collapse pressure P_{co} may be obtained. It is noted that both equations lead to elastic buckling pressure P_E and yield pressure P_0, for initially perfect tubes(δ_0=0).

The results estimated by Timoshenko and Haagsma and Schaap formula, for initial ovality of δ_0=0.0015 and 0.005 are compared with the present FEM results in Figure 3.2. It is observed that both equations give higher capacity than the FEM results for tubes with low initial ovality (δ_0=0.0015). When δ_0=0.005, the agreement between the equations and the FEM results is fairly good. Timoshenko equation gives better results than Haagsma and Schaap formula. However,

Timoshenko equation is expected to gives lower capacity than FEM results for tubes with large initial ovality, say δ_0>0.01.

3.2.5 Model uncertainties of collapse pressure formulae

A model parameter X is defined as $X = X^{true} / X^{pred}$, where X^{true} is the real value, determined by laboratory tests or finite element analysis and X^{pred} denotes the prediction due to the proposed equations. It is assumed that both X^{true} and X^{pred} are obtained for the same geometry and material parameters. The model parameter can be treated statistically by calculating its mean bias (Bias) and coefficient of variation (CoV) which are referred to as the model uncertainty and is defined as the standard deviation /mean value. According to Faulkner et al (1988), a good strength model should satisfy that:

- mean bias (Bias) tends to 1.0 - suggested 0.95-1.05
- CoV is as small as possible, suggested CoV<0.15
- there should be little if any dependence of bias on any basic variable

The collapse strength under external pressure depends upon D_0/t, δ_0, stress-strain curve. The variation of D_0/t, δ_0, E and σ_0 within the specimens is relatively small. However, it is noted that the thickness variation within ±2% implies a variation of the elastic buckling strength of ±6%. The variation of D_0 within ±1% is negligible. If the tolerance limit for δ_0 for real tubular is significantly larger than 0.15%, a strength correction factor to account for the systematic difference between δ_0 in specimens and real tubular, should be introduce. It is shown in Figure 3.2 that the Timoshenko formula predicts large differences in the strength corresponding to δ_0 = 0.15 and 0.5% than the FEM, especially for the material X-52. Also, the Timoshenko formula overpredicts the effect of ovalities for large δ_0.

There is a difference between the tensile and compressive yield strength as well as between axial σ_{0x} and circumferential $\sigma_{0\theta}$ yield stress incorporated in the model uncertainty. The pressure collapse strength is referred to $\sigma_{0\theta}$.

It should be noted that particular manufacturing processes like the UOE method, Kyriakides et.al (1991), may have a detrimental effect on the collapse load under external pressure, not covered by the present formulation and the uncertainties estimated herein. The reason for this effect is that the manufacturing induces large tensile strains. Then, when the external load is applied, compressive stresses/strains are set up and the stiffness and strength are reduced according to the Bauschinger effect.

The results of model uncertainty studies of the proposed equations, Eq. 3.2 and Eq. 3.3, are given in Table 3.1. The test results are given by Fowler (1990).

Table 3.1 Model uncertainties for external pressure

	Timoshenko, Eq. 3.2		Haagsma and Schaap, Eq. 3.3	
	Bias	CoV	Bias	CoV
Test results	1.038	0.110	0.931	0.081

3.3 Bending

Brazier (1927) solved a limit load type of instability of long elastic tubes in pure bending due to ovalization of the cross-section. The solution was extended by Ades(1957) for long elastic-plastic tubes in pure bending by assuming that the cross-section ovalized always into an elliptical form. For thinner tubes (larger D_0/t values), a bifurcation buckling (local shell buckling) occurs, Timoshenko and Gere (1961). However, the D_0/t value which separates the limit load instability and the bifurcation buckling depends on the material properties of the tubes. Experiments conducted by Kyriakides and Ju (1992) and Corona and Kyriakides (1988) show this D_0/t value for typical pipeline material is around 35 to 40. Therefore in the present study, only the limit type of instability is considered.

The FEM analysis is used to investigate the parametric dependence of the collapse moment and curvature. The purpose of the analysis is to provide a numerical data basis to derive an equation for the assessment of collapse of thick tubes under pure bending. The analysis is concentrated on the sensitivities to diameter to thickness ratio, D_0/t, yield parameter to Young modules ratio, σ_p/E, strain-hardening parameter, n, and yield anisotropy parameter S. It is noted that tube collapse under pure bending is defined as limit load point.

The curvature at limit moment point predicted by the present FEM analysis is identified as critical curvature. The agreement between two maximum moment points, from the experiment and from the FEM analysis, is excellent as shown in Appendix A. It is therefore decided to mainly look at the curvature at maximum moment in the present study.

The finding from the numerical studies will form the basic for equations for ultimate moment and curvature and the main finding are as follows:

The normalized collapse moment M_{co}/M_0 could be approximated by a linear function of D_0/t and increases linear with σ_p/E. The normalized collapse curvature κ_{co}/κ_0 is insensitive to D_0/t and is almost constant for different σ_p/E. The collapse moment and curvature are significantly affected by the strain-hardening parameter, n. They are decreasing rapidly with an increasing n. It is shown that the collapse moment and curvature depend linearly on the anisotropy parameter S.

3.3.1 Equations for ultimate moment and curvature

Collapse moment for tubes with $15<D_0/t<35$ given by design codes is approximately 0.95 M_0, see e.g. BS8010 (1993) . Significant effect of strain-hardening has not been considered in the design codes. Equations for collapse curvature in the design codes are also crude. This is due to the lack of experimental and numerical data. Therefore, the following equations have been derived based on least square curve fitting of the present parametric studies shown in Appendix A.

$$\frac{M_{co}}{M_0} = f_1(D_0/t,n) * f_2(\sigma_p/E) * f_3(S) \tag{3.4}$$

where

$$\begin{aligned} f_1(D_0/t,n) &= \left[1.0094 - 0.00184(D_0/t) + 0.0000333(D_0/t)^2\right] \\ &+ \left[0.14835 - 0.00275(D_0/t)\right](n/15)^{-1} \\ &+ \left[0.03913 - 0.001742(D_0/t) + 0.0000258(D_0/t)^2\right](n/15)^{-2} \end{aligned} \tag{3.5}$$

$$f_2(\sigma_p/E) = 0.971 + 15.5(\sigma_p/E) \tag{3.6}$$

$$f_3(S) = 0.861 + 0.139S \tag{3.7}$$

and

$$\kappa_{co}/\kappa_0 = 1.255 * f_4(n) * f_5(S) \tag{3.8}$$

where

$$f_4(n) = 0.5 + 0.586(n/15)^{-1} - 0.0939(n/15)^{-2} \tag{3.9}$$

$$f_5(S) = -0.19 + 1.19S \tag{3.10}$$

For a given set of geometric and material parameters, e.g. $D_0/t=25$, $n=15$, $\sigma_p/E=0.0012$ and $S=0.85$, Eq. 3.4 and Eq. 3.8 give $M_{co}/M_0= 1.1137$ and $\kappa_{co}/\kappa_0= 1.2611$. The obtained results agree well with the present finite element analysis results which are $M_{co}/M_0= 1.1124$ and $\kappa_{co}/\kappa_0= 1.2630$. Figure 3.3 shows the collapse bending moment and the curvature for different D_0/t and strain hardening.

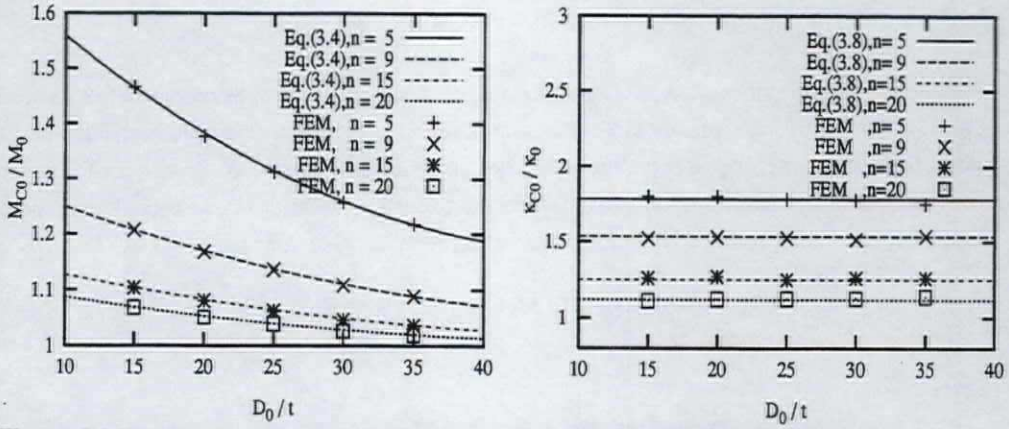

Figure 3.3 Bending moment and curvature as a function of D_0/t and strain hardening

3.3.2 Model uncertainties of the proposed equations

The bending capacity depends upon the stress-strain curve (E, σ_0, n). Data cover a D_0/t-range of 16 to 42, with a balance between large and small scale specimens, and a yield stress range of 290 to 500 MPa. The in specimen/batch parameter variability of D_0, t and σ_0 has a small influence on the uncertainty. The results of model uncertainty studies of the proposed equations, Eq. 3.4 and Eq. 3.8 , are given in Table 3.2.

Table 3.2 Model uncertainties pure bending

	Moment, Eq. 3.4		Curvature, Eq. 3.8	
	Bias	CoV	Bias	CoV
Test results	0.994	0.057	1.024	0.095

The prediction of Eq. 3.4 for ultimate moment has been compared with the experimental results, as shown in Figure 3.4. Test results are from Sherman (1976) and (1984), Fowler (1990), Kyriakides et al. (1987), Shilling (1965), Jirsa (1972) and Korol (1979). Figure 3.4 includes the experimental and finite element results.

Similarly, the predictions of Eq. 3.8 for critical curvature have been compared with the experimental results respectively, as shown in Figure 3.4. Test results are from Kyriakides and Corona (1987) and Kyriakides and Ju (1992). For perfect correlations, all points should lie on a 45^0 line of the plots of finite element and experimental results vs. predictions. It has been confirmed that the correlations are very good.

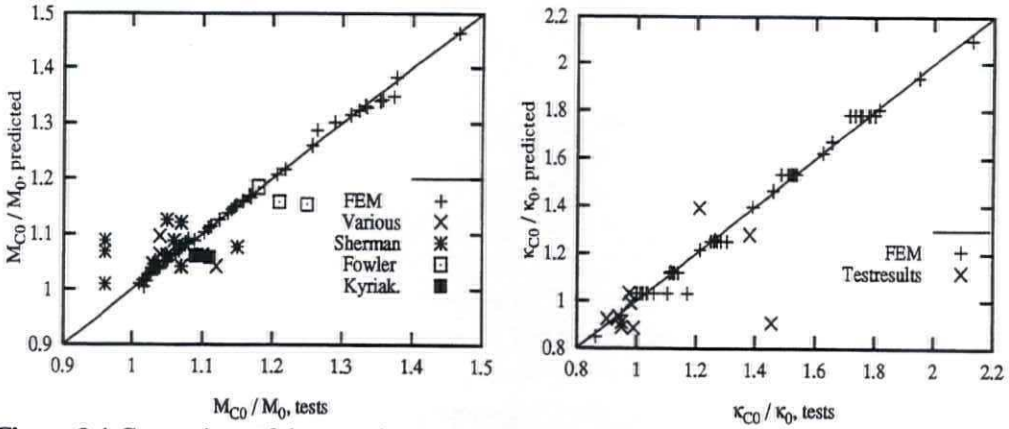

Figure 3.4 Comparison of the experimental ultimate moment, the critical curvature and the predicted equations

3.4 Tension

Apart from buckling and collapse, there is another failure mode - tension tearing rupture of material. The tension collapse is a rare failure mode for pipelines but the failure criteria has to be defined when considering tension tearing rupture.

During the last 30 years, many fracture mechanics criteria have been developed to predict material resistance, including both brittle fracture and tension tearing rupture(ductile fracture). Example of the criteria is the CTOD design curve approach, (Andersen 1990). For instance, the CTOD design curve is given by

$$\frac{\delta_c}{2\pi\varepsilon_0 a_{\max}} = \frac{\varepsilon_{co}}{\varepsilon_0} - 0.25 \qquad for \quad \frac{\varepsilon_{co}}{\varepsilon_0} > 0.5 \tag{3.11}$$

where δ_c is the critical CTOD value, ε_0 is yield strain and a_{max} denotes the equivalent through-thickness crack size. The major parameters governing the fracture are defect size and material fracture toughness. For pipeline material, typically, δ_c=0.2 and a_{max}=0.6 mm. This gives a critical strain ε_{co}=0.05, according to Eq. 3.11. However, it should be emphasized that the CTOD design curve applies to the localized strain near weld defects, and not to the strain from beam-column theory. The latter is the value determined from the extreme fibre strain of ABAQUS results. Therefore a smaller value, e.g. 0.02 should be used as the equivalent rupture strain.

On the other hand, for pipelines with surface flaws or through-wall flaws, systematic investigation on tensile failure criteria have been carried out by e.g. Wilkowski and Eiber (1981). The tensile failure is estimated using a flow stress concept. Several relationships between flow stress σ_f, yield

stress σ_0 and ultimate stress σ_u, have been proposed by Wilkowski and Eiber (1981), e.g.:

$$\sigma_f = 1.2\sigma_0 \tag{3.12}$$

$$\sigma_f = \frac{(\sigma_0 + \sigma_u)}{2} \tag{3.13}$$

$$\sigma_f = \sigma_0 + 68.9 Mpa \tag{3.14}$$

For typical pipeline material X-52 and X-77, the above equations give approximately $\sigma_f = 1.2\sigma_0$. In terms of strain, flow strain corresponding to $1.2\sigma_0$ is approximately 0.02. In this study the tension collapse is defined as maximum tension capacity, which is a function of yield stress and the hardening parameter n, Andersen (1990). The tension capacity is strongly influenced by the strain hardening , as shown in Figure 3.5.

$$T_{co} = \frac{1}{2} T_0 \left[1 + \frac{(0.002n)^{-\frac{1}{n}}}{\exp(\frac{1}{n})} \right] \tag{3.15}$$

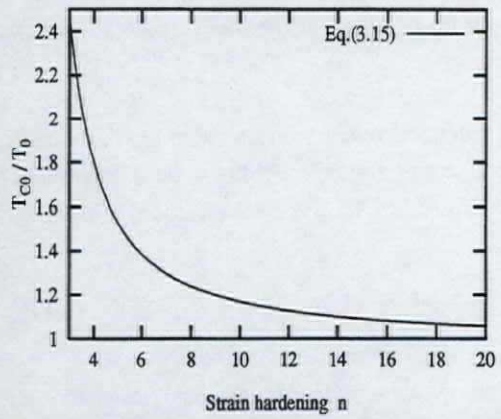

Figure 3.5 Collapse tension as a function of strain hardening

3.4.1 Model uncertainties for tension

The tensile capacity is not sensitive to a variation of the cross section area and the main contribution to the uncertainty is due to the stress-strain curve, and the definition of the failure criterion (limit state) itself, for the actual strain-hardening steels.

Data for only three tubular specimens tested until ultimate failure Fowler (1990), are available. The

results of model uncertainty studies of tension using Eq 3.15 as the predicted tension, are given in Table 3.3. Statistical uncertainties for the mean and the standard deviation are not included, according to Eq. 2.1 for the tensile case.

The stress (strain) level at which necking or fracture occurs in a real tube will be sensitive to defects and other stress concentrations. In the tensile specimens referred to here, failure occurred at an elongation of 20%, far beyond the level of 2% considered to be critical for welded specimens. For the steels X-52 and X-77 strain levels of 2% and 20% would imply stresses equal to about 1.2 and 1.5 times the yield stress, respectively. The yield stress corresponds to a strain of 0.5%.

Assuming that the tensile capacity varies between yield level and the stress corresponding to a 20% strain, the range of the bias factor, as referred to the yield strength, will be about 1.0 to 1.5. If the distribution of the bias is symmetric over the actual range, the mean bias is 1.25, which is quite close to the experimental value. It is reasonable to assume that this range should cover a significant part of the possible bias values. If the confidence interval for the bias is 0.99 and the bias is assumed to follow a normal distribution, the range 1.0 to 1.5 correspond to 5.2 standard deviations. This means that the standard deviation is $\sigma = (1.5 - 1.)/5.2 \sim 0.095$, and the CoV is $0.095/1.25 = 0.076$. This reasoning, hence leads to an estimated mean bias and CoV of 1.25 and 0.076, respectively.

Based on the above reasoning the model uncertainty of the tensile capacity determined by the yield strength, can conservatively be estimated to be a bias of 1.2 and a CoV of 0.08. Using Eq. 3.15, the bias can be estimated to 1.0 and a CoV of 0.08.

Table 3.3 Model uncertainties for tension, using Eq. 3.15

	Bias	CoV
Tests	1.058	0.13
Predicted	1.000	0.08

3.5 Pressure - Bending

3.5.1 General

In recent years, the understanding of collapse behaviour of thick tubes under bending load was further extended to the case when pressure is included. The state-of-art as well as literature review could be found from de Winter et al (1985), Corona and Kyriakides (1988) and Ju and Kyriakides (1991). It was shown by Corona and Kyriakides (1988) that the limit load type of instability could be numerically predicted provided the geometric and material parameters and loading path were known. They presented the sensitivity of pressure-curvature envelopes to D_0/t, initial ovality, yield

anisotropy and hardening parameters and loading paths.

Similar parameter studies are made in this work and the FEM analysis procedure for tubes under combined pressure and bending is validated through the simulation of the collapse tests, see Appendix A.

3.5.2 External pressure-moment interaction

The pressure-moment interaction is obtained based on the parameter study. A possible form of the equation is expressed as

$$\left(\frac{M_{co}}{M_{co}^{*}}\right)^{b} + \left(\frac{P_{co}}{P_{co}^{*}}\right)^{c} = 1 \tag{3.16}$$

where M_{co}^{*} denotes collapse moment when only moment load is applied, Eq. 3.4 and P_{co}^{*} is according to Timoshenko Eq. 3.2 . The value of the exponents b and c could be obtained by curve fitting. In Figure 3.6, the prediction of the proposed equation for b=1.9 and c=1.9 are compared with FEM results. The agreement is reasonable.

In some design rules, e.g. BS8010 (1993), the relationship between external pressure and curvature is linear. However, FEM results indicate that the collapse envelopes are lower than linear curves. The collapse envelopes are approximated in the form

$$\left(\frac{\kappa_{co}}{\kappa_{co}^{*}}\right)^{a} + \frac{P_{co}}{P_{co}^{*}} = 1 \tag{3.17}$$

where κ_{co}^{*} and P_{co}^{*} denote collapse curvature and collapse pressure when a single load is applied. In Figure 3.6 the results for a = 0.6 is compared with the present FEM results.

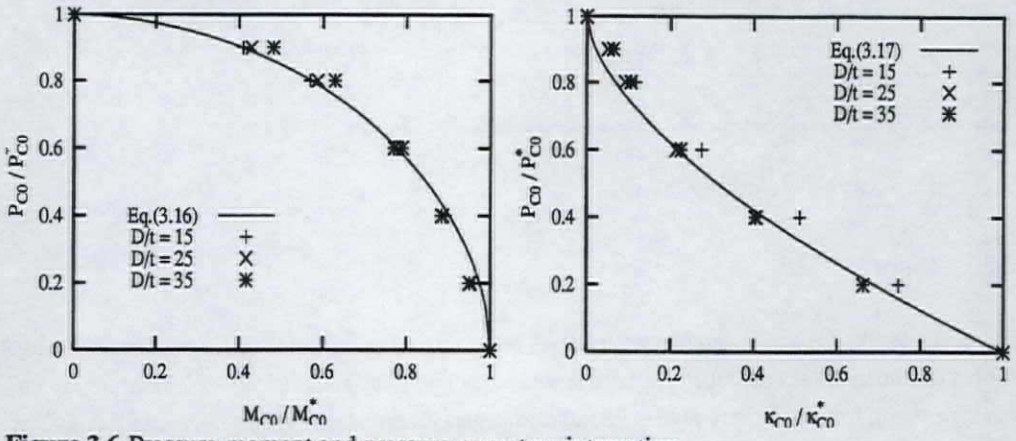

Figure 3.6 Pressure-moment and pressure-curvature interaction

3.6 Pressure - Tension

3.6.1 General

Collapse of tubes under combined tension and pressure loads is one of the most critical conditions for the design of deepwater casing. The tension load is due to the weight of the casing string. Some of the earliest experiments to establish a criterion for the design of oil-well casing under combined external pressure and tension loads were carried out by Edwards et al in 1939. Recent experimental investigations were presented by Kyogoku et al (1981), Tamano et al (1982). Babcock and Madhavan (1987) conducted a number of small scale tests and presented a systematic analysis considering the effects of initial ovality, yield anisotropy and strain hardening. They showed that for tubes with low initial ovalities changing the loading paths had very little effect on the tension-pressure collapse envelope unless tension load was dominant. However, for tubes with relatively large initial ovalities this conclusion should be further confirmed, e.g. by numerical simulation.

This section investigates the following problems associated with combined tension and pressure:

- In a previous study (Babcock and Madhavan 1987) it was concluded that for tubes with initial ovality amplitude δ_0 (less than 0.0015) the effect of load path is very small. The question is whether this conclusion is valid also for tubes with larger initial ovality parameter δ_0 (about 0.005)?
- It is well-known that the effect of (a small) axial tension can be accounted for by reducing the hoop yield stress according to the von Mises yield condition. For materials with anisotrophic yield properties the question is whether it is possible to account for the effect of tension load by using Hill yield condition.

3.6.2 Effect of load paths and initial ovality

Relatively large initial ovality magnitude(δ_0=0.005) is assumed and the material is X-52 grade steel. The P→T load path gives lower collapse envelopes than the T→P load path. Figure 3.7 show that the effect of load paths is negligible when the tension load is lower than T/T_0=0.6. On the other hand, the effect of load paths becomes significant when the tension load is dominant (T/T_0>0.6). In addition, the deviation between the two collapse envelopes is bigger for D_0/t=15 than for D_0/t=35. This is because the former involves larger plastic deformation and the load path effect is basically due to path dependency of plasticity.

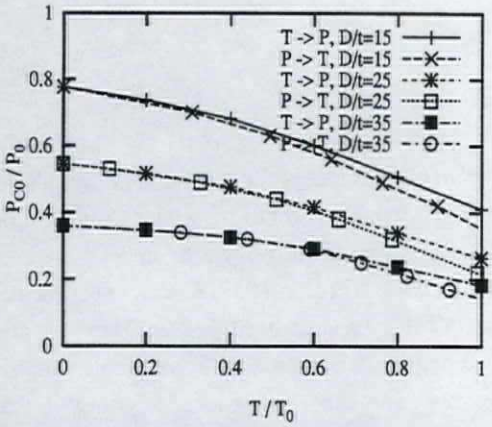

Figure 3.7 Pressure-tension interaction, effect of load path.

3.6.3 Formulae for pressure-tension envelopes

When plastic deformation is involved, the interaction between axial tension and external pressure can be considered as the problem of material yielding under bi-axial loads. The yield stress in the circumferential direction is reduced due to axial tension. Neglecting the stress component normal to the tube wall and all shear stress components, the Hill yield condition is expressed as e.g. (Corona and Kyriakides 1988):

$$\sigma_0^2 = \sigma_{0x}^2 - (1 + \frac{1}{S_\theta^2} - \frac{1}{S_r^2})\sigma_{0x}\sigma_{0\theta} + \frac{\sigma_{0\theta}^2}{S_\theta^2} \tag{3.18}$$

where $S_\theta = \sigma_{0\theta}/\sigma_{0x}$ and $S_r = \sigma_{0r}/\sigma_{0x}$ are the parameters describing the anisotrophy. For a given axial stress σ_{0x} (tension load), the circumferential yield stress can be obtained by solving Eq. 3.18 with respect to $\sigma_{0\theta}$. Substituting the obtained circumferential yield stress into for instance the Timoshenko formula, tension-pressure collapse envelopes could be evaluated. It is observed that the effect of tension on the collapse pressure of tubes with yield anisotropy could be considered by use of Hill yield function.

3.7 Bending - Tension

3.7.1 Loading paths and parameter study

For this load combination, there is no laboratory test data available. However, the finite element model has been validated using laboratory tests of pipes under combined tension and pressure and under combined bending and pressure.

The collapse behaviour of thick tubes under combined tension and bending is supposed to be greatly

influenced by the applied load path. Therefore two load paths T→κ and κ→T are considered.

The tension load T is first applied to a prescribed value for the T→κ. Then the tension load is fixed and the curvature κ is incremented. The moment and curvature at the limit point (maximum moment) represent collapse values. It has been shown that the collapse moment is reduced by the tension load applied. The tube is incrementally loaded to the chosen value of curvature at zero tension for the κ→T load path. There is no limit load point for this loading path. From the FEM analysis, it is concluded that T→κ load path is more severe than the κ→T load path. For more details see Appendix A.

The main conclusions of the parametric studies are:

When the failure criterion is limit load point, tubes with lower D_0/t values, lower hardening parameter n and higher yield anisotropy parameter S can sustain higher combinations of tension and bending (or curvature and tension). The collapse is insensitive to material grade (ratio of the yield parameter to Young modulus σ_y/E).

3.7.2 Interaction equations

Interaction equation between bending and tension is obtained based on the parametric studies presented. Finite element analysis results based on maximum capacity criteria are used and it has been found that the interactions could be approximated by :

$$\left(\frac{M_{co}}{M_{co}^{*}}\right) + \left(\frac{T_{co}}{T_{co}^{*}}\right)^{2.4} = 1 \qquad (3.19)$$

where M_{co}^{*} and T_{co}^{*} denote collapse moment from Eq. 3.4 and tension collapse from Eq. 3.15 under single load, respectively. In Figure 3.8 (a) moment-tension interaction curves due to the proposed equations is compared with finite element analysis results, for pipes with different hardening parameter (n=5, 9.05, 25).

Interactions in the form of curvature-tension are applicable to pipeline problems on the stinger during laying, since external load are applied on those components in displacement control. For pipeline applications, finite element analysis results based on limit load criterion have been used for derivation of interaction equations. From least square curve fitting it has been obtained that

$$\frac{\kappa_{co}}{\kappa_{co}^{*}} = 1 + 1.43\left(\frac{T_{co}}{T_{co}^{*}}\right)^{2.4} \qquad (3.20)$$

where κ_{co}^{*} denotes collapse curvature under single load, Eq. 3.8

Figure 3.8 (b) compares the predicted curvature-tension interactions with those of the finite element

analysis, for pipes with various diameter to thickness ratio (D_0/t=15, 25, 35). It has been shown that the proposed interaction equations agree well with the finite element analysis results.

The proposed interaction functions well describe the sensitivities of the collapse moment and critical curvature to the major parameters. The difference between the interaction function and finite element results for collapse moment at high tension load region is due to the criterion used (maximum moment criterion).

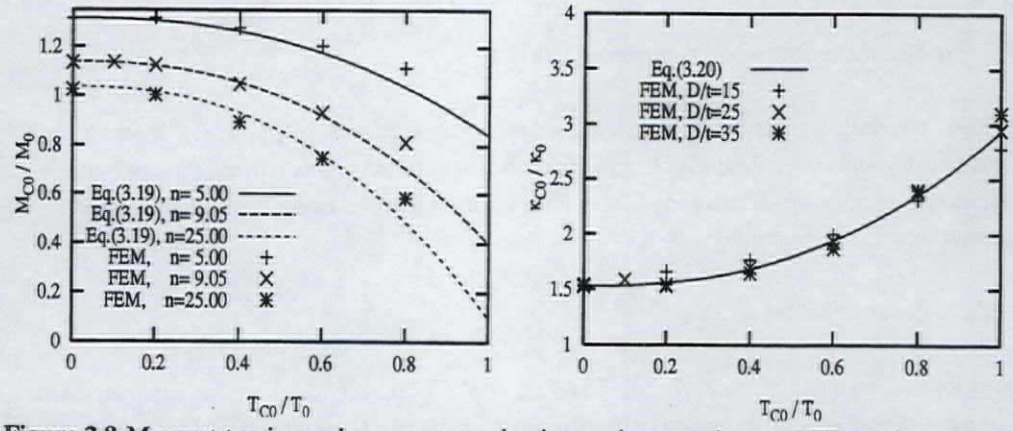

Figure 3.8 Moment-tension and curvature-tension interaction equations and FE-results.

3.8 Pressure - Tension - Bending

3.8.1 General

In the previous sections it is demonstrated that the FEM can accurately predict the collapse behaviour of thick tubes under combined pressure, tension and bending loads. In this section the FEM is applied to propose an equation for the capacity of tubes .

3.8.2 Pressure-tension-moment interaction

Based on numerical and experimental data bases, it has been proposed that the collapse strength for thick tubes simultaneously subjected to pressure, tension and bending loads could be estimated using the following equations:

$$\left(\frac{M_{co}}{M_{co}^{**}}\right)+\left(\frac{T_{co}}{T_{co}^{**}}\right)^{a} = 1 \qquad (3.21)$$

where

$$a = 2.4 - 2.5\left(\frac{P_{co}}{P_{co}^{*}}\right) + 1.5\left(\frac{P_{co}}{P_{co}^{*}}\right)^2 \tag{3.22}$$

and where M_{co}^{**} and T_{co}^{**} denote collapse moment and tension under coupled loads (after external pressure P_{co} is firstly applied), respectively. T_{co}^{**} denotes collapse tension load when pressure load P_{co} has been applied together, due to a combination of Hill yield function and Timoshenko equation. M_{co}^{**} could be obtained from the pressure-moment interactions Eq. 3.27. Collapse pressure P_{co}^{*} is pure pressure load estimated following the Timoshenko formula. A comparison between Eq. 3.21 and FEM-results are made and presented in Figure 3.9.

3.8.3 Pressure-tension-curvature interaction

It is proposed that the pressure-curvature-tension interaction is expressed in the form

$$\left(\frac{\kappa_{co}}{\kappa_{co}^{**}}\right)^{b} + \left(\frac{P_{co}}{P_{co}^{*}}\right) = 1 \tag{3.23}$$

where

$$b = 0.6 - 0.25\left(\frac{T}{T_{co}^{*}}\right) \tag{3.24}$$

where P_{co}^{*} and T_{co}^{*} could be obtained by the Timoshenko and the Anderson equation, respectively. The curvature-tension interaction, κ_{co}^{**}, could be approximated according to Eq. 3.20. For different level of tension, the interaction between pressure and curvature are compared with FEM-results in Figure 3.9.

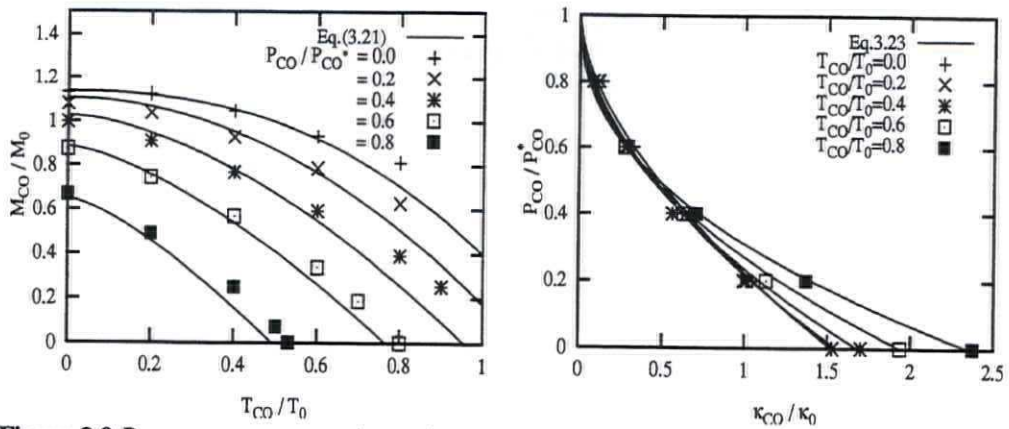

Figure 3.9 Pressure-moment-tension and pressure-curvature-tension interactions

3.9 Design Equations

3.9.1 General

Simple and accurate design interaction equations are developed based on extensive investigations of collapse behaviour. Comparison of the proposed equations and existing codes with experimental data indicated that the best performance was achieved by the proposed interaction equations in terms of Timoshenko equation for external pressure, bending capacity based on a new plastic collapse expression, pressure-axial interaction following von Mises yield condition, pressure-bending interaction using a newly developed equation and a new general interaction equation for acting pressure, axial and bending loads.

When dealing with a pipe section having displacement controlled load, interaction in form of strain are applicable. A strain-based interaction is proposed, based on the data base.

The equations outlined in the following will form the basic for the reliability study in Chapter 6.

3.9.2 Load controlled design condition

Basic failure modes

The collapse moment M_{co} under pure bending is obtained by substituting typical pipeline material properties into the general equations obtained as:

$$\frac{M_{co}}{M_0} = \left(1.35 - \frac{D_0/t}{90} + (\frac{D_0/t}{100})^2 \right) \tag{3.25}$$

The elastic-plastic collapse pressure P_{co}, of thick-walled pipe under pure pressure, is predicted using the Timoshenko equation Eq. 3.2. The critical axial load T_{co} is considered using Anderson (1990) with typical hardening parameter, given as:

$$T_{co} = 1.2 \cdot T_0 \tag{3.26}$$

Pressure-bending

The interaction between bending moment M and pressure P is expressed as

$$\left(\frac{M}{M_{co}} \right)^{1.9} + \left(\frac{P}{P_{co}} \right)^{1.9} = 1 \tag{3.27}$$

where M_{co} and P_{co} could be obtained from Eq. 3.25 and Eq. 3.2, respectively

Pressure-tension

The design format for interaction between pressure P and tension T is expressed as

$$\frac{P}{P_{co}^{*}} \leq 1 \tag{3.28}$$

P_{co}^{*} : for a given axial load (σ_{0x}, tension stress), the circumferential yield stress can be obtained by solving Eq. 3.18 with respect to $\sigma_{0\theta}$. Substituting the obtained circumferential yield stress into the Timoshenko formula, tension-pressure collapse envelopes could be evaluated.

Bending-tension

The collapse strength under bending moment M and axial load T could be estimated using the following equation :

$$\frac{M}{M_{co}} + \left(\frac{T}{T_{co}}\right)^{2.4} = 1 \tag{3.29}$$

where M_{co} and T_{co} could be obtained from Eq. 3.25 and Eq. 3.26, respectively

Pressure-tension-bending

The collapse strength for thick-walled pipes under simultaneous pressure P, axial load T and bending moment M could be estimated using the following equations :

$$\frac{M}{M_{co}^{p}} + \left(\frac{T}{T_{co}^{p}}\right)^{a} = 1 \tag{3.30}$$

The exponent 'a' is expressed as a function of the pressure load, Eq. 3.22. M_{co}^{p} and T_{co}^{p} could be obtained from the interaction equations for combined pressure and bending and combined pressure and axial load respectively. The interaction between axial load T and pressure P is considered using von Mises yield function as:

$$\left(\frac{T_0^p}{T_0}\right)^2 + \left(\frac{T_0^p}{T_0}\right)\left(\frac{P_0'}{P_0}\right) + \left(\frac{P_0'}{P_0}\right)^2 = 1 \tag{3.31}$$

where P_0' is the modified yield pressure due to the given collapse pressure. From Eq. 3.31 the reduced tension yield strength is found and can be used in Eq. 3.26. It is noted tensile axial load and external pressure are positively defined in the pressure-axial load interaction equation.

The interaction between bending moment M_{co}^{p} and pressure P is expressed as

$$\left(\frac{M_{co}^{p}}{M_{co}}\right)^{1.9}+\left(\frac{P}{P_{co}}\right)^{1.9}=1 \tag{3.32}$$

The collapse moment M_{co} is obtained by using Eq. 3.25. The elastic-plastic collapse pressure P_{co}, of thick-walled pipe under pure pressure, is predicted using the Timoshenko equation Eq. 3.2, excluding axial load correction.

The Figures 3.10 (a), (b) and (c) presents the envelopes for material X-52, $D_0/t=25$, $\delta_0=0.005$ and $P/P_0 = 0.00$, 0.22 and 0.44. The x-axis is critical tension load and the y-axis is critical bending moment, normalized with respect to yield 'loads', respectively.

3.9.3 Displacement controlled design condition

Basic failure mode

According to the finite element results, the critical bending strain is a linear function of t/D_0. A critical strain of 0.75 t/D_0 could be obtained from the critical curvature equation, Eq. 3.8, by assuming a hardening parameter n equal to 9.5. The linear approach is in agreement with Gellin (1980), Fabian (1981) and Jensen and Pedersen (1985). The hardening parameter is not so important when D_0/t is larger than 40, since collapse occurs at a stress level near the yielding point. However, for thick-walled pipe, the stress-strain curve needs to be determined using the yield and the ultimate points since collapse occurs at a large strain level and the collapse is more sensitive to strain hardening. Since the finite element results not account for this in a good way, Igland et al (1993), suggested an equation based on test results as

$$\varepsilon_{co} = 0.005+13\left(\frac{t}{D_0}\right)^2 \tag{3.33}$$

Pressure-bending

The pressure-bending strain interaction is expressed as

$$\frac{P}{P_{co}}+\left(\frac{\varepsilon}{\varepsilon_{co}}\right)^{0.6}=1 \tag{3.34}$$

where ε_{co} denotes the critical value of the maximum extreme fibre strain, Eq. 3.33.

Bending-tension

When axial strain exists, the interaction between axial strain and bending strain is very complex. Here the axial strain is defined as axial strain at the neutral axis and the bending strain is the strain linear from the neutral axis, based on a general beam theory. The proposed equation is based on

a conservative assumption, assuming a linear interaction between axial and bending strain.

Finite element analysis indicates that the existence of axial tensile load improves the critical bending strain. The design format for the interaction between bending and tension is suggested as

$$\frac{\varepsilon}{\varepsilon_{co}^{MT}} \leq 1 \tag{3.35}$$

where a linear interaction between axial strain and bending strain is assumed and ε_{co}^{MT} is bending strain when tensile load is applied together, given as

$$\frac{\varepsilon_{co}^{MT}}{\varepsilon_{co}} = 1 + 1.43\left(\frac{T}{T_{co}}\right)^{2.4} \tag{3.36}$$

ε_{co} is obtained by using Eq. 3.33, T_{co} is according to Eq. 3.26.

Pressure-tension-bending

An interaction equation for pressure-tension-bending strain is suggested as

$$\frac{P}{P_{co}} + \left(\frac{\varepsilon}{\varepsilon_{co}^{MT}}\right)^{0.6-0.25\frac{T}{T_{co}}} = 1 \tag{3.37}$$

where a linear interaction between axial strain and bending strain is assumed and ε_{co}^{MT} is bending strain when tensile load is applied together, given in Eq. 3.36.

Figure 3.10 (d) presents the pressure-strain envelopes for material X-52, $D_0/t=25$ and $\delta_0=0.005$. At the x-axis is strain normalized with respect to a reference strain equal to $0.5t/D_0$ and at the y-axis is the collapse pressure normalized with respect to yield pressure.

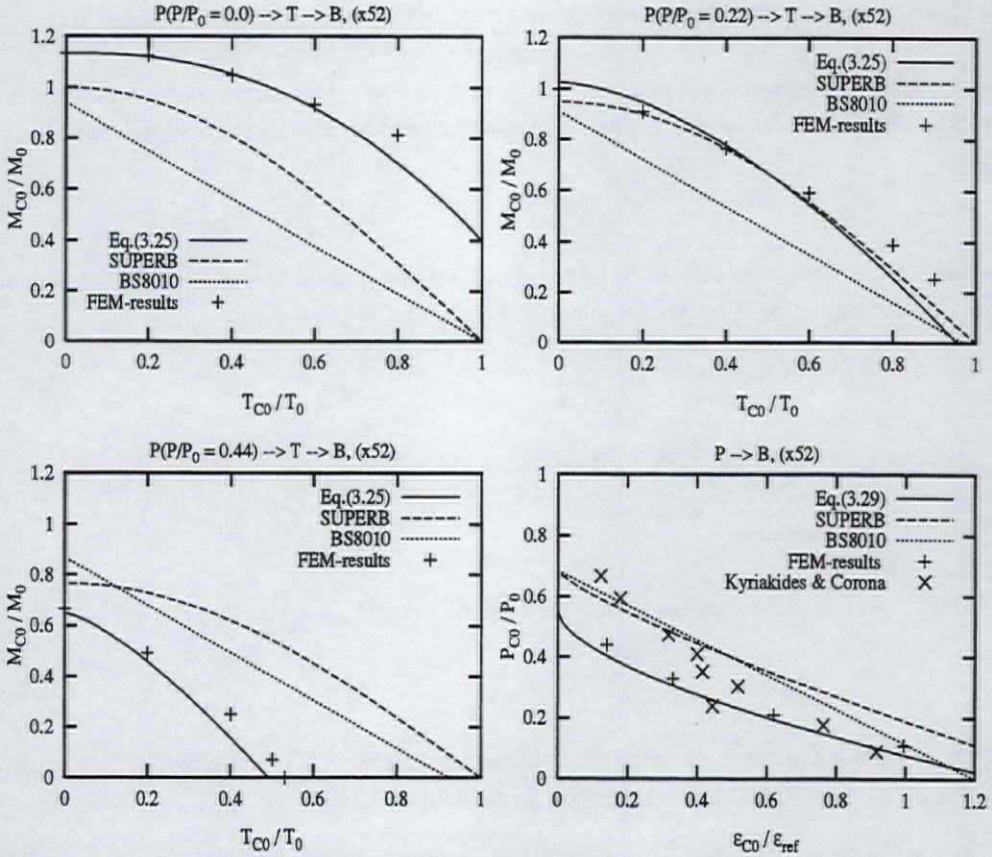

Figure 3.10 Predicted equations compared to design codes and FEM-results, $D_0/t = 25$, $\varepsilon_{ref} = 0.5 \cdot t/D_0$

3.9.4 Comparison with design codes

Comparisons of previous equations with traditional design practice/codes are made for SUPERB (1996) and BS8010 (1993) for load controlled and displacement controlled design conditions. Note, no safety and usage factors are included in the design equations.

The pressure-moment-axial load interaction is available in several design codes. Pressure-tension-bending interaction based on strain are not available in the codes but several interaction equations for pressure-bending strain are available.

The proposed equation, SUPERB (1996) and BS8010 (1993) are presented and compared with FE-results in Figure 3.10. In Figure 3.10 (d) , the predicted interaction due to SUPERB, BS8010 and the proposed interaction are compared with laboratory tests by Kyriakides and Corona (1987).

SUPERB

Pressure-moment-axial load interaction equations is suggested in the SUPERB (1996) guidelines:

$$\left(\frac{M_F+M_E}{M_{co}^T}\right)^2+\left(\frac{P}{P_{co}}\right)^2=1 \tag{3.38}$$

The critical bending moment $M_{co}{}^T$ is defined as

$$M_{co}^T = M_0\cos\left(\frac{\pi}{2}\frac{T_F+T_E}{T_0}\right) \tag{3.39}$$

where the subscript F and E are abbreviations for functional and environmental, respectively. T_0 is defined as yield axial load, and critical pressure is according to Haagsma and Schaap formula Eq. 3.3.

The strain based design equation accounting for external pressure and bending strain is given by

$$\left(\frac{\varepsilon_F+\varepsilon_E}{\varepsilon_{co}}\right)^{0.8}+\frac{P}{P_{co}} = 1 \tag{3.40}$$

where the buckling strain capacity is given by

$$\varepsilon_{co} = \frac{t}{D_0}-0.01 \tag{3.41}$$

BS8010

The following interaction equation was suggested in the BS8010 (1993) code

$$\left(\frac{M}{M_{co}}+\frac{T}{T_{co}}\right)^{1+300\frac{t}{D}}+\frac{P}{P_{co}} = 1 \tag{3.42}$$

where M_{co} can be outlined from

$$M_{co} = M_0(1-0.0024\frac{D}{t}) \tag{3.43}$$

and T_{co} is defined as yield tension and P_{co} is according to Haagsma and Schaap equation, Eq. 3.3. Note, for the calculations related to BS-formula the actual ovality was used in contrast with the BS recommendations that imposed an initial ovality not less than 0.025.

A linear interaction between pressure and bending strain was proposed by Murphey and Langner (1985) and adopted in BS8010 (1993):

$$\frac{P}{P_{co}}+\frac{\varepsilon}{\varepsilon_{co}}=1 \tag{3.44}$$

P_{co} is according to Haagsma and Schaap, Eq. 3.3 and ε_{co} is defined as $15(t/D)^2$

Figure 3.10 shows that the proposed equations take into account the effect of pressure in a good way, which is very important for deep water pipelines. For load controlled conditions SUPERB seems to underestimate the bending capacity for bending-tension conditions, SUPERB and the proposed equation is coincide for $P/P_0 = 0.22$ while for the extreme pressure combined with tension the bending capacity will be overestimated. This is in agreement with SUPERB (1997) where the equation is appropriate only in the moment and pressure dominant situations where the tension is moderate. BS8010 is conservative with respect to bending capacity, except for extreme pressure dominate conditions where the code may be unconcervative compare to the numerical results.

For displacement controlled conditions will the proposed equation underestimate the interaction for pressure dominated situation but coincide with the experimental results when the bending situation is dominated. The SUPERB equation coincide the experimental results very well for pressure dominated situations, but overestimate the bending capacity for pure bending. BS8010 fit the experimental results quit well.

Note, this comparison is made for D_0/t equal to 25 and several comparisons have to be made for final conclusions.

4 LOAD EFFECTS, STRAIN CONCENTRATION

4.1 General remarks

During S-laying installation of offshore pipelines, the pipe is exposed to plastic strains when the pipe passes over a stinger exceeding a certain curvature. Two special aspects are then occurring, twisting of the pipe due to reversing the bending at the sagbend and strain concentration due to discontinuity of the concrete coating. Endal et al. (1995) show that the pipeline lies along a straight line on the sea bottom, and no instabilities are experienced as a consequence of residual curvature. Furthermore, the pipeline twist (roll) is found to occur with negligible out-of-plane displacements.

Offshore pipelines are usually coated with concrete in order to counteract buoyancy and ensure on-bottom stability of the pipeline. Generally the presence of the concrete is neglected in laying analyses. However, because of the discontinuity in the concrete coating, several additional problems arise (Konuk, 1984). The most important of which is the occurrence of strain concentrations at the field joints during bending of the pipe, Figure 4.1.

It is of considerable interest to determine the strain concentrations since a discussion concerning maximum allowable strain on the stinger and in the sagbend region is presently taking place (Sriskandarajah and Mahendran, 1992).

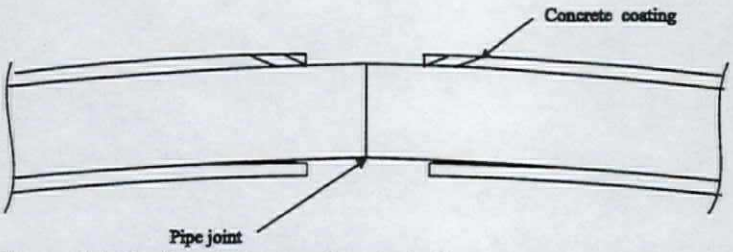

Figure 4.1 Pipeline during bending, including concrete coating

The magnitude of the strain concentrations are reduced because of the weak bond between the steel pipe and the concrete coating. This is due to the small shear-transfer capacity of the anti-corrosion coating, allowing the concrete to move towards the field joint during bending of the pipe.

During the last decades several experimental tests have been carried out in order to better understand the behaviour of concrete coated pipelines in pure bending (Jirsa et al. (1969), Mogbo et al. (1971), Archer and Adams (1983), Akten et al. (1985), Lund et al. (1993)). The main characteristics described in these papers can be summarized as follows:

- The pipeline is discontinuously concrete coated, which introduces strain concentrations at the field joints. Small shear strength in the anti-corrosion layer implies weak bond between the steel pipe and the concrete coating. Bending of the pipeline implies sliding between the steel and the concrete.

- The shear strength of the corrosion layer is dependent on the material used. Asphalt and epoxy are the most commonly used anti-corrosion layers. The shear strength, τ, is in the range 0.1 to 0.2 MPa or in the range 0.0 to 0.1 MPa for asphalt and epoxy, respectively. The true shear strength increases considerably if methods to prevent sliding are used.

- The strain concentrations at the field joints are dependent on the temperature and the time it takes to deform the pipe since the anti-corrosion material is visco-elastic.

- Analytically the problem is difficult to model, especially when the strains in the field joint enter the nonlinear area.

The experimental tests have shown that the physical behaviour of a concrete coated pipeline exposed to pure bending is complex. Many different parameters are of great influence on the behaviour, e.g. time used for performing the test, temperature, concrete cracking. However, the test-results do not give unique answers to important questions like the effect of the material properties of the anti-corrosion coating.

Experimental tests are therefore still necessary in order to establish a deeper understanding of the physical behaviour. At the same time it will be of great advantage if one is able to develop numerical models which predict the test results.

In this chapter a numerical model is established in order to develop an equation which predict the strain concentration for a pipeline being bent over the stinger during laying. The FE analysis in this chapter is based on Endal (1993), which was partly supervised by the author.

The strain concentration found in this Chapter will be taken into account when the load effect is calculated and the subsequent reliability analysis is performed in Chapter 6.

4.2 Numerical modelling

The problem of a coated pipeline is very complex, three material properties are involved and interact. Numerical modelling of the physical problem requires a program which allows for proper modelling of nonlinear material steel property, concrete cracking and slipping between steel and concrete.

The numerical study is based on the nonlinear finite element program DIANA (1992).

4.2.1 Finite element model

The pipeline is welded together of sections of 12 m length, at each end of the sections a 0.35 m long end is uncoated. Only one half of a 12m-section is modelled due to symmetry during uniform bending and due to small shear transfer capacity of the anti-corrosion coating which imply no strain concentration in the area where the concrete coating is ended. The finite element model is shown in Figure 4.2. The pipe is fixed at the left end (cross section deformation still possible), and a bending moment is applied at the opposite end.

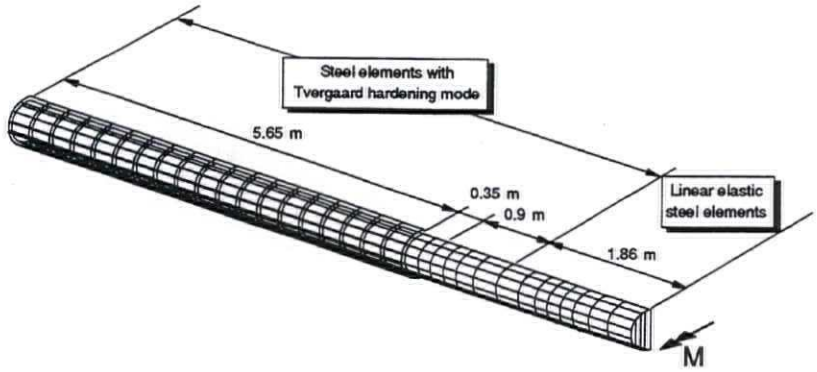

Figure 4.2 The finite element model

4.2.2 Elements

Steel

Curved shell element CQ40S is used for the steel pipe, eight nodes serendip element with five degrees of freedom at each node. The element is used due to a large length/width ration and the 8-nodes element present a linear variation of stress and strain within each element, compared to a 4-nodes when the stress and strain are constant over the element length. This shell element formulation is based on plane stress condition ($\sigma_{zz} = 0$) and quadratic isoparametric interpolation. To avoid 'shear locking' a 2*2 Gauss-integration is used (one time under-integration).

Concrete / Reinforcement

Shell element CQ40S is also used for the concrete coating. Reinforcement is modelled as embedded in the concrete elements, the so-called mother elements. The strains are computed from the displacement field of the mother element. This implies perfect bond between the reinforcement and the surrounding material.

Corrosion Coating

The shell elements are interconnected by the use of an interface-element (CQ48I) with specified bond-slip material properties to model the anti-corrosion coating (asphalt) and the slipping between the steel pipe and the concrete coating. These elements describe the interface between two planes in 3-D configuration in terms of a relation between the normal and the shear traction and the normal and shear relative displacement across the interface. The formulation of the plane interface elements are fully isoparametric. Quadratic interpolation and Newton-Cotes integration scheme is used, where the interpolation points are located in the nodes. The interface elements have only translation as degree of freedom.

4.2.3 Material models

Steel

Tvergaard material model is used in this study, for further details see Eq. A5 in Appendix A.

Concrete / Reinforcement

Concrete is a composite material. The physical behaviour is complex and depend very much on how the concrete is prepared, e.g. water-cement ratio and concrete strength. Drücker-Prager material model is used for the concrete modelling. The Drücker-Prager criterion, formulated in 1952, is a

simplified modification of the von Mises criterion, where the influence of hydrostatic stress component on failure is introduced by inclusion of an additional term in the von Mises expression. The failure surface in the principal space is a right-circular cone, Chen et al (1987), as shown in Figure 4.3.

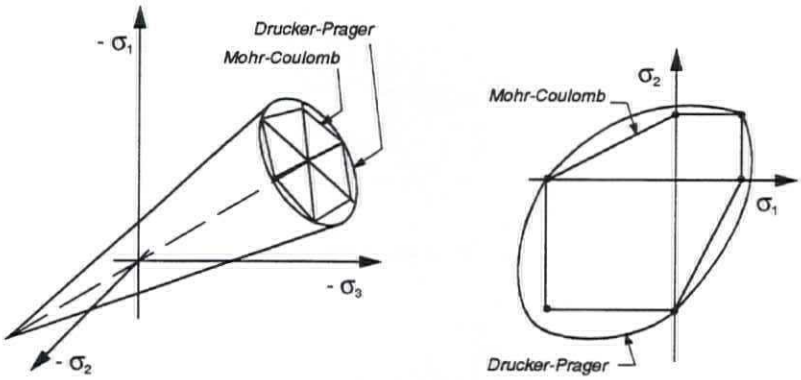

Figure 4.3 Drücker-Prager material model

The concrete is modelled with a uniaxial compressive strength equal to 40 MPa and a friction angle equal to 30°. Cracking is specified as constant tension cut-off, linear tension softening and constant shear retention. The model is shown in Figure 4.4.

The embedded reinforcement is modelled as Von Mises yield-criteria, the yield stress is defined equal to 500 Mpa.

Corrosion Coating

The bond-slip model set a nonlinear relation between the shear traction t_t and the shear slip δu_t. Shear relations for positive and negative values of slip are equal. Specification is done in an absolute sense, i.e. refers to the positive part of the diagram, Figure 4.5. The shear traction is independent of the normal traction t_n, i.e. no 'friction-effect'.

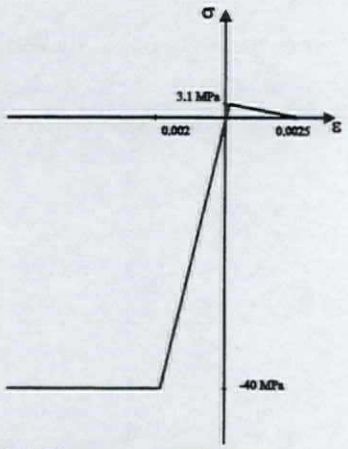

Figure 4.4 Concrete material model

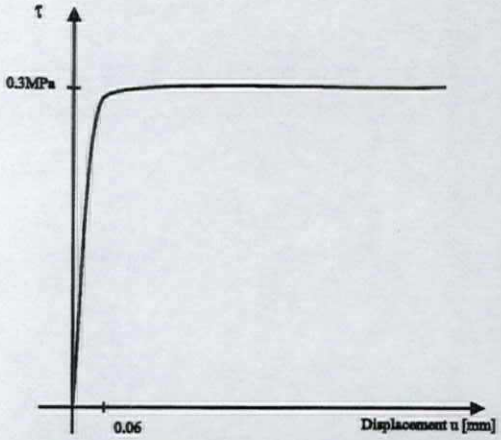

Figure 4.5 Corrosion coating material model, Bond-slip

4.2.4 Bending the pipe

A deformation-controlled loading is used. At the end of the model 3 noded beam element is used, where one of the nodes is located at the neutral axis (Master node) and the other nodes (Slave nodes) are connected to the top and bottom of the pipe model, as shown in Figure 4.6. The master node is rotated about z-axis and the end plane is corresponding rotated. This element rotation is a non-conservative approach. In order to trace the bending moment level easily, linear elastic elements are used at the right end. At the end where the bending moment is introduced, the pipe is further elongated in order to avoid end-effects in the field joint area.

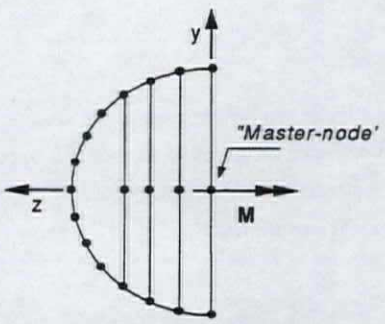

Figure 4.6 End-plane of FE-model, location of Master node.

4.2.5 Compromises and problems in the modelling

Some simplifications are made in the numerical modelling. The material properties of the anti-corrosion coating are idealized by a linearly elastic-perfect plastic bond-slip model. However, experimentally the material properties are found to be visco-elastic. The shear transfer capacity of the anti-corrosion coating is also idealized as being independent of the contact pressure (no `friction-effect').

In addition, it is experienced that numerical convergence or divergence is very dependent on the normal stiffness of the interface element. It is often necessary to calibrate the normal stiffness when analysing a new case in order to obtain convergence.

One should also keep in mind that the pipe in the numerical model is exposed to pure bending (constant moment along the pipe). This is an idealization of the situation on the lay barge stinger. In reality, discontinuous concrete coating results in non-uniform stiffness along the pipe. Furthermore, roller supports on the stinger result in peaks of the moment level at every roller support, as shown in Figure 4.7. However, in this numerical study these two effects are neglected.

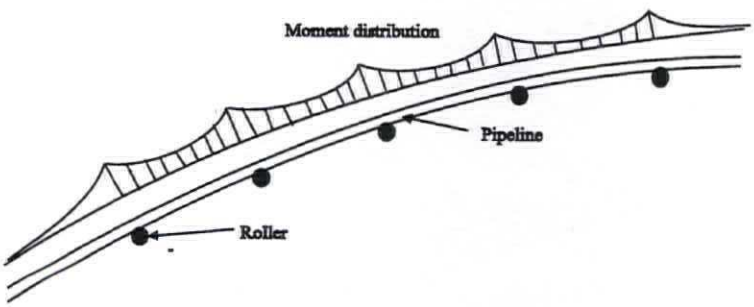

Figure 4.7 Bending moment distribution over stinger

4.3 Numerical results

4.3.1 Base case vs. uncoated pipe

A pipeline with outer diameter equal to 20" is used as base case in the present study. 20" pipeline is frequently used as transportation system for oil and gas in the North Sea, Robertson et al (1995). Data for the base case 20" pipe are given in Table 4.1.

The results from the numerical study are taken from several points along the pipeline (x1-x9), as shown in Figure 4.8.

Table 4.1 Data for Base Case

Steel	Outer diameter	508 mm
	Wall thickness	17.9 mm
	Yield strength	448 MPa
	Nominal length	12.0 m
Anti-corrosion coating	Thickness	6 mm
	Shear transfer capacity	0.3 MPa
Concrete	Thickness	80 mm
	Compressive strength	40 MPa
	Tension strength	3.1 MPa
	Nominal length	11.3 m
Reinforcement	Hoop direction, t_{eq} [1]	0.45 %
	Axial direction, t_{eq}	0.01 %

[1] teq = 0.45 % means that the equivalent thickness of the reinforcement equals 0.45 % of the concrete thickness.

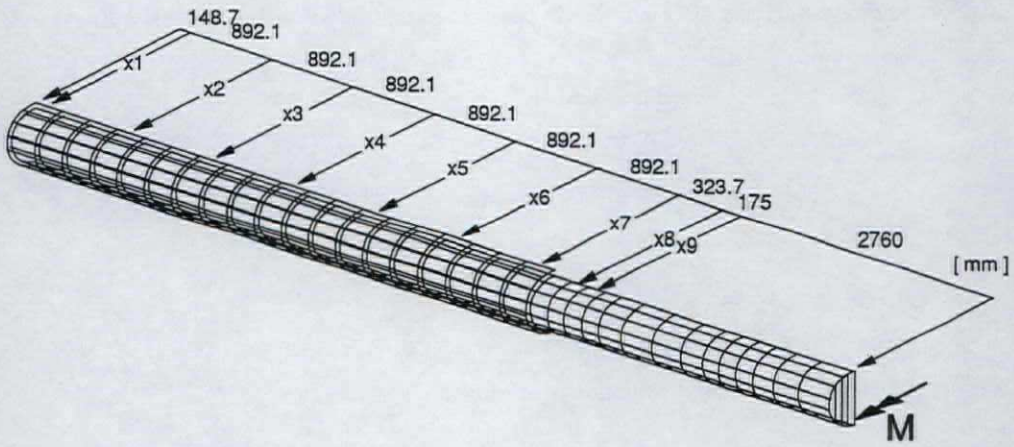

Figure 4.8 FE-Model including location of result- presentation

Figure 4.9 shows moment-global curvature relationship for the coated pipe specified in Table 4.1 and for a uncoated steel pipe. The pipeline with concrete coating is somewhat stiffer than the uncoated pipeline. The behaviour of the concrete coated pipe can be divided into three main phases: Initially, the pipe is very stiff, but at M ≈ 0.22 MNm the concrete cracked on the tension side, and the structure softened. An almost linear relationship is experienced until the third phase is reached at M ≈ 1.3 MNm. The steel now entered into the non-linear area, and the slope of the curve decreased.

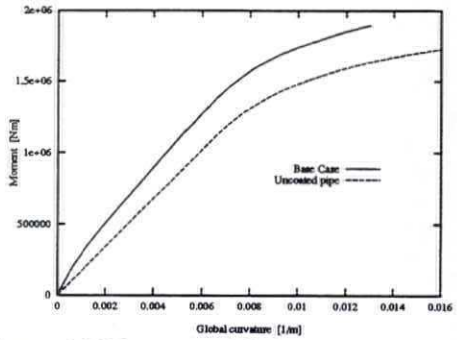

Figure 4.9 Moment - global curvature

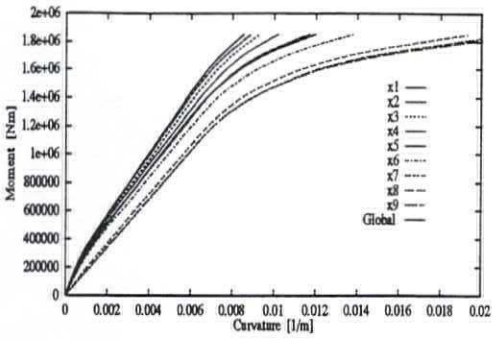

Figure 4.10 Local and global moment - curvature

Figure 4.10 shows moment versus local curvature in the points marked x1 - x9 in Figure 4.8. The global moment-curvature relationship is also shown, and this curve lies in between the local curves. It is seen that the pipe becomes gradually less stiff as one moves towards the field joint. The moment-curvature for location x9 (field point) coincides with the moment-curvature for a uncoated pipeline, Figure 4.9, which means no strain concentration due to change in thickness where the concrete coating ends. The distribution is similar for the steel compressive strains along the pipeline. But at the tension side the curves are much more gathered than on the compression side. This is due to the concrete contribution to the stiffness being larger on the compression side than on the tension side of the pipe (after cracking of the concrete on the tension side).

Figure 4.11 shows the ovalization at the field joint as a function of the global curvature of the pipe. The ovalization of an uncoated pipe is also presented. It is seen that the field joint experiences larger ovalization than an uncoated pipe when the global curvature is equal. This is natural, since the concrete coated pipe needs a larger moment in order to obtain the same global deformation as an uncoated pipe.

Figure 4.12 shows the sliding of the concrete coating (location x7) relative to the steel pipe in the field joint area. Positive sliding means that the concrete moves towards the field joint. It is seen from Figure 4.12 that the concrete slides monotonicly in the positive direction at the compressive side of the pipe, while on the tension side it initially slides in the negative direction (ca. 0.3mm), but later on changes direction so that the concrete at the tension side also slides towards the field joint. This change of direction is mainly due to the concrete coating being continuous in the hoop direction. As the positive sliding increases on the compression side, the tension side is dragged along. Concrete cracking on the tension side amplifies this tendency.

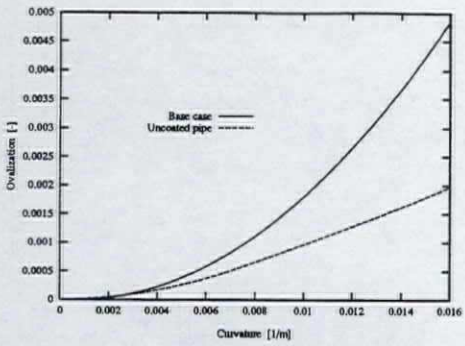

Figure 4.11 Ovalisation at field joint

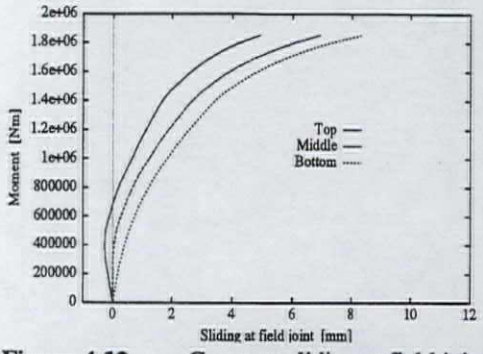

Figure 4.12 Concrete sliding at field joint

4.3.2 Validation of the model

The numerical study of the strain concentration in the field joint was made in front of a bending test performed by Statoil in 1994, Verley (1995). The FE-model was not verified during the analysis, due to lack of reliable data. The FE-model and material model have been validated according to these bending tests.

Figure 4.13 show the stress-strain curve from tests which are calculated from the moment-curvature curve in the field joint during bending tests. The curves represent probably a more accurate stress-strain relation than predicted by a few coupon, Verley et al (1995). In the tests a material grade X60 is used, where the expected yield stress is about 10% higher than the characteristic value. The material model used in FE-model, underestimate slightly the yield stress and the strain hardening. Figure 4.14 shows that the asphalt corrosion coating in the tests have a shear strength of 0.42-0.55MPa. The behaviour of the anti-corrosion in the FE-model is idealized as elastic-perfect plastic. The tests show that the FE-model is too stiff, but when the maximum capacity is achieved the behaviour is perfect plastic as the FE-model. This idealization may underestimate the sliding in the initial bending, but not affect the sliding when maximum shear strength is achieved. The parameter study will cover the range of maximum capacity.

The moment-global curvature is compared with Test 2 of the bending tests. The FE-model and Test 2 are in very good agreement, as shown in Figure 4.15 , the FE-model may be some stiffer when the moment come into the plastic region. The FE-model is quite similar to the test model with respect to D_0/t, concrete thickness and material properties.

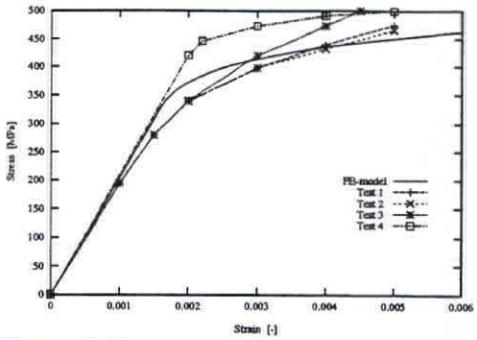

Figure 4.13 Validation of material model, Steel

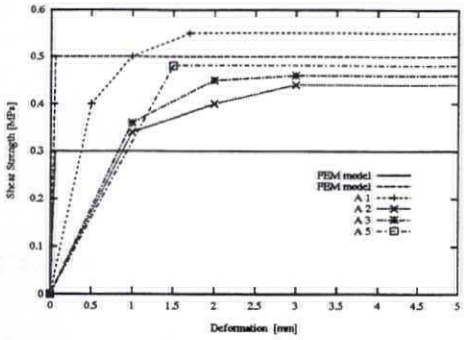

Figure 4.14 Validation of material model, corrosion coating

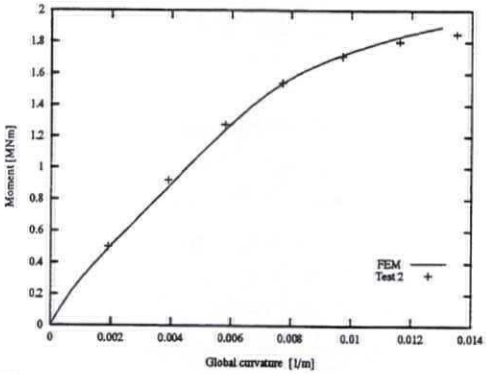

Figure 4.15 Validation of FE-model

4.4 Strain concentration model

A simplified strain concentration model is established based on results from a parametric study. The parameters considered have been varied sequentially within their predefined variation ranges keeping the other parameters at base case values. It is noted that the parameter studies are limited in the following range:

Concrete thickness; $40 < CT < 120$, diameter to thickness ratio; $23 < D/t < 35$, shear strength ; $0.1 < \tau < 0.5$, reinforcement along the pipe; $0.01 <$ % of CT < 2.0, reinforcement hoop direction; $0.01 <$ % of CT < 2.0.

Parametric studies on the amount of reinforcement showed that the strain concentration factor is practically independent of the reinforcement in the hoop direction, but increased with increasing amount of longitudinal reinforcement. This effect, however, is negligible since longitudinal reinforcement for all practical cases is limited.

Results from the parametric study will be presented as an equation in terms of the strain concentration factor C and the nominal strain ε_{norm}, where ε_{norm} = nominal strain defined as maximum strain for a bare steel pipe during bending. This means that :

$$\varepsilon_{norm} = \frac{r_{mean}}{R} \tag{4.1}$$

where

r_{mean} = mean radius of the steel pipe, (D-t)/2.
R = global curvature radius.

The strain concentration factor, C, is defined as:

$$C = \frac{maximum\ field\ joint\ strain}{\varepsilon_{norm}} \tag{4.2}$$

The strain concentration is large at the starting of bending due to the stiffness contribution from the concrete is intact before the concrete cracking, as shown in Figure 4.9. The cause for a decreasing C after cracking may be explained in Figure 4.9. The moment curvature curve for "Base Case" after cracking is practically parallel to the curve for uncoated pipe. This implies that the relative difference in stiffness is decreasing with increased moment and this means that the relative difference in strain is decreasing (<=> C is decreasing for increase ε_{norm}). This trend will continue until the strain in the field joint will extend to the nonlinear area, and a minimum point is obtained.

4.4.1 Equations

The equation outlined in the following is limited to a 20" pipeline, material grade X60, concrete thickness; $40 < CT < 120$, diameter to thickness ratio; $23 < D/t < 35$ and shear strength ; $0.1 < \tau < 0.5$.

The strain concentration follow an negative exponential function when starting bending the pipeline and further will the strain concentration increase linear. A trial-and-error approach is applied to find the optimal coefficients in the equation. From the numerical parametric studies, the following equation can be made.

$$C = ae^{-b\frac{\varepsilon}{0.0015}} + c\left(\frac{\varepsilon}{0.0015}\right) \tag{4.3}$$

where

$$a = (1 + 0.0031 CT^{1.3}) \cdot (0.687 + 0.011 D_0/t) \cdot (0.934 + 0.220\tau) \tag{4.4}$$

$$b = 0.138 \cdot CT^{0.6} \cdot \tau^{0.2} \tag{4.5}$$

$$c = 0.144 \cdot CT^{0.5} \cdot (0.75 + 0.009 D_0/t) \cdot \tau^{0.3} \tag{4.6}$$

CT : Concrete coating [mm]
τ : Shear strength [MPa]
D_0/t : Diameter-thickness ratio

Figure 4.16 shows the strain concentration factor C as a function of the nominal strain and the concrete thickness. For the uncoated steel pipe, C = 1. As seen in Figure 4.16 the strain concentration factor is strongly dependent on the concrete thickness. During installation of offshore pipelines the field joint strains are kept in the elastic range or slightly into the plastic range. In Figure 4.16, the most interesting value of C is thus the minimum one.

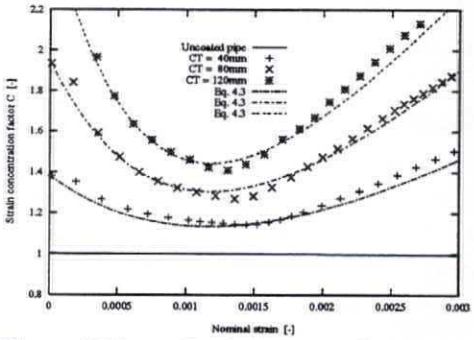

Figure 4.16 Strain concentration, effect of concrete thickness

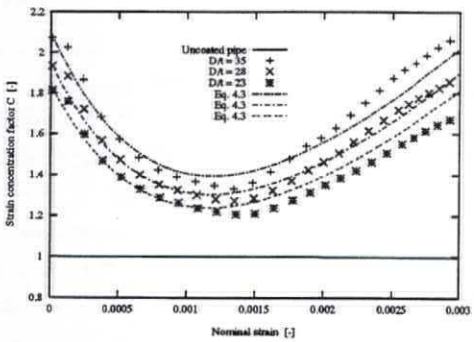

Figure 4.17 Strain concentration, effect of D/t

Figure 4.17 shows the dependency of C on the D_0/t-ratio. As seen in the figure the concrete is of greater significance as the D_0/t-ratio is increased. This is to be expected, since the concrete then represents a relatively larger contribution to the total stiffness.

Figure 4.18 shows C as a function of the nominal strain and the shear transfer capacity of the anti-corrosion coating. As seen from the figure the strain concentration factor changes considerably as the shear strength varies from 0.1MPa to 0.5MPa. Experimental tests of the anti-corrosion layer properties have shown that the average shear transfer capacity is within the range 0.1MPa to 0.5MPa, Lund et al. (1993), Verley et al (1995) .

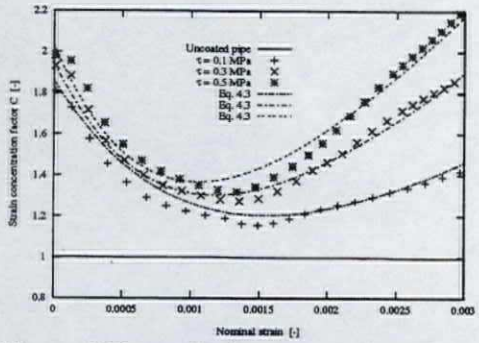

Figure 4.18 Strain concentration, effect of shear strength

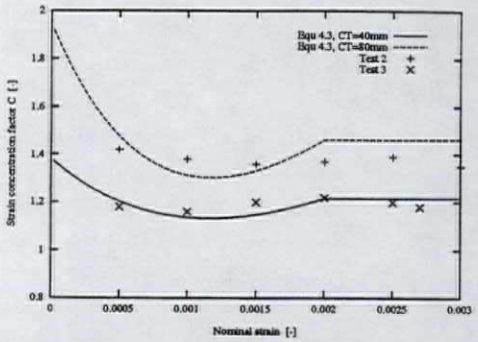

Figure 4.19 Validation of strain concentration

4.4.2 Equation vs test results

The numerical model show that the strain concentration in the field joint is very dependent on the shear strength of the anti-corrosion coating, the concrete coating thickness and the D_o/t ratio. The strain concentration have been validated and modified according to test and analytical results, Verley et al (1995), Ness et al (1995). The strain concentration is compared with test results for different concrete thickness, 40 and 80 mm, Figure 4.19. The strain concentration is held constant for the nominal strain of 0.002, since the numerical model does not include crushing of the concrete. This crushing is predicted to occur at a nominal strain of 0.002, Ness et al (1995). The agreement between tests and FE-model seems to be good for the two concrete thicknesses.

For practical purposes a constant strain concentration should be used, but the strain concentration should vary dependent on the shear strength of the anti-corrosion coating, the concrete coating thickness and the D_o/t ratio.

4.5 Model uncertainty

The test results show variation due to concrete thickness but a smaller variation of the strain concentration than the numerical results predict during bending of the pipeline. For practical use a constant strain concentration for a given concrete thickness will be used for the reliability analysis. Bias and the CoV the test results are given in Table 4.2.

Table 4.2 Model uncertainty for strain concentration

Case	Bias	CoV
Test 2 / 1.4	0.981	0.03
Test 3 / 1.2	0.990	0.02

5 LOAD EFFECTS AND RESPONSE SURFACES

5.1 General remarks

Different technologies and equipments are adopted to install marine pipelines. The pipeline is welded offshore on location or the pipeline is welded onshore and then transported to the offshore site.

The S-lay and J-lay methods fall into the first group. S-lay, J-lay and Reel-lay experience differences in the loading as far as the upper end is concerned due to the differences in laying equipment and procedures, Figure 5.1.

S-lay is applied to lay the vast majority of large diameter (larger than 16 in) pipelines in the North Sea as well as in the Sicily Channel. The maximum depth is governed by tension capacity, the stinger length, curvature and tip slope.

The near-horizontal ramp includes welding stations, one or more tensioners, a non-destructive-test station and field joint stations, where girth welds are coated and concrete coated joints filled in. A stinger bear the pipe through rollers adequately spaced for a certain length and curvature to the tip, where the slope ensures a smooth departure from the supports.

Once welded, the pipe is fed into the sea by moving the vessel towards on its anchors. Dynamic positioning is adopted to help or even substitute the mooring lines. The stinger radius controls the overbend curvature and the sagbend curvature is controlled by the tension applied to the pipe by tensioners on the barge. The required tension depends on the water depth, the submerged weight of the pipe, the allowable radius of curvature at the overbend and the allowable stress at the sagbend. The pipeline is generally in a state of residual tension as it reaches the seabed.

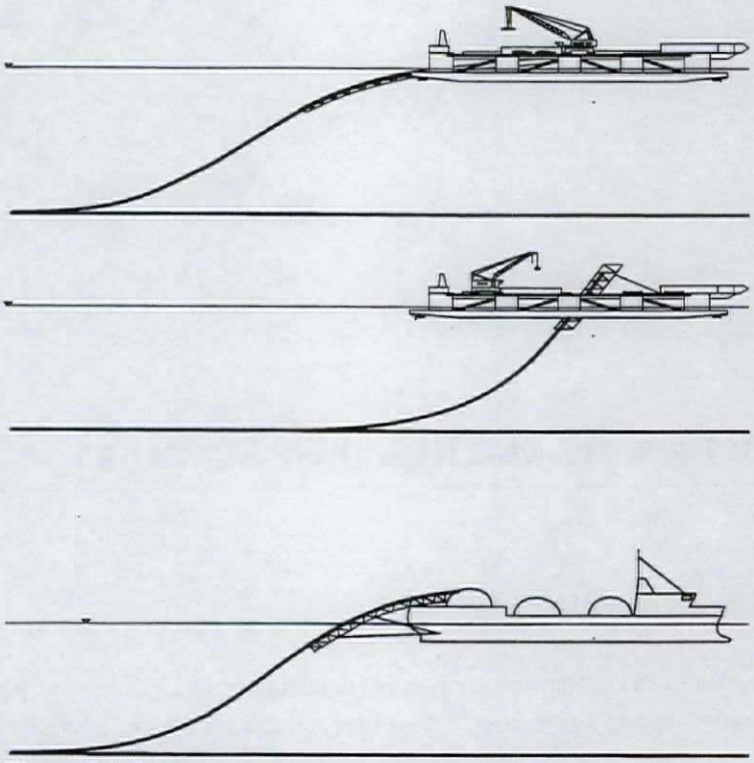

Figure 5.1 S-lay, J-lay and reeling configurations

The J-lay method is a method presently being developed for very deep waters. The J-configuration is achieved by lowering the pipe almost vertically into the water, thus totally eliminating the curvature required on overbend and supplied by the stinger. The J-lay method allows pipelaying at much lower tensions, to control the state of stress on the sagbend. Further residual lay tension on the seabed after J-lay can be negligible compared to the S-lay method. Dynamic positioning must be used to keep the J-lay barge on course.

The reel barge method, which fall into the second group, consists of spooling the pipe into a large reel. The reel barge then proceeds to the offshore installation site and unspool the pipe and lay it on the seabed. A tensioner and a straightener on the stern ramp to annul the reeling curvature and to control the lay span. Another methods which fall into the second group, includes the tow methods: surface tow, controlled-depth tow and bottom tow. These three methods require onshore assembly of pipe into long strings. Once the pipe string is fabricated then it is towed directly to the offshore installation site. The three methods differ in the buoyancy/weight preparation of the pipe strings and in the manner of towing and connecting the pipe strings in the field.

The S-lay method of lay operation will be consider in the succeeding pages.The mechanics of loading and the uncertainties related to lay operations will be discussed in Chapter 5.2.

The maximum load effect is calculated for extreme sea state for the lay operation. The load effect is calculated in two ways, first using a nominal case and complementary experiments where only one of the variables has been given a different value from the nominal one. Second using randomizing the variables and calculate the load effect for several sets of experiments. The maximum load effect is given as response surfaces. The assessment of the load effect is described in succeeding pages in Chapter 5.3. The load effect given as response surfaces will be used in the reliability analysis in Chapter 6.

5.2 Mechanics of loading

In general, the term "load effect" denotes any kind of response of a structure subjected to given loading. In the pipelaying case, the loading consists of direct hydrodynamic forces, forced end displacements (from lay vessel motions) and discrete support forces. The pipeline response from this loading, e.g. bending moments, axial forces and shear forces, make the *load effects*.

The most appropriate representation of the load effects depends on the configuration of the pipesection. A displacement controlled situation is defined for a pipe section for which curvature and configuration is governed by the stinger properties; stinger radius, relative length of the stinger and roller positions/properties.The pipeline is in a displacement controlled situation at the upper part of the stinger, while the pipeline is in a load controlled situation at the lower part of the stinger since no contact is allowable for the pipeline and the last roller. A load controlled situation is defined for a pipe section which curvature is controlled by the loads, as sections at the sagbend the bending moment is directly related to the 'live' loads acting along the pipeline.

Load and load effects are classified as functional and environmental categories, where the functional load effect is a static configuration while the environmental load effect is related to the dynamic behaviour.

The following parameters govern the static configuration :

- applied lay vessel tension
- stinger geometry (radius, length) and roller positions
- lift-off (departure angle) from the supporting means on the lay vessel
- pipe characteristics (weight and bending stiffness)
- water depth

All factors mentioned above are governing for the static as well as the dynamic load effects. In the dynamic case, additional factors are:

- the sea state (H_S,T_P) and it frequency content (short or long crested seas)
- the lay vessel response to wave excitation (Response Amplitude Operators)
- the tensioner position and working characteristics

So far the factors controlling the *global* behaviour of the pipeline are presented. The previous chapter

showed an additional factor that affect the load effects *locally*.The presence of discontinuous concrete coating and/or buckle arrestors may cause a concentration of deformation in the parts of the pipeline having lower bending stiffness (e.g. the field joints) than in the nominal case, considering constant stiffness along the pipe.

5.2.1 Assessment of load effects

Assessment of load effects in the installation phase is an important part in pipeline design and specification of installation procedures. In the following a brief description of the steps to be undertaken in such a process is given, considering the S-lay method, see Figure 5.2

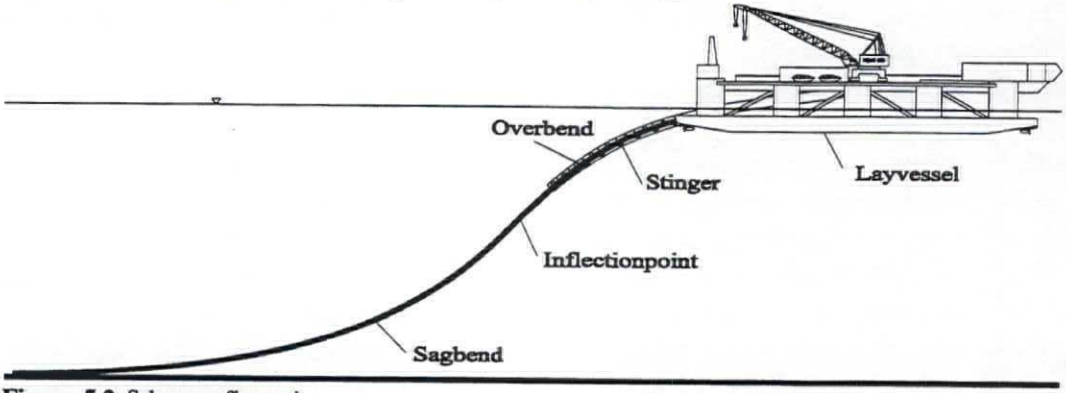

Figure 5.2 S-lay configuration

Assessment of the pipeline installation procedure starts with the identification of maximum layable weight versus the water depth and the stinger length. Limitations are applied on the resulting stress/strain levels, for example, on the maximum bending strain occurring along the pipe section supported by the stinger, or on the maximum equivalent stress along the sagbend.

The calculation of maximum static load effects is usually performed setting the stinger/roller system to have supporting points along a predefined radius. The pulling force at the tensioner or at the sea bottom and the roller positions are then adjusted to give well distributed contact (reactions) on the pipeline.

The numerical assessment of the pipeline *static* equilibrium configuration and corresponding stresses/strains can be achieved using large displacement-rotation theory of deflected beams. The problem can be considered three-dimensional or two-dimensional (vertical plane only); the latter being more rapid and of general use, provided that the envisaged route is almost rectilinear and cross currents are negligible. Numerical methods based on the finite element formulation are usually preferred, however analytical methods have also been developed. The finite element approach consists of a stepwise determination of the deflected pipe shape; the pipeline is subdivided into finite elements with an assumed initial configuration. The tension, weight and buoyancy are then gradually applied.

The numerical calculation results in a global bending moment or bending strain which:

- in the overbend is directly related to the radius of the stinger
- in the sagbend depends on the equilibrium condition achieved by the suspended span under the action of the pipe weight, pulling force and lift-off angle on the stinger.

Local load effects caused by contact forces and/or differential bending stiffness are then superimposed to the effects from global bending of the pipeline. Alternatively, local effects can be taken into account in the assessment through a proper modelling of the pipe sections with different bending stiffness.

Dynamic pipelay analysis is necessary as the lay vessel and the suspended span are subjected to hydrodynamic loading from waves. The dynamic behaviour of a pipeline during installation is mainly related to the response of the lay vessel to wave action; the pipe is supported down to a certain water depth by the stinger/lay ramp, and the effects of direct wave action on the pipeline can be considered of minor importance, Lund (1993).

Wave direction with respect to the lay heading will influence the pipe dynamic behaviour due to the dependency to lay vessel response. Pitch motion of the lay vessel gives the largest dynamic excitation on the pipeline, and consequently head/stern sea will represent the worst case. In shallow water, surge motion of the lay vessel may also give large dynamic excitation.

Dynamic excitation due to vortex shedding may have important effects upon the pipe in some particular situations with strong currents and deep water depths.

Calculation of the dynamic behaviour of a pipeline during laying involves a number of non-linearities:

- contact between pipe and stinger/lay ramp in the overbend
- a tensioner working inside a working range
- fluid-pipe interaction (minor importance)
- non-linear pipe sectional behaviour
- geometric stiffness from axial tension

Different procedures to perform a dynamic analysis are outlined below:

- A regular wave approach, where the load effect is calculated for a single regular wave with a characteristic height and an associated wave period. A characteristic wave height to be used can be defined as e.g. the largest expected wave occurring in a 3-hour seastate, H_{max}. The associated period may be varied over an interval to cover of all realistic wave conditions. In general, the results from this approach will give conservative results.

- A linearized approach, where the pipe response function is defined. Such a function gives the amplitude of any dynamic response parameter for a unit wave height and wave periods within a certain range. The pipe response operator is then combined with a given sea-state spectrum, giving the corresponding response spectrum. The response spectrum contains all the necessary information to estimate response statistics. The performance of this approach is very efficient, but does not include the nonlinearities discussed previous.

- A complete irregular time-domain approach, where the dynamic response is calculated for a sequence of irregular waves with a certain duration (e.g. 3-hours). The analysis is performed for a series of wave sequences, and the maximum response from each sequence forms the basis for a statistical analysis. Then, the expected peak response (in terms of load effects) for the selected sea state (e.g. storm of a certain duration), including all nonlinear effects can be predicted. Time-domain approach is very time-consuming, but an efficient method has been used by Passano (1995) for risers and will also be applied in this study. This method needs both linearized and nonlinear analysis and is explained in Chapter 5.2.3.

The limiting seastate must be related to the operational weather window. The relationship between the limiting seastate and the weather window is given by in site wave measurements for the relevant laying period (scatter diagram).

5.2.2 Structural modelling and response calculation

The load effect analysis for pipelaying is performed by use of the FEM program LAYFLEX (1994). LAYFLEX is a tailor-made computer program system for static and dynamic analysis of pipelines during lay operations. The basis for LAYFLEX is the RIFLEX Program System (1995), which was originally designed for non-linear static and dynamic analysis of flexible riser systems.

LAYFLEX is based on a Finite Element Method formulation allowing large displacements and rotations based on 3-D beam elements. In order to handle the large displacement and rotations found in marine pipelines a beam element without any displacement limitations is used. This is achieved by using the co-rotated ghost reference system and a Bernoulli-Euler beam element.

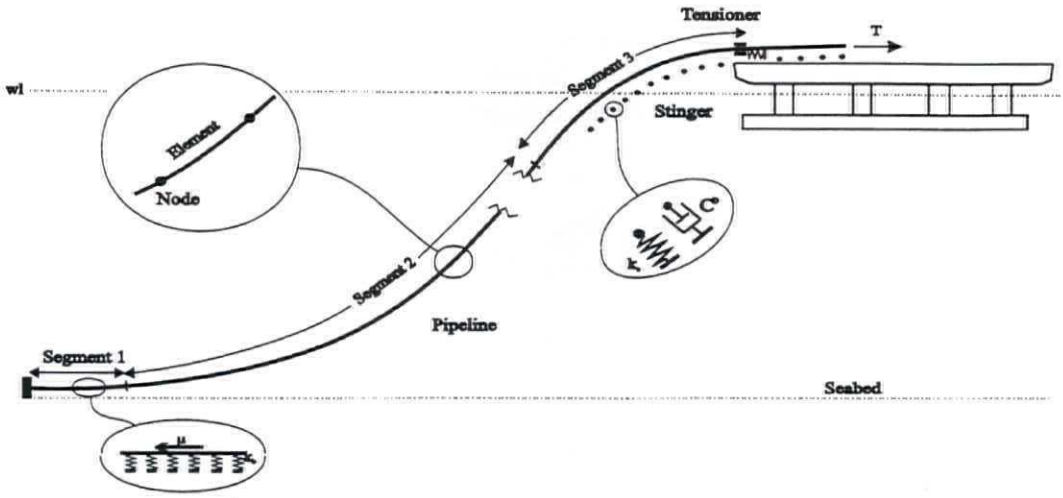

Figure 5.3 FE-model for S-lay configuration

The pipeline system is shown in Figure 5.3 and modelled in the following way:

The seafloor contact is modelled as a tangent plane specification with vertical bi-linear springs and horizontal friction forces in the axial and the lateral directions. The stiffness matrix will normally be re-established at each step and iteration in the time domain analysis. Nodes may therefore obtain or loose seafloor contact, and sliding behaviour is included. The interaction forces are introduced into the unbalanced force vector during equilibrium iterations.

The Pipeline is composed of several segments. Each segment has uniform cross section properties.

Cross section properties are specified in terms of area, mass and stiffness. Rotation symmetric cross section is used. Structural response is always computed as global deformations and stress resultants (axial force, moments). Cross-sections are modelled with 12 DOF beam elements. Nonlinear cross section behaviour is modelled by introducing nonlinear relations between global deformation parameters and stress resultants, i.e. axial force versus axial elongation, bending moment versus curvature and torsional moment versus twist angle. The pipeline is described as homogenous, and possible differential bending stiffness along the pipeline is not considered in the FE-analysis.

Stinger The stinger is modelled as a structure with rollers with stiffness and damping properties. The contact between the pipeline and the rollers are modelled by nonlinear springs and dash pot dampers. Possible frictional forces are not included. The contact force is assumed to act normal to the pipe and the roller. It is treated as a discrete element load acting on the pipe, while the contact force acting on the roller is transferred as a nodal load to the stinger.

During nonlinear analysis the computation of the contact force is based on the relative positions between the pipe and the roller and the roller stiffness characteristics. In addition, the incremental stiffness relation of the contact force contributes to the system stiffness. The incremental stiffness relation consists of a term associated with the roller spring stiffness and terms corresponding to change in the contact force direction at the point of attack.

Tensioner. The force from the tensioner acting on the pipe is directed along the pipe and should be within an upper and lower limit (working range). Due to possible dynamic behaviour of the lay barge and/or the pipe, the tensioner force may increase/decrease, but it will not exceed the upper limit nor decrease below the lower limit. Between the upper and lower limit the tensioner is described as a linear spring having a relatively large stiffness.

During static analysis, a constant tensioner force directed along the pipe is applied. This force is within the upper and the lower limit.

In nonlinear dynamic analysis the tensioner is modelled by the actual tensioner force (static value) and incremental stiffness based on the tensioner spring stiffness. The working range setting is ±10% in which the pipeline is kept in an approximately fixed position to the lay vessel. Outside the working range, the pipeline is free to move with an applied tension according to the working range limits, shown in Figure 5.4.

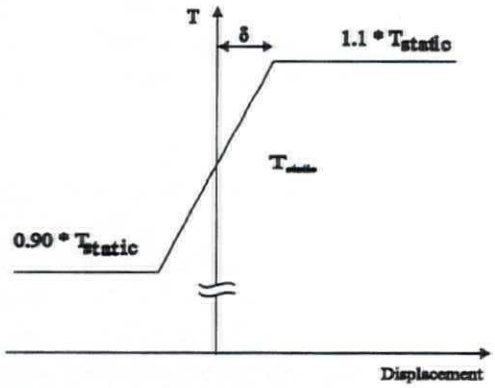

Figure 5.4 Tensioner characteristics

Hydrodynamic load models

Hydrostatic pressure effects on marine risers have been discussed by several authors in the open literature, e.g. Morgan and Peret (1974), Sparks (1984). This discussion normally involves the following notions that need to be defined.

- Effective tension: force in the pipe that affects stability. This force is relevant for governing the shape of cables and pipes, including buckling analysis, and is used for calculation of geometric

stiffness in the finite element method.

- Axial stress resultant: force found by integrating normal stresses over the cross section. In the presence of external hydrostatic pressure this force is different from the effective tension.

In LAYFLEX hydrostatic effects is modelled by conservative, vertical forces. No hydrostatic force variation is accounted for caused by deformations, except for possible increase or decrease of submerged volume and wetted pipe surface at the sea surface. These forces are in equilibrium with the effective tension, which implies that axial stresses need not necessarily be calculated during an iteration for equilibrium. The theoretical foundation for this way of modelling hydrostatic forces is given by Sparks (1984).

Hydrostatic pressure is therefore treated in terms of effective weight and effective tension defined as:

$$w = m_p g - A_e \rho g + A_i \rho_i g \tag{5.1}$$

$$T = T_p + A_e P_e - A_i P_i \tag{5.2}$$

where

T - effective tension
T_p - tension in pipe wall, i.e. resulting force from normal stresses
A_e, A_i - external/internal cross sectional area
P_e, P_i - external/internal hydrostatic pressure
w - effective weight per unit length, i.e. submerged weight of pipe including content
m_p - mass of pipe per unit length
ρ_i - density of internal fluid
ρ - water density
g - acceleration of gravity

Hydrodynamic forces are dependent on wave, current and structure motions. The wave elevation is desribed by the spectral formulation. An irregular sea state is described by Jonswap standard wave spectrum.

In order to generate time series of surface elevation, water particle velocities and accelerations, the short crested irregular sea is discretized into a set of harmonic components. Fast Fourier Transformation is used. Times series of wave particle velocity and acceleration are calculated at specific position along all loaded elements using Airy wave theory.

The current velocity is normally assumed to be constant with time. The current velocity at a given

position is described by the speed and the direction. It is done by input of discrete values and interpolation to actual node positions or by definition of standard profiles.

The time series of wave loads are calculated by applying Morison equation.

Forced motion of line is dependent on vessel motions. The pipeline is connected to a vessel in one end. Motions of this vessel must therefore be known during a dynamic pipeline analysis. Generation of motion time series is consistent with generated time series for wave induced water particle velocities and accelerations. The rigid body motion responses comprise six degrees of freedom, surge, sway, heave, roll, pitch and yaw referred to the global (X, Y, Z)-coordinate system.

The motion model consists of a set of high-frequency (wave frequency) motions in all six degrees of freedom and a set of low-frequency motions in the three horizontal degrees of freedom: surge, sway and yaw. For most dynamic pipeline problems it is sufficient to include only the HF-motions. The effects of typical LF-motions, with periods of 60-180 s, can often be covered by suitable selection of static (mean) position.

The wave frequency-, or HF motions are treated as linear responses to the waves. Thus, the HF motions are described by a set of complex transfer functions $H_{HF_j}(\beta, \omega)$, j = 1, 2.....6 where:

$$H_{HF_j}(\beta,\omega) = \frac{x_j(\beta,\omega)}{\zeta_a(\beta,\omega)} \tag{5.3}$$

$$S_{x_j}(\beta,\omega) = |H_{HF_j}(\beta,\omega)|^2 \, S_\zeta(\beta,\omega) \tag{5.4}$$

and the motions are denoted by x. The transfer function, H_{HF}, is calculated using sink-source method for a semisubmerged lay barge.

Analysis procedures for Layflex

Static analysis.

The basis for finite element analysis is starting from stress free configuration. The incremental loading is carried out in the following sequence:

1. Volume forces (weight and buoyancy) and contact forces, (i.e. contact between elastic contact surface and pipeline)
2. Specified displacements (i.e. displacements from stress free configuration to final position of nodal points with specified boundary conditions)

3. Specified forces (nodal point loads)
4. Position dependent forces (current forces) and bottom friction.

Incrementation and iteration parameters are specified separately for each load type. Pure Newton-Raphson iteration procedure is used for each load type.

The state of the discretized finite element model is completely determined by the nodal displacement vector. The purpose of the static analysis is to determine the nodal displacement vector so that the complete system is in static equilibrium. The static equilibrium configuration is therefore found as the solution of the following system of equations

$$\boldsymbol{R}^S(\boldsymbol{r}) = \boldsymbol{R}^E(\boldsymbol{r}) \tag{5.5}$$

where

$\mathbf{r}$ - Nodal displacement vector including all degrees of freedom for the system i.e. displacements and rotations for a beam model. Both displacements and rotations are relative to the stress free reference configuration.

$\mathbf{R}^S(\mathbf{r})$- Internal structural reaction force vector found by assembly of element contributions. Contact forces are also treated as internal reaction forces.

$\mathbf{R}^E(\mathbf{r})$- External force vector accounting for specified external forces and contribution from distributed loading (i.e. weight, buoyancy and current forces) assembled from all elements.

Both internal reaction forces and external loading will in general be nonlinear functions of the nodal displacement vector. Numerically, the static equilibrium is found by application of a incremental loading procedure with equilibrium iteration at each load step (i.e. a so-called incremental-iterative procedure with Euler-Cauchy incrementation).

The basic principle in this approach is to accumulate the external loading in a number of small load increments. The static configuration at each load step is then found by iterative solution of Eq. 5.5 for the accumulated external load vector using the displacement vector from previous load increment as start solution.

Dynamic analysis

The dynamic equilibrium of a spatial discretized finite element system model can in general be expressed as:

$$\boldsymbol{R}^I(\boldsymbol{r},\ddot{\boldsymbol{r}},t) + \boldsymbol{R}^D(\boldsymbol{r},\dot{\boldsymbol{r}},t) + \boldsymbol{R}^S(\boldsymbol{r},t) = \boldsymbol{R}^E(\boldsymbol{r},\dot{\boldsymbol{r}},t) \tag{5.6}$$

where

$\boldsymbol{R}^I$ - inertia force vector
$\boldsymbol{R}^D$ - damping force vector
$\boldsymbol{R}^S$ - internal structural reaction force vector
$\boldsymbol{R}^E$ - external force vector
$\boldsymbol{r},\dot{\boldsymbol{r}},\ddot{\boldsymbol{r}}$ - structural displacement, velocity and accelerations vectors

This is a nonlinear system of differential equations due to the displacement dependencies in the inertia and the damping forces and the coupling between the external load vector and structural displacement and velocity. In addition, there is a nonlinear relationship between internal forces and displacements.

All force vectors are established by assembly of element contributions and specified discrete nodal forces. A description of the internal reaction force vector is given in the static procedure, the other terms in Eq. 5.6 are further detailed in the following.

The external force vector accounts for:

- weight and buoyancy
- forced displacements due to support vessel motions
- drag and wave acceleration terms in Morison equation
- specified discrete nodal point forces

The inertia force vector can be expressed as:

$$\boldsymbol{R}^I(\boldsymbol{r},\ddot{\boldsymbol{r}},t) = [\boldsymbol{M}^S + \boldsymbol{M}^H(\boldsymbol{r})]\ \ddot{\boldsymbol{r}} \tag{5.7}$$

where
$\boldsymbol{M}^S$ - structural mass matrix
$\boldsymbol{M}^H(\boldsymbol{r})$- displacement dependent hydrodynamic mass matrix accounting for the structural acceleration terms in the Morison equation as added mass contributions in local directions

The damping force vector is expressed as:

$$\boldsymbol{R}^D(\boldsymbol{r},\dot{\boldsymbol{r}}) = [\boldsymbol{C}^S(\boldsymbol{r}) + \boldsymbol{C}^H(\boldsymbol{r}) + \boldsymbol{C}^D(\boldsymbol{r})]\ \dot{\boldsymbol{r}} \tag{5.8}$$

where
$\boldsymbol{C}^S(\boldsymbol{r})$ - internal structural damping matrix, to account for energy dissipation in the structure itself.
$\boldsymbol{C}^H(\boldsymbol{r})$ - hydrodynamic damping matrix accounting for diffraction effects of partly submerged elements
$\boldsymbol{C}^D(\boldsymbol{r})$ - matrix of specified discrete dashpot dampers

The most important nonlinear effects that is considered in dynamic analyses are:

- Geometric stiffness (i.e. contribution from axial force to transverse stiffness).
- Nonlinear material properties.
- Hydrodynamic loading according to the generalized Morison equation expressed by relative velocities.
- Integration of loading to actual surface elevation.
- Contact problems (bottom contact, pipe/stinger contact, etc.).

The nonlinear time domain analysis technique used in the work is summaried in the following :

Step by step numerical integration (Newmark β-family) of the incremental dynamic equilibrium equations, with a Newton-Raphson type of equilibrium iteration at each time step. This approach allows for a proper treatment of all the described nonlinearities. Nonlinear dynamic analysis is, however, rather time consuming due to repeated assembly of system matrices (mass, damping and stiffness) and triangularisation during the iteration process at each time step.

5.2.3 Stochastic method description

The response of the pipeline during laying may be significantly non-Gaussian due to nonlinear structural behaviour and in a sense nonlinear hydrodynamics. Together with the stochastic nature of the environmental loads, this makes simulation of the dynamic response to irregular waves necessary for estimation of extreme response. As each simulation gives only one realization of the response, a long simulation is needed in order to limit the statistical uncertainty of the response. An efficient method for establishing the maxima of a non-Gaussian response quantity in a given seastate, originally developed for analysis of flexible risers (Passano 1995), is therefore adopted. A description of the applied method is given below.

Procedure for response estimates

The following practical estimation procedure have been adapted :

- Identify the locations in the sagbend and overbend where the most severe load effect occur.
- Define the area of the stinger where a displacement controlled response takes place.
- Decide a location (node) at the pipeline which represent a characteristic load effect for the sagbend or the overbend. A timeseries and corresponding response spectrum will be made for this location.
- Decide a practical simulation length on the basis of the complexity of the structural system and load effect level, giving sufficient confidence in the response spectrum estimation for the response quantities, such as bending moment, curvature, tension and tension strain.

- The response spectra are established for the sea states analysed, from which linear *estimates* of different response realizations (3-hours) can be generated.
- In n generated realization, the maximum response and the corresponding time of occurrence is identified.
- Then, performing a complete nonlinear time-domain simulation around this point in the corresponding wave record, a consistent prediction of the response maxima is obtained.

Verification of method

Given that the time of occurrence of the largest maxima is correctly identified, this method provides a fast and efficient method of predicting maximum dynamic response in pipelines during laying. Figure 5.5 and Figure 5.6 show a comparison between a time series Fourier transformed (FFT) from a linear response estimate and the corresponding response time series from a complete nonlinear time-domain simulation. The comparison shows conformity in determination of the time of occurrence of the largest maximum load effects.

In general, this method holds good for determination of dynamic load effects for pipelaying analysis and the method is easily applicable compared to a complete time-domain simulation.

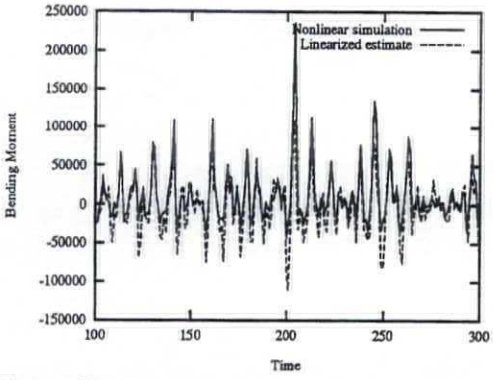

Figure 5.5 Time of occurence of maximum load effect. Nonlinear simulation vs. linear estimate, overbend

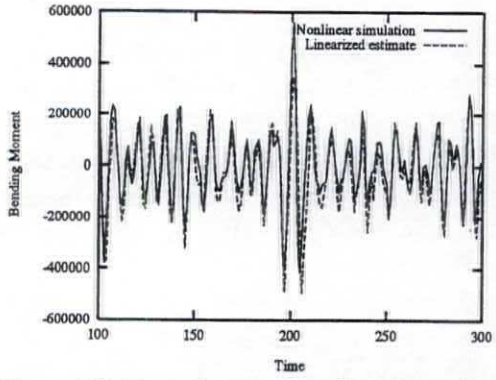

Figure 5.6 Time of occurence of maximum load effect. Nonlinear simulation vs. linear estimate, sagbend

5.2.4 Uncertainties in the load effect assessment

Structural reliability assessment should be based on a rational treatment of the uncertainties related to the physical quantities and models governing the structural behaviour and methods for predicting the safety of structural design. Concerning the design of submarine pipelines for installation subjected to vessel motions and to external wave, most of the governing variables are random quantities and

information about their probabilistic properties should be properly represented by any rational design method.

The governing uncertainties are due to:

- Pipe structural properties in terms of bending stiffness which to a certain extent will influence on the static configuration as well as dynamic response (stiffness effects)
- The pipe mass, affecting the pipeline configuration in the static case as well as dynamic response (inertia effects).
- The lay equipment, in particular the stinger (and roller) stiffness which will influence the dynamic response.
- The lay vessel behaviour, which is the main variable affecting the dynamic response
- In a given seastate, the variability in peak period T_P will affect the dynamic response, due to possible resonant phenomena.
- Uncertainty from wave realization.

Assumtions made for other variables

The roller positions are treated as deterministic variable in this study, i.e assuming that the roller positioning is always performed to ensure an optimal behaviour of the pipeline on the overbend. This assumption, reflects the actual practice for which a uniform roller reaction along the stinger is obtained with adjustment of the roller position. If, however, the installation procedures do not include any specific control/adjustment of the roller positions from initial setting, it will be correct to include some uncertainty of the roller positions in the safety assessment, e.g. the total static load effect uncertainty in the overbend prediction. The rollers positioning as assumed to be completely controllable, i.e. no uncertainty in this variable is considered.

Contact between the pipeline and the last roller on the stinger is not allowable according to the actual practice of design. Since the contact is controllable , no uncertainty in this variable is considered.

Lay vessel trim is a result of either deliberate actions or crane movements on deck. The trim-angle will affect the departure-angle for the pipeline and influence the characteristic vessel behaviour. Possible deliberate lay vessel trim represent a bias on the obtained results, depending on the scenarioes and the uncertainties related to the effect of change in characteristic vessel behavior is taken into account for the uncertainty related to the transfer function. Trim is therefore not included in the response surface as an uncertain variable.

The tensioner modelling is made in terms of a static value and a working range setting of ±10% in which the pipeline is kept in an approximately fixed position to the lay vessel. Outside the working range, the pipeline is free to move with an applied tension according to the working range limits. Given a static

configuration, the uncertainty related to tension is assossiated to the reliability of the tensioner. The measurement of the reliability of the tensioner is difficult to obtain, which imply a deterministic consideration of the tensioner variable.

The uncertainty variables accounted for in load effect prediction, mass, yield strength, stinger stiffness, transfer function and peak period are described below.

Mass

The mass is composed of sectional mass and added mass, the sectional mass will influence the tension and the static configuration of the pipeline, while the added mass is a function of dynamic movement. In sagbend the added mass is equal to the displaced volume of the pipe, but the variability of the diameter have a minor effect compared to a variability in the sectional mass which influence the tension and the static configuration. At overbend only the sectional mass will influence the tension and the curvature for the pipeline.

The sectional mass variability is due to the uncertainties in steel wall thickness and concrete coating thickness and density. The sectional weight is proportional to all contributing thicknesses, thus the total (mass) variability yields the sum of steel wall thickness variability and concrete coating thickness variability. The CoV for the nominal steel wall thickness is found to be 3.3 %, Jiao et al (1995), and the CoV for concrete coating thickness and density is taken as 5%.
The total sectional CoV then yields (independent variables):

$$CoV_{section} = \frac{\sqrt{\sigma^2_{W_{steel}} + \sigma^2_{W_{coat}}}}{\mu_{W_{steel}} + \mu_{W_{coat}} + \mu_{W_{add}}} \tag{5.9}$$

and for a 20" pipeline, D/t=28, 50 mm concrete thickness and density equal to 2500 kg/m^3 the $\mu_{w\_steel} \approx \mu_{w\_coat} \approx \mu_{w\_add.mass}$:

$$CoV_{section} = \frac{\mu\sqrt{0.033^2 + 0.05^2}}{3\mu} \approx 2\% \tag{5.10}$$

Now, considering the entire suspended span of a pipeline during laying, the pipe string is an assembly of separate pipeline sections (usually of 12 m length). The sections are seperatly produced on-shore so the thickness and density will vary from one section to another. Then asssuming that the pipe mass, X_n, are equally distributed with mean μ, variance σ and correlated, then according to the central limit theorem the total sectional mass Y yields:

$$Y = \sum_{i=1}^{n} X_i$$

$$Var(Y) = \sum_{i=1}^{n} var(X_i) + \sum_{i \neq j}^{n} \sum \rho_{ij} \sigma_{x_i} \sigma_{x_j} \qquad (5.11)$$

$$CoV_Y = \frac{\sqrt{\sigma^2(n+n(n-1)\rho)}}{n\mu} = \sqrt{\frac{1+(n-1)\rho}{n}} \frac{\sigma_x}{\mu}$$

The length of the suspended span is mainly a function of the water depth, but usually longer than 10 pipe sections (125 m) and n > 10, which imply that the total sectional mass CoV is a function of the correlation between the sections. A positive correlation is assumed, the correlation between all the sections is the same, with average coefficient of correlation equal to 0.6.

A normal distribution is applied for the total mass. The nominal mass is taken as the mean value, and the CoV is taken as 1.5%.

Yield strength

Uncertainty in the yield strength depends on the actual material specification, pipe producer, and in-batch production results. For most pipeline material, the yield strength, is defined as the stress corresponding to a total strain of 0.5% according to the API 5L specification. The Specified Minimum Yield Strength (SMYS) is a characteristic value of the yield strength. Commonly used pipe steel grades , X60 and X65, and corresponding SMYS values are 413 Mpa and 448 Mpa, respectively.

A data base has been used to derive uncertainty measures, contains detailed information on pipe material and dimensional parameters, established with a very large amount of measurement data obtained from representative European and Japanese pipe makers.

The pipe material covers normal to high strength carbon steel, namely, API 5L X60 - X80. For steel tensile strength parameters including the yield strength, ultimate tensile strength and ultimate tensile strain, measurements are available for parent metal in the longitudinal and transverse directions, and weld metal in the cross-weld direction (for seam-welded pipes).

For a particular parameter, the first step is to assess each individual sample by estimating its moments and inspecting the corresponding histogram. A suitable probability distribution function is then applied to fit the sample histogram. When there are several samples available, uncertainty measure for this parameter is made based on an overall assessment of all the samples. Usually, a conservative recommendation, e.g., an upper bound, is given.

In the longitudinal direction, there are 11 test samples available for welded pipes of steel grade X60 and X65, and 2 samples for seamless pipes of steel grade X65.

Table 5.1 presents the combined sample statistics, that is, the statistics are estimated for each steel grade by combining all relevant samples obtained from pipes of different dimensions and from different steel mills. No obvious difference between welded and seamless pipes is observed.

Table 5.1 Combined sample statistics for the longitudinal yield strength

Steel grade	No. of tests	Max. (MPa)	Min. (MPa)	Mean (MPa)	St. dev. (MPa)	CoV (%)
X60	748	506.0	416.0	456.5	14.75	3.2
X65	2754	557.1	451.0	480.6	13.45	2.8

Based on the above analysis, the following conclusions are obtained:

- Either a lognormal or normal distribution may be applied for the yield strength. The scatter in the yield strength is independent of the steel grade, a normalized uncertainty measure can thus be applied. Being conservative, a normal distribution is recommended for general application.
- There is little difference between the yield strength in the hoop direction and that in the longitudinal direction.

Although uncertainty measures are dependent on the quality of pipe producer reflected by a slight variation of the normalized mean and CoV values, a reasonable upper bound can be obtained. It is considered that a CoV of 4% is currently achievable in general for good quality steel mills, and the corresponding mean value is taken as two standard deviations above the SMYS.

Stinger stiffness

The "stinger stiffness" model includes the flexibility of the stinger structure. The uncertainty in the stinger stiffness reflects both the uncertainties in stinger/roller properties as well as roller positioning. The stinger structure is gradullay more flexible from the attachment point to the stinger tip. The stinger structure in the FE-model is taken infinitely stiff and in addition elastic stiffness from the roller.

The rollers positioning are made optimal, with an optimal uniform contact force measured during laying. This position will be constant during laying, and will not affect the uncertainties from the dynamic responses.

A FEM has been used to calculate the stiffness of the stinger. An unit load has been applied successive at each roller position and the associated deformation has been measured.

The uncertainty reflects the method used for calculate the stiffness, the effect of local deformation and the fact that the pipeline is a continous structure. A normal distribution is applied for the stinger stiffness with a mean value equal to the nominal value, and the CoV is taken as 10%.

Response Amplitude Operator

The uncertainties for the Response Amplitude Operator (RAO) for a semisubmerged laybarge, depend on the method used for calculating the transfer function and the water depth. The method that are avalible are numerical simulation and model testing. Two numerical methods which are often used are the strip theory and sink-source theory, the latter is used for the laybarge in this study.

Sink-source, called panel method, is a 3-D theory. Potential theory is assumed, and the method is based distributing panel elements on the wetted surface of the vessel, on a restricted part of the free surface, and on a control surface surrounding the computational domain. The effect of interaction betweeen columns and the pontoons is taken care of.

The uncertainty in the RAO for the lay vessel accounts for both the actual uncertainty related to the specific lay vessel characteristics applied in this study in addition to the variability in different lay vessel characteristics.

A normal distribution is applied for the RAOs with a mean value equal to the nominal value and a CoV of 10%.

Peak period, T_P

In each short term condition (3-hours) with a corresponding H_S, there is a variability in the peak period T_p. For summer condition the variability is shown in Figure 5.7, the representative data is for the North Sea, see Table 2.2.

The variability of T_p depends on the level of H_s and the conditional distribution of T_p given H_s is reasonally well fitted by a lognormal model. At least as long as the upper tail regions of the distribution are not too important, Haver and Nyhus (1986). Figure 5.7 compares the distribution of T_p with lognormal models with a CoV equal to 0.2. A CoV equal to 0.2 seems to fit the distribution reasonably well and with a mean value equal to the nominal value, the lognormal distribution is taken for the variability of T_p.

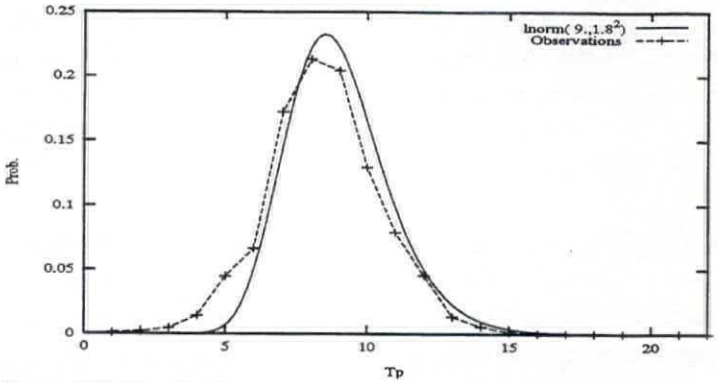

Figure 5.7 The distribution of Tp compared to lognormal models, Table 2.2

Uncertainty from wave realizations

Uncertainty is present in the prediction of pipeline response due to the variability of the wave realization in the time domain. The maximum pipeline response will be dependent on the actual wave time series used in the simulation. In this work, the uncertainty due to wave realization is determined investigating the variability in the load effects directly, based on obtained response for different wave realizations.

5.2.5 Pipelaying scenarios

The selected scenarios cover different water depths, which being of great importance with respect to the section criticality (sagbend/overbend). In deep waters, the response of the pipeline in the sagbend is less pronounced than in the overbend and vice versa. The static configuration for the different pipelay scenarios are determined on basis of the following criteria:

- The total axial strain (bending plus axial strain) equal to a predefined value.
- No contact between the pipeline and (at least) the last roller on the stinger

A pipeline with outer diameter equal to 20" and a diameter to thickness ratio as 28.4 is used as base case in the present study. For all scenarios, a steel grade API X60 material is used. In order to obtain the effect of extreme dynamic load levels, the analysis is performed utilizing two different irregular sea states; H_S = 3m, T_P = 8s and H_S = 4m, T_P = 10s, which are the operational sea states for the given lay barge and the anchor handling system, Pulici and Ronzoni (1995).Scenario S1 and S2 are overbend cases while S3 and S4 are sagbend cases. Table 5.2 shows the selected lay scenarios considered in the load effect assessment.

Table 5.2 Lay scenarios

Scenario	H_s (m)	T_p (s)	Specific gravity	Water depth (m)	Stinger radius (m)	Top tension (kN)	Nominal strain, static (%)
S1	3	8	1.27	300	140	900	0.20
S2	4	10	1.27	300	140	900	0.20
S3	3	8	1.42	100	130	293	0.20
S4	4	10	1.42	100	130	293	0.20

5.3 Results from the load effect assessment

5.3.1 General remarks

Two experiment data bases are made, one for overbend, scenario S1, and the other for sagbend, scenario S4. The data bases are established using LAYFLEX and are based on randomizing of the variables, yield strength, mass of the pipe, stiffness of stinger system, RAO and peak period of the spectrum. The data bases are enclosed in Appendix B.

The experiment data bases are made for establishing response surfaces and to compare the different types of response surfaces. In the present investigation four response-surface-models have been explored; multiplicative model, linear plane, polynomial without interaction and polynomial including interaction between the variables.

For multiplicative model and polynomial models comparisons between load effects from experiments and load effects from response surfaces are made. Uncertainty measures are made for all the models and compared to experimental results.

5.3.2 Response surface results

Polynomial models

The coefficients of the response surfaces are established by least square fitting of the results from LAYLEX, based on randomizing of the variables, yield strength, mass of the pipe, stiffness of stinger system, RAO and peak period of the spectrum.

Use of polynomial models will show the important variables of the response surface directly from the estimated coefficients when the variables are normalized and the centre of the variables is at the nominal value. The normalized variables and the results from the analysis are summarized in Appendix B.

Maximum response for a linear hyper plane is given by Eq. 2.32. The linear plane is the simplest model and the number of required experiments is small. The drawback with this model is that no nonlinear effect of the variation of the variables will be taken into account when calculating the load effect.

For a polynomial model without interaction between the variables, the maximum response is given by Eq. 2.33. This model take into account the effect of the variables and the effect of the variables in the power of 2. To establish this model still the number of experiments are small.

The polynomial model including interaction between the variables is given by Eq. 2.34. This model will in addition to the previous models take into account the interaction between the variables, i.e interaction between the yield strength and the mass, interaction between the mass and the peak spectrum period, etc.

Multiplicative model

The multiplicative model consists of a nominal case and complementary experiments where only one of the variables has been varied. The maximum response is given by Eq. 2.31. The model is simple and the control of the results from FE-analysis is good when only one of the variables is changed from one analysis to another.

Comparisons

The polynomial models are established from the entire number of experiments to reduce the statistical uncertainties for the models. For the linear and polynomial models, comparisons between load effect from experiment and load effect from response surface are made. The same values of the variables are used for FE-analysis and response surface, the comparison is graphically shown in Figure 5.8 and Figure 5.9. In the Figures the load effect is normalized with respect to the mean value from the experiments. The three models are quit similar, especially at sagbend, some deviations are observed for the dynamic load effect at overbend. The linear and polynomial model without interaction overestimate the load effect compared to the polynomial model with interaction between the variables.

The multiplicative model and polynomial model with interaction between the variables are compared in the same way. The different in this approach is that the multiplicative model is established using deterministic value of the variables. The models show the same trend as previous, the variation is worst for the dynamics at overbend. The load effect from the multiplicative model will vary more than the polynomial model, as shown in Figure 5.10 and Figure 5.11.

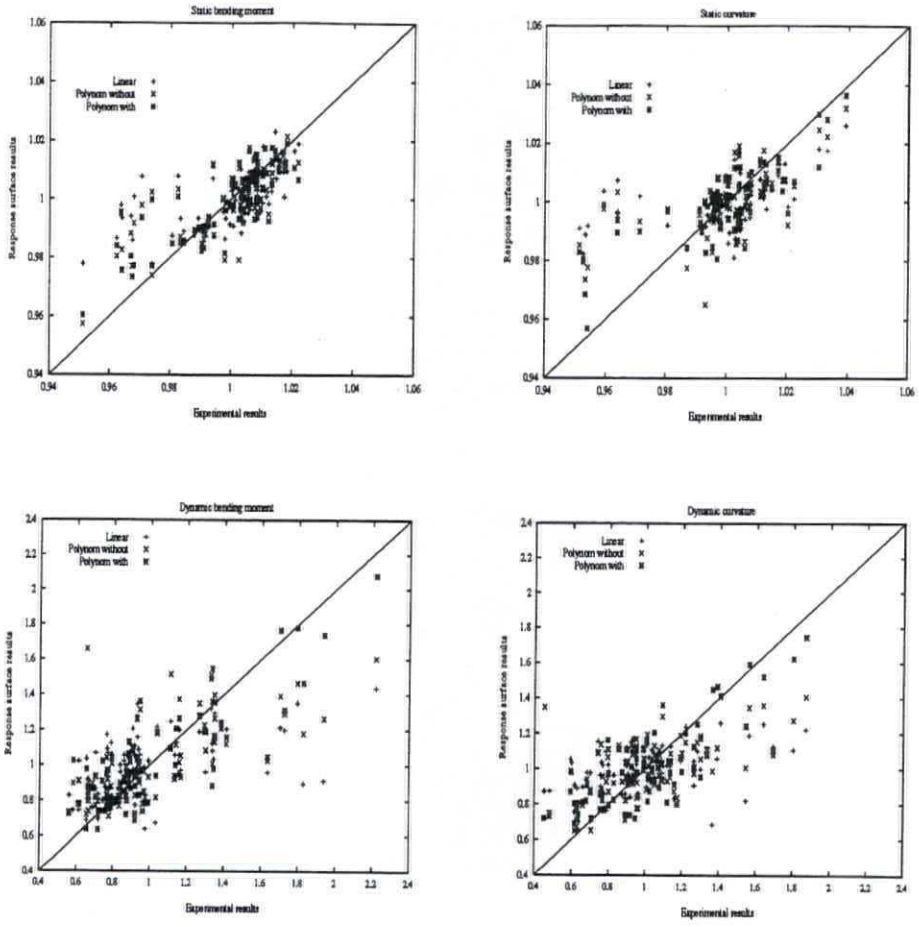

Figure 5.8 Response surface, Overbend, comparison between polynomial models, normalized with respect to mean value for experimental results.

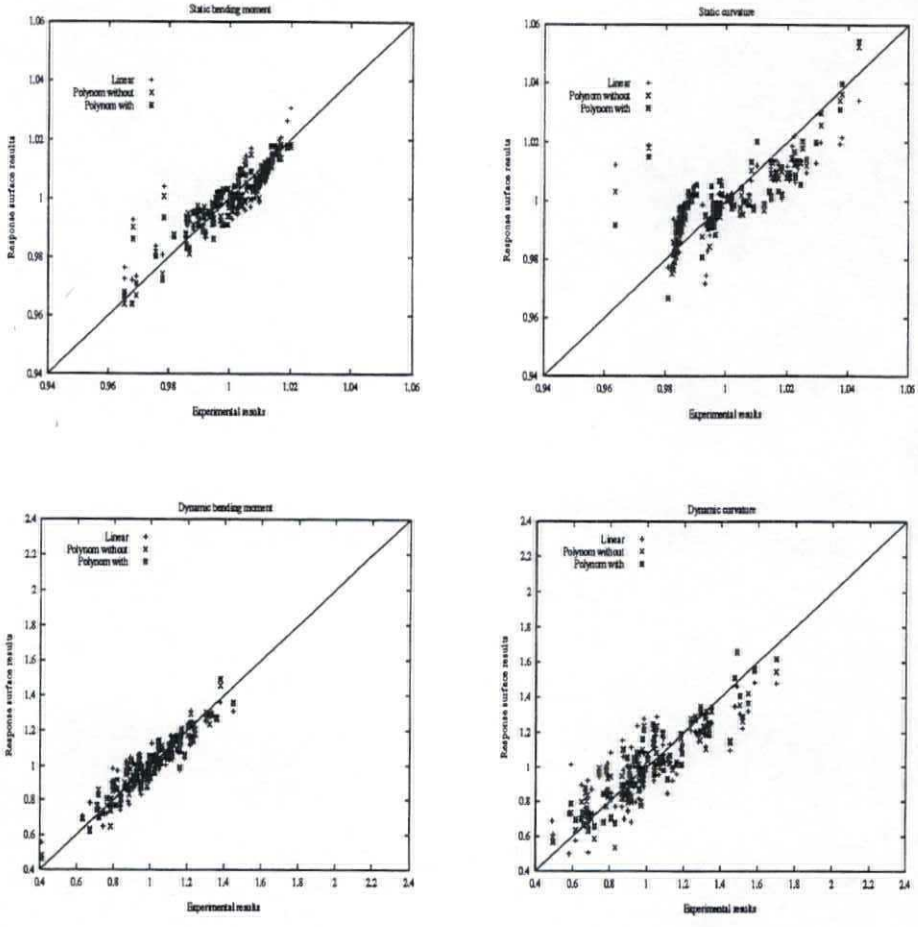

Figure 5.9 Response surface, Sagbend, comparison between polynomial models, normalized with respect to mean value for experimental results.

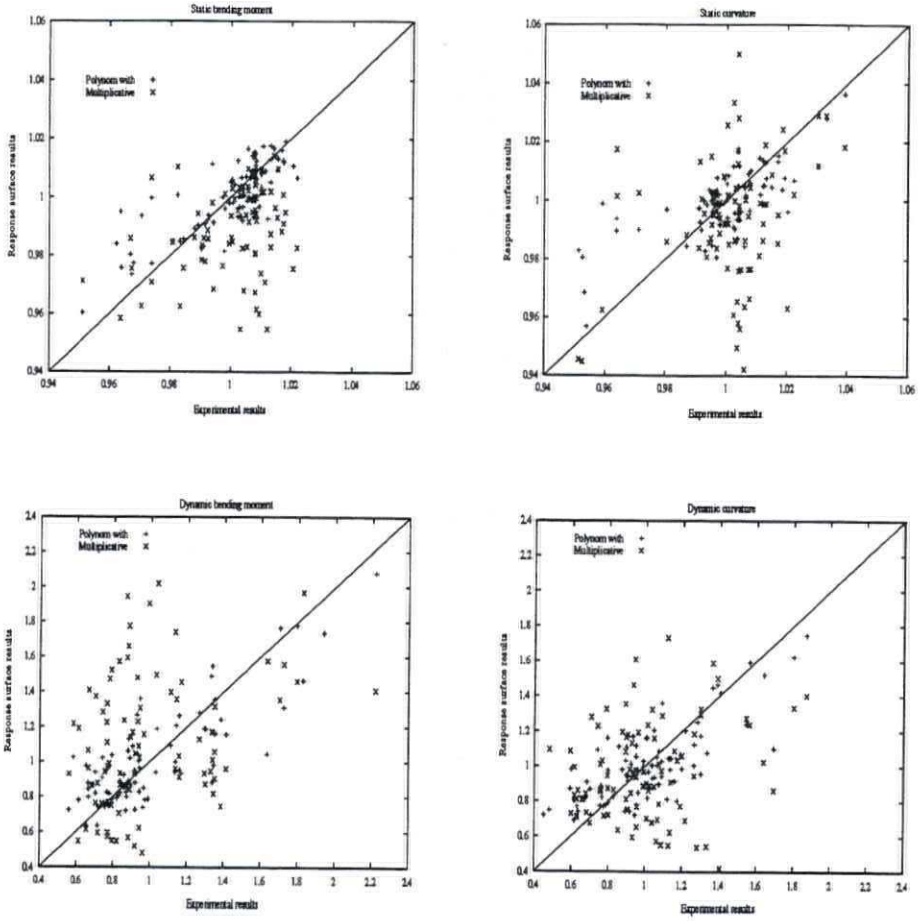

Figure 5.10 Response surface, Overbend, comparison between multiplicative and polynomial model, normalized with respect to mean value for experimental results.

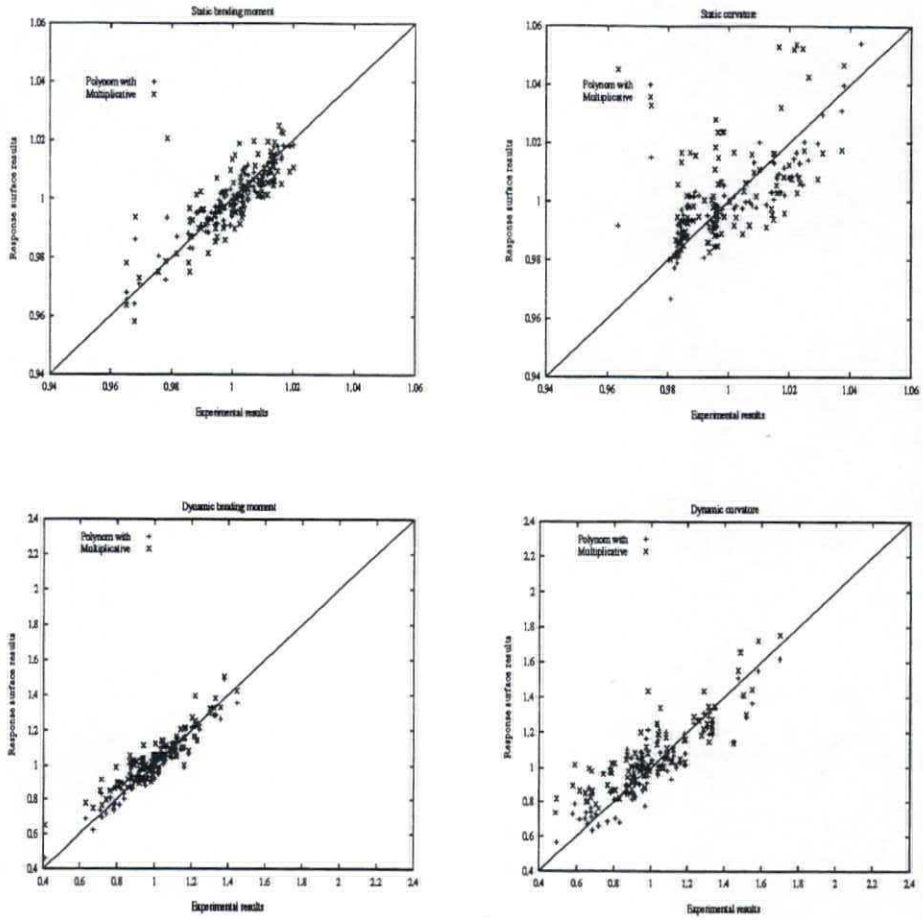

Figure 5.11 Response surface, Sagbend, comparison between multiplicative and polynomial model, normalized with respect to mean value for experimental results.

Uncertainty measures are made for all the models, presented in Table 5.3. The bias for the polynomials is equal or very close to 1.0, as expected since the response surfaces are fitted to the experiments. The uncertainty for the static load effect is about 1%, which means that for practical purpose there is no different between the models. For dynamic load effect the three models are quit different from each other. The linear model is coarse compared to the polynomial including interaction between the variables. This implies that there are some nonlinear effect and the interaction between the variables have to be considered when using response surface modelling.

The uncertainties for the dynamic load effect is quit different if the displacement controlled condition or load controlled condition are considered. For displacement controlled conditions very small measurements are observed for dynamic curvature and the variation may be relatively large when two small numbers are divided.

The multiplicative model estimate the static load effect quit well, the uncertainties is about twice as high but still acceptable. The model seems to be coarse for the dynamic load effect for displacement controlled condition where the uncertainties are about twice as for the polynomials. For the load controlled conditions the uncertainties are similar to the polynomials. The uncertainties for the dynamic load effect for sagbend will be better than the linear model and worse than the polynomials, which means that some nonlinear effects have to be included in the response surface model.

The multiplicative model underestimate the dynamic load effect for overbend and slightly overestimate the dynamic load effect for the sagbend. This implies that a model uncertainty for the multiplicative response surface have to be used.

The response surface modelling is used in reliability analysis to take into account the uncertainties in the load effects which will not be accounted for in ordinary design. The model uncertainty for the response surface will take into account the uncertainty using response surface compared to interactive use complete FE analysis in the reliability analysis. When using the multiplicative model it is important to find a nominal case which is close to the design point to avoid extrapolation and model uncertainty. When doing the previous comparison, a wide range of the variables is used to find the model uncertainty which means that for a good chosen nominal case the model uncertainty given in Table 5.3 including the uncertainties for the basic variable twice. Using an engineering judgement, the bias and corresponding CoV for dynamic curvature at overbend and dynamic moment at sagbend are presented in Table 5.4

The following conclusion may be drawn from the load effect assessment:

Use of the polynomial model with interaction between the variables is found to give a good prediction of the actual load effects, the drawback using this model is the large number of experiments required for establishing the response surface.

Use of the multiplicative model is found to give a well prediction of the actual load effects, given that extraction of response is done *within* the range of points defining the response surface, no coupling effects are included in this approach.

The multiplicative model will be used for the reliability analysis in the next Chapter, including model uncertainties as presented in Table 5.4.

Table 5.3 Uncertainty measures from experiments and response surfaces

Scenario	Load effect	Linear plane		Polynomial without interaction		Polynomial with interaction		Multiplicative	
		Bias	CoV	Bias	CoV	Bias	CoV	Bias	CoV
S1	S. Mom	1.000	1.2	1.000	1.0	1.000	1.0	1.015	2.0
	S. Curv	1.000	1.4	1.000	1.2	1.000	1.1	1.010	2.4
	D. Mom	1.003	28.3	0.999	21.0	1.002	18.7	0.994	37.5
	D. Curv	1.002	26.8	1.000	21.7	1.000	18.9	1.110	42.2
S4	S. Mom	1.000	0.6	1.000	0.5	1.000	0.5	1.000	0.8
	S. Curv	1.000	1.1	1.000	1.0	1.000	0.9	0.996	1.7
	D. Mom	1.000	8.4	1.000	6.6	1.000	5.7	0.964	7.5
	D. Curv	1.002	16.7	1.001	13.5	1.000	11.7	0.929	14.1

S. Mom, S. Curv, D. Mom and D. Curv are abbveriates for static moment, static curvature, dynamic moment and dynamic curvature, respectively.

Table 5.4 Model uncertainties for the dynamic load effect for the multiplicative model

Condition	Distribution	X_m^{RS}	CoV (%)
Displacement control	Normal	1.05	10
Load control	Normal	0.95	5

6 STRUCTURAL RELIABILITY ANALYSIS, DESIGN FORMATS AND CALIBRATIONS

6.1 General remarks

Structural reliability methods consider structural analysis models in conjunction with available information of the involved variables and their associated uncertainties. The applied models are not always perfect and the knowledge about the involved variables are usually limited. While physical randomness of a quantity in nature is objective, the implementation of this uncertainty in the reliability model is subjective. Thus, the reliability as assessed by reliability methods is generally not an objective physical property of the pipeline itself in the given operational and environmental condition, but rather a nominal measure of the reliability given a certain physical and probabilistic modelling and analysis procedure applied. The results from the reliability analysis should hence not be associated with a frequency interpretation of observed failures but may be regarded as a comparative measure related to the amount of information available.

SUPERB (1997) presents the design format for buckling and collapse adopted in the Design Guideline from the SUPERB project and in the new DNV-96 Rules for Submarine Pipeline Systems. The design format including usage and safety factors for load controlled and displacement controlled conditions are presented. Similar to SUPERB, the present work aims at a reliability based calibration of a semi-probabilistic limit state design approach. The limit states in the present work have been established before the SUPERB project, while the load effect analysis is performed in parallell with SUPERB project. The calibration of design format is performed after SUPERB project, with a more refined response surface model and consideration of pipeline system reliability model.

The main objective of this chapter is to use reliability procedures for laying operation. The study includes : using response surfaces for the load effects, the effect of strain concentration, system reliability and probability of failure for a laying period. Design format for displacement and load controlled design conditions will be outlined in Chapter 6.2. Calibration of design format will be described in Chapter 6.3.

6.2 Design format

6.2.1 General remarks

The fundamental principle of the partial safety factor method or load and resistance factor design (LRFD) method is to verify that factored design loads do not exceed factored design resistances for all considered limit states (i.e., failure modes).

The safety factors in each design equation (format) account for different sources of uncertainties entering the limit state of consideration, and are so calibrated that the target safety level set forth in Chapter 2 is satisfied. The design format is set-up for the local buckling limit state according to equations outlined in Chapter 3.

6.2.2 Buckling/Collapse

Buckling and collapse are the most important failure modes for the lay operation. Two load conditions have to be considered when designing pipeline for laying: displacement controlled condition and load controlled condition. Displacement controlled curvature is relevant for the pipeline on the stinger and the pipeline adapting to a very uneven seabed. Load controlled situation is relevant for a pipe section which is curvature controlled by its load, as a pipe section at the sagbend. The design formats for the two conditions are presented in this context.

The presence of the concrete is neglected in laying analysis. However, because of the discontinuity in the concrete coating, occurrence of strain concentrations at the field joints during bending of the pipe. The effect of strain concentration is accounted for in the load effect used for displacement controlled conditions.

6.2.3 Limit state format

The proposed equations outlined in Chapter 3 express the interaction between external pressure, tension and bending in a good way, especially for pressure dominant conditions where the existing codes may overestimate the capacity compared to the FE-results. The limit state functions for displacement and load controlled condition will be outlined in the following.

Displacement Controlled Curvature

For the displacement condition on the stinger a load combination of tension and bending will occur. The effect of tension is taken into account for the bending capacity of the tube. The following design equation for bending and tension is applicable for the pipeline on the stinger:

$$\frac{\gamma_F \, \varepsilon_{F,c} + \gamma_E \, \varepsilon_{E,c}}{\eta_\varepsilon \, \varepsilon_{co,c}^{\,T}} \leq 1.0 \tag{6.1}$$

where

$\varepsilon_{F,c}$ - characteristic maximum functional (static) strain load effect, calculated using response surface for functional load effect.

$\varepsilon_{E,c}$ - characteristic maximum environmental (dynamic) strain load effect, calculated using response surface for environmental load effect.

$\varepsilon_{co,c}^{\,T}$ - characteristic maximum strain capacity, accounting for the effect of tension

T_c - characteristic load effect, tension

$T_{co,c}$ - characteristic collapse tension

and where the characteristic bending strain capacity is calculated by

$$\varepsilon_{co,c}^{\,T} = \varepsilon_{co,c}\left(1.0+1.43\cdot\left(\frac{T_c}{\eta_T \, T_{co,c}}\right)^{2.4}\right) \tag{6.2}$$

$$\varepsilon_{co,c} = 0.005 + 13\cdot\left(\frac{t_{nom}}{D_0}\right)^2 \tag{6.3}$$

$$T_{co,c} = SMYS\,\pi D_0 t_{nom} \tag{6.4}$$

The corresponding limit state equation, including strain concentration and model uncertainty for bending strain, collapse tension and response surface, is :

$$g(x) = 1.0 - \frac{X_1\cdot(\varepsilon_F + X_m^{\,RS}\varepsilon_E)}{X_m^{\,\varepsilon}\cdot\varepsilon_{co}^{\,T}} \tag{6.5}$$

where the actual bending strain, ε_F and ε_E, are calculated by response surface using random value of the parameters affecting the load effect. The actual bending strain capacity is calculated by

$$\varepsilon_{co}{}^{T} = \varepsilon_{co}\left(1.0 + 1.43\cdot\left(\frac{T}{X_m{}^{T}\cdot T_{co}}\right)^{2.4}\right) \tag{6.6}$$

and

$$\varepsilon_{co} = 0.005 + 13\left(\frac{t}{D_0}\right)^2 \tag{6.7}$$

where the model uncertainties and strain concentration are denoted as

$X_m{}^{\varepsilon}$ = model uncertainty for critical bending strain
$X_m{}^{T}$ = model uncertainty for collapse tension
$X_m{}^{RS}$ = model uncertainty for dynamic load effect when response surface is used
X_I = strain intensification factor

In the reliability analysis using normalized variables are advantageous with respect to convergence criteria when the design point is calculated. Then introducing the following terms:

q_ε	$= \varepsilon_{E,c}/\varepsilon_{F,c}$	ratio of characteristic dynamic to static strain (load level)
q_T	$= T_c/T_{co,c}$	ratio of tension to collapse tension
X_F	$= \varepsilon_F/\varepsilon_{F,c}$	normalized static strain load effect
X_E	$= \varepsilon_E/\varepsilon_{E,c}$	normalized dynamic strain load effect
$X\varepsilon_{co}{}^{T}$	$= \varepsilon_{co}{}^{T}/\varepsilon_{co,c}{}^{T}$	normalized bending strain capacity
X_T	$= T/T_c$	normalized load effect, tension
X_{Tco}	$= T_{co}/T_{co,c}$	normalized collapse tension capacity

Using Eq. 6.1 and Eq. 6.5 and the normalized variables, the normalized limit state function can then be written:

$$g(x) = 1.0 - \frac{\eta_\varepsilon\, X_I\,(X_F + X_m{}^{RS} X_E\, q_\varepsilon)}{X_m{}^{\varepsilon}\cdot X_{\varepsilon_{co}}{}^{T}\,(\gamma_F + \gamma_E\, q_\varepsilon)} \tag{6.8}$$

$$X_{\varepsilon_{co}}{}^{T} = X_I\cdot\left(\frac{1.0 + 1.43\cdot\left(\dfrac{X_T\cdot q_T}{X_m{}^{T}\cdot X_{T_{co}}}\right)^{2.4}}{1.0 + 1.43\left(\dfrac{q_T}{\eta_T}\right)^{2.4}}\right) \tag{6.9}$$

$$X_{T_{co}} = X_\sigma \cdot X_t \tag{6.10}$$

Load Controlled Design Conditions

The limit state and design equations are based on the bending moment, the tension and the external pressure acting on a pipe section as for the pipeline in the sagbend or on-bottom pipeline in free span conditions. The following design equation including safety factors is applicable:

$$\frac{\gamma_F M_{F,c} + \gamma_E M_{E,c}}{\eta_M \cdot M_{co,c}^{\ P}} + \left(\frac{T_c}{\eta_T \cdot T_{co,c}^{\ P}} \right)^{\alpha} \leq 1 \tag{6.11}$$

where:

α = $2.4 - 2.5(P_c/P_{co,c}) + 1.5(P_c/P_{co,c})^2$

$M_{F,C}$ - characteristic maximum functional moment for the design load condition, calculated using characteristic values of the parameters entering the response surface for functional load effect.

$M_{E,C}$ - characteristic maximum environmental moment load effect, calculated using environmental response surface.

$M_{co,c}$ - characteristic maximum bending moment capacity

T_c - characteristic load effect, tension

$T_{co,c}$ - characteristic collapse tension

P_c - characteristic external pressure load effect

$P_{co,c}$ - characteristic collapse pressure

and

$$M_{co,c}^{\ P} = M_{co,c} \left(1.0 - (\frac{P_c}{P_{co,c}})^{1.9} \right)^{\frac{1}{1.9}} \tag{6.12}$$

$$M_{co,c} = M_0 \left(1.35 - (\frac{D_o/t_{nom}}{90}) + (\frac{D_o/t_{nom}}{100})^2 \right), \quad M_0 = SMYS\ D_o^2\ t_{nom} \tag{6.13}$$

$$T_{co,c}^{P} = 1.2 T_{0,c}^{P} \tag{6.14}$$

$$\left(\frac{T_{0,c}^{p}}{T_{0,c}}\right)^2+\left(\frac{T_{0,c}^{p}}{T_{0,c}}\right)\left(\frac{P_{0,c}^{/}}{P_{0,c}}\right)+\left(\frac{P_{0,c}^{/}}{P_{0,c}}\right)^2=1 \tag{6.15}$$

$$\frac{P_{0,c}^{/}}{P_{0,c}}=\frac{P_c}{P_{0,c}}\left(1.0-\frac{3.0\delta_0\frac{D}{t}}{\frac{P_c}{P_{E,c}}-1.0}\right) \tag{6.16}$$

The corresponding limit state equation including model uncertainty is:

$$g(x)=1.0-\frac{M_F+X_m^{RS}M_E}{X_m^{M}\cdot M_{co}^{P}}-\left(\frac{T}{X_m^{T}\cdot T_{co}^{P}}\right)^{\alpha} \tag{6.17}$$

$$\alpha=2.4-2.5\left(\frac{P}{X_m^{P}\cdot P_{co}}\right)+1.5\left(\frac{P}{X_m^{P}\cdot P_{co}}\right)^2 \tag{6.18}$$

where

X_m^{M} = model uncertainty for critical bending moment
X_m^{T} = model uncertainty collapse tension
X_m^{P} = model uncertainty collapse pressure
X_m^{RS} = model uncertainty for dynamic load effect when response surface is used

Using normalized variables the following terms are introduced:

q_M	$= M_{E,c}/M_{F,c}$	ratio of characteristic dynamic to static moment (load level)
q_T	$= T_{e,c}/T_{co,c}$	ratio of tension to collapse tension
q_P	$= P_{e,c}/P_{co,c}$	ratio of external pressure to collapse pressure
X_F	$= M_F/M_{F,c}$	normalized static moment load effect
X_E	$= M_E/M_{E,c}$	normalized dynamic moment load effect
X_{Mco}^{P}	$= M_{co}^{P}/M_{co,c}^{P}$	normalized moment capacity
X_T	$= T/T_c$	normalized load effect, tension
X_{Tco}^{P}	$= T_{co}^{P}/T_{co,c}^{P}$	normalized collapse tension capacity
X_P	$= P_e/P_{e,c}$	normalized external overpressure load effect
X_{Pco}	$= P_{co}/P_{co,c}$	normalized collapse pressure capacity

From Eq. 6.11 and Eq. 6.17 and using normalized variables, the normalized limit state function can then be written:

$$g(x) = 1.0 - \left(\frac{\eta_M \, (X_F + X_m^{RS} X_E \, q_M)}{X_m^{M} \cdot X_{M_{co}}^{P} \, (\gamma_F + \gamma_E \, q_M)} \right) \left(1 - (\frac{q_T}{\eta_T})^{\alpha} \right) - \left(\frac{X_T}{X_m^{T} \cdot X_{T_{co}}^{P}} \, q_T \right)^{\alpha} \tag{6.19}$$

$$\alpha = 2.4 - 2.5(\frac{X_P}{\eta_P \cdot X_m^{P} \cdot X_{P_{co}}} q_P) + 1.5(\frac{X_P}{\eta_P \cdot X_m^{P} \cdot X_{P_{co}}} q_P)^2 \tag{6.20}$$

$$X_{M_{co}}^{P} = X_\sigma \cdot X_t \cdot \frac{\left(1.0 - (\frac{X_p}{X_m^{P} \cdot X_{P_{co}}} q_P)^{1.9} \right)^{\frac{1}{1.9}}}{\left(1.0 - (q_P)^{1.9} \right)^{\frac{1}{1.9}}} \tag{6.21}$$

$$X_{T_{co}}^{P} = X_\sigma \cdot X_t \cdot \frac{\cos(\frac{\pi}{2} \frac{X_p}{X_m^{P} \cdot X_{P_{co}}} q_P)}{\cos(\frac{\pi}{2} q_P)} \tag{6.22}$$

where a cosine function is used for a simplification of Eq. 6.15 and Eq. 6.16.

6.3 Design calibration

6.3.1 General remarks

The premises for the calibration imply a varying degree of conservatism for the individual design equations depending on the knowledge of the prevailing functional and environmental loadings, pipe capacities, safety systems, mitigation measures, etc. The safety factors applied to a specific design format in this section are calibrated in accordance with Chapter 2. The safety factors are derived to cover a wide range of load effect level.

Installation is a temporary condition, which implies that the failure probability should relate to the time period relevant for lay operation, herein the summer season (June-August) is considered. The effect of number of sea states occurring in the laying period and the way the resistance is modelled will influence on the probability of failure and will be outlined in the following.

The failure of probability for one element is considered in section 6.3.3 using Eq. 2.22. The effect of the number of sea states in a laying period is taken into account, using the scaling factor for

dynamic load effect, Eq. 2.25 combined with Eq. 2.22. The system effect is included in Eq. 2.22 when a high correlation between the resistance from one element to another is assumed. The sensitivity of this assumption is outlined in section 6.3.4.

6.3.2 Uncertainties for the reliability analysis

The functional and environmental load effects, X_F and X_E, are calculated using the multiplicative response surface model, described in Chapter 2 and 5, as following :

$$X_F = \frac{RS_F(X_\sigma, X_{Mass}, X_{Stiff}, X_{RAO}, X_{Tp})}{RS_F(1.0,1.0,1.0,1.0,1.0)} \tag{6.23}$$

$$X_E = \frac{RS_E(X_\sigma, X_{Mass}, X_{Stiff}, X_{RAO}, X_{Tp})}{RS_E(1.0,1.0,1.0,1.0,1.0)} \tag{6.24}$$

where RS_F and RS_E are abbreviated for response surface, functional and environmental, respectively.

The sampling of the uncertainty variables (X_σ, X_{Mass}, X_{Stiff}, X_{RAO}, X_{Tp}) is done in accordance with the statistical properties as described in Table 6.1. In Table 6.2 and Table 6.3 the uncertainties used for displacement and load controlled design conditions, respectively are presented.

Table 6.1 Common random variables for load and displacement controlled conditions

Variable		Distribution	Mean	CoV (%)
X_σ	σ / SMYS	Lognormal	1.08	4
X_{mass}	Linear mass / nominal mass	Normal	1.0	1.5
X_{stiff}	Stinger stiffness/nominal value	Normal	1.0	10
X_{RAO}	RAO/ nominal RAO	Normal	1.0	10
X_{Tp}	Tp/ nominal Tp	Lognormal	1.0	20

Table 6.2 Uncertainties for displacement controlled design conditions

Parameter		Distribution	Mean	CoV, (%)
X_t	Wall thickness/Thickness_{nom}	Normal	1.000	3.3
X_I	$\text{Strain}_{joint}/\text{Strain}_{nom}$	Normal	1.200	3
X_T	Tension/E[Tension]	Normal	1.000	5
$X_m^{\ \varepsilon}$	$(\varepsilon_{co})_{test} / (\varepsilon_{co})_{pred}$	Normal	1.032	20
$X_m^{\ T}$	$(T_{co})_{test} / (T_{co})_{pred}$	Normal	1.000	8
$X_m^{\ RS}$	$RS_{F\_test} / RS_{F\_pred}$	Normal	1.100	10

Table 6.3 Uncertainties for load controlled design conditions

Parameter		Distribution	Mean	CoV, (%)
X_t	Wall thickness/Thickness$_{nom}$	Normal	1.000	3.3
X_T	Tension/E[Tension]	Normal	1.000	5
X_P	Pressure/E[Pressure]	Normal	1.000	2
X_m^M	$(M_{co})_{test} / (M_{co})_{pred}$	Normal	0.994	5.7
X_m^T	$(T_{co})_{test} / (T_{co})_{pred}$	Normal	1.000	8
X_m^P	$(P_{co})_{test} / (P_{co})_{pred}$	Normal	1.038	11
X_m^{RS}	$RS_{B, test} / RS_{B, pred}$	Normal	0.950	5
X_{Pco}	$P_{co} / (P_{co})_c$	Normal	1.010	11

Note, tension and pressure are taken as the expected value, but including a statistical uncertainty, according to a load combination where bending moment or bending strain is the most severe load effect.

6.3.3 Calibration of design code

The objective of the calibration is to establish a simple and practical design format capable of providing a uniform reliability level for a large parameter variation and wide range of design scenarios.

Reliability formulations for pipelines are outlined in Chapter 2. The calibration of the safety and usage factors will be performed using a single short term period as reference, using resistance for one element and maximum load effect in a short term (3 hours) period. The effect of laying period will then be demonstrated, i.e the number of sea states in a laying period is taken into account, using a scaling factor for dynamic load effect. This is achieve using Eq. 2.25 combined with Eq. 2.22. Finally the effect of using the minimum resistance combined with maximum load effect will be demonstrated.

Failure probability

The multi-dimensional failure probability integral in Eq. 2.7 is calculated by importance sampling simulation technique. The computer program ISPUD (Bourgund and Bucher, 1986) is used for the design calibration. ISPUD uses a combination of design point calculation and important sampling procedure when calculating the probability of failure. ISPUD use an optimalization procedure for establish the design point. This is a powerful technique which has the advantage of operation in the original space of the random variables, without transformation to the normal space, as outlined in Chapter 2.2.3. The important sampling is performed in the area around the design point where the contribution to the failure probability has its maximum, as shown in Eq. 2.12 and Figure 2.2.

Model uncertainty

The bending load effect is the most severe load effect for the sagbend and overbend. This implies that the model uncertainty for the interaction will be dominated by the model uncertainty for bending moment capacity. Therefore will the model uncertainties for the basic failure modes be used for the interaction between bending and tension and pressure, tension and bending in the limit states for design calibration.

Load combination

For time varying load effects (bending and tension) that are uncorrelated and independent of each other the philosophy implied by Turkstra's rule is considered to be an acceptable approximation when one of the load effect is dominant.

Load level

The safety factors are derived to cover a wide range of load effect level. The load levels q_e and q_M are defined as ratio of characteristic dynamic load effect to static load effect. The load levels considered in this study cover the range 0.05 to 0.4. The load level q_e and q_M will cover the effect of Hs, while the effect of peak period is included in the response surfaces.

The load levels for the extreme sea state (3 hours) which are used as basis for the response surfaces, q_e are 0.04 and 0.06 for the curvature at the overbend and q_M are 0.10 and 0.24 for the bending moment at the sagbend, for Hs3/Tp8 and Hs4/Tp10, respectively.

The load levels for tension and pressure are defined as ratio between characteristic load and critical capacity.

Load effect from response surface

Calibration of the design equations are made using response surface. The response surfaces are used by ISPUD in the calculation of the load effect and the probability of failure. Response surfaces based on significant wave height, Hs equal to 4m and peak spectrum period, Tp equal to 10 sec are used, which are representative for extreme lay operation conditions. As outlined in Chapter 5, the response surfaces represent the overbend conditions, displacement controlled situation, which represent a deep water condition and the sagbend conditions, load controlled situation, which represents a shallow water condition.

Probability of failure for an element for a single short term period

A calibration of the safety and usage factors is performed for a short term period. A trial- and -error approach is applied to find the optimal safety and usage factors.

Figures 6.1 and 6.2 show the probability of failure for the overbend and the sagbend, respectively, as function of load level for bending, tension and pressure. In the figures one of the load effects is varied while the other is kept constant, i.e. q_e vary, q_T= 0.1 means that the tension is kept at 10% of critical tension capacity, while the dynamic load effect for bending strain is varied from 0.05 to 0.3 of the static load effect.

The probability of failure is uniform for overbend but will vary somewhat for the sagbend for extreme load level of q_M, q_T and q_P. Figure 6.3 and Figure 6.4 show the sensitivity of the safety factor for the dynamic load effect compare to the safety factor for the static load effect. The load controlled situation is more affected by dynamic load effect than for the displacement controlled situation, as shown in these figures.

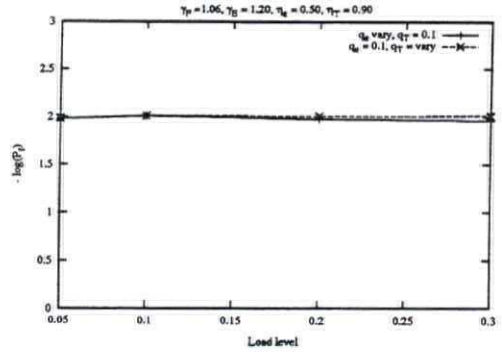

Figure 6.1 P_f for overbend as function of load level

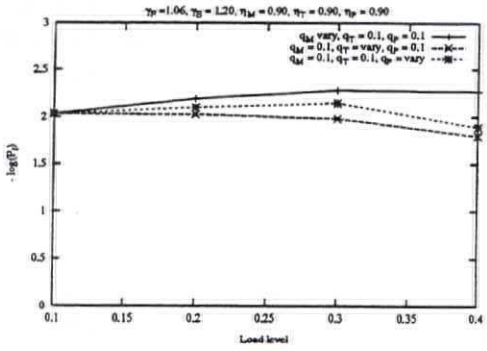

Figure 6.2 P_f for sagbend as function of load level

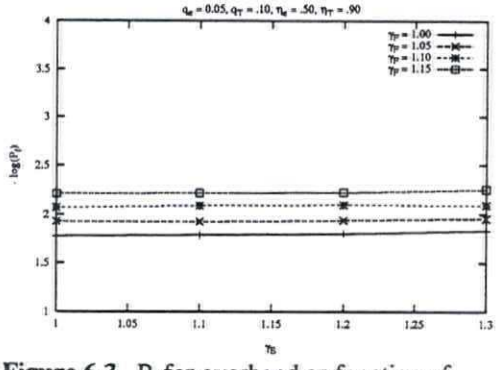

Figure 6.3 P_f for overbend as function of safety factors, γ_F and γ_E

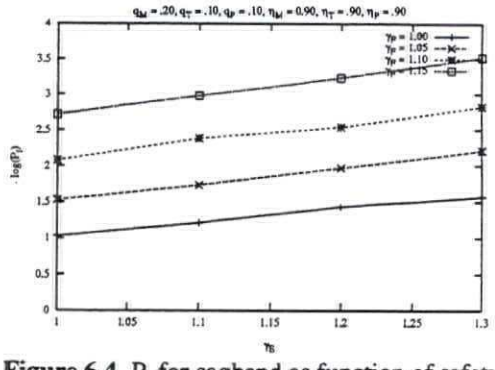

Figure 6.4 P_f for sagbend as function of safety factors, γ_F and γ_E

Table 6. 4 shows the proposed load and usage factors for the laying conditions for one element during a 3 hours period.

Table 6.4 Load and resistance factors for overbend and sagbend, 3 hours period

	γ_F	γ_E	η_p	η_T	η_e	η_M
Overbend	1.06	1.2	---	0.90	0.50	---
Sagbend	1.06	1.2	0.90	0.90	---	0.90

Considering γ_F= 1.06, γ_E = 1.2, η_ϵ = 0.5, η_T = 0.9, q_ϵ=0.05 and q_T=0.10 the design point and important factors given in Table 6.5 are obtained for the displacement conditions. The most important parameter is the model uncertainty for the bending strain capacity, while the load effect has a negligible effect on the probability of failure. X_o, X_{mass}, X_{stiff}, X_{RAO} and X_{Tp} are the variables that affect the load effects.

For load controlled conditions, γ_F= 1.06, γ_E = 1.2, η_M = 0.90, η_T = 0.90 and η_P = 0.90, q_M= 0.20, q_T = 0.10 and q_P= 0.10 the design point and important factors given in Table 6.6 are obtained. The most important parameter is the model uncertainty for the bending moment capacity, while the load effect has a minor effect on the probability of failure, as seen for X_o, X_{mass}, X_{stiff}, X_{RAO} and X_{Tp}.

Table 6.5 Design point and important factors for displacement controlled conditions

Variable	Design point	Parametric sensitivity factor	Important factor
X_o	0.9935	-0.0690	0.0048
X_{mass}	0.9990	-0.0376	0.0014
X_{stiff}	1.0044	0.0190	0.0004
X_{RAO}	1.0021	0.0090	0.0001
X_{Tp}	0.9967	-0.0070	0.0001
X_t	0.9929	-0.0933	0.0087
X_I	1.2049	0.0706	0.0050
X_T	0.9998	-0.0017	0.0000
X_m^e	0.5726	-0.9897	0.9795
X_m^T	1.0006	0.0034	0.0000
X_m^{RS}	1.0533	0.0143	0.0002

Table 6.6 Design point and important factors for load controlled conditions

Variable	Design point	Parametric sensitivity factor	Important factor
X_o	0.9849	-0.1484	0.0220
X_{mass}	1.0011	0.2945	0.0867
X_{stiff}	1.0000	0.0002	0.0000
X_{RAO}	1.0028	0.0112	0.0001
X_{Tp}	0.9758	-0.0476	0.0023
X_t	0.9629	-0.4442	0.1973
X_T	1.0014	0.0109	0.0001
X_P	1.0002	0.0030	0.0009
X_m^M	0.8743	-0.8244	0.6780
X_m^T	0.9964	-0.0176	0.0003
X_m^P	1.0335	-0.0160	0.0003
X_m^{RS}	0.9646	0.1145	0.0131
X_{Pco}	1.0054	-0.0163	0.0003

6.3.4 Sensitivity of system modelling

Probability of failure for a continuous laying process

The laying of a continuous pipeline will take 1-3 months. The effect of number of sea states will influence the expected maximum dynamic load effect and hence affect the probability of failure for a laying period. Herein the effect of the number of sea states will be shown using a constant, Eq. 2.25 to scale the dynamic load effect combined with Eq. 2.22. This implies that the safety factor for dynamic load effect is a function of number of sea state of a given H_s and of the uncertainty in the dynamic load effect.

Under displacement controlled conditions and load controlled conditions, the effect of number of sea states is considerable. Figure 6.5 and Figure 6.6 show the probability of failure as function of load level, q_c and q_M, including scaling of dynamic load effect and using different safety factors for dynamic load effect. To achieve a target level of 0.01 when system model is applied, the safety factor for dynamic load effect has to be increased from 1.2 to 1.4. In the figures tension and pressure are kept constant, q_T=0.1 and q_P=0.1. The failure probability is approximately uniform for both conditions when taking into account the effect of number of sea states.

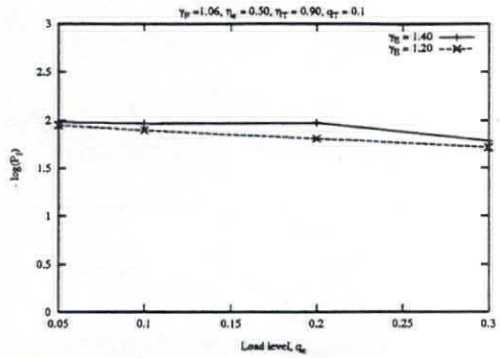

Figure 6.5 P_f for overbend as function of load level

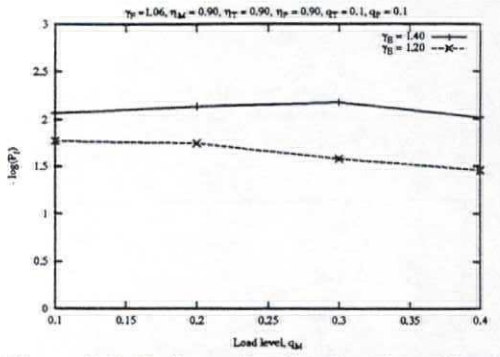

Figure 6.6 P_f for sagbend as function of load level

Effect of series system of resistances in a short term period

In the previous section, the effect of series system in time was included in Eq. 2.22 and Eq. 2.25, assuming a very high correlation between the variables for the resistance from element to another and assuming that the simultaneous occurrence of minimum resistance (R^{min}) and maximum load effect (S^{max}) will be extreme rare and conservative combination, i.e. R^{min} - (S_{static} + $S_{dyn}{}^{max}$). Anyway it may be of interest to see the effect on usage factors by using R^{min} for independent R_i instead of using R_i for the series system. This effect will be investigated in the following using the same target level as previous. This is an assumption since the target level should be evaluated when the method is modified.

System effects are relevant in scenarios where many elements are subjected to identical load conditions and potential failure occur in connection with lowest structural capacity. For the series system, the failure probability will depend on the uncertainty of each element of the pipeline and the number of elements. The uncertainty for the resistance in a pipeline element mostly depends on the uncertainty for the yield strength and the wall thickness. Herein, the wall thickness is considered using minimum value distribution since this variable is common for displacement controlled and load controlled conditions and is one of the most important variables in the reliability analysis, in compliance with Table 6.5 and Table 6.6. Yield strength is considered with uncertainty within each element.

In this case the load effect is taken to be the expected maximum in a design period and the most important parameter in the resistance follow a minimum distribution for N_E independent elements, as following :

$$F_{\min}(x) = 1. - (1. - F(x))^{N_E} \tag{6.25}$$

where F(x) is the cumulative distribution for the most important parameter and N_E is the number of elements.

For this series systems it is assumed that an average number of elements pass the most critical position pr extreme sea state (3 hour) : N_E equal to 10 as a minimum and N_E equal to 100 as the maximum where several extreme conditions is follow each other.

The statistical moments for the normalized wall thickness using Eq. 6.25 are presented in Table 6.7 for different number of elements. The extreme value distribution is for illustration given in Figure 6.7 for N_E = 1, 10, 100 and assuming a Normal distribution $N(1.0, 0.033^2)$ for X_t in compliance with Table 6.2 and Table 6.3.

Table 6.7 Statistical properties for minimum value of normalized wall thickness, X_t

Number of elements	Distribution	μ	CoV (%)
1	Normal	1.00	3.3
10	Normal	0.95	2.0
100	Normal	0.91	1.5

The different statistical properties listed in Table 6.7 in combination with uncertainties listed in Tables 6.1 - Table 6.3 are used in the reliability analysis to find the effect of series system using independent resistance.

Figures 6.8 and 6.9 show the failure probability as function of usage factor for bending capacity. From the figures, the usage factor will be found for different N_E and in Table 6.8 these are presented for N_E in the range from 1 to 100. Note, the target level is kept at the same level, P_f equal to 0.01.

Table 6.8 Usage factor for bending capacity, for target level $P_f = 0.01$

Number of elements	Displacement control	Load control
1	0.50	0.90
10	0.47	0.87
100	0.46	0.84

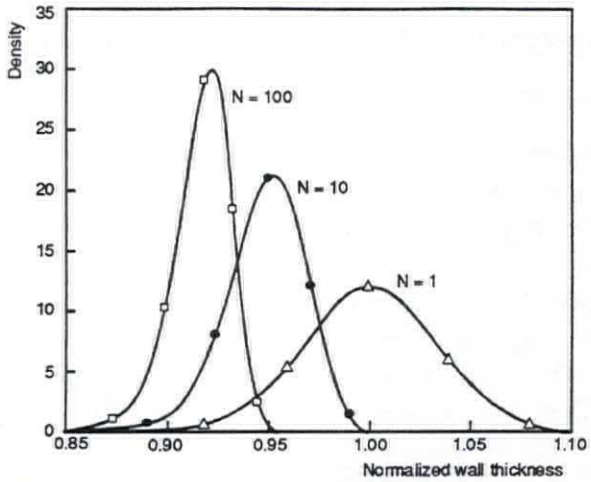

Figure 6.7 Density function for normalized wall thickness for normal and extreme conditions

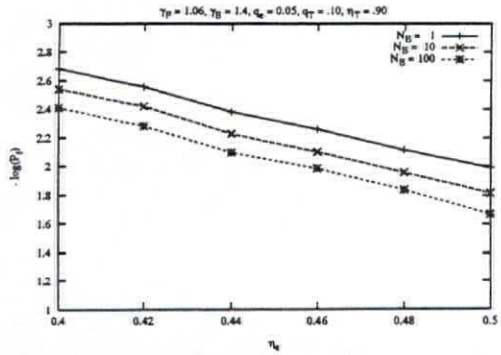

Figure 6.8 P_f for overbend as a function of η_e and the number of elements

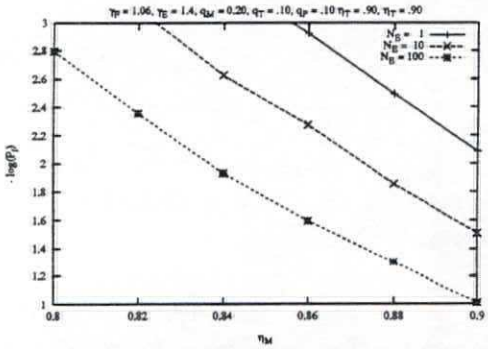

Figure 6.9 P_f for sagbend as a function of η_M and the number of elements

It is seen that the system reliability implies a reduction of the usage factor of about 5% when considering the minimum wall thickness among N_E independent elements and the yield strength for one element. The number of elements N_E is between 10 and 100.

As discussed in Chapter 2, it is a conservative approach to consider a minimum of independent element resistance of the pipeline in combination with maximum load effect. Combined with a realatively small effect of the above analysis for independent variables, the assumption made above using the resistance of one element is considered combined with maximum load effect is a reasonable assumption.

The following conclusions may be drawn from the calibration :

The most important parameter is the model uncertainty for the bending moment capacity, while the load effect has a minor effect on the probability of failure. The effect of weather window is important when the safety factor for dynamic load effect is considered. The effect of series system of the resistance will affect the usage factor of the capacity of the pipeline, but when a high correlation between the resistance from one element to another the effect is less than 5%. Table 6.9 presents the proposed safety factors for the laying period including effect of series system.

Table 6.9 Load and usage factors for overbend and sagbend for the laying period

	γ_F	γ_E	η_p	η_T	η_e	η_M
Overbend	1.06	1.4	---	0.90	0.50	---
Sagbend	1.06	1.4	0.90	0.90	---	0.90

In SUPERB (1997) the safety and usage factors are somewhat different from those the presented in Table 6.9. This is caused by different limit states function, different response surface model, model uncertainties for the capacity as well as reliability model. The different design formats can only be compared by comparing designs resulting from different formats.

This study also shows the importance of consistently choosing reliability methodology and target level.

7 CONCLUSIONS

7.1 General remarks

This work has two main objectives. The first one is to study the ultimate strength of tubes under combined loading. The second objective is to apply reliability theory to achieve a more uniform and consistent safety level for design criteria for pipelines with different geometry and load conditions during laying. The finding from the first part of the work have formed the basis for the reliability study. The collapse strength calculation, parametric studies and the subsequent reliability calculations are performed for pipeline laid in North Sea condition.

7.2 Capacity of tubes under combined loads

Finite element analyses for the collapse of thick tubes ($15<D_0/t<35$) under combined external pressure, tension and bending loads are studied. The effects of initial ovality, residual stress, strain-hardening, yield anisotropy and loading paths were accounted for in the analysis. Extensive comparisons between the analysis and laboratory tests, demonstrate that the analysis can accurately predict collapse behaviour of thick tubes under combined external pressure, tension and bending loads.

A series of parametric studies on collapse of thick tubes were carried out. The following observations can be made from the results of the study:

- The responses of thick tubes under simultaneous external pressure(P), tension(T) and bending(κ) are significantly affected by the loading paths. Three loading paths have been studied: P→T→κ, T→P→κ and P→κ→T. The P→T→κ loading path is more severe than the

P→κ→T and T→P→κ loading paths.

- The external pressure reduces moment-tension envelopes.
- Lower diameter to thickness ratio leads to higher collapse envelopes.
- Since collapse under pressure is sensitive to initial ovality, the collapse under combined loads is also sensitive to initial ovality. However, any residual stress effect seems to be very small.
- Material properties, e.g. yield stress, hardening parameter and anisotropy parameter, play important roles in collapse behaviour and collapse envelopes. A higher yield stress to Young's moduls ratio, or lower hardening parameter or higher anisotropy parameter leads to higher collapse envelopes.

A set of interaction equations is proposed accounting for major factors affecting collapse envelopes. Extensive comparisons with the present finite element analysis results confirm the suitability of the proposed equations.

7.3 Load effect, strain concentration

The presence of the concrete is neglected in laying analysis. However, because of the discontinuity in the concrete coating occurrence of strain concentrations at the field joints arise during bending of the pipe.

Finite element analyses for the bending of pipelines including concrete coating are performed. The effects of concrete coating thickness, diameter to thickness ratio, shear strength of the corrosion coating and reinforcement in longitudinal and hoop direction were accounted for in the analysis.

Comparisons between the analysis and laboratory tests, demonstrate that the analysis can predict the strain concentration, defined as maximum strain in joint / nominal global strain, in the field joints. Simple formulae are proposed to account for major factors affecting strain concentration. A strain concentration factor is found to vary in the range of 1.1 to 1.6.

7.4 Load effect and response surface

In the pipe laying case, the load effect denotes the response of loading from direct hydrodynamic forces, forced end displacements (from lay vessel motions) and discrete support forces. The load effect is categorized in two ways, displacement controlled condition and load controlled condition.

Finite element analyses for the behaviour of the pipeline under ultimate sea state for S-lay operations are studied. The effects of uncertainties for yield stress, mass, stiffness of the stinger, RAO and Tp were accounted for in the analysis.

The maximum load effect is given as response surfaces. The response surface is a parameterization

of the response in terms of the basic random parameter. The maximum load effect is calculated in two ways, first using a nominal case and complementary experiments where only one of the parameters has been varied. Second using randomizing of the variables and calculate the load effect for several sets of experiments. In the present investigation four response-surface-models have been explored; multiplicative model, linear plane, polynomial without interaction and polynomial including interaction between the variables.

The linear and polynomial model without interaction overestimate the load effect compared to the polynomial model with interaction between the variables.

Use of the polynomial model with interaction between the variables is found to give a good prediction of the actual load effects, the drawback using this model is the large number of experiments required for establishing the response surface.

Use of the multiplicative model is found to give a well prediction of the actual load effects, given that extraction of response is done *within* the range of points defining the response surface, no coupling effects are included in this approach.

7.5 Structural reliability analysis, design format and calibration

Structural reliability methods consider structural analysis models in conjunction with available information of the involved variables and their associated uncertainties. Hence, upon introducing structural reliability and a target safety level to be met, methods for the reliability analysis and procedures for the probabilistic modelling must be specified.

The study include calibration of safety factors for design format: using the response surfaces for the load effects, including the effect of strain concentration, take into account the effect of series system of pipe sections and consider the probability of failure for a laying period as reference unit. A combination of design point calculation and important sampling procedure is used when calculating the probability of failure.

The most important parameter is the model uncertainty for bending capacity while the load effects have minor importance of the probability of failure.

The system effect is taken into account considering a high correlation between the resistance from one element to another, the effect on the usage factor for bending capacity is less than 5% compared to independent resistance. Considering the probability of failure for the total laying period, the safety factor for environmental load effect should be increased compared to considering the failure of a element during a 3 hour period.

7.6 Suggestion for further work

Capacity of tubes

- Although the proposed equations agree with laboratory tests for tubes under single loads or combined loads, it is necessary to verify the formulations by tests on tubes under simultaneous external pressure, tension and bending loads.

- The model uncertainty for bending capacity for the strain based design requirer more test-results to make a good model for the bending strain capacity and reduce the CoV.

Load effect, strain concentration

- The effect of large diameter pipeline for the strain concentration should be verified through full scale measurements.

Load effect analysis

- The load effect analysis with focus on the interaction between pipeline and the roller at the stinger should be performed.

- For the load effect analysis a good contact formulation for interaction between the pipeline and stinger is required to avoid numerical problem during FE-analysis. A more consistent formulation should be used in the FE-algorithm.

Structural reliability, response surface, design format and calibration

- A more extensive study may be performed to calibrate the design code using a refined response surface model including more random variables and using a response surface for tension.

- Consider the total period of lay operation as a union of sea states and taken into account the correlation between resistance and load effect.

With these future visions in mind, it is still hoped that the present study represent a valuable contribution to the analysis and design of offshore pipeline.

8 REFERENCES

ABAQUS (1992) , *User's Manual, Theoretical Manual and Example Problem Manual*, Version 4.9, Hibbitt, Karlsson and Sorensen, Inc.

Ades, C.S. (1957), "Bending strength of tubing in the plastic range", *Journal of Aeronautical Sciences*, Vol 24, pp 605-610.

Akten, H.T., Lund, S. og Miller, D.M. (1985): "On the Design and Construction of Statpipe Pipeline System", *Proc. Offshore Technology Conference*, OTC 4922, pp. 247-257.

Andersen, T.L.(1990), Elastic-plastic fracture mechanics - A critical review, *SSC report no.345*, (U.S.A.), Dec. 1990.

Ang A H-S and Tang W H, (1975), *Probability Concepts in Engineering Planning and Design*, John Wiley & Sons, New York,

Archer, G.L. and Adams, A.J. (1983): "The Behavior of Concrete over Thin Film Epoxy Coatings on Offshore Pipelines", *Proc. Offshore Technology Conference*, OTC 4453, pp. 85-95.

Ayyub B M and Haldar A, (1984), "Practical Structural Reliability Techniques." Journal of Sructural Engineering, Vol 110, No.8, pp.1707-1724.

Babcock, C.D. and Madhavan, R.(1987), "Pipe collapse under combined axial tension and external pressure", in Factors affecting pipe collapse, Phase 2, *EMRL Report No. 87/8, Department of Aerospace Engineering and Engineering Mechanics*, The University of Texas at Austin, August 1987.

Bai, Y., Igland, R. and Moan, T.(1992). "Collapse of Thick Tube under Pressure, Tension and Bending and their Combinations." *Proc 2nd ISOPE 1992, Vol IV, pp 568-576.*

Bai, Y., Igland, R. and Moan, T.(1993). "Limit States for Tendon and Production Riser Bodies, -Numerical Data Basis."*SINTEF Report STF70 F93070,* Trondheim.

Bai, Y., Igland, R. and Moan, T.(1993). "Tube Collapse under Combined Pressure, Tension and Bending Loads." *International Journal of Offshore and Polare Engineering* . Vol3, No 2, June

Bai, Y., Igland, R. and Moan, T.(1993). "Limit States of Pipes under Tension and Bending." *Proc 3th ISOPE 1993, Vol II, pp 1-9.*

Bai, Y., Igland, R. and Moan, T.(1994). "Ultimate Limit States of Pipes under Tension and Bending.", *International Journal Offshore and Polar Engineering*., Vol 4, No 4, December 1994

Bai, Y., Igland, R. and Moan, T.(1995). "Collapse of Thic Tubes under Combined Tension and Bending Loads.", *Journal of Construction Steel Research*., Vol 32 1995, pp 233-257

Bai, Y., Igland, R. and Moan, T.(1997). "Tube Collapse Under Combined External Pressure, Tension and Bending loads." *Marine Structures* . Vol 10 No 5, pp 389-410

Brazier, L.G.(1927), "On the flexure of thin cylindrical shells and other thin sections", *Proceeding of Royal Society of London*, Series A, Vol. 116, pp.104-114.

BS8010 (1993). "Practice for pipelines - Part 3 pipeline subsea: Design, construction and installation." *Codes* by British Standards Institute.

Bourgund U. and Bucher C.G. (1986), " Important sampling Procedure Using Design Points (ISPUD)" - *A User manual*, Institute of Engineering Mechanics, Univercity of Innsbruck, Report 8-86

Bucher C.G. and Borgund U. (1990), " A Fast and Effecient Response Surface Approach for Structural Reliability Problems", *Structural Safety*, 7, pp 57-66

Chen W F and Han D J, (1987), *Plasticity for Structural Engineers*, Springer-Verlag, New York

Corona, E. and Kyriakides, S.(1988), "On the collapse of inelastic tubes under combined bending and pressure", *International Journal of Solids and Structures*, Vol. 24, pp.505-535.

CSA, Canadian Standard Assosiation, (1987) *General Requirements, design Criteria, Environment and Loads*,Preliminary Standard S471

DIANA 5.0, (1992), *User's Manual*, TNO Building and Construction Research - Department of Computational Mechanics, Delft, The Netherlands

DnV (1981), Det norske Veritas, *Rules of Submarine Pipeline Systems*, Høvik, Norway, 1982

DNV Classification, (1992), "Structural Reliability Analysis of Marine Structures", *Classification Notes No : 30.6*, Høvik, Norway, July, 1992

Edwards, S.H. and Miller, C.P.(1939), "Discussion on the effect of combined longitudinal loading and external pressure on the strength of oil-well casing", *Drilling and Production Practice, American Petroleum Institute*, pp.483-502.

Endal Geir, (1993), 'Rørledning med betongkappe ved ekstrem bøyning', *Diplom-thesis*, The University of Trondheim, The Norwegian institute of Technology, Department of Structural Engineering, 1993, (in norwegian).

Endal G., Ness O. B., Verley R, Holte K and Remseth S. (1995), 'Behaviour of offshore pipelines subjected to residual curvature during laying.', *Offshore Mechanics and Arctic Engineering*, OMAE Conference 1995

Fabian, O.(1981). "Elastic-plastic collapse of long tubes under combined bending and pressure load." *Ocean Engineering*, **8** (3), pp 295-330.

Farnes K.A, (1990), " Long-term Statistics of Response in Non-linear Marine Structures", *Dr.Ing Thesis, MTA Report 1990:74*, Norwegian Institute of Technology, Trondheim, 1990

Farnes K.A and Moan T (1993), "Extreme Dynamic Response of Fixed Platforms Using a Complete Long-term Approach", *Applied Ocean Research*, 1993

Faulkner , D, Guedes Soares, C and Warwick D M, (1988), " Modelling Requirements for Structural Design and Assessment", *Integrity of Offshore Structures-3, ISO-87, Elsevier Applied Science*.

Ferry-Borges, J and Castenheta, M (1971), *Structural Safety*, Laboratoria Nacional de Engenhera Civil, Lisbon

Fowler, J.R. (1990)."Pipe Collapse - Large Scale Tests," *Stress Engineering Services Inc. Report (PR-201-818)*, Prepared for the American Gas Association, June 1990.

Gellin, S. (1980),"The Plastic Buckling of Long Cylindrical Shells under Pure Bending", *International Journal Solids Structures*, Vol. 16 pp 397-407

Gumbel E J (1958), *Statistics of Extremes*, Columbia University Press

Haagsma S. H. and Schaap, D, (1981), "Collapse Resistance of Submarine Lines Studied", *Oil & Gas*, February 1981

Haver S and Nyhus K A (1986), "A Wave Response Climate Description for Long Term Calculations ", OMAE

Hill R, (1950), *The Mathematical Theory of Plasticity*, Oxford University Press, Oxford

Hohenbichler, M. and Rackwitz, R., (1988): "Improvement of Second-Order Reliability Estimates by Importance Sampling", *Journal of Engr. Mech.*, ASCE. 114(12), 2195-2199.

Hughes, T.J.R. and Liu, W.K.(1981), Nonlinear finite element analysis of shells (Part 1) - Three-dimensional shells, *Computer Methods in Applied Mechanics and Engineering*, Vol.26, pp.331-362.

Igland R T and Moan T (1993), "Reliability Analysis of Deep Water Pipelines During Laying, for Combined Pressure, Tension and Bending Loads", *Proc. of ISOPE 93*, Vol IV, pp 613-621

ISO/TC98/SC2/WG1, (1995), *General Principles on reliability for Structures*, 14th draft, May 1995

Jensen J J and Pedersen P T, (1985), " The buckling of submarine pipelines", *Advances in Offshore Oil & Gas Pipeline Technology*

Jiao, G. & Moan, T.(1994), "Target Safety Levels for Limit State Based Design", *SINTEF Report SFT70 94037*, Trondheim, Norway, 1994.

Jiao G., Sotberg T. and Igland R.T (1995), " Basic Uncertainty Measures for Reliability Analysis of Offshore Pipelines", *Sintef Report STF70 F95212*

Jirsa, J.O., Wilhoit Jr., J.C., Aguirre, M. and Mogbo, N.C. (1969): "Effect of Concrete Coating on the Rigidity of 12 3/4-in. Line Pipe", *Offshore Technology Conference*, OTC 1074.

Jirsa, J.O., Lee, F.E., Wilhoit, J.C. and Merwin, J.E (1972) "Ovaling of Pipelines under Pure Bending", *Offshore Technology Conference*, OTC 1569

Jordaan, I.J. (1988),"Safety Levels Implied in Offshore Structural Design Codes: Application to CSA Program for Offshore Structures", Memorial University, St John's, New Foundland, September

Ju, G.T. and Kyriakides, S.(1991), "Bifurcation buckling versus limit load instabilities of elastic-plastic tubes under bending and pressure", *Journal of Offshore Mechanics and Arctic Engineering, Transactions of the ASME*, Vol. 113, pp.43-52.

Kendall M and Stuart A, (1977), *The advance Theory of Statistics*, Vol. I, Charles Griffing & Company Limited, London 1977

Khuri A I and Cornell J A, (1987) *Response Surfaces, Design and Analysis*, Marcel Dekker, Inc, ASQC, Quality Press

Konuk, I. (1984): "Some Considerations on the Effect of Concrete Coating on the Pipeline Design",*Offshore Mechanics and Arctic Engineering*, OMAE Conference, New Orleans.

Korol, R.M., (1979),"Critical Buckling Strains of Round Tubes in Flexure",*International Journal of Mechanical Science*, Vol 21, pp 719-730

Kyogoku, T., Tokimasa, K., Nakanishi, H. and Okazawa, T.(1981), "Experimental study on the effect of axial tension load on the collapse strength of oil well casing", *Proceedings of the 13th Offshore Technology Conference*, OTC 4108.

Kyriakides, S. and Corona, E.(1987). "Pipe collapse under combined bending and pressure.", *Factors affecting pipe collapse - Phase II, EMRL* report No.87/8(PR-106-521), prepared for the American Gas Association, August 1985.

Kyriakides, S., Corona, E. and Fischer F. J (1991). "On the Effect of the UOE Manufacturing Process on the Collapse Pressure of Long Tubes", OTC 6758, Houston, May 1991.

Kyriakides, S. and Ju G.T.(1992), "Bifurcation and localization instabilities in cylindrical shells under bending-I. Experiments", *International Journal of Solids and Structures*, Vol.29(9), pp.1117-1142.

LAYFLEX (1994), *Sintef Report STF70 F95227*, SINTEF/Snamprogetti, Trondheim

Leadbetter, M.R, Lindgren, G. and Rootzen, H, (1983) *Extremes and Related Properties of Random Sequences and Processes*, Springer-Verlag, New-York

Lund, K.M, (1993), "Analyse av ekstreme påkjenninger i rørledninger under utlegging", *Diplom Thesis*, Norwegian Institute of Technology, Trondheim, 1993 (in norwegian).

Lund, S., Bruschi, R., Montesi, M., Sintini, L. (1993): "Laying criteria versus strain concentration at field joints for heavily coated pipelines" *Offshore Mechanics and Arctic Engineering* , Volume V, pp 41-56.

Madsen, H.O., Krenk, S. & Lind, N. "Methods of Structural Safety" Prentice Hall Inc., Englewood Cliffs, N.J., 1986.

Melhers, R E (1987), *Structural Reliability Analysis and Prediction*, Ellis Hoorwood Limited, Great Britan

Moan, T. (1988) "The Inherent Safety of Structures Designed according to NPD Regulations", *SINTEF Report STF71 F88043*, Trondheim

Moan T. and Jiao G.(1990)," Probabilistic Calibration of Design Criteria for Marine Risers", *Integrity of Offshore Structures (IOS-4)*, Elviers Science Publication

Mogbo, N.C., Jirsa, J.O. and Wilhoit Jr., J.C. (1971): "Effective Stiffness of Concrete Coated Line Pipe", *ASME* paper no. 71.

Morgan, G.W. and Peret, J.W. (1975): *Applied Mechanics of Marine Riser Systems* Petroleum Engineer, Oct. 1974 - Oct. 1975.

Murphey , C.E. and Langner C.G. (1985),"Ultimate Pipe Strength Under Bending, Collapse and Fatigue", *Int. Conference Offshore Mechanics and Arctics Eng.*, Vol 1, pp 467-477

Myers R H, (1976), *Response Surface Methodology*, Library of Congress Catalog Card No: 71-125611, USA

Mørk, K, Spiten J. Torselletti, E., Ness O.B. and Verley R. (1997), "The SUPERB Project, Buckling and Collapse Limit State ", *Proc. Of OMAE*, Vol V, pp 79-89

Ness O.B. and Verley R. (1995) ' Strain Concentration in Pipeline with Concrete Coating An Analytical Model', *Offshore Mechanics and Arctic Engineering*, OMAE Conference 1995, pp 507-514

NKB (1978), *Guidelines for Load and Safety Regulations for Load-carrying Structures*, Report No.55, Nordic Committee for Building Regulations.

NPD (1990), *Regulations for the Structural Design of Load-carrying Structures Intended for Explotations of Petroleum Resourses*, Norwegian Petroleum Directorate, Stavanger

Passano, E.A, (1994), "Efficient Analysis of Non-linear Slender Marine Structures", *Dr.Ing Thesis, MTA Report 1994:26*, Norwegian Institute of Technology, Trondheim, 1994

Pulici, M. and Ronzoni, R. (1995), " Gibraltar Strait Crossing : Dynamic Pipelay analysis in Irregular Sea State", *Offshore Mechanics and Arctic Engineering*, OMAE Conference 1995, Vol. V, pp 547-554

Ramberg W and Osgood W R, (1943), 'Description of Stress-Strain Curves by Three Parameters', *NACA Technical Note 902*

Riflex Program System (1995),"Flexible Riser System Analysis Program", *Report STF70 A95217*

Robertson J L M, Smart D and Al-Hassan T (1995), "Offshore North Sea Pipeline and Riser Loss of Containment Study (PARLOC) - Applications and Limitations in the Assessment of Operating Risks", *Proc. of OMAE 1995*, Volum V, pp 315-322

Rubinstein, R.Y., (1981): *Simulation and the Monte Carlo method*, J. Wiley & Sons, New York.

Schall, G., Gollwitzer, S., and Rackwitz, R., (1988): "Integration of Multinormal Densities on Surfaces",*Proc. of 2nd IFIP Working Conference on Reliability and Optimization on Structural Systems*, edited by P. Thoft-Christensen, Springer Verlag.

Schilling, G.S. (1965), "Buckling Strength of Circular Tobes", *Journal of Structure Division*, ASCE, Vol 91, pp 325-348

Sherman, D.R. (1976), "Tests of Circular Tubes in Bending", *Journal of Structure Division*, ASCE, Vol 102, pp 2181-2195

Sotberg T (1996), "The SUPERB Project: Reliability Based Design Guidelines for Submerged Pipelines", *OTC 8220* 1996

Sotberg T, Moan T, Bruschi R, Jiao G and Mørk K (1997), "The SUPERB Project, Recommended Target Safety Levels for Limit States Based Design", *Proc. of OMAE* , Vol V pp 71-77

Sparks, C.P. (1984): "The influence of tension, pressure and weight on pipe and riser deformations and stresses", *Journal of Energy Resources Technology*, Vol. 106, pp. 46-54.

Sriskandarajah, T. and Mahendran, I.K. (1992): "Critique of Offshore Pipelay Criteria and Its Effect on Pipeline Design", *Proc. Offshore Technology Conference* , OTC 6847, pp. 533-542.

SUPERB (1996), "Limit state Design Guideline for Offshore Pipeline", *Sintef report STF22 F96745*, Trondheim

SUPERB (1997),K Mørk, J spiten, E Torselletti, O B Ness and R Verley, " Buckling and Collapse Limit State", *Offshore Mechanics and Arctic Engineering*, OMAE Conference 1997, pp 79 -91

Sødahl N.R, (1991), "Methods for Design and Analysis of Flexible Risers", *Dr.Ing Thesis, MTA Report 1991:81,* Norwegian Institute of Technology, Trondheim, 1990

Tamano, T., Mimura, H. and Yanagimoto, S.(1982), Examination of commercial casing collapse strength under axial loading, *Proceedings of the 1st Offshore Mechanics/Arctic Engineering/Deep Sea Systems Symposium*, ASME, pp.113-118.

Thoft-Cristiansen P and Baker M J (1982) *Structural Reliability Theory and its Applications*, Springer Verlag, Berlin, Germany.

Timoshenko, S.P. and Gere, J.M.(1961), *Theory of elastic stability, 2nd edition*, McGraw-Hill International Book Company, pp.287-297.

Timoshenko, S.P. and Goodier, J.N. (1970), *Theory of elasticity*, 3rd Edition, McGraw-Hill Book Inc., pp.71-80

Tokimasa ,K. and Tanaka, K.(1986), "FEM analysis of the collapse strength of a tube", *Journal of Pressure Vessel Technology,* Transactions of the ASME, Vol.108, pp.158-164.

Turkstra C. J. (1970), *Theory of Structural Design Decisions Study No.2*, Solid Mechanics Division, University of Waterloo, Ontario

Tvergaard V, (1976), 'Buckling of elasto-plastic oval cylindrical shells under axial compression', *International Journal of Solids and Structures*, Vol. 12, pp. 683-691

Verley R.and Ness O.B. (1995) ' Strain Concentration in Pipeline with Concrete Coating Full Scale Bending Tests and Analytical Calculations', *Offshore Mechanics and Arctic Engineering*, OMAE Conference 1995, pp. 499-506

Wilkowski, G.M. and Eiber, R.J.(1981), "Evaluation of tensile failure of girth weld repair grooves in pipe subjected to offshore laying stresses", *Journal of Energy Resources Technology,* Transactions of the ASME, Vol. 103(1981), pp. 48-55.

Winter, P.E. De, Stark, J.W.B. and Witteveen, J.(1985), "Collapse behaviour of submarine pipelines", *Shell Structures: Stability and Strength, Ed. R.Narayanan, Elsevier Applied Science Publishers,* pp. 221-246.

Yeh, M.K. and Kyriakides, S.(1986), "On the collapse of inelastic thick-walled tubes under external pressure", *Journal of Energy Resources Technology,* Transactions of the ASME, Vol.108, pp. 35-47.

Yeh, M.K. and Kyriakides,S.(1988), "Collapse of deepwater pipelines", *Journal of Energy Resources Technology,* Transactions of the ASME, Vol. 110, pp.1-11.

A NUMERICAL DATA BASE FOR CAPACITY OF TUBES UNDER COMBINED LOADS

A.1 General remarks

The appendix presents FE-results of the collapse behaviour of thick tube under combined external pressure, tension and bending loads, as shown in Figure A1(a). A numerical data base, shown in Table A.1 - Table A.12 is established by a systematic parametric study using the proposed finite element modelling. The validation of the model and the parameter studies are shown in Figures A3 - A28. The data base have been used in Bai et al (1992), Bai et al (1993a), Bai et al (1993b), Bai et al (1993c), Bai et al (1994),Bai et al (1995) and Bai et al (1997).

It is noted the parameter studies for thick tubes under combined pressure, tension and bending are limited to the following ranges:

Mean diameter D_0=25.4 mm; tube length=infinite; Young's modulus E=2.05×10^5 MPa (N/mm^2); Poison's ratio ν=0.3; Diameter to thickness ratio $10<D_0/t<40$; The ratio between the yield parameter and Young's modulus $0.001<\sigma_p/E<0.003$; The strain-hardening parameter $5<n<25$; The yield anisotropy parameter $0.8<S<1.2$; Initial imperfection parameter $0.0015<\delta_0<0.005$; The residual stress parameter $-0.4<\sigma_r/\sigma_0<0.4$

A.1.1 FEM-modelling

FEM-modelling

The tube is modelled as a long circular cylinder with mean diameter D_0, wall thickness t, under simultaneous action of external pressure, tension and bending. Figure A1(b) shows a shell mesh for collapse under combined external pressure, tension and bending loads.

The elastic-plastic large deflection analysis is carried out by means of the finite element program ABAQUS (1992). In the following the modelling and computational technique used, are described.

The mean diameter D_0 is fixed at 25.4mm and relevant D_0/t ratios are obtained by changing the tube thickness t.

Since initial ovality is the most important factor affecting tube pressure collapse, it is modelled carefully, by defining the initial coordinates of the nodes. An initial ovality parameter defined as follows is adopted:

$$\delta_0 = \frac{D_{max} - D_{min}}{D_{max} + D_{min}} \tag{A.1}$$

where D_{max} and D_{min} represent the maximum and minimum diameters measured at a weakest cross-section. The initial shape of the cross-section is approximated as the ring pressure buckling mode:

$$R_\theta = 0.25(D_{max} + D_{min})(1 + \delta_0 \cos(2\theta)) \tag{A.2}$$

Manufacturing processes which do not involve complete annealing will leave residual stresses in the tubes. The amount and distribution of the residual stress depend on the type of manufacturing process involved. In the present study, the distribution of the residual stress is assumed as a linear solution of pure bending of a curved bar (Timoshenko and Goodier 1970), and is expressed by the following formula:

$$\sigma_{r\theta} = -4k\left[-\left(\frac{R_i^2 R^2}{r^2}\right)\ln\left(\frac{R}{R_i}\right) + R^2 \ln\left(\frac{r}{R}\right) + R_i^2 \ln\left(\frac{R_i}{r}\right) + R^2 - R_i^2\right] \tag{A.3}$$

where r is a polar coordinate, $R_i \le r \le R$. R_i and R denote inner radius and out radius, respectively. For a prescribed residual stress σ_r, the constant k is obtained from Eq. A.4, where $\sigma_{r\theta}$ is according to Eq.A.3 and therefore the distribution of residual stress $\sigma_{r\theta}$ is evaluated from Eq. A.3 .

$$\sigma_r = \sigma_{r\theta}(r = R_i) \tag{A.4}$$

The residual stress is approximately linear across the thickness, as shown in Figure A1(c). The residual stress is maximum on the inner wall and minimum on the tube outer wall. A positive

residual stress is defined as tensile stresses on the inner wall. The effect of residual stress is accounted for by setting initial stress at integration points of element layers.

The cylindrical surface is modelled by a shell element of the type S8R5. The element is a general isoparametric shell element mainly based on the theory by Hughes and Liu(1981). The thick shell is modelled using 7-11 layers over the thickness and using numerical integration over the thickness. In the calculation of the element stiffness matrices, reduced integration is employed to overcome artificial locking. The Kirchhoff hypothesis of zero transverse shear is imposed directly at the integration points based on the penalty function concept. Traditionally, RIP(reduced integration, penalty method) shell elements have been developed by direct approximation in three-dimensional continuum theory (Hughes and Liu 1981). Instead of that, the shell element in ABAQUS is derived by a numerical approximation of a two-dimensional shell theory.

It is assumed that all variables involved in the analysis are constant along the tube length. This assumption is valid for long tubes (when the effect of end constraints can be neglected) until localized buckle occurs. In this way the modelling is reduced to a two-dimensional one and only one element is required in the longitudinal direction of the tube. The complexity of the problem is dramatically simplified compared with a model which is necessary to reproduce local (bifurcation) buckling modes.

A.1.2 Boundary and load conditions

Adequate boundary conditions are applied (ABAQUS 1992). The plane z=0 is a plane of symmetry, implying that nodes on that plane must satisfy: $u_z=\phi_x=\phi_y=0$. To remove the rigid body rotation mode about the z-axis, rotations around z-axis ϕ_z is constrained at the plane x=0. For all nodes on that plane the symmetry constraints are $u_x=\phi_y=\phi_z=0$. To impose the symmetry conditions about the rotated end plane (the other end of the tube piece), a "beam node" is introduced to represent the motion of the end plane, and the nonlinear multi-point constraints capacity (ABAQUS 1992) is applied.

The pressure load is applied as pressure acting on shell elements. The tension load is directly applied at the "beam node". Both pressure and tension loads are incremented using a load control procedure. However, bending load is applied using a displacement control procedure, incrementing the curvature of cross-section. This is achieved by imposing rotation at the "beam node". For all loads, rigorous tolerance criteria for equilibrium iterations are applied and the size of increment is automatically determined according to the number of iterations cost in the previous increments. Mesh convergence studies have demonstrated that six element for a modelling are sufficient to accurately predict collapse behaviour. It has been confirmed that seven integration points through the wall thickness are sufficient for the elastic-plastic analysis.

A.1.3 Material parameters

Stress(σ)-strain(ε) relationship used in the analysis is crucial to correctly predict collapse behaviour of the tubes. Therefore a realistic stress-strain curve (e.g. expressed by a Ramberg-Osgood curve) is approximated by multi-linear curves. More than 20 points are used to get the correct multi-linear curves so that actual stress-strain relationships could be simulated accurately over all of the strain range involved. An isotropic hardening rule is employed in the analysis.

In the parametric studies, the material parameters for pipeline steel grades X-52, X-65 and X-77 given by Tvergaard (1976) have been adopted. The stress-strain relationship is defined as

$$\begin{aligned} \sigma &= E\varepsilon && \varepsilon \le \varepsilon_p \\ \sigma &= \sigma_p \left(\frac{nE\varepsilon}{\sigma_p} + 1 - n \right)^{\frac{1}{n}} && \varepsilon > \varepsilon_p \end{aligned} \tag{A.5}$$

where σ_p, ε_p and n are linear stress limit, linear strain limit and strain hardening parameter, respectively. E denotes Young's modulus.

For grade X-52: $E=2.05\times10^{11}$ N/m^2; $\nu=0.3$; $\sigma_p/E=0.0012$; $n=9.05$
For grade X-65: $E=2.05\times10^{11}$ N/m^2; $\nu=0.3$; $\sigma_p/E=0.0016$; $n=9.65$
For grade X-77: $E=2.05\times10^{11}$ N/m^2; $\nu=0.3$; $\sigma_p/E=0.0020$; $n=10.0$

where ν denotes Poisson's ratio. Note, the quality of the above values of σ_p/E and n may be improved if material tests are conducted for these material grades.

The material stress-strain curves used in the present finite element analysis are defined using Tvergaard curves. However, in many cases, the stress-strain curves are defined using Ramberg-Osgood curves as, (see Ramberg and Osgood (1943)) :

$$\varepsilon = \frac{\sigma}{E}\left[1 + \frac{3}{7}\left(\frac{\sigma}{\sigma_R}\right)^{n_R-1}\right] \tag{A.6}$$

or

$$\frac{E}{E_s} = \frac{E\varepsilon}{\sigma} = 1 + \frac{3}{7}\left(\frac{\sigma}{\sigma_R}\right)^{n_R-1} \tag{A.7}$$

Linear stress limit σ_p of the Tvergaard curves could be defined as the stress at which $E_s=0.95E$ of the Ramberg-Osgood curves. The stress-strain curves due to the Tvergaard curves and those due to the Ramberg-Osgood curves have been compared in Figure A2 for $n=n_R=5$ and 10, assuming σ_p of the Tvergaard curves equals to σ_R of the Ramberg-Osgood curves.

Many of the thick tubes are drawn, and many of the plates used for welded pipes are rolled. Such kind of manufacturing processes (rolling and drawing) tend to induce material anisotropy. In most situations, the anisotropy occurs in the form of differences in the yield stresses in the hoop, thickness and axial directions. The yield anisotropy is accounted for by using Hill's yield function (ABAQUS, 1992), Hill (1950) . Neglecting the stress component normal to the tube wall and all shear stress components, the Hill's yield condition is expressed as :

$$\sigma_0^2 = \sigma_{0x}^2 - \left(1+\frac{1}{S_\theta^2}-\frac{1}{S_r^2}\right)\sigma_{0x}\sigma_{0\theta} + \frac{1}{S_\theta^2}\sigma_\theta^2 \qquad (A.8)$$

where $S_\theta = \sigma_{0\theta} / \sigma_{0x}$ and $S_r = \sigma_{0r} / \sigma_{0x}$ are the anisotropic parameters.

A.2 Validation of the FE-model approach

A.2.1 External pressure

Hoop collapse takes place when a tube is subjected to large external pressure. The collapse involves change of cross-section from the uniformly circular to a nonuniformly oval configuration. The collapse of a long, circular tube is modelled as a unit length ring since the effect of boundary conditions at both ends is negligible.

The FEM analysis procedure was validated through a comparison with a series of full-scale experiments using X-42 and X-65 grade steel tubes (Yeh and Kyriakides 1988). All of the test specimens in this study were analysed, and the biggest deviation in terms of collapse pressure between the experimental and the present numerical results was less than 5 percent.

A.2.2 Bending

The finite element modelling has been validated through a systematic comparison with results from an experimental investigation of thick tubes under pure bending due to Kyriakides and Ju (1992). The agreement between the two maximum moment points, from the experiment and from the finite element analysis, is excellent, Figure A3. The experimental results show that the three critical curvatures corresponding to ripples, maximum moment point, and catastrophic collapse (kink, or local buckling), respectively, are close to each other if D_0/t is equal to 35. It is therefore decided to mainly look at the curvature at maximum moment in the present study.

A.2.3 Tension

For pipelines with surface flaws or through-wall flaws, systematic investigation on tensile failure criteria have been carried out by e.g. Wilkowski and Eiber (1981). The tensile failure is estimated using a flow stress concept. For typical pipeline material X-52 and X-77, the flow stress is approximately $\sigma_f = 1.2\sigma_0$. In terms of strain, flow strain corresponding to $1.2\sigma_0$ is approximately 0.02. For tubes under combined loads, a stretch failure is defined when mean axial strain is increased up to 0.005. The validation is made for combination of Pressure-Tension, Babcock and Madhavan (1987), Figure A5(a) - A5(e).

A.2.4 Pressure - Bending

The FEM analysis procedure for tubes under combined pressure and bending is validated through the simulation of the collapse tests. In Figure A3(a) - Figure A3(c) moment-curvature relationships of tubes obtained by the present FEM analysis and experimental and analytical results due to Ju and Kyriakides (1991), are compared. It is seen that the present analysis predicts both load-deformation relationships and maximum moments (curvatures) very well.

A more extensive comparison is made with experimental results by Corona and Kyriakides (1988). The pressure-curvature envelopes for D_0/t=24.5 and for D_0/t=34.7 are presented in Figure A4 (a) and A4(b), respectively. The P→κ and κ→P load paths are considered. The agreement between the present analysis and experiments is again excellent. It is clearly shown that the P→κ collapse envelope is substantially lower than the κ→P collapse envelope. The pressure and bending interact through the ovalization of cross-section and yielding under bi-axial loads. For bending dominant cases, bending collapse takes place. In contrast, the interaction leads to hoop collapse when the pressure load is dominant.

A.2.5 Pressure - Tension

Figure A5 (a) - (e) show a comparison of the present FEM analysis and experimental and analytical results obtained by Babcock and Madhavan (1987). The tension-pressure collapse envelopes for $D_0/t = 27.2$ (P→T) and for $D_0/t = 12.2$ - $D_0/t = 38.3$ (T→P) are presented. The circumferential yield stress is reduced due to the axial stress following Hill's yield function. Therefore, the collapse pressure decreases with the increase of the tension load.

In the present FEM analysis, material anisotropy is included by Hill's yield condition. The stress-strain relationship of the material is represented by multi-linear curves and an isotropic hardening rule. It is seen that excellent agreement has been achieved. The present FEM analysis gives better prediction than Babcock and Madhavan's analysis.

A.2.6 Bending - Tension and Pressure - Tension - Bending

For these load combinations, there are no laboratory test data available. However, the finite element model has been validated using laboratory tests of pipes under combined tension and pressure and under combined bending and pressure in the previous sections.

A.3 Parameter study

The analysis is made under the following assumptions: X-52 (σ_y/E=0.0012), n=9.05, σ_r=0, S=1, D_0/t=25 and δ_0=0.005. In the following, sensitivity of collapse envelopes to basic parameters are studied by changing one of the parameters each time from the base case.

A.3.1 Pressure

Two problems which have not been resolved for the collapse pressure, are studied : the effect of residual stress and the effect of initial imperfection on the collapse pressure. The first problem is chosen because some researchers claimed that the residual stress greatly reduces the collapse strength while others showed that the effect is very small.

Figures A6 (a) and (b) show the effect of residual stress on the collapse pressure for typical pipe material X-52 and X-77. In the figures, P_{co}^* denotes collapse pressure of tubes free from residual stress. The collapse strength is linearly reduced with the increase of the amount of residual stress $\sigma_{\theta r}/\sigma_0$. However, the biggest reduction for a residual stress $\sigma_{\theta r}/\sigma_0$ equal to 0.5, is less than 5 percent. This effect is basically in agreement with Yeh and Kyriakides(1986). However, even if the material is assumed to be elastic-perfectly-plastic as assumed by Tokimasa and Tanaka(1986), the large reduction shown by them, has not been obtained. The reduction is almost zero when D_0/t is 15 for material X-52 and D_0/t is 35 for material X-77. This implies that in the fully plastic collapse region and fully elastic collapse region, there is no residual stress effect. Even in elastic-plastic collapse region, the effect of residual stress seems to be small and could normally be neglected.

Figure A7 shows how the collapse strength is reduced by varying the initial ovality between δ_0= 0.0015 and 0.005. The results for material X-52 and X-77 are presented in Figures A7 (a) and (b), respectively. The slenderness ratio λ is defined as

$$\lambda = (P_0/P_E)^{1/2} = (D_0/t)[\frac{(1-\nu^2)}{E}\sigma_0]^{1/2} \qquad (A.9)$$

A typical tolerance level for the initial ovality magnitude δ_0 in design codes for pipelines may be 0.005. For D_0/t in the range between 15 and 35, the difference between collapse pressure for imperfection amplitudes 0.0015 and 0.005 is about 15 percent.

A.3.2 Bending

Maximum moment and corresponding curvature are presented in the following, the effect of diameter to thickness ratio D_0/t, the effect of the ratio between the yield parameter and Young's modulus, σ_p/E, the effect of the strain-hardening parameter n and the effect of the yield anisotropy parameter S are considered.

Figures A8 (a) and (b) show maximum moments and corresponding curvatures as a function of diameter to thickness ratio D_0/t. It is found that the normalized collapse moment M_{co}/M_0 could be approximated by a linear function of D_0/t. The normalized collapse curvature κ_{co}/κ_0 is insensitive to D_0/t.

Figures A9 (a) and (b) presents the normalized collapse moment and curvature as a function of the ratio between the yield parameter and Young's modulus σ_p/E. It is shown that the normalized collapse moment increases with σ_p/E and the normalized collapse curvature is almost constant for different σ_p/E.

The effect of the strain hardening parameter n on the maximum moment and corresponding curvature is presented in Figures A10 (a) and (b). It is seen that the collapse moment and curvature are significantly affected by the strain-hardening parameter n. They are decreasing rapidly with an increasing n.

The difference in yield stress in the longitudinal and circumferential directions may have a significant effect, even for tubes under pure bending. A yield anisotropy parameter S is defined as the ratio between yield stress in the circumferential and longitudinal directions. Figures A11 (a) and (b) show the effect of the yield anisotropy parameter S on the collapse moment and curvature, respectively. It is shown that the collapse moment and curvature depend linearly on the anisotropy parameter S.

A.3.3 Pressure-Tension

Figure A12(a) presents the effect of load paths for D_0/t=15; 25 and 35. The P→T load path gives lower collapse envelopes than the T→P load path. It has been shown that the effect of load paths is negligible when the tension load is lower than T/T_0=0.6. On the other hand, the effect of load paths becomes significant when the tension load is dominant(T/T_0>0.6). In addition, the deviation between the two collapse envelopes is bigger for D_0/t=15 than for D_0/t=35. This is because the former involves larger plastic deformation and the load path effect is basically due to path dependency of plasticity.

In Figure A12(b) predicted tension-pressure collapse envelopes for the P→T path are presented as a function of the initial ovality, δ_0. It is shown that the collapse envelopes are significantly reduced

when the initial ovality parameter is increased from 0.0015 to 0.005, especially when the pressure load is dominant.

A.3.4 Bending-Tension

The collapse behaviour of thick tubes under combined tension and bending load is supposed to be greatly influenced by the load path applied. Therefore the two load paths T→κ and κ→T are considered.

Figure A13 presents responses for the T→κ. The tension load T is first applied to a prescribed value. Then the tension load is fixed and the curvature κ is incremented. Predicted moment-curvature, ovalization-curvature and (mean) axial strain-curvature responses for T/T_0=0; 0.4; 0.8 are shown in Figures A13 (a) (b) and (c), respectively. The moment and curvature at the limit point (maximum moment) represent collapse values. It has been shown that the collapse moment is reduced by the tension load applied. However, the ovalization-curvature relationship is insensitive to the tension load. Since the axial tension is kept at a given level, the axial strain is increasing when the curvature is incremented.

Figure A14 presents responses for the κ→T load path. The tube is incrementally loaded to the chosen value of curvature at zero tension. Calculated moment-curvature and ovalization-curvature response for this part of the path are shown in Figures A14 (a) and (b), respectively. The tension is then incremented while the curvature is fixed at κ/κ_0=0.7; 1.0; and 1.3. The ovalization grows further and the bending load eventually decreases during the tension part of the loading path as shown in Figures A14(a) and (b). In addition, mean axial strain-tension curve is presented in Figure A14(c). There is no limit load point for this loading path.

From the above analysis, it is concluded that T→κ load path is more severe than the κ→T load path, and therefore in the following only T→κ load path is considered.

For the tension-bending interaction two other criterion are considered. First a ductile rupture criterion, herein the flow stress concept is considered, where the flow strain corresponding to 1.2 σ_0 is approximately 0.02. Secondly, the mean axial strain equal to 0.005 is adopted as a failure criterion since in offshore design rules equivalent stress estimated from beam theory is not allowed to exceed yield stress, which is equivalent to strain 0.005.

The normalized moment-tension, curvature-tension and curvature-axial strain envelopes for a basic case obtained based on the maximum capacity criteria, extreme fibre strain criteria (2%) and mean axial strain criteria (0.5%) are presented in Figures A15(a), (b) and (c), respectively. As shown from the figure the interaction is very sensitive to which criterion that is chosen. The Figures A15 - A19 show the sensitivity of D_0/t, σ_y/E, strain hardening and anisotropy.

Figure A16 shows the moment-tension envelopes and curvature-tension (mean-axial strain) envelopes for D_0/t=15 and 35. When the failure criterion is limit load point, tubes with lower D_0/t values can sustain higher combinations of tension and bending(or curvature and tension). However, the collapse envelopes based on extreme fibre strain and mean axial strain criteria are insensitive to D_0/t.

Figure A17 shows how the moment-tension envelopes vary with material grade(X-52 vs. X-77). The hardening parameter for both materials are approximately same. So the major difference between the materials is the ratio of the yield parameter to Young's modulus, σ_p/E. It is found that the collapse envelopes are insensitive to material grade (ratio of the yield parameter to Young's modulus σ_p/E).

Figure A18 shows the effect of hardening parameter n on the collapse envelopes. The values of n are 5 and 25. Lower n implies larger strain-hardening effect and therefore tubes with lower n can sustain higher loads. It is found that the effect of hardening parameter n is significant.

Figure A19 shows the variation of the collapse envelopes with the material anisotropy parameter S(=0.85 and 1.15). The parameter S is the ratio between circumferential and axial yield stresses. The material exhibits isotropic yielding if S=1. Since σ_p/E and n are material properties in the axial direction of the tube, larger S leads to higher load carrying capacity.

A.3.5 Pressure-Tension-Bending

The FEM is applied to study the collapse behaviour of tubes under various load paths and especially the sensitivity of the collapse envelopes to various parameters.

Figures A20(a) and (b) shows the effect of external pressure on the collapse envelopes based on maximum capacity criterion. The individual collapse envelopes for various P/P_{co}(=0.0, 0.2, 0.4, 0.6, 0.8) are presented. It is demonstrated that the external pressure reduces the moment-tension collapse envelopes.

Figures A20 (c) and (d) show the pressure-tension-moment envelopes based on the tearing rupture criterion and the axial collapse criterion respectively. The moment-tension interactions for various pressure loads P/P_{co} (=0, 0.2, 0.4, 0.6, 0.8) are presented. Comparing Figure A20(a) and Figures A20(c) and (d), it is found that the maximum capacity criterion leads to the lowest interaction envelope. Therefore, in the following, only finite element results due to this criterion are discussed.

The collapse behaviour of thick tubes under combined tension and bending load is supposed to be greatly influenced by the load path applied. Therefore the two load paths $T \rightarrow \kappa$ and $\kappa \rightarrow T$ are considered.

Figure A21 presents responses for the P→T→κ and T→P→κ . For the former load path is the pressure first applied to P/P_{co} = 0.4, then is the tension load T applied to a prescribed value. Then the pressure and the tension are fixed and the curvature κ is incremented. Predicted moment-curvature, ovalization-curvature and (mean) axial strain-curvature responses for T/T_0=0; 0.4; 0.8 are shown in Figures A21(a), (b) and (c), respectively. The moment and curvature at the limit point (maximum moment) represent collapse values. It has been shown that the collapse moment is reduced by the tension load applied. However, the ovalization-curvature relationship is insensitive to the tension load. Since the axial tension is kept at a given level, the axial strain is increasing when the curvature is incremented. T→P→κ is presented in the same figure, as shown, no significant effect of this load path is observed.

Figure A22 presents responses for the P→κ→T loading path. Tension load is incremented while the curvature is fixed at κ/κ_0=0.2, 0.4 and 0.6. The ovalization grows further and the bending load eventually starts to decrease during the tension part of the path as shown in Figures A22(a) and (b). The mean axial strain-tension relationships are presented in Figure A22(c). Both ovalization and mean axial strain increase rapidly when T/T_0 approaches a collapse load level.

From Figures A21-A22, it is concluded that the P→T→κ load path is more severe than the load paths T→P→κ and P→κ→T. Therefore, in the following parametric study, only the P→T→κ load path is considered, and the analysis is made under the following assumptions: X-52 (σ_y/E=0.0012), n=9.05, σ_r=0, S=1, D_0/t=25, δ_0=0.005 and P/P_{co}=0.4. In the following, sensitivity of collapse envelopes to basic parameters are studied by changing one of the parameters each time from the basic case.

Figure A23 shows how the pressure-tension-moment interaction based on maximum capacity criterion varies with D_0/t for P/P_{co}=0.4 and 0.8. It is found that the effect of D_0/t on the shape of collapse envelopes is small. However, tubes with lower D_0/t values can sustain higher combinations of pressure, tension and bending.

Figure A24 compares pressure-tension-moment interactions for different levels of initial ovality δ_0 (=0.0015, 0.0035 and 0.005). Since collapse pressure is sensitive to the initial ovality, the collapse envelopes are reduced with the increase of initial ovality.

Figure A25 shows how the circumferential residual stress affects the pressure-tension-moment interaction. The values of σ_r are $-0.4\sigma_0$, 0, $0.4\sigma_0$. It is shown that the effect of residual stress on the collapse envelopes is negligible.

Figure A26 shows how the pressure-tension-moment interaction varies with material grade. The major difference between the material X-52 and X-77 is the ratio of the yield parameter to Young's modulus. The load carrying capacity is lower for tubes with lower σ_y/E. This is confirmed by Figure

A26(c) which shows the sensitivity of the pressure-tension-moment interaction to yield stress/Young's modulus ratio σ_p/E.

Figure A27 presents the variation of the pressure-tension-moment interaction with the strain-hardening parameter n. Lower n implies larger strain-hardening effect and therefore leads to higher collapse envelopes.

Figure A28 shows the variation of the pressure-tension-moment interaction with the material anisotropy parameter S(=0.85, 1.0, 1.15). The circumferential yield stress is lower than that in the axial direction if S<1. It is demonstrated that S<1 leads to lower collapse loads. On the other hand, S>1 leads to higher collapse envelopes.

From Figures A20 - A28, it is concluded that material properties play an important role to the collapse of thick tubes under combined external pressure, tension and bending loads. Higher values of σ_p/E, lower values of n or higher values of S lead to higher collapse envelopes.

A.4 Figures, based on the data base

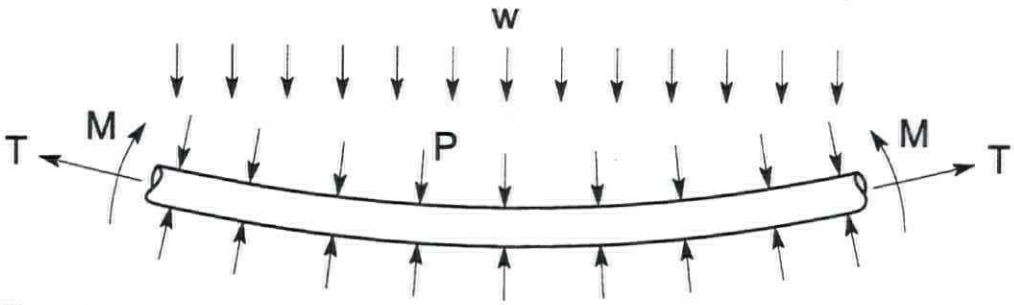

Figure A1a Tube under combined pressure, tension and bending

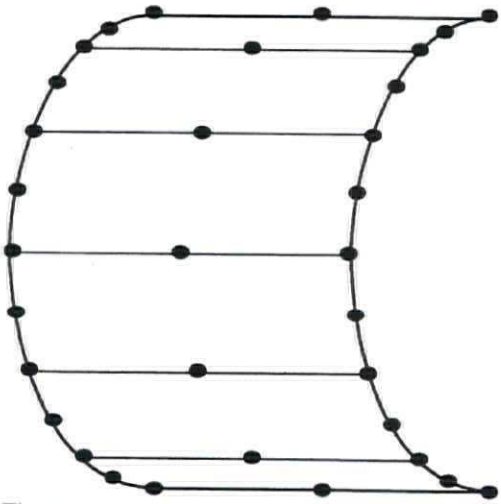

Figure A1b Finite element model

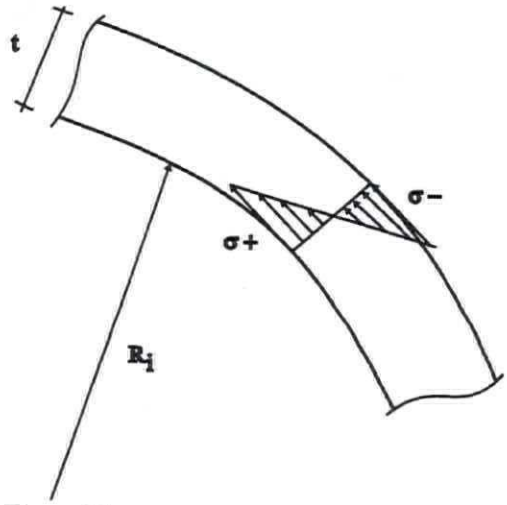

Figure A1c Residual stress

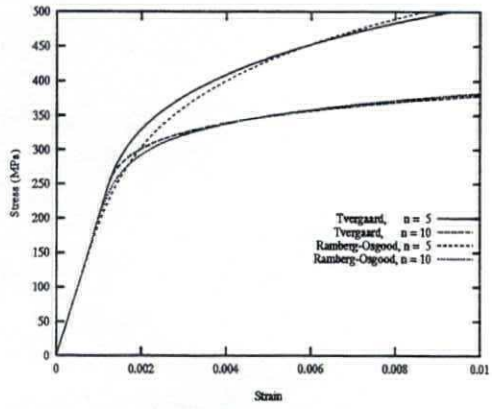

Figure A2 The stress-strain curve, Tvergaard and Ramberg-Osgood

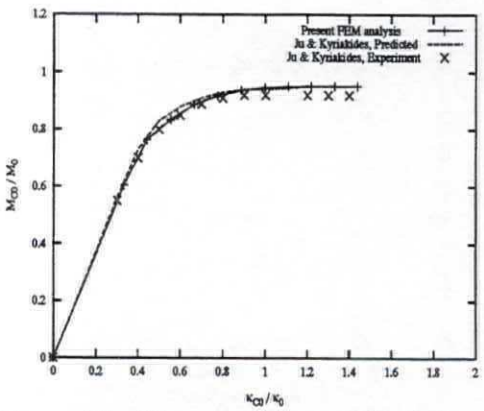

Figure A3a Moment-curvature, P/P_0=0.0

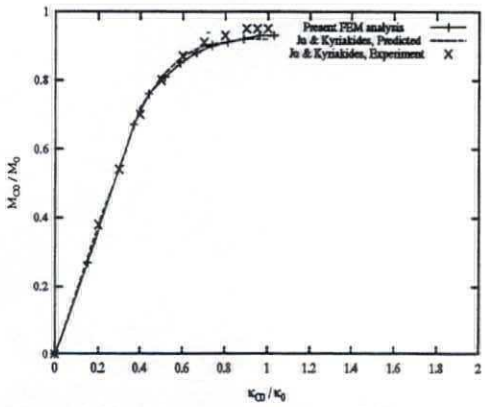

Figure A3b Moment-curvature, P/P_0=0.21

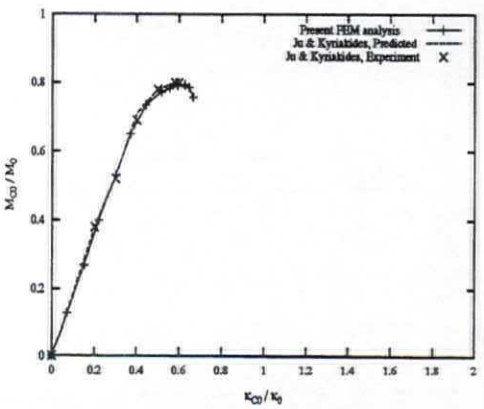

Figure A3c Moment-curvature, P/P_0=0.62

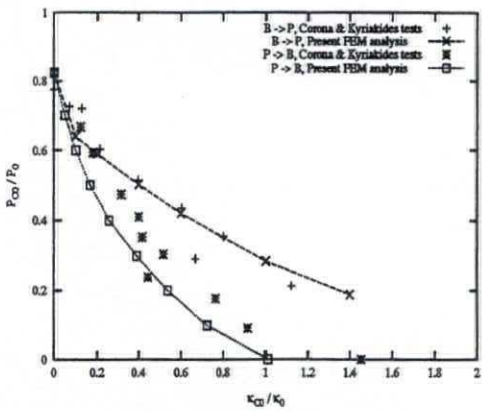

Figure A4a Pressure-curvature, D/t=24.5

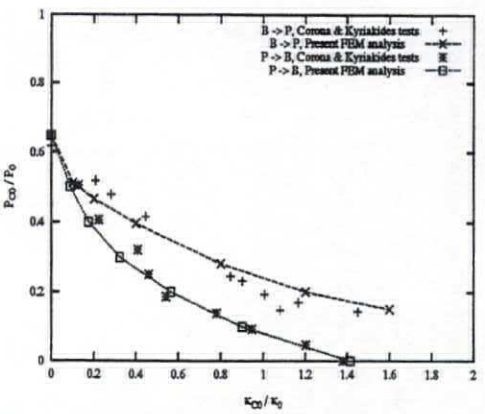

Figure A4b Pressure-curvature, D/t=34.7

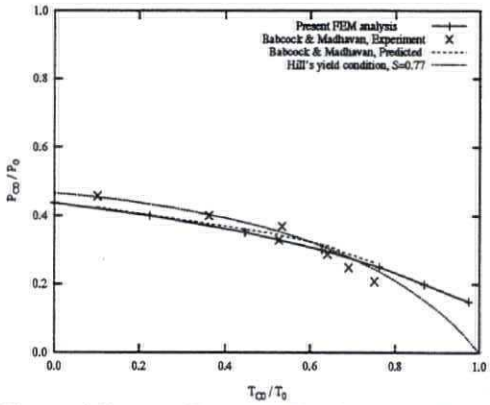

Figure A5a Pressure-Tension, D/t=27.2

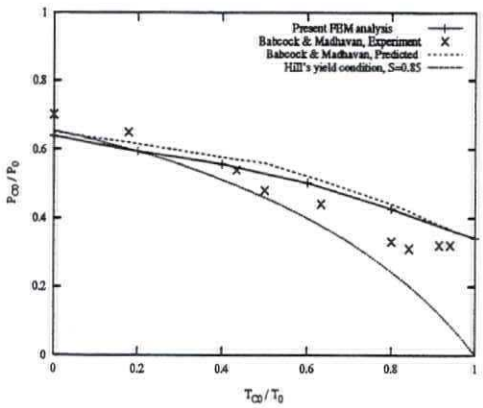

Figure A5b Tension-Pressure, D/t=18.2

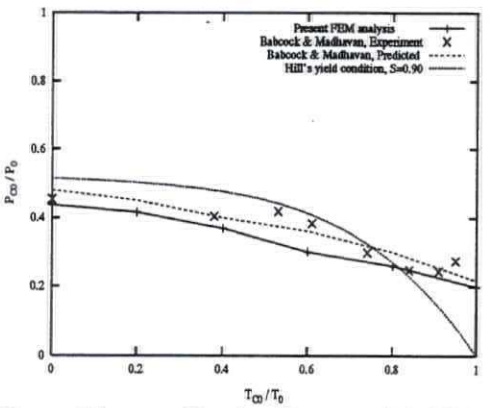

Figure A5c Tension-Pressure, D/t=38.3

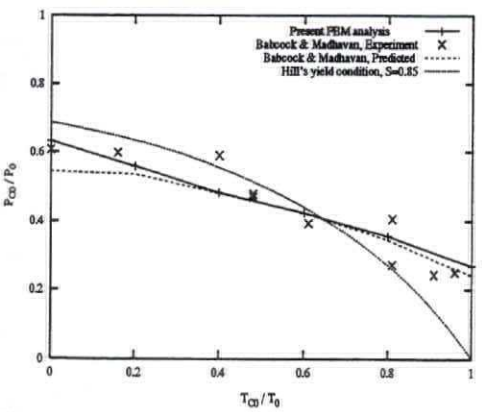

Figure A5d Tension-Pressure, D/t=24.5

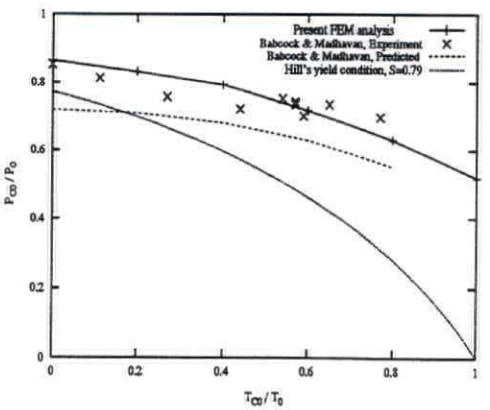

Figure A5e Tension-Pressure, D/t=12.2

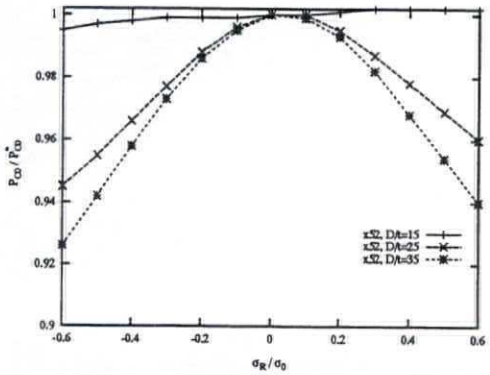

Figure A6a Collapse pressure, residual stress, X52

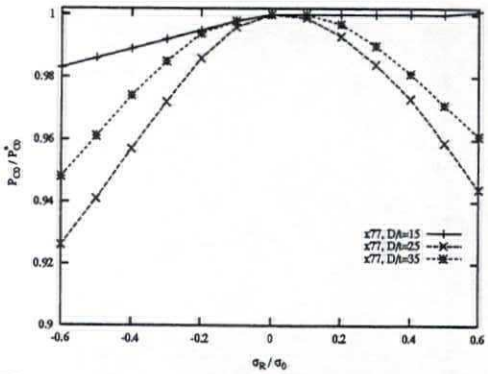

Figure A6b Collapse pressure, residual stress, X77

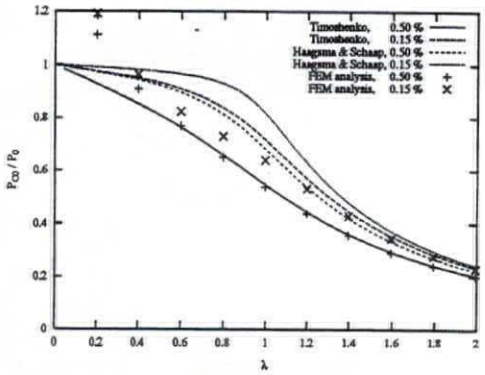

Figure A7a Collapse pressure, initial ovality, X52

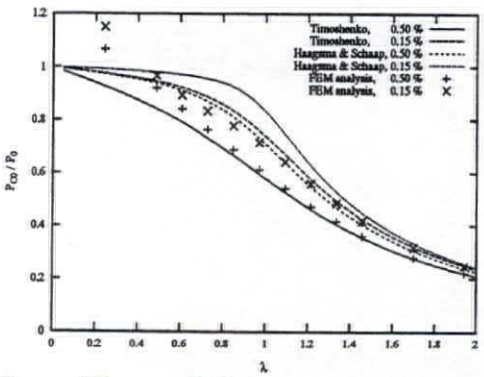

Figure A7b Collapse pressure, inital ovality, X77

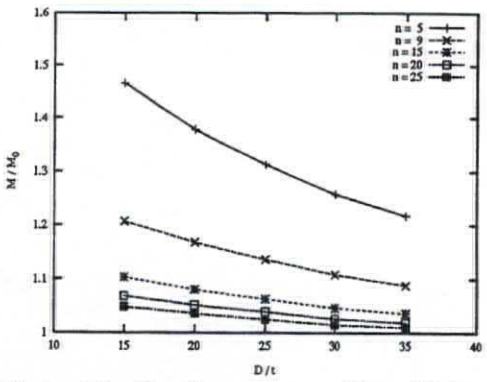

Figure A8a Bending moment, effect of D/t

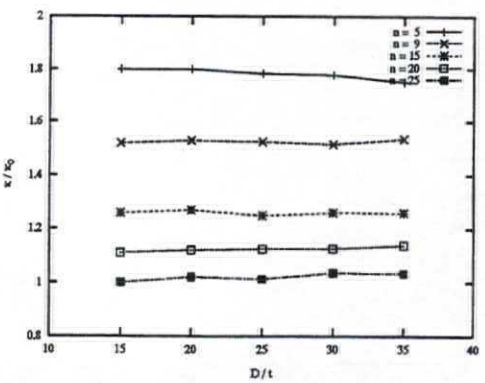

Figure A8b Bending curvature, effect of D/t

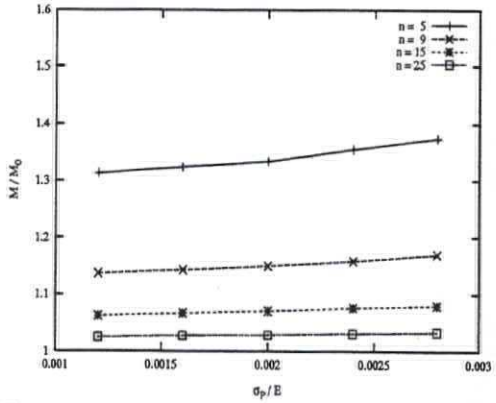

Figure A9a Bending moment, effect of σ_p/E

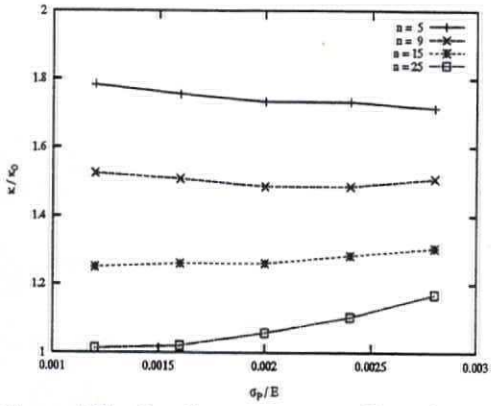

Figure A9b Bending curvature, effect of σ_p/E

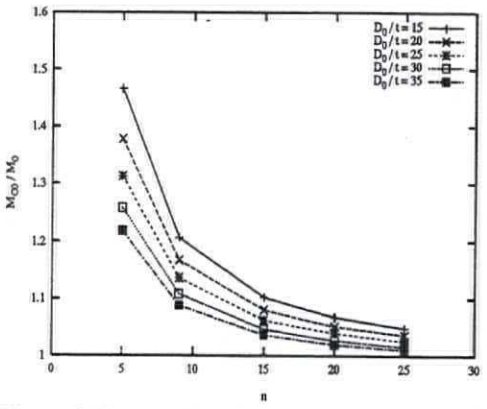

Figure A10a Bending moment, effect of n

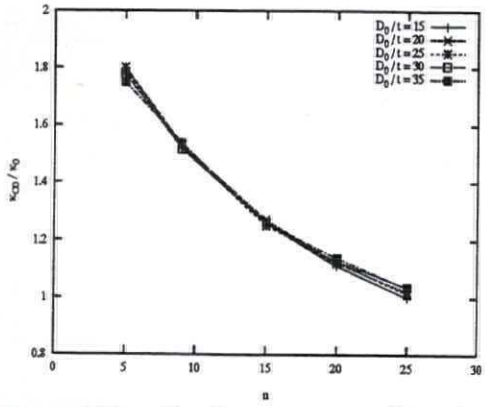

Figure A10b Bending curvature, effect of n

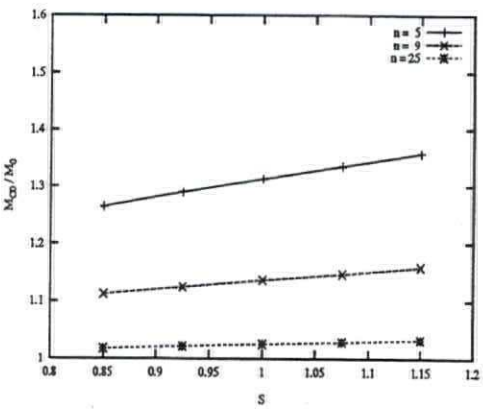

Figure A11a Bending moment, effect of S

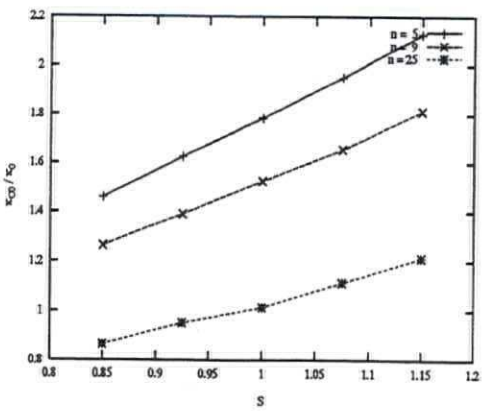

Figure A11b Bending curvature, effect of S

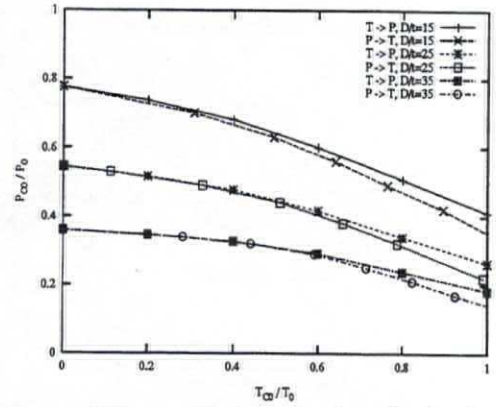

Figure A12a Pressure-tension, loadpath

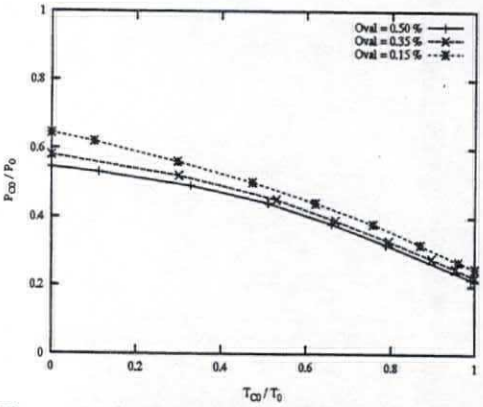

Figure A12b Pressure-tension, initial ovality

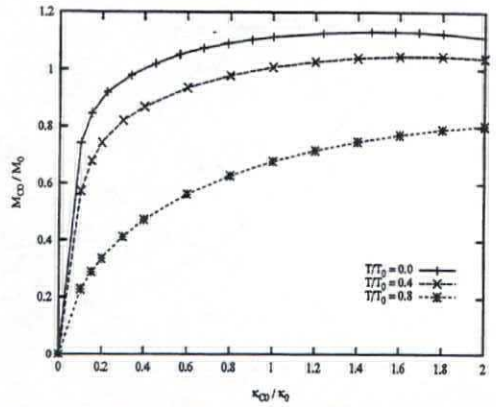

Figure A13a Tension-bending, moment-curvature

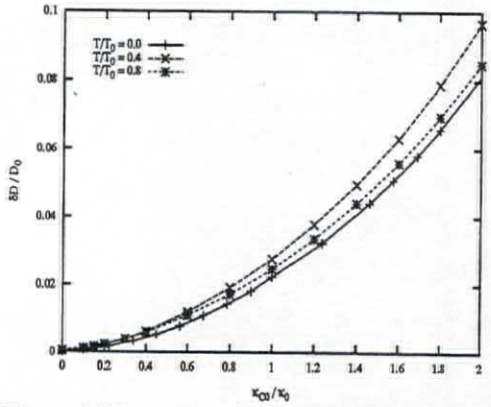

Figure A13b Tension-bending, ovalisation-curvature

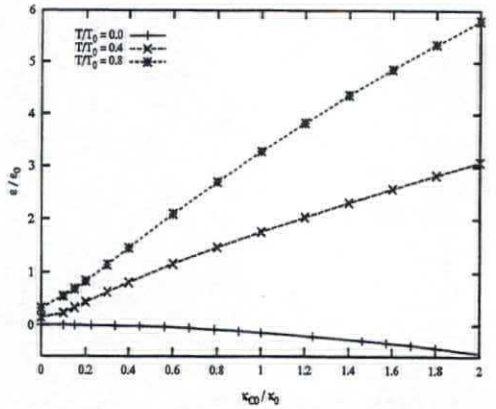

Figure A13c Tension-bending, mean axial strain-curvature

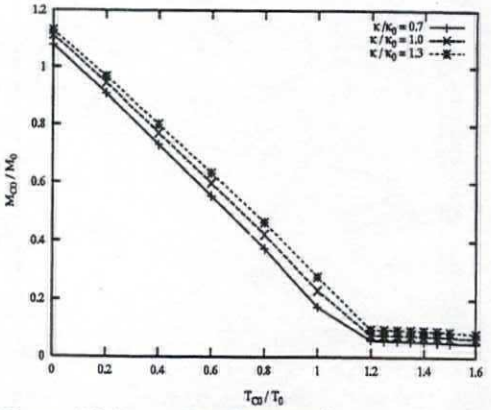

Figure A14a Bending-tension, ovalisation-tension response

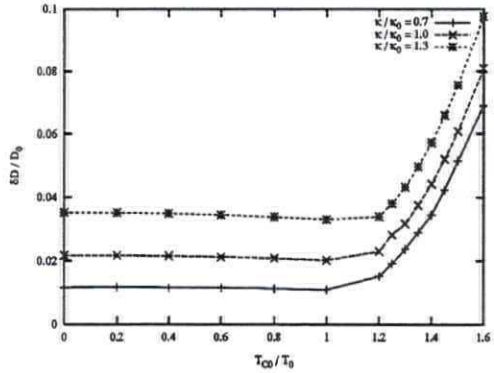

Figure A14b Bending-tension, moment-tension response

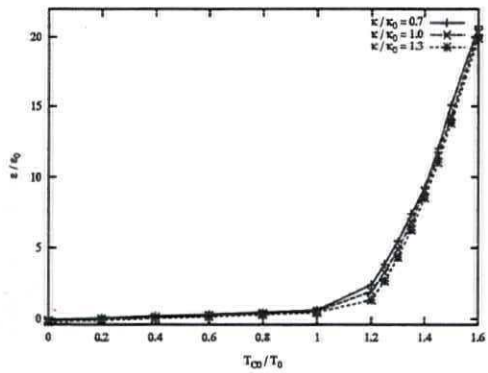

Figure A14c Bending-tension,mean axial strain-tension response

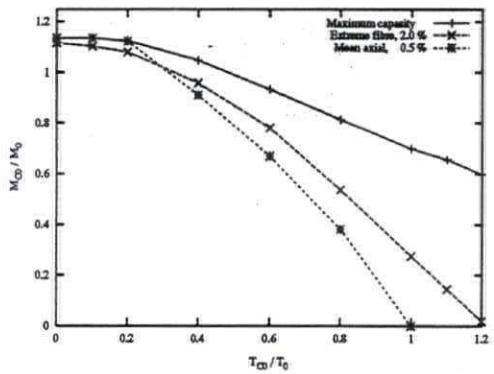

Figure A15a Tension-bending, moment-tension interaction

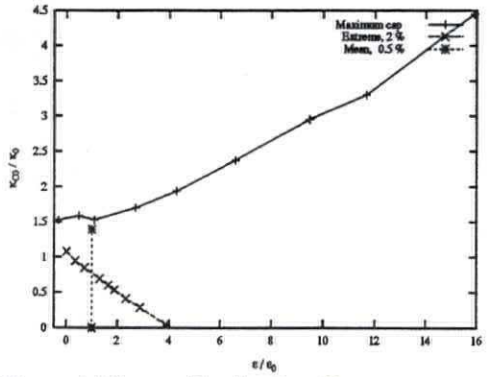

Figure A15b Tension-bending, curvature-mean axial strain

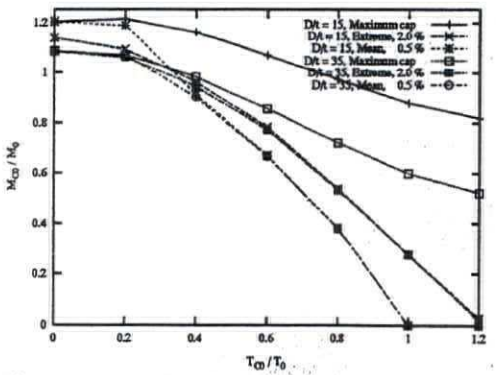

Figure A16a Tension-bending, effect of D/t

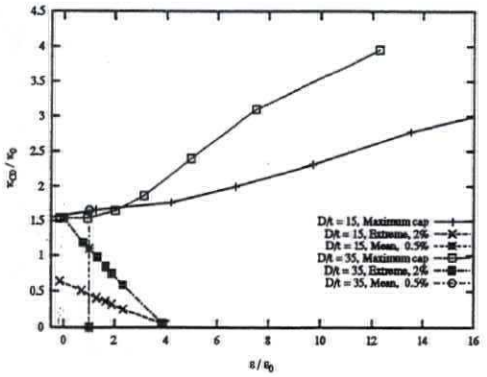

Figure A16b Tension-bending, curvature-strain, effect of D/t

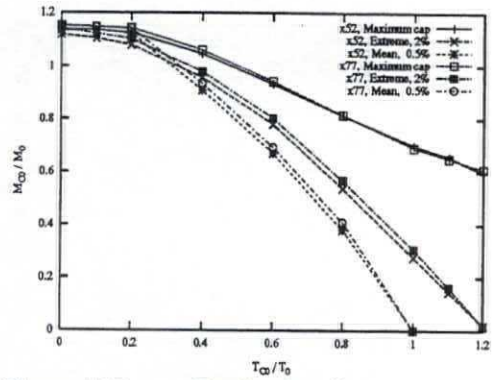

Figure A17a Tension-bending, moment-tension response, effect of steel grade

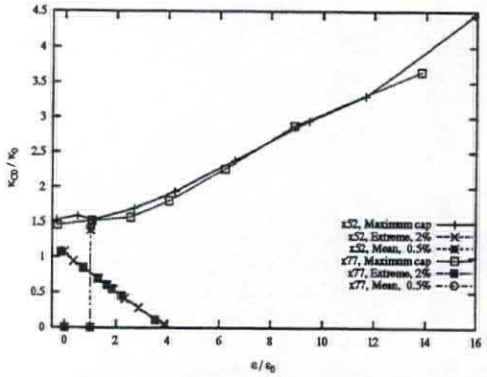

Figure A17b Tension-bending, mean axial strain-tension response, X52/X77

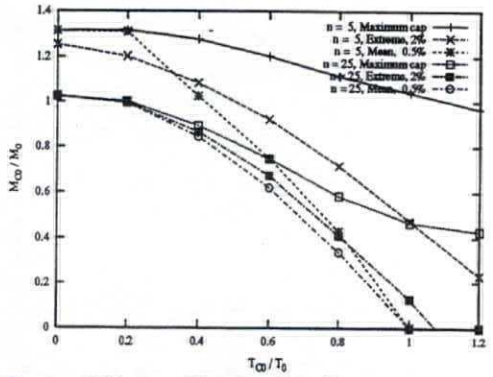

Figure A18a Tension-bending, moment-tension interaction, effect of hardening (n).

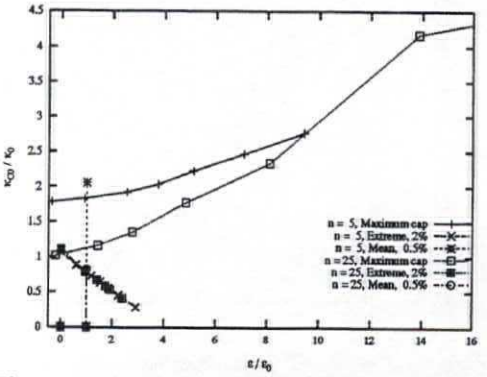

Figure A18b Tension-bending, curvature-mean axial strain , effect of n.

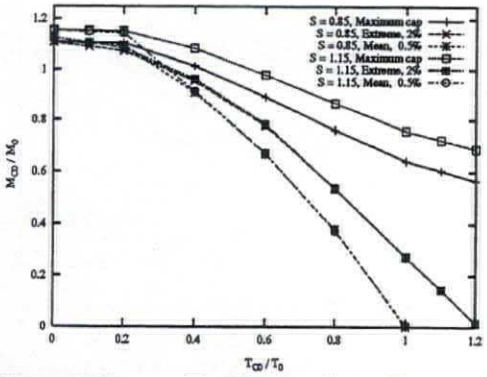

Figure A19a Tension-bending, effect of anisotropy (S).

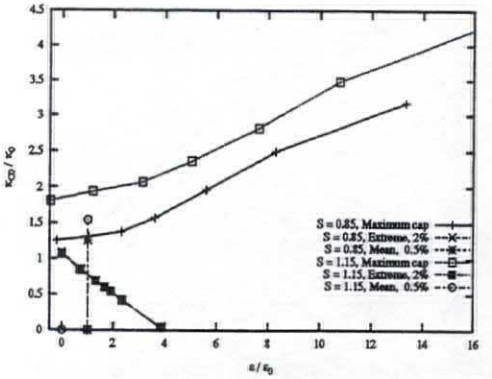

Figure A19b Tension-bending, curvature-strain, effect of anisotropy (S).

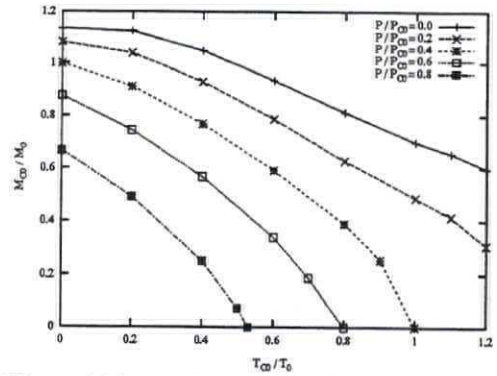

Figure A20a Pressure-tension-bending, maximum cap. criterion, moment-tension.

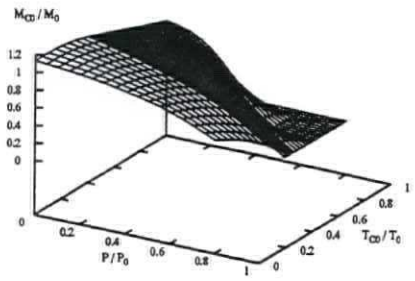

Figure A20b Pressure-tension-bending, maximum cap. criterion, collapse surface

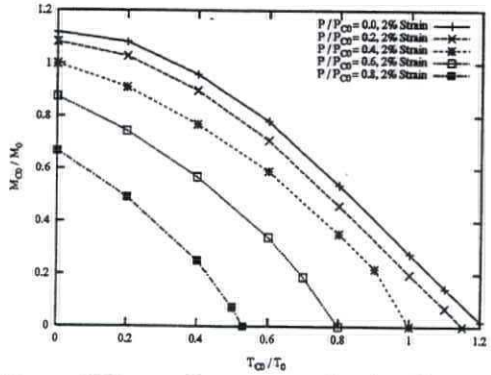

Figure A20c Pressure-tension-bending, extreme fibre strain criterion, moment-tension

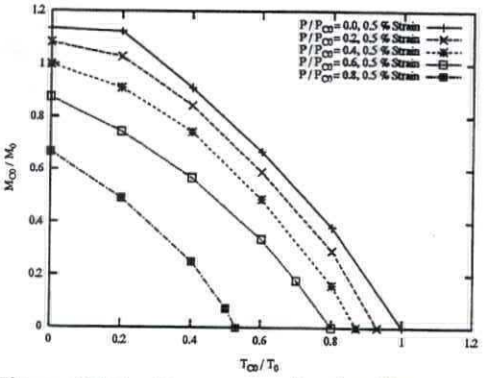

Figure A20d Pressure-tension-bending, mean axial strain criterion, curvature-axial strain

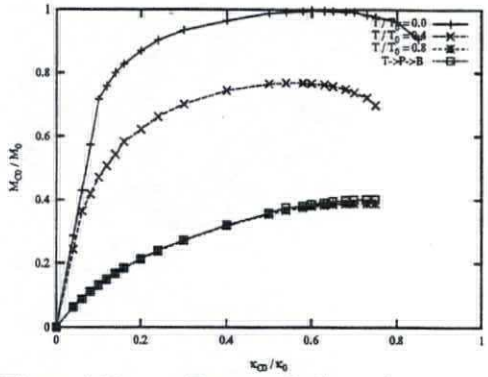

Figure A21a Pressure(0.4)-tension-bending, moment-curvature response

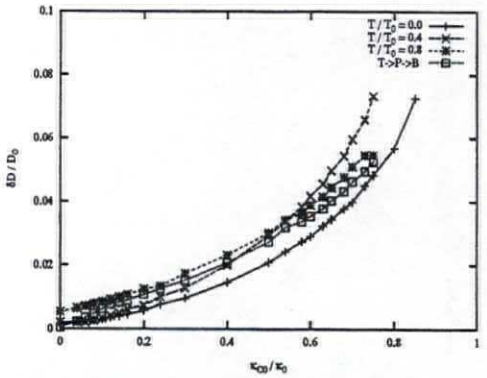

Figure A21b Pressure(0.4)-tension-bending, ovalisation-curvature response

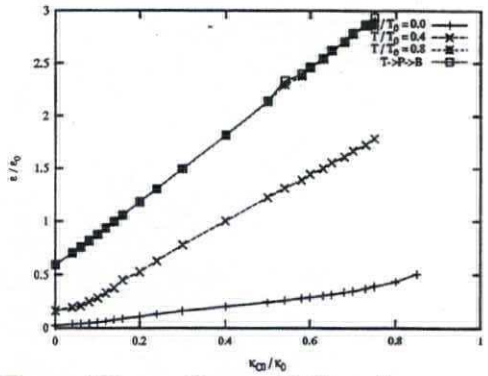

Figure A21c Pressure(0.4)-tension-bending, mean axial strain-curvature

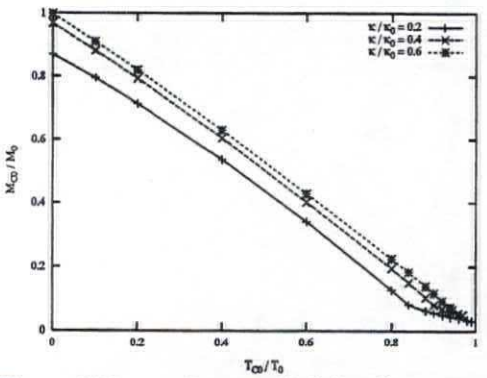

Figure A22a Pressure(0.4)-bending-tension, moment-tension response

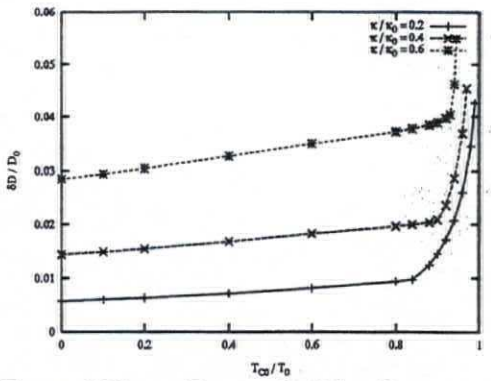

Figure A22b Pressure(0.4)-bending-tension, ovalisation-tension response

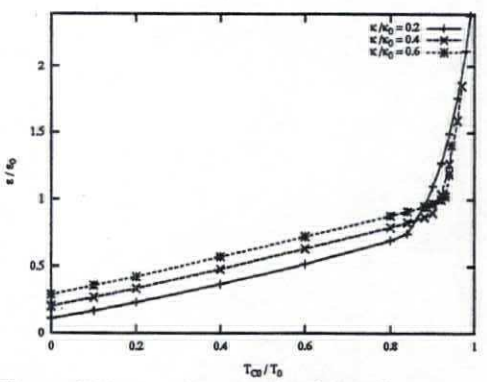

Figure A22c Pressure(0.4)-bending-tension, mean axial strain-tension response

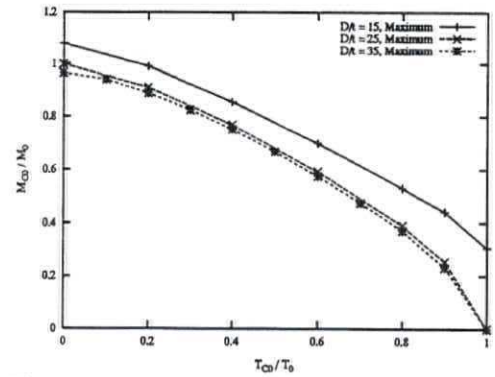

Figure A23a P(0.4) - T - B, moment-tension interaction, effect of D/t

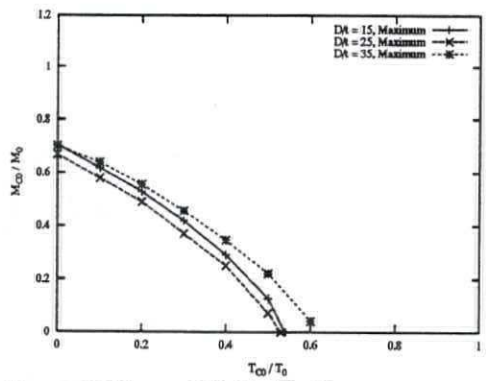

Figure A23b P(0.8) - T - B, moment-tension interaction, effect of D/t

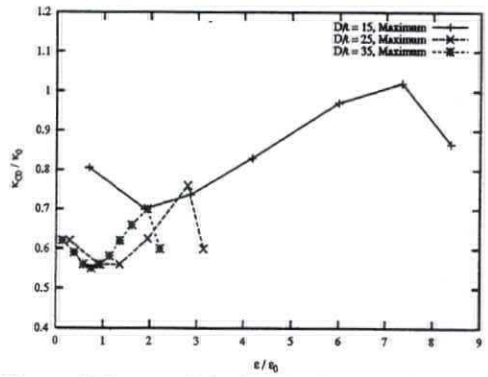

Figure A23c P(0.4) - T - B, curvature-axial strain envelope, effect of D/t

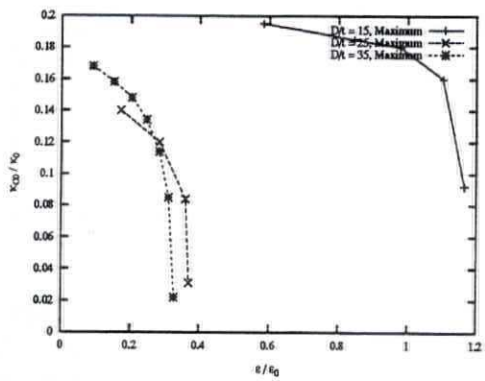

Figure A23d P(0.8) - T - B, curvature-axial strain evelope effect of D/t

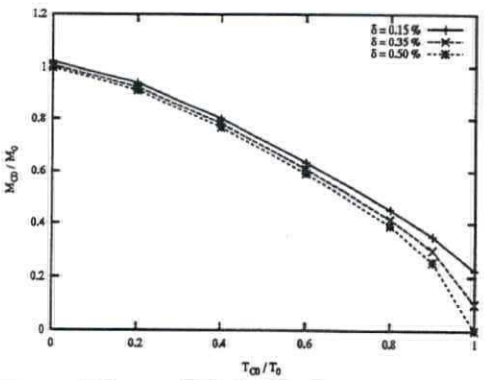

Figure A24a P(0.4) - T - B, moment-tension interaction, effect of initial ovality

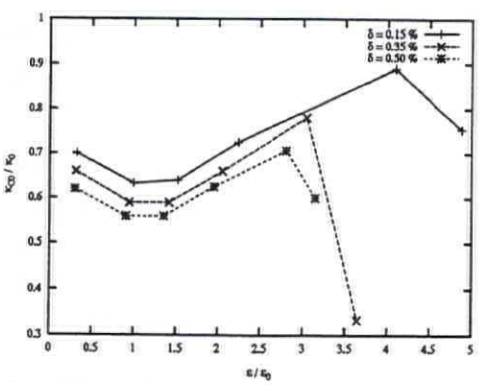

Figure A24b P(0.4) - T - B, curvature-axial strain envelope, effect of initial ovality

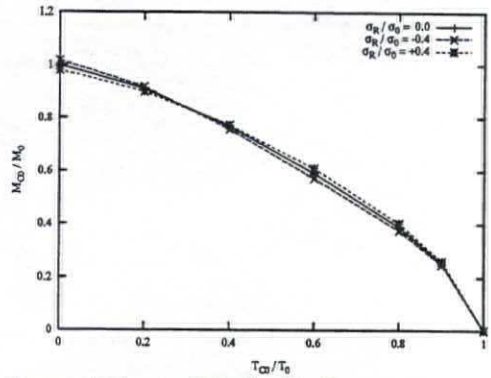

Figure A25a P(0.4) - T - B, moment-tension interaction, effect of residual stress

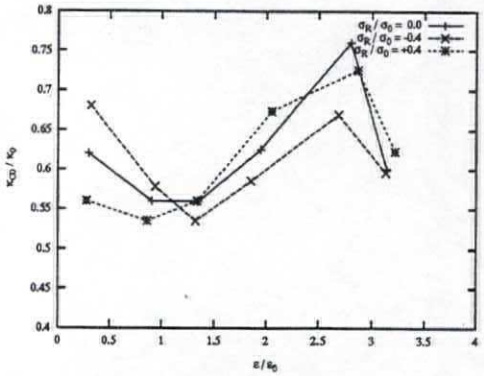

Figure A25b P(0.4) - T - B, curvature-axial strain envelope, effect of residual stress

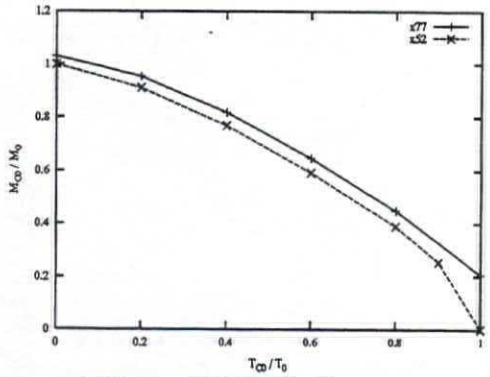

Figure A26a P(0.4) - T - B, moment-tension interaction, effect of steel grade

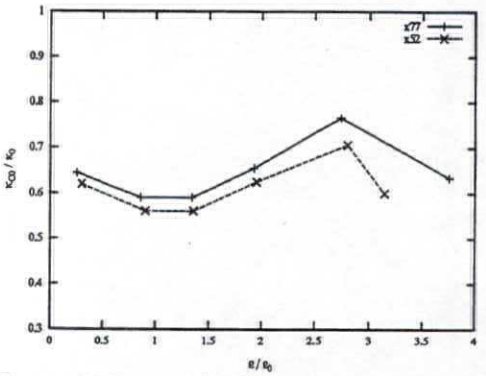

Figure A26b P(0.4) - T - B, curvature axial strain, effect of steel grade

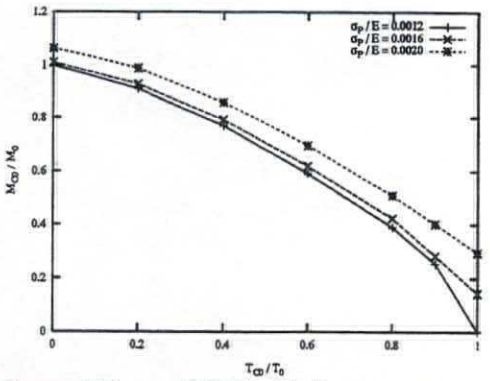

Figure A26c P(0.4) - T - B, moment-tension interaction, effect of σ_p/E

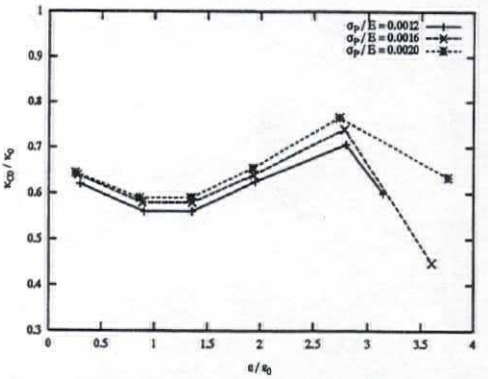

Figure A26d P(0.4) - T - B, curvature axial strain, effect of σ_p/E

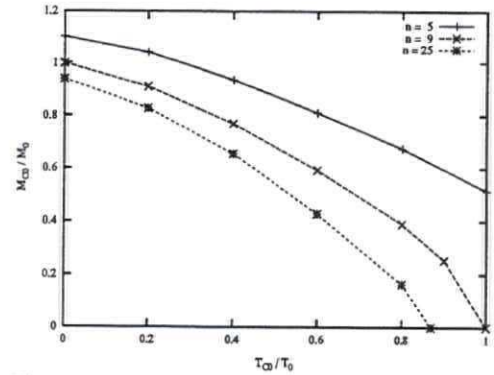

Figure A27a P(0.4) - T - B, moment-tension interaction, effect of n

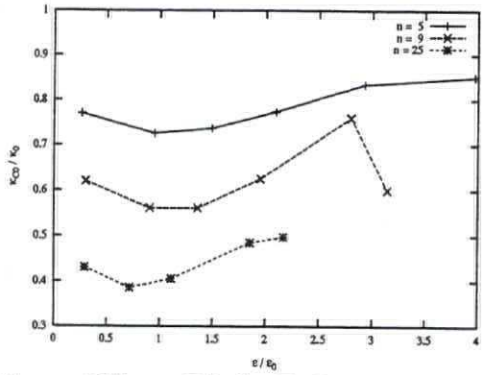

Figure A27b P(0.4) - T - B, curvature-axial strain, effect of n

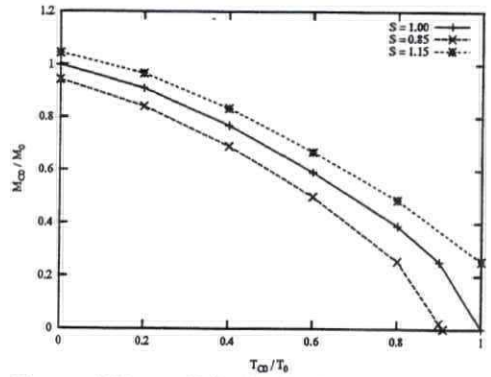

Figure A28a P(0.4) - T - B, moment-tension interaction, effect of anisotropy

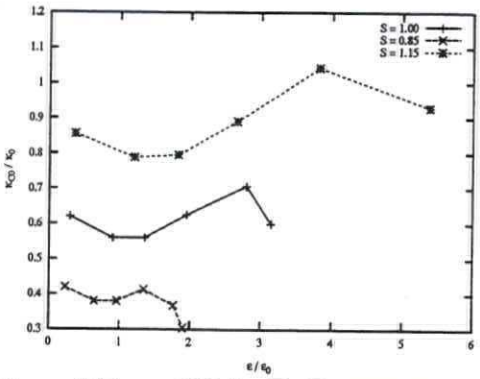

Figure A28b P(0.4) - T - B, curvature-axial strain, effect of anisotropy

A.5 Table, Numerical data base

The parameter studies is summarized in Table A.1 to A.12.

Case	1 - 96	Pressure
Case	97 - 149	Bending
Case	150 - 183	Pressure -Tension
Case	184 - 233	Bending - Tension
Case	234 - 360	Pressure - Tension - Bending

Table A.1

No	D_0/t	oval	σ_p/E	n	σ_R/σ_0	σ_Θ/σ_0	P_∞/P_0	T_∞/T_0	M_∞/M_0	κ_∞/κ_0
01	5	0.0015	0.0012	9.05	0.000	1.000	1.192	0.000	0.000	0.000
02	10	0.0015	0.0012	9.05	0.000	1.000	0.964	0.000	0.000	0.000
03	15	0.0015	0.0012	9.05	0.000	1.000	0.824	0.000	0.000	0.000
04	20	0.0015	0.0012	9.05	0.000	1.000	0.730	0.000	0.000	0.000
05	25	0.0015	0.0012	9.05	0.000	1.000	0.640	0.000	0.000	0.000
06	30	0.0015	0.0012	9.05	0.000	1.000	0.533	0.000	0.000	0.000
07	35	0.0015	0.0012	9.05	0.000	1.000	0.429	0.000	0.000	0.000
08	40	0.0015	0.0012	9.05	0.000	1.000	0.344	0.000	0.000	0.000
09	45	0.0015	0.0012	9.05	0.000	1.000	0.279	0.000	0.000	0.000
10	50	0.0015	0.0012	9.05	0.000	1.000	0.230	0.000	0.000	0.000
11	5	0.0035	0.0012	9.05	0.000	1.000	1.158	0.000	0.000	0.000
12	10	0.0035	0.0012	9.05	0.000	1.000	0.920	0.000	0.000	0.000
13	15	0.0035	0.0012	9.05	0.000	1.000	0.791	0.000	0.000	0.000
14	20	0.0035	0.0012	9.05	0.000	1.000	0.681	0.000	0.000	0.000
15	25	0.0035	0.0012	9.05	0.000	1.000	0.575	0.000	0.000	0.000
16	30	0.0035	0.0012	9.05	0.000	1.000	0.470	0.000	0.000	0.000
17	35	0.0035	0.0012	9.05	0.000	1.000	0.381	0.000	0.000	0.000
18	40	0.0035	0.0012	9.05	0.000	1.000	0.310	0.000	0.000	0.000
19	45	0.0035	0.0012	9.05	0.000	1.000	0.255	0.000	0.000	0.000
20	50	0.0035	0.0012	9.05	0.000	1.000	0.212	0.000	0.000	0.000
21	5	0.0050	0.0012	9.05	0.000	1.000	1.114	0.000	0.000	0.000
22	10	0.0050	0.0012	9.05	0.000	1.000	0.909	0.000	0.000	0.000
23	15	0.0050	0.0012	9.05	0.000	1.000	0.768	0.000	0.000	0.000
24	20	0.0050	0.0012	9.05	0.000	1.000	0.651	0.000	0.000	0.000
25	25	0.0050	0.0012	9.05	0.000	1.000	0.540	0.000	0.000	0.000
26	30	0.0050	0.0012	9.05	0.000	1.000	0.439	0.000	0.000	0.000
27	35	0.0050	0.0012	9.05	0.000	1.000	0.357	0.000	0.000	0.000
28	40	0.0050	0.0012	9.05	0.000	1.000	0.291	0.000	0.000	0.000
29	45	0.0050	0.0012	9.05	0.000	1.000	0.241	0.000	0.000	0.000
30	50	0.0050	0.0012	9.05	0.000	1.000	0.201	0.000	0.000	0.000

Table A.2

No	D_0/t	oval	σ_p/E	n	σ_R/σ_0	σ_Θ/σ_0	P_{co}/P_0	T_{co}/T_0	M_{co}/M_0	κ_{co}/κ_0
31	5	0.0015	0.0020	10.0	0.000	1.000	1.150	0.000	0.000	0.000
32	10	0.0015	0.0020	10.0	0.000	1.000	0.967	0.000	0.000	0.000
33	15	0.0015	0.0020	10.0	0.000	1.000	0.833	0.000	0.000	0.000
34	20	0.0015	0.0020	10.0	0.000	1.000	0.714	0.000	0.000	0.000
35	25	0.0015	0.0020	10.0	0.000	1.000	0.559	0.000	0.000	0.000
36	30	0.0015	0.0020	10.0	0.000	1.000	0.417	0.000	0.000	0.000
37	35	0.0015	0.0020	10.0	0.000	1.000	0.317	0.000	0.000	0.000
38	40	0.0015	0.0020	10.0	0.000	1.000	0.248	0.000	0.000	0.000
39	5	0.0035	0.0020	10.0	0.000	1.000	1.132	0.000	0.000	0.000
40	10	0.0035	0.0020	10.0	0.000	1.000	0.937	0.000	0.000	0.000
41	15	0.0035	0.0020	10.0	0.000	1.000	0.791	0.000	0.000	0.000
42	20	0.0035	0.0020	10.0	0.000	1.000	0.647	0.000	0.000	0.000
43	25	0.0035	0.0020	10.0	0.000	1.000	0.500	0.000	0.000	0.000
44	30	0.0035	0.0020	10.0	0.000	1.000	0.379	0.000	0.000	0.000
45	35	0.0035	0.0020	10.0	0.000	1.000	0.293	0.000	0.000	0.000
46	40	0.0035	0.0020	10.0	0.000	1.000	0.232	0.000	0.000	0.000
47	5	0.0050	0.0020	10.0	0.000	1.000	1.066	0.000	0.000	0.000
48	10	0.0050	0.0020	10.0	0.000	1.000	0.919	0.000	0.000	0.000
49	15	0.0050	0.0020	10.0	0.000	1.000	0.763	0.000	0.000	0.000
50	20	0.0050	0.0020	10.0	0.000	1.000	0.611	0.000	0.000	0.000
51	25	0.0050	0.0020	10.0	0.000	1.000	0.470	0.000	0.000	0.000
52	30	0.0050	0.0020	10.0	0.000	1.000	0.359	0.000	0.000	0.000
53	35	0.0050	0.0020	10.0	0.000	1.000	0.279	0.000	0.000	0.000
54	40	0.0050	0.0020	10.0	0.000	1.000	0.222	0.000	0.000	0.000
55	15	0.005	0.0012	9.05	0.000	1.000	1.000	0.000	0.000	0.000
56	25	0.005	0.0012	9.05	0.000	1.000	1.000	0.000	0.000	0.000
57	35	0.005	0.0012	9.05	0.000	1.000	1.000	0.000	0.000	0.000
58	15	0.005	0.0012	9.05	0.200	1.000	1.001	0.000	0.000	0.000
59	25	0.005	0.0012	9.05	0.200	1.000	0.995	0.000	0.000	0.000
60	35	0.005	0.0012	9.05	0.200	1.000	0.993	0.000	0.000	0.000

Table A.3

No	D_0/t	oval	σ_p/E	n	σ_R/σ_0	σ_θ/σ_0	P_∞/P_0	T_∞/T_0	M_∞/M_0	κ_∞/κ_0
61	15.0	0.005	0.0012	9.05	0.400	1.000	1.002	0.000	0.000	0.000
62	25.0	0.005	0.0012	9.05	0.400	1.000	0.978	0.000	0.000	0.000
63	35.0	0.005	0.0012	9.05	0.400	1.000	0.968	0.000	0.000	0.000
64	15.0	0.005	0.0012	9.05	0.600	1.000	1.002	0.000	0.000	0.000
65	25.0	0.005	0.0012	9.05	0.600	1.000	0.960	0.000	0.000	0.000
66	35.0	0.005	0.0012	9.05	0.600	1.000	0.940	0.000	0.000	0.000
67	15.0	0.005	0.0012	9.05	-0.20	1.000	0.999	0.000	0.000	0.000
68	25.0	0.005	0.0012	9.05	-0.20	1.000	0.988	0.000	0.000	0.000
69	35.0	0.005	0.0012	9.05	-0.20	1.000	0.986	0.000	0.000	0.000
70	15.0	0.005	0.0012	9.05	-0.40	1.000	0.998	0.000	0.000	0.000
71	25.0	0.005	0.0012	9.05	-0.40	1.000	0.966	0.000	0.000	0.000
72	35.0	0.005	0.0012	9.05	-0.40	1.000	0.958	0.000	0.000	0.000
73	15.0	0.005	0.0012	9.05	-0.60	1.000	0.995	0.000	0.000	0.000
74	25.0	0.005	0.0012	9.05	-0.60	1.000	0.945	0.000	0.000	0.000
75	35.0	0.005	0.0012	9.05	-0.60	1.000	0.926	0.000	0.000	0.000
76	15.0	0.005	0.0020	10.0	0.000	1.000	1.000	0.000	0.000	0.000
77	25.0	0.005	0.0020	10.0	0.000	1.000	1.000	0.000	0.000	0.000
78	35.0	0.005	0.0020	10.0	0.000	1.000	1.000	0.000	0.000	0.000
79	15.0	0.005	0.0020	10.0	0.200	1.000	1.000	0.000	0.000	0.000
80	25.0	0.005	0.0020	10.0	0.200	1.000	0.993	0.000	0.000	0.000
81	35.0	0.005	0.0020	10.0	0.200	1.000	0.997	0.000	0.000	0.000
82	15.0	0.005	0.0020	10.0	0.400	1.000	1.000	0.000	0.000	0.000
83	25.0	0.005	0.0020	10.0	0.400	1.000	0.973	0.000	0.000	0.000
84	35.0	0.005	0.0020	10.0	0.400	1.000	0.981	0.000	0.000	0.000
85	15.0	0.005	0.0020	10.0	0.600	1.000	1.001	0.000	0.000	0.000
86	25.0	0.005	0.0020	10.0	0.600	1.000	0.944	0.000	0.000	0.000
87	35.0	0.005	0.0020	10.0	0.600	1.000	0.961	0.000	0.000	0.000
88	15.0	0.005	0.0020	10.0	-0.20	1.000	0.995	0.000	0.000	0.000
89	25.0	0.005	0.0020	10.0	-0.20	1.000	0.986	0.000	0.000	0.000
90	35.0	0.005	0.0020	10.0	-0.20	1.000	0.994	0.000	0.000	0.000

Table A.4

No	D_0/t	oval	σ_p/E	n	σ_R/σ_0	σ_Θ/σ_0	P_{co}/P_0	T_{co}/T_0	M_{co}/M_0	κ_{co}/κ_0
91	15.0	0.005	0.0020	10.0	-0.40	1.000	0.989	0.000	0.000	0.000
92	25.0	0.005	0.0020	10.0	-0.40	1.000	0.957	0.000	0.000	0.000
93	35.0	0.005	0.0020	10.0	-0.40	1.000	0.974	0.000	0.000	0.000
94	15.0	0.005	0.0020	10.0	-0.60	1.000	0.983	0.000	0.000	0.000
95	25.0	0.005	0.0020	10.0	-0.60	1.000	0.926	0.000	0.000	0.000
96	35.0	0.005	0.0020	10.0	-0.60	1.000	0.948	0.000	0.000	0.000
97	25.0	0.0050	0.0012	5.00	0.000	1.000	0.000	0.000	1.313	1.783
98	25.0	0.0050	0.0016	5.00	0.000	1.000	0.000	0.000	1.324	1.755
99	25.0	0.0050	0.0020	5.00	0.000	1.000	0.000	0.000	1.333	1.733
100	25.0	0.0050	0.0024	5.00	0.000	1.000	0.000	0.000	1.354	1.733
101	25.0	0.0050	0.0028	5.00	0.000	1.000	0.000	0.000	1.374	1.715
102	25.0	0.0050	0.0012	9.05	0.000	1.000	0.000	0.000	1.136	1.525
103	25.0	0.0050	0.0016	9.05	0.000	1.000	0.000	0.000	1.142	1.508
104	25.0	0.0050	0.0020	9.05	0.000	1.000	0.000	0.000	1.149	1.485
105	25.0	0.0050	0.0024	9.05	0.000	1.000	0.000	0.000	1.158	1.485
106	25.0	0.0050	0.0028	9.05	0.000	1.000	0.000	0.000	1.170	1.508
107	25.0	0.0050	0.0012	15.0	0.000	1.000	0.000	0.000	1.062	1.250
108	25.0	0.0050	0.0016	15.0	0.000	1.000	0.000	0.000	1.066	1.260
109	25.0	0.0050	0.0020	15.0	0.000	1.000	0.000	0.000	1.070	1.260
110	25.0	0.0050	0.0024	15.0	0.000	1.000	0.000	0.000	1.076	1.283
111	25.0	0.0050	0.0028	15.0	0.000	1.000	0.000	0.000	1.080	1.305
112	25.0	0.0050	0.0012	25.0	0.000	1.000	0.000	0.000	1.025	1.013
113	25.0	0.0050	0.0016	25.0	0.000	1.000	0.000	0.000	1.027	1.020
114	25.0	0.0050	0.0020	25.0	0.000	1.000	0.000	0.000	1.028	1.058
115	25.0	0.0050	0.0024	25.0	0.000	1.000	0.000	0.000	1.031	1.103
116	25.0	0.0050	0.0028	25.0	0.000	1.000	0.000	0.000	1.033	1.170
117	25.0	0.0050	0.0012	5.05	0.000	0.850	0.000	0.000	1.265	1.459
118	25.0	0.0050	0.0012	5.05	0.000	0.925	0.000	0.000	1.289	1.625
119	25.0	0.0050	0.0012	5.05	0.000	1.075	0.000	0.000	1.335	1.950
120	25.0	0.0050	0.0012	5.05	0.000	1.150	0.000	0.000	1.357	2.130

Table A.5

No	D_0/t	oval	σ_p/E	n	σ_R/σ_0	σ_Θ/σ_0	P_∞/P_0	T_∞/T_0	M_∞/M_0	κ_∞/κ_0
121	25.0	0.0050	0.0012	9.05	0.000	0.850	0.000	0.000	1.112	1.263
122	25.0	0.0050	0.0012	9.05	0.000	0.925	0.000	0.000	1.124	1.390
123	25.0	0.0050	0.0012	9.05	0.000	1.075	0.000	0.000	1.147	1.655
124	25.0	0.0050	0.0012	9.05	0.000	1.150	0.000	0.000	1.159	1.813
125	25.0	0.0050	0.0012	25.0	0.000	0.850	0.000	0.000	1.018	0.863
126	25.0	0.0050	0.0012	25.0	0.000	0.925	0.000	0.000	1.021	0.950
127	25.0	0.0050	0.0012	25.0	0.000	1.075	0.000	0.000	1.029	1.113
128	25.0	0.0050	0.0012	25.0	0.000	1.150	0.000	0.000	1.032	1.213
129	15.0	0.0050	0.0012	5.00	0.000	1.000	0.000	0.000	1.466	1.799
130	15.0	0.0050	0.0012	9.05	0.000	1.000	0.000	0.000	1.207	1.520
131	15.0	0.0050	0.0012	15.0	0.000	1.000	0.000	0.000	1.103	1.260
132	15.0	0.0050	0.0012	20.0	0.000	1.000	0.000	0.000	1.068	1.110
133	15.0	0.0050	0.0012	25.0	0.000	1.000	0.000	0.000	1.048	1.000
134	20.0	0.0050	0.0012	5.00	0.000	1.000	0.000	0.000	1.377	1.800
135	20.0	0.0050	0.0012	9.05	0.000	1.000	0.000	0.000	1.168	1.530
136	20.0	0.0050	0.0012	15.0	0.000	1.000	0.000	0.000	1.080	1.270
137	20.0	0.0050	0.0012	20.0	0.000	1.000	0.000	0.000	1.051	1.120
138	20.0	0.0050	0.0012	25.0	0.000	1.000	0.000	0.000	1.036	1.020
139	25.0	0.0050	0.0012	20.0	0.000	1.000	0.000	0.000	1.039	1.125
140	30.0	0.0050	0.0012	5.00	0.000	1.000	0.000	0.000	1.258	1.778
141	30.0	0.0050	0.0012	9.05	0.000	1.000	0.000	0.000	1.108	1.516
142	30.0	0.0050	0.0012	15.0	0.000	1.000	0.000	0.000	1.046	1.261
143	30.0	0.0050	0.0012	20.0	0.000	1.000	0.000	0.000	1.026	1.126
144	30.0	0.0050	0.0012	25.0	0.000	1.000	0.000	0.000	1.015	1.036
145	35.0	0.0050	0.0012	5.00	0.000	1.000	0.000	0.000	1.218	1.750
146	35.0	0.0050	0.0012	9.05	0.000	1.000	0.000	0.000	1.088	1.536
147	35.0	0.0050	0.0012	15.0	0.000	1.000	0.000	0.000	1.036	1.260
148	35.0	0.0050	0.0012	20.0	0.000	1.000	0.000	0.000	1.019	1.138
149	35.0	0.0050	0.0012	25.0	0.000	1.000	0.000	0.000	1.010	1.033
150	25.0	0.0015	0.0012	9.05	0.000	1.000	0.270	0.960	0.000	0.000

Table A.6

No	D_0/t	oval	σ_p/E	n	σ_R/σ_0	σ_Θ/σ_0	P_∞/P_0	T_∞/T_0	M_∞/M_0	κ_∞/κ_0
151	25.0	0.0015	0.0012	9.05	0.000	1.000	0.440	0.622	0.000	0.000
152	25.0	0.0015	0.0012	9.05	0.000	1.000	0.620	0.100	0.000	0.000
153	27.2	0.0015	0.0012	9.05	0.000	1.000	0.436	0.000	0.000	0.000
154	27.2	0.0015	0.0012	9.05	0.000	1.000	0.400	0.225	0.000	0.000
155	27.2	0.0015	0.0012	9.05	0.000	1.000	0.350	0.446	0.000	0.000
156	27.2	0.0015	0.0012	9.05	0.000	1.000	0.300	0.627	0.000	0.000
157	27.2	0.0015	0.0012	9.05	0.000	1.000	0.250	0.762	0.000	0.000
158	27.2	0.0015	0.0012	9.05	0.000	1.000	0.200	0.869	0.000	0.000
159	27.2	0.0015	0.0012	9.05	0.000	1.000	0.150	0.975	0.000	0.000
160	12.2	0.0015	0.0012	9.05	0.000	1.000	0.864	0.000	0.000	0.000
161	12.2	0.0015	0.0012	9.05	0.000	1.000	0.832	0.200	0.000	0.000
162	12.2	0.0015	0.0012	9.05	0.000	1.000	0.793	0.400	0.000	0.000
163	12.2	0.0015	0.0012	9.05	0.000	1.000	0.718	0.600	0.000	0.000
164	12.2	0.0015	0.0012	9.05	0.000	1.000	0.630	0.800	0.000	0.000
165	12.2	0.0015	0.0012	9.05	0.000	1.000	0.519	1.000	0.000	0.000
166	18.2	0.0015	0.0012	9.05	0.000	1.000	0.638	0.000	0.000	0.000
167	18.2	0.0015	0.0012	9.05	0.000	1.000	0.594	0.200	0.000	0.000
168	18.2	0.0015	0.0012	9.05	0.000	1.000	0.557	0.400	0.000	0.000
169	18.2	0.0015	0.0012	9.05	0.000	1.000	0.502	0.600	0.000	0.000
170	18.2	0.0015	0.0012	9.05	0.000	1.000	0.426	0.800	0.000	0.000
171	18.2	0.0015	0.0012	9.05	0.000	1.000	0.340	1.000	0.000	0.000
172	24.5	0.0015	0.0012	9.05	0.000	1.000	0.632	0.000	0.000	0.000
173	24.5	0.0015	0.0012	9.05	0.000	1.000	0.559	0.200	0.000	0.000
174	24.5	0.0015	0.0012	9.05	0.000	1.000	0.482	0.400	0.000	0.000
175	24.5	0.0015	0.0012	9.05	0.000	1.000	0.423	0.600	0.000	0.000
176	24.5	0.0015	0.0012	9.05	0.000	1.000	0.355	0.800	0.000	0.000
177	24.5	0.0015	0.0012	9.05	0.000	1.000	0.269	1.000	0.000	0.000
178	38.3	0.0015	0.0012	9.05	0.000	1.000	0.437	0.000	0.000	0.000
179	38.3	0.0015	0.0012	9.05	0.000	1.000	0.416	0.200	0.000	0.000
180	38.3	0.0015	0.0012	9.05	0.000	1.000	0.368	0.400	0.000	0.000

Table A.7

No	D_0/t	oval	σ_p/E	n	σ_R/σ_0	σ_Θ/σ_0	P_{co}/P_0	T_{co}/T_0	M_{co}/M_0	κ_{co}/κ_0
181	38.3	0.0015	0.0012	9.05	0.000	1.000	0.300	0.600	0.000	0.000
182	38.3	0.0015	0.0012	9.05	0.000	1.000	0.259	0.800	0.000	0.000
183	38.3	0.0015	0.0012	9.05	0.000	1.000	0.199	1.000	0.000	0.000
184	15.0	0.0050	0.0012	9.05	0.000	1.000	0.000	0.000	1.204	1.520
185	15.0	0.0050	0.0012	9.05	0.000	1.000	0.000	0.200	1.215	1.660
186	15.0	0.0050	0.0012	9.05	0.000	1.000	0.000	0.400	1.161	1.770
187	15.0	0.0050	0.0012	9.05	0.000	1.000	0.000	0.600	1.070	2.000
188	15.0	0.0050	0.0012	9.05	0.000	1.000	0.000	0.800	0.973	2.310
189	15.0	0.0050	0.0012	9.05	0.000	1.000	0.000	1.000	0.880	2.780
190	15.0	0.0050	0.0012	9.05	0.000	1.000	0.000	1.200	0.817	3.260
191	25.0	0.0050	0.0012	9.05	0.000	1.000	0.000	0.000	1.134	1.525
192	25.0	0.0050	0.0012	9.05	0.000	1.000	0.000	0.100	1.135	1.588
193	25.0	0.0050	0.0012	9.05	0.000	1.000	0.000	0.200	1.124	1.531
194	25.0	0.0050	0.0012	9.05	0.000	1.000	0.000	0.400	1.048	1.700
195	25.0	0.0050	0.0012	9.05	0.000	1.000	0.000	0.600	0.933	1.938
196	25.0	0.0050	0.0012	9.05	0.000	1.000	0.000	0.800	0.813	2.375
197	25.0	0.0050	0.0012	9.05	0.000	1.000	0.000	1.000	0.698	2.950
198	25.0	0.0050	0.0012	9.05	0.000	1.000	0.000	1.100	0.656	3.300
199	25.0	0.0050	0.0012	9.05	0.000	1.000	0.000	1.200	0.598	4.450
200	35.0	0.0050	0.0012	9.05	0.000	1.000	0.000	0.000	1.086	1.540
201	35.0	0.0050	0.0012	9.05	0.000	1.000	0.000	0.200	1.071	1.540
202	35.0	0.0050	0.0012	9.05	0.000	1.000	0.000	0.400	0.983	1.650
203	35.0	0.0050	0.0012	9.05	0.000	1.000	0.000	0.600	0.856	1.870
204	35.0	0.0050	0.0012	9.05	0.000	1.000	0.000	0.800	0.721	2.400
205	35.0	0.0050	0.0012	9.05	0.000	1.000	0.000	1.000	0.599	3.100
206	35.0	0.0050	0.0012	9.05	0.000	1.000	0.000	1.200	0.522	3.950
207	25.0	0.0050	0.0020	10.0	0.000	1.000	0.000	0.000	1.151	1.460
208	25.0	0.0050	0.0020	10.0	0.000	1.000	0.000	0.200	1.142	1.570
209	25.0	0.0050	0.0020	10.0	0.000	1.000	0.000	0.400	1.061	1.810
210	25.0	0.0050	0.0020	10.0	0.000	1.000	0.000	0.600	0.943	2.260

Table A.8

No	D_0/t	oval	σ_p/E	n	σ_R/σ_0	σ_Θ/σ_0	P_{co}/P_0	T_{co}/T_0	M_{co}/M_0	κ_{co}/κ_0
211	25.0	0.0050	0.0020	10.0	0.000	1.000	0.000	0.800	0.815	2.880
212	25.0	0.0050	0.0020	10.0	0.000	1.000	0.000	1.000	0.690	3.650
213	25.0	0.0050	0.0020	10.0	0.000	1.000	0.000	1.200	0.610	3.650
214	25.0	0.0050	0.0012	9.05	0.000	0.850	0.000	0.000	1.110	1.260
215	25.0	0.0050	0.0012	9.05	0.000	0.850	0.000	0.200	1.105	1.310
216	25.0	0.0050	0.0012	9.05	0.000	0.850	0.000	0.400	1.013	1.380
217	25.0	0.0050	0.0012	9.05	0.000	0.850	0.000	0.600	0.890	1.570
218	25.0	0.0050	0.0012	9.05	0.000	0.850	0.000	0.800	0.761	1.960
219	25.0	0.0050	0.0012	9.05	0.000	0.850	0.000	1.000	0.641	2.490
220	25.0	0.0050	0.0012	9.05	0.000	0.850	0.000	1.200	0.566	3.170
221	25.0	0.0050	0.0012	9.05	0.000	1.150	0.000	0.000	1.156	1.810
222	25.0	0.0050	0.0012	9.05	0.000	1.150	0.000	0.200	1.153	1.940
223	25.0	0.0050	0.0012	9.05	0.000	1.150	0.000	0.400	1.083	2.070
224	25.0	0.0050	0.0012	9.05	0.000	1.150	0.000	0.600	0.977	2.360
225	25.0	0.0050	0.0012	9.05	0.000	1.150	0.000	0.800	0.866	2.820
226	25.0	0.0050	0.0012	9.05	0.000	1.150	0.000	1.000	0.757	3.480
227	25.0	0.0050	0.0012	9.05	0.000	1.150	0.000	1.200	0.687	4.230
228	25.0	0.0050	0.0012	9.05	0.000	1.000	0.000	0.000	1.134	1.525
229	25.0	0.0050	0.0012	9.05	0.000	1.000	0.000	0.200	1.124	1.531
230	25.0	0.0050	0.0012	9.05	0.000	1.000	0.000	0.400	1.048	1.700
231	25.0	0.0050	0.0012	9.05	0.000	1.000	0.000	0.600	0.933	1.938
232	25.0	0.0050	0.0012	9.05	0.000	1.000	0.000	0.800	0.813	2.375
233	25.0	0.0050	0.0012	9.05	0.000	1.000	0.000	1.000	0.698	2.950
234	25.0	0.0050	0.0012	9.05	0.000	1.000	0.200	0.000	1.081	1.051
235	25.0	0.0050	0.0012	9.05	0.000	1.000	0.200	0.200	1.038	0.994
236	25.0	0.0050	0.0012	9.05	0.000	1.000	0.200	0.400	0.928	1.010
237	25.0	0.0050	0.0012	9.05	0.000	1.000	0.200	0.600	0.787	1.130
238	25.0	0.0050	0.0012	9.05	0.000	1.000	0.200	0.800	0.628	1.370
239	25.0	0.0050	0.0012	9.05	0.000	1.000	0.200	1.000	0.487	1.713
240	25.0	0.0050	0.0012	9.05	0.000	1.000	0.400	0.000	0.998	0.620

Table A.9

No	D_0/t	oval	σ_p/E	n	σ_R/σ_0	σ_θ/σ_0	P_{co}/P_0	T_{co}/T_0	M_{co}/M_0	κ_{co}/κ_0
241	25.0	0.0050	0.0012	9.05	0.000	1.000	0.400	0.200	0.910	0.560
242	25.0	0.0050	0.0012	9.05	0.000	1.000	0.400	0.400	0.768	0.560
243	25.0	0.0050	0.0012	9.05	0.000	1.000	0.400	0.600	0.592	0.625
244	25.0	0.0050	0.0012	9.05	0.000	1.000	0.400	0.800	0.390	0.706
245	25.0	0.0050	0.0012	9.05	0.000	1.000	0.400	0.900	0.254	0.600
246	25.0	0.0050	0.0012	9.05	0.000	1.000	0.400	1.000	0.000	0.000
247	25.0	0.0050	0.0012	9.05	0.000	1.000	0.600	0.000	0.874	0.330
248	25.0	0.0050	0.0012	9.05	0.000	1.000	0.600	0.200	0.744	0.280
249	25.0	0.0050	0.0012	9.05	0.000	1.000	0.600	0.400	0.567	0.290
250	25.0	0.0050	0.0012	9.05	0.000	1.000	0.600	0.600	0.338	0.275
251	25.0	0.0050	0.0012	9.05	0.000	1.000	0.600	0.700	0.188	0.205
252	25.0	0.0050	0.0012	9.05	0.000	1.000	0.600	0.800	0.000	0.000
253	25.0	0.0050	0.0012	9.05	0.000	1.000	0.800	0.000	0.667	0.140
254	25.0	0.0050	0.0012	9.05	0.000	1.000	0.800	0.200	0.491	0.120
255	25.0	0.0050	0.0012	9.05	0.000	1.000	0.800	0.400	0.250	0.084
256	25.0	0.0050	0.0012	9.05	0.000	1.000	0.800	0.500	0.072	0.031
257	25.0	0.0050	0.0012	9.05	0.000	1.000	0.800	0.530	0.000	0.000
258	15.0	0.0050	0.0012	9.05	0.000	1.000	0.400	0.000	1.080	0.804
259	15.0	0.0050	0.0012	9.05	0.000	1.000	0.400	0.200	0.990	0.699
260	15.0	0.0050	0.0012	9.05	0.000	1.000	0.400	0.400	0.855	0.737
261	15.0	0.0050	0.0012	9.05	0.000	1.000	0.400	0.600	0.698	0.830
262	15.0	0.0050	0.0012	9.05	0.000	1.000	0.400	0.800	0.531	0.969
263	15.0	0.0050	0.0012	9.05	0.000	1.000	0.400	0.900	0.441	1.019
264	15.0	0.0050	0.0012	9.05	0.000	1.000	0.400	1.000	0.306	0.866
265	15.0	0.0050	0.0012	9.05	0.000	1.000	0.800	0.000	0.704	0.195
266	15.0	0.0050	0.0012	9.05	0.000	1.000	0.800	0.100	0.617	-----
267	15.0	0.0050	0.0012	9.05	0.000	1.000	0.800	0.200	0.529	0.185
268	15.0	0.0050	0.0012	9.05	0.000	1.000	0.800	0.300	0.419	0.180
269	15.0	0.0050	0.0012	9.05	0.000	1.000	0.800	0.400	0.292	0.160
270	15.0	0.0050	0.0012	9.05	0.000	1.000	0.800	0.500	0.127	0.092

Table A.10

No	D_0/t	oval	σ_y/E	n	σ_R/σ_0	σ_Θ/σ_0	P_∞/P_0	T_∞/T_0	M_∞/M_0	κ_∞/κ_0
271	15.0	0.0050	0.0012	9.05	0.000	1.000	0.800	0.540	0.000	0.000
272	35.0	0.0050	0.0012	9.05	0.000	1.000	0.400	0.000	0.964	0.620
273	35.0	0.0050	0.0012	9.05	0.000	1.000	0.400	0.100	0.940	0.590
274	35.0	0.0050	0.0012	9.05	0.000	1.000	0.400	0.200	0.889	0.560
275	35.0	0.0050	0.0012	9.05	0.000	1.000	0.400	0.300	0.824	0.550
276	35.0	0.0050	0.0012	9.05	0.000	1.000	0.400	0.400	0.752	0.560
277	35.0	0.0050	0.0012	9.05	0.000	1.000	0.400	0.500	0.667	0.581
278	35.0	0.0050	0.0012	9.05	0.000	1.000	0.400	0.600	0.575	0.620
279	35.0	0.0050	0.0012	9.05	0.000	1.000	0.400	0.700	0.475	0.660
280	35.0	0.0050	0.0012	9.05	0.000	1.000	0.400	0.800	0.371	0.700
281	35.0	0.0050	0.0012	9.05	0.000	1.000	0.400	0.900	0.232	0.600
282	35.0	0.0050	0.0012	9.05	0.000	1.000	0.400	1.000	0.000	0.000
283	35.0	0.0050	0.0012	9.05	0.000	1.000	0.800	0.000	0.699	0.168
284	35.0	0.0050	0.0012	9.05	0.000	1.000	0.800	0.100	0.638	0.158
285	35.0	0.0050	0.0012	9.05	0.000	1.000	0.800	0.200	0.555	0.148
286	35.0	0.0050	0.0012	9.05	0.000	1.000	0.800	0.300	0.456	0.134
287	35.0	0.0050	0.0012	9.05	0.000	1.000	0.800	0.400	0.347	0.114
288	35.0	0.0050	0.0012	9.05	0.000	1.000	0.800	0.500	0.221	0.085
289	35.0	0.0050	0.0012	9.05	0.000	1.000	0.800	0.600	0.041	0.022
290	25.0	0.0015	0.0012	9.05	0.000	1.000	0.400	0.000	1.021	0.700
291	25.0	0.0015	0.0012	9.05	0.000	1.000	0.400	0.200	0.939	0.633
292	25.0	0.0015	0.0012	9.05	0.000	1.000	0.400	0.400	0.802	0.640
293	25.0	0.0015	0.0012	9.05	0.000	1.000	0.400	0.600	0.634	0.725
294	25.0	0.0015	0.0012	9.05	0.000	1.000	0.400	0.800	0.453	0.870
295	25.0	0.0015	0.0012	9.05	0.000	1.000	0.400	0.900	0.350	0.890
296	25.0	0.0015	0.0012	9.05	0.000	1.000	0.400	1.000	0.223	0.753
297	25.0	0.0035	0.0012	9.05	0.000	1.000	0.400	0.000	1.008	0.660
298	25.0	0.0035	0.0012	9.05	0.000	1.000	0.400	0.200	0.922	0.590
299	25.0	0.0035	0.0012	9.05	0.000	1.000	0.400	0.400	0.783	0.590
300	25.0	0.0035	0.0012	9.05	0.000	1.000	0.400	0.600	0.609	0.660

Table A.11

No	D_0/t	oval	σ_p/E	n	σ_R/σ_0	σ_θ/σ_0	P_∞/P_0	T_∞/T_0	M_∞/M_0	κ_∞/κ_0
301	25.0	0.0035	0.0012	9.05	0.000	1.000	0.400	0.800	0.415	0.725
302	25.0	0.0035	0.0012	9.05	0.000	1.000	0.400	0.900	0.299	0.720
303	25.0	0.0035	0.0012	9.05	0.000	1.000	0.400	1.000	0.099	0.330
304	25.0	0.0050	0.0016	9.65	0.000	1.000	0.400	0.000	1.008	0.640
305	25.0	0.0050	0.0016	9.65	0.000	1.000	0.400	0.200	0.928	0.580
306	25.0	0.0050	0.0016	9.65	0.000	1.000	0.400	0.400	0.791	0.580
307	25.0	0.0050	0.0016	9.65	0.000	1.000	0.400	0.600	0.619	0.640
308	25.0	0.0050	0.0016	9.65	0.000	1.000	0.400	0.800	0.423	0.740
309	25.0	0.0050	0.0016	9.65	0.000	1.000	0.400	1.000	0.143	0.448
310	25.0	0.0050	0.0020	9.00	0.000	1.000	0.400	0.000	1.062	0.665
311	25.0	0.0050	0.0020	9.00	0.000	1.000	0.400	0.200	0.988	0.610
312	25.0	0.0050	0.0020	9.00	0.000	1.000	0.400	0.400	0.858	0.610
313	25.0	0.0050	0.0020	9.00	0.000	1.000	0.400	0.600	0.696	0.670
314	25.0	0.0050	0.0020	9.00	0.000	1.000	0.400	0.800	0.509	0.780
315	25.0	0.0050	0.0020	9.00	0.000	1.000	0.400	1.000	0.295	0.770
316	25.0	0.0050	0.0020	10.0	0.000	1.000	0.400	0.000	1.030	0.645
317	25.0	0.0050	0.0020	10.0	0.000	1.000	0.400	0.200	0.953	0.590
318	25.0	0.0050	0.0020	10.0	0.000	1.000	0.400	0.400	0.818	0.590
319	25.0	0.0050	0.0020	10.0	0.000	1.000	0.400	0.600	0.646	0.655
320	25.0	0.0050	0.0020	10.0	0.000	1.000	0.400	0.800	0.449	0.765
321	25.0	0.0050	0.0020	10.0	0.000	1.000	0.400	1.000	0.206	0.634
322	25.0	0.0050	0.0012	5.00	0.000	1.000	0.400	0.000	1.103	0.770
323	25.0	0.0050	0.0012	5.00	0.000	1.000	0.400	0.200	1.041	0.725
324	25.0	0.0050	0.0012	5.00	0.000	1.000	0.400	0.400	0.936	0.736
325	25.0	0.0050	0.0012	5.00	0.000	1.000	0.400	0.600	0.810	0.773
326	25.0	0.0050	0.0012	5.00	0.000	1.000	0.400	0.800	0.675	0.834
327	25.0	0.0050	0.0012	5.00	0.000	1.000	0.400	1.000	0.516	0.851
328	25.0	0.0050	0.0012	25.0	0.000	1.000	0.400	0.000	0.939	0.430
329	25.0	0.0050	0.0012	25.0	0.000	1.000	0.400	0.200	0.827	0.385
330	25.0	0.0050	0.0012	25.0	0.000	1.000	0.400	0.400	0.655	0.405

Table A.12

No	D_0/t	oval	σ_y/E	n	σ_R/σ_0	σ_Θ/σ_0	P_∞/P_0	T_∞/T_0	M_∞/M_0	κ_∞/κ_0
331	25.0	0.0050	0.0012	25.0	0.000	1.000	0.400	0.600	0.427	0.485
332	25.0	0.0050	0.0012	25.0	0.000	1.000	0.400	0.800	0.163	0.497
333	25.0	0.0050	0.0012	25.0	0.000	1.000	0.400	0.869	0.000	0.000
334	25.0	0.0050	0.0012	25.0	0.400	1.000	0.400	0.000	0.979	0.560
335	25.0	0.0050	0.0012	25.0	0.400	1.000	0.400	0.200	0.899	0.535
336	25.0	0.0050	0.0012	25.0	0.400	1.000	0.400	0.400	0.773	0.560
337	25.0	0.0050	0.0012	25.0	0.400	1.000	0.400	0.600	0.610	0.673
338	25.0	0.0050	0.0012	25.0	0.400	1.000	0.400	0.800	0.403	0.725
339	25.0	0.0050	0.0012	25.0	0.400	1.000	0.400	0.900	0.261	0.623
340	25.0	0.0050	0.0012	25.0	0.400	1.000	0.400	0.995	0.000	0.000
341	25.0	0.0050	0.0012	25.0	-0.40	1.000	0.400	0.000	1.016	0.680
342	25.0	0.0050	0.0012	25.0	-0.40	1.000	0.400	0.200	0.917	0.578
343	25.0	0.0050	0.0012	25.0	-0.40	1.000	0.400	0.400	0.758	0.535
344	25.0	0.0050	0.0012	25.0	-0.40	1.000	0.400	0.600	0.572	0.585
345	25.0	0.0050	0.0012	25.0	-0.40	1.000	0.400	0.800	0.376	0.669
346	25.0	0.0050	0.0012	25.0	-0.40	1.000	0.400	0.900	0.249	0.596
347	25.0	0.0050	0.0012	25.0	-0.40	1.000	0.400	0.998	0.000	0.000
348	25.0	0.0050	0.0012	25.0	0.000	0.850	0.400	0.000	0.942	0.420
349	25.0	0.0050	0.0012	25.0	0.000	0.850	0.400	0.200	0.841	0.380
350	25.0	0.0050	0.0012	25.0	0.000	0.850	0.400	0.400	0.690	0.380
351	25.0	0.0050	0.0012	25.0	0.000	0.850	0.400	0.600	0.499	0.413
352	25.0	0.0050	0.0012	25.0	0.000	0.850	0.400	0.800	0.256	0.368
353	25.0	0.0050	0.0012	25.0	0.000	0.850	0.400	0.900	0.021	0.304
354	25.0	0.0050	0.0012	25.0	0.000	0.850	0.400	0.910	0.000	0.000
355	25.0	0.0050	0.0012	25.0	0.000	1.150	0.400	0.000	1.043	0.855
356	25.0	0.0050	0.0012	25.0	0.000	1.150	0.400	0.200	0.966	0.788
357	25.0	0.0050	0.0012	25.0	0.000	1.150	0.400	0.400	0.833	0.795
358	25.0	0.0050	0.0012	25.0	0.000	1.150	0.400	0.600	0.669	0.890
359	25.0	0.0050	0.0012	25.0	0.000	1.150	0.400	0.800	0.487	1.043
360	25.0	0.0050	0.0012	25.0	0.000	1.150	0.400	1.000	0.256	0.930

B RESPONSE SURFACES

B.1 General remarks

The appendix presents the response surfaces and the basic for the polynomial models. In the present investigation four response-surface-models have been explored; multiplicative, linear plane, polynomial without interaction and polynomial included interaction between the variables.

The variables ; yield strength, mass of the pipe, stiffness of stinger system, response amplitude operator and peak period of the wave spectrum, are employed in the response surfaces.

The maximum load effect for the multiplicative model are given for the nominal case and the complementary experiments. For the polynomial model the maximum load effect are given for all the experiments and the fitted polynomial coefficients.

B.2 Multiplicative model

The model consists of a nominal case and complementary experiments where only one of the parameters has been varied. The results from the analysis are summarized in Table B.1 - Table B.4

The maximum response is given by :

$$r = r^0 \prod_{i=1}^{m} \left(\frac{r_i}{r^0} \right) \qquad \text{B.1}$$

where r_i is found by interpolation/extrapolation of the values given in Table B.1 - Table B.3 for random values of the variables x_1 - x_5.

B.2.1 Hs 3 Tp 8

Table B.1 Maximum response for multiplicative model, Overbend, S1, Hs = 3m, Tp = 8s

		Static		Dynamic	
Variable	x_i / x_{i0}	Moment	Curvature	Moment	Curvature
Nominal (r_0)	1.00	.12834E+07	.75575E-02	.42040E+05	.41738E-03
Yield strength	0.90	.12427E+07	.78701E-02	.17244E+05	.23585E-03
x_1	1.20	.13041E+07	.75132E-02	.36500E+05	.23247E-03
Mass	0.98	.12221E+07	.71538E-02	.86450E+05	.60933E-03
x_2	1.02	.12762E+07	.75099E-02	.58043E+05	.54894E-03
Stiff	0.90	.12788E+07	.75270E-02	.36322E+05	.33241E-03
x_3	1.50	.12869E+07	.75809E-02	.68433E+05	.74680E-03
RAO	0.90	---	---	.36320E+05	.34188E-03
x_4	1.30	---	---	.62733E+05	.65267E-03
Tp	0.80	---	---	.46500E+05	.38659E-03
x_5	1.25	---	---	.59557E+05	.58033E-03
	1.50	---	---	.54688E+05	.55250E-03

Table B.2 Maximum response for multiplicative model, Sagbend, S3, Hs = 3m, Tp = 8s

		Static		Dynamic	
Variable	x_i / x_{i0}	Moment	Curvature	Moment	Curvature
Nominal (r_0)	1.00	.13177E+07	.78488E-02	.12935E+06	.16450E-02
Yield strength	0.90	.12626E+07	.81422E-02	.11909E+06	.20145E-02
x_1	1.20	.13393E+07	.77373E-02	.17574E+06	.11283E-02
Mass	0.98	.12819E+07	.12819E+07	.98574E+05	.10991E-02
x_2	1.03	.13144E+07	.13144E+07	.21735E+06	.30690E-02
Stiff	0.90	.13178E+07	.78501E-02	.12939E+06	.16455E-02
x_3	1.50	.13168E+07	.78372E-02	.12988E+06	.16517E-02
RAO	0.90	---	---	.11733E+06	.14921E-02
x_4	1.30	---	---	.17167E+06	.21833E-02
Tp	0.80	---	---	.11333E+06	.14414E-02
x_5	1.25	---	---	.10607E+06	.13489E-02
	1.50	---	---	.88087E+05	.11203E-02

B.2.2 Hs 4 Tp 10

Table B.3 Maximum response for multiplicative model, Overbend, S2, Hs = 4m, Tp = 10s

		Static		Dynamic	
Variable	x_i / x_{i0}	Moment	Curvature	Moment	Curvature
Nominal (r_0)	1.00	.12834E+07	.75578E-02	.48027E+05	.47309E-03
Yield strength	0.90	.12364E+07	.77841E-02	.53211E+05	.72615E-03
x_1	1.20	.12932E+07	.74497E-02	.97965E+05	.62022E-03
Mass	0.98	.12828E+07	.75540E-02	.61714E+05	.63628E-03
x_2	1.02	.12840E+07	.75617E-02	.14090E+05	.10307E-03
Stiff	0.90	.12788E+07	.75274E-02	.40702E+05	.36072E-03
x_3	1.50	.12921E+07	.76148E-02	.62829E+05	.70727E-03
RAO	0.90	---	---	.54367E+05	.56037E-03
x_4	1.30	---	---	.55217E+05	.55725E-03
Tp	0.80	---	---	.39617E+05	.35893E-03
x_5	1.20	---	---	.51887E+05	.51475E-03

Table B.4 Maximum response for multiplicative model, Sagbend, S4, Hs = 4m, Tp = 10s

		Static		Dynamic	
Variable	x_i / x_{i0}	Moment	Curvature	Moment	Curvature
Nominal (r_0)	1.00	.13177E+07	.78487E-02	.31636E+06	.75655E-02
Yield strength	0.90	.12513E+07	.79877E-02	.24656E+06	.85221E-02
x_1	1.20	.13272E+07	.76596E-02	.52684E+06	.54846E-02
Mass	0.98	.13196E+07	.78733E-02	.30252E+06	.73751E-02
x_2	1.03	.13016E+07	.76777E-02	.41724E+06	.12314E-01
Stiff	0.90	.13064E+07	.77089E-02	.31612E+06	.75589E-02
x_3	1.50	.13055E+07	.77030E-02	.31562E+06	.74958E-02
RAO	0.90	---	---	.31384E+06	.74419E-02
x_4	1.30	---	---	.32116E+06	.78007E-02
Tp	0.80	---	---	.31784E+06	.76401E-02
x_5	1.20	---	---	.29134E+06	.67571E-02

B.3 Polynomial models

The coefficients of the response surfaces are established by least square fitting of the results from LAYLEX, based on randomizing of the variables, yield strength, mass of the pipe, stiffness of stinger system, RAO and peak period of the wave spectrum.

The following parameters are employed in the response surface :

Yield strength :

$$x_1 = \frac{\sigma}{\sigma_0} - 1.0$$

Mass :

$$x_2 = \frac{mass}{mass_{nom}} - 1.0$$

Stinger stiffness :

$$x_3 = \frac{stiff}{stiff_{nom}} - 1.0$$

Response Amplitude Operator :

$$x_4 = \frac{RAO}{RAO_{nom}} - 1.0$$

Peak period of the wave spectra :

$$x_5 = \frac{T_P}{T_{P_{nom}}} - 1.0$$

Linear hyper plane

Maximum response for a linear hyper plane is given by :

$$r = A_0 + A_1 \cdot x_1 + A_2 \cdot x_2 + A_3 \cdot x_3 + A_4 \cdot x_4 + A_5 \cdot x_5 \qquad \text{(B.2)}$$

where A_0 - A_5 are given in Table B.5 - B.6

Polynomial without interaction

Maximum response for a polynomial model without interaction is given as :

$$r = B_0 + B_1 \cdot x_1 + B_2 \cdot x_2 + B_3 \cdot x_3 + B_4 \cdot x_4 + B_5 \cdot x_5 + B_6 \cdot x_1^2 + B_7 \cdot x_2^2 + B_8 \cdot x_3^2 + B_9 \cdot x_4^2 + B_{10} \cdot x_5 \qquad \text{(B.3)}$$

where B_0 - B_{10} are given in Table B.7 - B.8.

Polynomial including interaction between variables

Maximum response for the polynomial model including interaction is given as :

$$\begin{aligned} r = {} & C_0 + C_1 \cdot x_1 + C_2 \cdot x_2 + C_3 \cdot x_3 + C_4 \cdot x_4 + C_5 \cdot x_5 \\ & + C_6 \cdot x_1 \cdot x_1 + C_7 \cdot x_1 \cdot x_2 + C_8 \cdot x_1 \cdot x_3 + C_9 \cdot x_1 \cdot x_4 + C_{10} \cdot x_1 \cdot x_5 \\ & + C_{11} \cdot x_2 \cdot x_2 + C_{12} \cdot x_2 \cdot x_3 + C_{13} \cdot x_2 \cdot x_4 + C_{14} \cdot x_2 \cdot x_5 + C_{15} \cdot x_3 \cdot x_3 \\ & + C_{16} \cdot x_3 \cdot x_4 + C_{17} \cdot x_3 \cdot x_5 + C_{18} \cdot x_4 \cdot x_4 + C_{19} \cdot x_4 \cdot x_5 + C_{20} \cdot x_5 \cdot x_5 \end{aligned} \qquad \text{(B.4)}$$

where C_0 - C_{20} are given in Table B.9 - B.10.

B.3.1 Coefficients of the Polynomials

Table B.5 Coefficients for linear hyper plane, Overbend, S1, Hs = 3m, Tp = 8s

Coef.	Static		Dynamic	
	Moment	Curvature	Moment	Curvature
A_0	.1270129E+07	.7509714E-02	.6072512E+05	.5669372E-03
A_1	.2367374E+06	-.1065923E-02	.2167199E+06	-.1048373E-02
A_2	.1944023E+06	.1637040E-02	.2551889E+06	.3486970E-02
A_3	.4280310E+05	.3743421E-03	.1357633E+05	.2208593E-03
A_4	---	---	-.1277619E+05	-.1130986E-03
A_5	---	---	.1441763E+05	.1635682E-03

Table B.6 Coefficients for linear hyper plane, Sagbend, S4, Hs = 4m, Tp = 10s

Coef.	Static		Dynamic	
	Moment	Curvature	Moment	Curvature
A_0	.1307903E+07	.7812663E-02	.3148289E+06	.7524575E-02
A_1	.3515458E+06	-.2064846E-02	.9037394E+06	-.7678715E-02
A_2	-.3473470E+06	-.3280740E-02	.2315230E+07	.1003943E+00
A_3	-.1365828E+04	.8283091E-04	-.1558304E+05	-.8101476E-03
A_4	---	---	.2032127E+05	.7884295E-03
A_5	---	---	-.4884268E+05	-.2578507E-02

Table B.7 Coefficients for polynomial without interaction, Overbend, S1, Hs = 3m, Tp = 8s

Coef.	Static		Dynamic	
	Moment	Curvature	Moment	Curvature
B_0	.1277915E+07	.7527286E-02	.5578182E+05	.5211593E-03
B_1	.2598171E+06	-.7041093E-03	.1740798E+06	-.1410396E-02
B_2	-.1736807E+06	-.1269119E-02	.7242742E+06	.6418040E-02
B_3	.4040928E+05	.3769203E-03	.1614614E+05	.2497293E-03
B_4	---	---	-.1233912E+05	-.1536171E-03
B_5	---	---	.1575167E+05	.1752797E-03
B_6	-.1950917E+07	.6602106E-02	.6433759E+06	.6067896E-02
B_7	-.3872150E+08	-.2664391E+00	.4494048E+08	.3063105E+00
B_8	.3577474E+05	.1413544E-03	-.5503502E+05	.1199666E-04
B_9	---	---	-.3700380E+05	-.1284149E-02
B_{10}	---	---	-.1246881E+05	.2120301E-03

Table B.8 Coefficients for polynomial without interaction, Sagbend, S4, Hs = 4m, Tp = 10s

Coef.	Static		Dynamic	
	Moment	Curvature	Moment	Curvature
B_0	.1311800E+07	.7803137E-02	.3233689E+06	.8100005E-02
B_1	.3356280E+06	-.1983453E-02	.8886111E+06	-.8945361E-02
B_2	-.3211189E+06	-.3409391E-02	.2252976E+07	.9866408E-01
B_3	.2116693E+04	.2053250E-04	-.3539690E+04	.2789977E-04
B_4	---	---	.2927944E+05	.1112553E-02
B_5	---	---	-.2995112E+05	-.1431179E-02
B_6	-.1620991E+07	.1690309E-01	-.8635936E+06	-.1231481E+00
B_7	-.8130380E+07	-.7078158E-01	.2560473E+08	.1166031E+01
B_8	-.2877152E+05	-.1178688E-04	-.3854134E+05	-.2625383E-02
B_9	---	---	-.2238939E+06	-.1177977E-01
B_{10}	---	---	-.2482783E+06	-.1268923E-01

Table B.9 Coefficients for polynomial with interaction, Overbend, S1, Hs = 3m, Tp = 8s

Coef.	Static		Dynamic	
	Moment	Curvature	Moment	Curvature
C_0	.1278718E+07	7532415E-02	.5590657E+05	.5175325E-03
C_1	.2759380E+06	-.6361572E-03	.1896323E+06	-.1483374E-02
C_2	-.2866422E+06	-.2032740E-02	.1085182E+07	.9470424E-02
C_3	.4790388E+05	.3801402E-03	.1731343E+05	.3519908E-03
C_4	---	---	-.8192936E+04	-.1378205E-03
C_5	---	---	.1606708E+05	.1904086E-03
C_6	-.1914479E+07	.6470385E-02	.5429926E+06	.4028640E-02
C_7	.5635282E+07	.4540644E-01	-.3454412E+05	-.1326978E-01
C_8	.3759987E+06	.1264506E-03	-.5736277E+05	-.2834935E-03
C_9	---	---	-.1504026E+05	.1383502E-02
C_{10}	---	---	.1911556E+06	.3678415E-03
C_{11}	-.4250190E+08	-.2884721E+00	.5073088E+08	.3507164E+00
C_{12}	-.2695286E+07	-.2262751E-01	.1613931E+07	.2569820E-01
C_{13}	---	---	.1798980E+07	.1043342E-01
C_{14}	---	---	.3588466E+07	.3070799E-01
C_{15}	-.2862058E+05	-.3060589E-03	-.1399173E+05	.8292739E-03
C_{16}	---	---	.1344184E+06	.1113905E-02
C_{17}	---	---	.3997497E+05	.1161000E-02
C_{18}	---	---	.9524768E+04	-.1080484E-02
C_{19}	---	---	-.5761274E+04	-.4215227E-03
C_{20}	---	---	-.3873303E+05	.1209776E-03

Table B.10 Coefficients for polynomial with interaction, Sagbend, S4, Hs = 4m, Tp = 10s

Coef.	Static		Dynamic	
	Moment	Curvature	Moment	Curvature
C_0	.1312013E+07	.7803654E-02	.3251786E+06	.8166181E-02
C_1	.3365755E+06	-.1993659E-02	.8499092E+06	-.1086121E-01
C_2	-.3535775E+06	-.3510433E-02	.2375396E+07	.1016091E+00
C_3	.1759894E+04	.3003595E-04	.7322823E+04	.2792347E-03
C_4	---	---	.8296681E+04	.2982468E-03
C_5	---	---	-.2933937E+05	-.1322306E-02
C_6	-.1732621E+07	.1686435E-01	-.7371735E+05	-.9395749E-01
C_7	-.2947955E+07	-.3003124E-02	.8004204E+07	.2963561E-01
C_8	-.1040492E+06	-.4456815E-03	.1065501E+07	.5044463E-01
C_9	---	---	-.6976401E+06	-.3466959E-01
C_{10}	---	---	.4658061E+06	.2355156E-01
C_{11}	-.9487812E+07	-.8113746E-01	.2392380E+08	.1151556E+01
C_{12}	-.5744744E+06	-.7838056E-02	.5906970E+06	.1803366E-01
C_{13}	---	---	-.1441210E+07	-.5171335E-02
C_{14}	---	---	-.6299577E+06	-.1620182E-01
C_{15}	-.3626982E+05	-.9329940E-04	-.1695756E+06	-.1053917E-01
C_{16}	---	---	.3734170E+06	.1840552E-01
C_{17}	---	---	-.1574175E+06	-.5192032E-02
C_{18}	---	---	-.4330474E+06	-.1941954E-01
C_{19}	---	---	.2789117E+06	.1321310E-01
C_{20}	---	---	-.2287930E+06	-.1167588E-01

B.3.2 Experiment Data Base for the Coefficients of the Polynomials

Maximum load effects are given for the overbend case S1, Hs 3 Tp 8 and the sagbend case S4, Hs 4 Tp 10. In the Tables B 11 to B 18. The value of the random variables are given and the maximum bending moment and corresponding curvature for all the cases.

Table B.11 Maximum load effect, Over bend Hs 3 Tp 8

Random variable					Load effect					
σ_0	Mass	RAO	Stiff	Tp	Static Mom.	Static Curv.	Dynamic Mom.	Dyn. Mom. Std	Dynamic Curv.	Dyn. Curv. Std
1.052	0.992	0.967	1.033	0.823	.12898E+07	.75446E-02	.53850E+05	.46629E+04	.35200E-03	.30545E-04
0.992	1.011	1.012	1.111	0.676	.12740E+07	.75043E-02	.67378E+05	.21753E+05	.72006E-03	.27826E-03
1.061	1.014	1.001	1.011	1.373	.12806E+07	.74755E-02	.12807E+06	.40329E+05	.99773E-03	.43791E-03
1.056	0.978	0.984	0.864	1.016	.12303E+07	.71518E-02	.99533E+05	.86512E+04	.65001E-03	.56650E-04
1.005	0.995	1.322	0.770	0.783	.12905E+07	.75985E-02	.45510E+05	.56779E+04	.43590E-03	.71889E-04
1.025	1.008	1.058	0.834	0.908	.12776E+07	.74920E-02	.74700E+05	.17828E+05	.56355E-03	.22331E-03
1.068	0.993	0.875	1.071	0.896	.12871E+07	.75112E-02	.52320E+05	.11135E+05	.34141E-03	.72567E-04
1.027	0.994	1.013	1.121	0.845	.12768E+07	.74848E-02	.40590E+05	.10504E+05	.26623E-03	.68966E-04
1.026	1.001	1.034	0.991	1.149	.12874E+07	.75558E-02	.81514E+05	.31451E+05	.70017E-03	.39082E-03
1.004	1.005	0.990	0.932	0.793	.12721E+07	.74776E-02	.66890E+05	.59687E+04	.59546E-03	.75749E-04
1.014	1.003	1.012	1.107	1.405	.12749E+07	.74851E-02	.65850E+05	.10783E+05	.51753E-03	.13625E-03
1.109	0.990	0.989	0.928	0.622	.12953E+07	.75263E-02	.53660E+05	.64921E+04	.34832E-03	.42226E-04
1.030	0.998	0.990	0.930	0.739	.12783E+07	.74915E-02	.53020E+05	.91703E+04	.34820E-03	.60861E-04
1.022	0.969	1.001	1.013	0.654	.12270E+07	.71629E-02	.11194E+06	.45926E+04	.75555E-03	.54151E-04
1.042	1.005	0.995	0.973	0.988	.12778E+07	.74753E-02	.79880E+05	.29250E+05	.57468E-03	.30274E-03
0.980	1.001	0.992	0.953	1.155	.12717E+07	.75022E-02	.77629E+05	.29840E+05	.93733E-03	.38448E-03
0.910	0.991	1.227	1.152	0.937	.12464E+07	.78015E-02	.53189E+05	.13633E+05	.71949E-03	.18419E-03
0.993	0.998	0.927	1.042	1.394	.12896E+07	.76061E-02	.44263E+05	.36263E+05	.51461E-03	.46122E-03
0.986	1.000	0.962	0.998	1.237	.12691E+07	.74773E-02	.52957E+05	.28130E+05	.54903E-03	.36113E-03
1.020	0.995	1.044	1.056	0.794	.12862E+07	.75543E-02	.49650E+05	.15946E+04	.34071E-03	.19781E-04
0.939	0.997	1.167	1.049	0.712	.12642E+07	.77357E-02	.44889E+05	.13314E+05	.59526E-03	.17623E-03
0.967	0.986	0.901	0.897	0.714	.12718E+07	.75651E-02	.42910E+05	.77652E+04	.55724E-03	.10092E-03
0.956	1.012	0.842	0.980	0.713	.12569E+07	.74769E-02	.50340E+05	.68648E+04	.65971E-03	.90099E-04
1.059	1.018	0.962	1.001	0.618	.12779E+07	.74597E-02	.64080E+05	.47100E+04	.41874E-03	.30760E-04
1.006	1.001	1.070	0.955	0.680	.12776E+07	.75126E-02	.54440E+05	.94371E+04	.45871E-03	.11953E-03

Table B.12 Maximum load effect, Over bend Hs 3 Tp 8

Random variable					Load effect					
σ_0	Mass	RAO	Stiff	Tp	Static Mom.	Static Curv.	Dynamic Mom.	Dyn. Mom. Std	Dynamic Curv.	Dyn. Curv. Std
0.984	1.006	1.133	0.968	0.698	.12782E+07	.75403E-02	.55850E+05	.11787E+05	.66355E-03	.15152E-03
1.014	1.011	1.033	0.985	0.994	.12453E+07	.72919E-02	.77933E+05	.30878E+05	.58045E-03	.32191E-03
1.010	1.005	0.914	0.970	0.873	.12748E+07	.74894E-02	.51480E+05	.73935E+04	.37821E-03	.86863E-04
1.080	0.985	1.013	1.117	0.806	.12937E+07	.75423E-02	.59940E+05	.71207E+04	.39078E-03	.46409E-04
0.967	0.992	0.973	1.074	1.011	.12745E+07	.76011E-02	.43620E+05	.77826E+04	.56710E-03	.10126E-03
0.947	1.009	0.993	0.954	1.216	.12257E+07	.72365E-02	.75057E+05	.26878E+05	.90707E-03	.35424E-03
1.066	1.015	0.815	0.930	0.910	.12714E+07	.74105E-02	.76733E+05	.19691E+05	.50079E-03	.12860E-03
1.007	0.979	0.920	1.002	0.960	.12216E+07	.71425E-02	.94420E+05	.93822E+04	.64101E-03	.83517E-04
1.039	0.996	0.959	0.979	0.805	.12598E+07	.73608E-02	.65600E+05	.15966E+05	.42995E-03	.10459E-03
0.988	0.983	0.911	0.956	1.125	.12786E+07	.75380E-02	.50522E+05	.50388E+04	.56130E-03	.64512E-04
0.998	1.004	0.915	0.979	1.035	.12344E+07	.72369E-02	.45725E+05	.33973E+05	.33135E-03	.26774E-03
1.016	0.963	1.074	0.979	1.241	.12708E+07	.74564E-02	.37680E+05	.12562E+05	.24998E-03	.86931E-04
1.002	0.977	0.994	0.967	0.894	.12831E+07	.75529E-02	.51130E+05	.68822E+04	.48415E-03	.87323E-04
1.000	1.014	0.958	0.973	1.398	.12724E+07	.74847E-02	.98275E+05	.19952E+05	.10354E-02	.25378E-03
1.008	0.997	0.840	0.976	1.301	.12783E+07	.75145E-02	.51700E+05	.29793E+05	.42444E-03	.36833E-03
0.936	1.009	0.938	1.123	0.778	.12553E+07	.76515E-02	.39620E+05	.10260E+05	.52648E-03	.13637E-03
0.976	0.991	1.085	1.036	0.696	.12804E+07	.75895E-02	.45033E+05	.46564E+04	.58096E-03	.59979E-04
0.992	1.016	1.147	1.006	0.972	.12783E+07	.75318E-02	.77067E+05	.21510E+05	.86468E-03	.27486E-03
0.972	0.992	1.025	0.918	0.885	.12779E+07	.75992E-02	.38350E+05	.63544E+04	.49703E-03	.82293E-04
1.028	0.991	1.052	1.144	0.813	.12890E+07	.75633E-02	.65410E+05	.26026E+05	.49388E-03	.32246E-03
0.948	0.978	0.951	0.924	0.897	.12649E+07	.76596E-02	.33470E+05	.56904E+04	.44029E-03	.74735E-04
0.996	0.989	1.095	1.092	1.116	.12844E+07	.75682E-02	.57230E+05	.99509E+04	.61993E-03	.12696E-03
1.031	1.006	0.854	1.005	0.685	.12707E+07	.74405E-02	.77290E+05	.87181E+04	.52931E-03	.79981E-04
0.945	0.999	0.994	0.962	0.779	.12581E+07	.76037E-02	.44580E+05	.76450E+04	.58879E-03	.10098E-03
0.998	0.983	0.918	0.993	0.785	.12797E+07	.75352E-02	.50890E+05	.90084E+04	.49445E-03	.11451E-03

Table B.13 Maximum load effect, Over bend Hs 3 Tp 8

Random variable					Load effect					
σ_0	Mass	RAO	Stiff	Tp	Static Mom.	Static Curv.	Dynamic Mom.	Dyn. Mom. Std	Dynamic Curv.	Dyn. Curv. Std
0.938	1.002	0.884	1.117	0.951	.12562E+07	.76460E-02	.44570E+05	.90927E+04	.59160E-03	.12062E-03
0.995	0.971	0.947	0.880	0.874	.12220E+07	.71570E-02	.10549E+06	.79732E+04	.85523E-03	.10178E-03
0.943	0.978	0.933	1.082	0.833	.12198E+07	.72015E-02	.59590E+05	.13753E+05	.70050E-03	.18153E-03
0.940	0.993	0.911	0.957	1.177	.12604E+07	.76752E-02	.41310E+05	.47901E+04	.54748E-03	.63332E-04
1.027	1.013	1.032	0.976	0.830	.12780E+07	.74922E-02	.73120E+05	.52546E+04	.52631E-03	.60101E-04
1.057	1.013	1.197	1.102	1.009	.12856E+07	.75124E-02	.10354E+06	.28407E+05	.76958E-03	.27137E-03
0.945	1.002	1.106	0.776	1.018	.12538E+07	.75379E-02	.51114E+05	.10221E+05	.67450E-03	.13479E-03
0.884	1.003	0.948	0.890	0.969	.12056E+07	.75369E-02	.56317E+05	.12313E+05	.77822E-03	.16990E-03
1.076	1.012	0.971	1.057	0.690	.12813E+07	.74658E-02	.77850E+05	.11549E+05	.50745E-03	.75165E-04
0.987	0.986	0.883	1.110	0.887	.12780E+07	.75353E-02	.47940E+05	.57075E+04	.53279E-03	.73248E-04
1.028	1.014	0.947	0.877	0.839	.12751E+07	.74726E-02	.66744E+05	.47107E+04	.44182E-03	.40929E-04
0.951	1.000	0.919	0.996	0.864	.12579E+07	.75364E-02	.45910E+05	.83847E+04	.60297E-03	.11025E-03
0.934	0.998	0.921	1.005	1.025	.12431E+07	.75100E-02	.55538E+05	.20526E+05	.73850E-03	.27304E-03
0.999	1.001	0.982	0.815	0.705	.12759E+07	.75085E-02	.49590E+05	.83651E+04	.44322E-03	.10650E-03
0.996	0.995	0.893	0.784	1.118	.12785E+07	.75290E-02	.44540E+05	.49194E+04	.42157E-03	.62841E-04
0.968	0.996	0.908	0.938	0.810	.12669E+07	.74894E-02	.40720E+05	.61122E+04	.52878E-03	.79357E-04
0.916	0.999	1.086	1.038	0.767	.12478E+07	.77558E-02	.41450E+05	.10569E+05	.55838E-03	.14234E-03
0.964	0.997	1.194	1.096	0.945	.12677E+07	.75371E-02	.38200E+05	.31011E+05	.49674E-03	.40389E-03
0.986	0.994	0.917	0.986	1.224	.12679E+07	.74699E-02	.35338E+05	.18878E+05	.32805E-03	.22593E-03
0.968	0.991	1.162	1.038	1.064	.12782E+07	.76357E-02	.44178E+05	.74049E+04	.57347E-03	.96040E-04
0.928	1.001	0.972	1.066	0.884	.12555E+07	.77356E-02	.35350E+05	.61100E+04	.47283E-03	.81543E-04
0.962	0.998	0.946	0.869	0.746	.12684E+07	.75668E-02	.48130E+05	.10128E+05	.62832E-03	.13234E-03
0.965	0.995	0.883	1.113	0.919	.12726E+07	.75918E-02	.32120E+05	.92318E+04	.41841E-03	.12015E-03
1.003	0.998	0.934	1.087	0.902	.12682E+07	.74537E-02	.48411E+05	.18025E+05	.37564E-03	.20091E-03
0.911	0.998	0.940	1.166	1.094	.12263E+07	.75255E-02	.37771E+05	.17376E+05	.51117E-03	.23488E-03

Table B.14 Maximum load effect, Over bend Hs 3 Tp 8

Random variable					Load effect					
σ_0	Mass	RAO	Stiff	Tp	Static Mom.	Static Curv.	Dynamic Mom.	Dyn. Mom. Std	Dynamic Curv.	Dyn. Curv. Std
0.999	0.996	0.915	0.977	1.001	.12805E+07	.75389E-02	.42744E+05	.10973E+05	.38828E-03	.12886E-03
1.001	0.997	1.060	0.877	1.332	.12844E+07	.75626E-02	.44150E+05	.95435E+04	.41079E-03	.12122E-03
0.966	0.998	1.000	1.007	1.179	.12753E+07	.76200E-02	.48444E+05	.13152E+05	.63036E-03	.17109E-03
1.025	1.007	1.009	1.081	0.889	.12764E+07	.74838E-02	.77867E+05	.24403E+05	.60316E-03	.29435E-03
0.991	1.002	0.795	0.901	1.014	.12652E+07	.74470E-02	.54400E+05	.20917E+05	.51671E-03	.24730E-03
0.961	0.989	1.048	1.090	0.781	.12731E+07	.76349E-02	.38440E+05	.50204E+04	.50142E-03	.65511E-04
1.023	0.990	0.952	0.926	0.929	.12844E+07	.75389E-02	.54130E+05	.36080E+04	.36547E-03	.41183E-04
0.929	1.010	0.691	0.803	0.863	.12346E+07	.74429E-02	.53120E+05	.69168E+04	.70956E-03	.92329E-04
0.988	1.016	1.086	1.042	0.852	.12772E+07	.75287E-02	.54560E+05	.53359E+04	.60433E-03	.68297E-04
0.950	1.002	0.845	0.987	0.892	.12523E+07	.74711E-02	.47460E+05	.13299E+05	.62456E-03	.17506E-03
0.995	0.985	1.007	1.063	1.148	.12821E+07	.75538E-02	.50311E+05	.41804E+04	.52312E-03	.53425E-04

Table B.15 Maximum load effect, Sag bend Hs 4 Tp 10

Random variable					Load effect					
σ_0	Mass	RAO	Stiff	Tp	Static Mom.	Static Curv.	Dynamic Mom.	Dyn. Mom. Std	Dynamic Curv.	Dyn. Curv. Std
1.044	1.003	1.033	0.983	0.962	.13128E+07	.77031E-02	.36138E+06	.41080E+05	.69959E-02	.19239E-02
1.017	0.979	0.896	0.857	0.901	.13239E+07	.78049E-02	.30884E+06	.28813E+05	.67665E-02	.13892E-02
1.038	1.001	1.018	0.821	1.068	.13243E+07	.77835E-02	.34118E+06	.12456E+05	.68499E-02	.58743E-03
0.984	0.977	1.026	0.927	1.012	.13133E+07	.79416E-02	.27180E+06	.24766E+05	.66128E-02	.12341E-02
1.000	1.002	1.116	0.899	1.357	.13172E+07	.78374E-02	.25364E+06	.30793E+05	.48682E-02	.15091E-02
1.017	1.002	0.924	1.024	0.888	.13213E+07	.77880E-02	.32832E+06	.19453E+05	.75652E-02	.93767E-03
0.904	1.013	1.136	0.978	0.950	.12642E+07	.81151E-02	.22194E+06	.27250E+05	.74041E-02	.14856E-02
0.974	0.986	1.125	0.943	0.826	.13077E+07	.79653E-02	.26960E+06	.19708E+05	.69389E-02	.99444E-03
0.996	0.995	0.845	0.985	0.858	.13172E+07	.78769E-02	.29540E+06	.21937E+05	.71817E-02	.10816E-02
1.025	1.003	0.996	0.982	1.197	.13222E+07	.77848E-02	.32306E+06	.33117E+05	.68196E-02	.15817E-02
1.106	0.995	1.050	1.107	0.989	.13324E+07	.77700E-02	.41168E+06	.29146E+05	.60824E-02	.12847E-02
1.024	0.995	1.115	0.896	1.243	.13227E+07	.77889E-02	.28530E+06	.32341E+05	.50839E-02	.15472E-02
1.024	1.034	0.909	0.944	0.915	.13053E+07	.76739E-02	.42650E+06	.32303E+05	.11189E-01	.17591E-02
1.044	0.986	1.152	1.018	1.336	.13262E+07	.77906E-02	.31684E+06	.29481E+05	.54090E-02	.13817E-02
1.033	0.991	1.132	0.964	1.283	.13243E+07	.77902E-02	.29274E+06	.17925E+05	.49170E-02	.84828E-03
1.029	1.005	1.011	1.093	1.052	.13105E+07	.77038E-02	.34616E+06	.47880E+05	.71832E-02	.22786E-02
0.980	0.996	0.929	1.052	0.878	.13103E+07	.79352E-02	.30538E+06	.33323E+05	.84028E-02	.16677E-02
0.937	0.994	1.018	0.812	1.031	.12873E+07	.80657E-02	.21968E+06	.27411E+05	.59339E-02	.14379E-02
0.990	0.999	1.014	1.146	1.041	.13010E+07	.77197E-02	.29132E+06	.39772E+05	.67189E-02	.19698E-02
0.985	1.025	1.128	0.951	0.959	.12948E+07	.76873E-02	.37724E+06	.39656E+05	.11101E-01	.20077E-02
0.967	1.005	0.928	1.044	0.670	.13031E+07	.79669E-02	.26884E+06	.29243E+05	.71177E-02	.14847E-02
0.980	0.978	0.974	1.084	1.179	.13116E+07	.79578E-02	.27366E+06	.10429E+05	.68960E-02	.52307E-03
1.039	0.966	1.038	1.014	1.052	.13280E+07	.78074E-02	.26918E+06	.74299E+05	.43607E-02	.18896E-02
1.002	0.993	1.157	1.029	0.900	.13185E+07	.78385E-02	.30520E+06	.14540E+05	.73377E-02	.71148E-03
0.991	1.008	0.904	0.918	1.020	.13004E+07	.77068E-02	.33676E+06	.42773E+05	.89084E-02	.21179E-02

Table B.16 Maximum load effect, Sag bend Hs 4 Tp 10

Random variable					Load effect					
σ_0	Mass	RAO	Stiff	Tp	Static Mom.	Static Curv.	Dynamic Mom.	Dyn. Mom. Std	Dynamic Curv.	Dyn. Curv. Std
1.012	0.994	0.977	1.118	1.036	.13215E+07	.77936E-02	.32654E+06	.16604E+05	.78152E-02	.80457E-03
0.943	1.015	0.906	0.931	1.428	.12889E+07	.80284E-02	.24370E+06	.24972E+05	.68832E-02	.13031E-02
0.972	1.011	1.044	1.060	0.871	.12880E+07	.77251E-02	.36680E+06	.27875E+05	.11432E-01	.19029E-02
1.062	1.002	0.826	0.948	1.338	.13154E+07	.77023E-02	.34354E+06	.47922E+05	.52897E-02	.19298E-02
0.895	0.987	1.027	0.940	1.376	.12608E+07	.81635E-02	.12672E+06	.29568E+05	.26408E-02	.16060E-02
0.954	1.035	0.892	0.712	1.039	.12774E+07	.77615E-02	.36028E+06	.27391E+05	.11908E-01	.17457E-02
1.002	0.991	0.866	1.039	0.873	.13194E+07	.78430E-02	.30612E+06	.26149E+05	.73652E-02	.12786E-02
1.029	0.989	1.103	1.181	0.775	.13241E+07	.77925E-02	.29140E+06	.31767E+05	.51115E-02	.15115E-02
0.994	1.004	1.260	1.213	1.222	.13152E+07	.78673E-02	.30834E+06	.19189E+05	.78513E-02	.94586E-03
1.092	0.998	1.010	1.091	1.017	.13308E+07	.77728E-02	.42056E+06	.29205E+05	.72920E-02	.13042E-02
0.987	1.015	0.914	0.972	0.906	.12971E+07	.77014E-02	.35940E+06	.38395E+05	.10165E-01	.19100E-02
1.055	1.009	1.024	0.911	0.766	.13131E+07	.76941E-02	.40836E+06	.47437E+05	.84591E-02	.21971E-02
1.067	1.003	1.017	0.724	0.903	.13274E+07	.77754E-02	.37232E+06	.15132E+05	.65712E-02	.69263E-03
1.016	0.988	0.970	1.051	1.196	.13228E+07	.77978E-02	.30460E+06	.45394E+05	.65212E-02	.21883E-02
1.032	0.999	1.231	1.157	0.968	.13116E+07	.77082E-02	.32242E+06	.36959E+05	.58864E-02	.17541E-02
0.986	0.972	0.941	1.192	1.273	.12780E+07	.75371E-02	.25908E+06	.34649E+05	.46343E-02	.13674E-02
1.001	0.982	0.956	0.957	0.920	.13200E+07	.78631E-02	.29788E+06	.34238E+05	.70703E-02	.16761E-02
0.959	0.992	1.041	1.035	0.944	.12996E+07	.80048E-02	.29246E+06	.19749E+05	.87384E-02	.10124E-02
1.028	0.985	0.992	0.949	1.067	.13247E+07	.77975E-02	.32418E+06	.32326E+05	.67561E-02	.15407E-02
0.957	0.984	1.128	0.953	0.990	.12989E+07	.80182E-02	.26002E+06	.27018E+05	.72040E-02	.13885E-02
0.958	0.988	0.941	1.205	1.432	.12994E+07	.80137E-02	.24262E+06	.35982E+05	.62501E-02	.18447E-02
0.995	1.007	0.968	1.036	0.893	.13028E+07	.77025E-02	.35432E+06	.34022E+05	.96213E-02	.16770E-02
0.978	1.020	1.035	0.995	1.294	.12906E+07	.77026E-02	.34608E+06	.33062E+05	.98466E-02	.16580E-02
0.969	0.977	0.989	0.926	1.347	.13062E+07	.79915E-02	.19570E+06	.39028E+05	.37149E-02	.14411E-02
1.039	1.017	0.979	1.152	0.786	.13099E+07	.76889E-02	.37716E+06	.44242E+05	.79073E-02	.20814E-02

Table B.17 Maximum load effect, Sag bend Hs 4 Tp 10

Random variable					Load effect					
σ_0	Mass	RAO	Stiff	Tp	Static Mom.	Static Curv.	Dynamic Mom.	Dyn. Mom. Std	Dynamic Curv.	Dyn. Curv. Std
1.006	0.996	1.006	1.055	0.993	.13191E+07	.77936E-02	.32434E+06	.27776E+05	.80182E-02	.13539E-02
0.989	1.009	0.998	0.992	0.850	.12987E+07	.80284E-02	.35800E+06	.59505E+05	.10050E-01	.29513E-02
1.011	1.013	1.170	1.053	0.820	.13064E+07	.77251E-02	.38430E+06	.28122E+05	.10060E-01	.13635E-02
1.009	0.981	1.064	0.918	1.209	.13214E+07	.77023E-02	.26612E+06	.37442E+05	.51168E-02	.18201E-02
0.999	0.996	0.881	1.098	0.701	.13180E+07	.81635E-02	.27542E+06	.40142E+05	.60498E-02	.19700E-02
0.937	1.004	0.820	0.938	1.039	.12745E+07	.77615E-02	.30444E+06	.23310E+05	.99286E-02	.12234E-02
0.981	0.994	0.971	1.063	0.850	.13108E+07	.78430E-02	.31690E+06	.13976E+05	.89411E-02	.69990E-03
0.990	1.018	0.933	1.080	0.791	.12986E+07	.77925E-02	.35318E+06	.44522E+05	.97108E-02	.22061E-02
0.970	1.010	0.894	0.810	1.234	.12877E+07	.78673E-02	.30556E+06	.45891E+05	.82152E-02	.23231E-02
0.976	1.002	0.937	1.119	0.715	.12915E+07	.77728E-02	.30954E+06	.28774E+05	.81935E-02	.14475E-02
0.983	1.008	1.070	0.957	0.759	.12953E+07	.77014E-02	.34438E+06	.44338E+05	.96942E-02	.24107E-02
0.977	0.989	1.166	1.047	1.530	.13092E+07	.76941E-02	.20794E+06	.20838E+05	.36767E-02	.10464E-02
1.031	0.996	1.027	0.942	0.657	.13238E+07	.77754E-02	.31138E+06	.38284E+05	.59262E-02	.18189E-02
0.939	1.002	0.910	0.950	1.010	.12878E+07	.77978E-02	.24848E+06	.22506E+05	.73382E-02	.11774E-02
1.017	1.019	0.851	0.999	1.138	.13067E+07	.77082E-02	.38180E+06	.41903E+05	.94969E-02	.20166E-02
0.970	0.984	1.099	1.122	0.931	.13060E+07	.75371E-02	.29454E+06	.13660E+05	.83696E-02	.69068E-03
0.958	0.994	1.003	1.025	0.970	.12988E+07	.78631E-02	.28036E+06	.19925E+05	.81758E-02	.10212E-02
0.990	1.004	1.080	1.012	0.782	.13002E+07	.80048E-02	.31326E+06	.33920E+05	.77822E-02	.16812E-02
0.981	1.018	0.951	0.922	0.864	.12927E+07	.77975E-02	.37644E+06	.27978E+05	.11318E-01	.14763E-02
0.970	1.004	1.136	0.977	0.918	.12884E+07	.80182E-02	.35872E+06	.26631E+05	.10924E-01	.13482E-02
0.981	1.004	1.104	1.203	0.857	.13096E+07	.80137E-02	.31786E+06	.45187E+05	.89604E-02	.22607E-02
0.981	1.010	0.861	1.025	1.124	.12937E+07	.77025E-02	.31368E+06	.34828E+05	.81683E-02	.17425E-02
0.976	1.007	0.999	1.001	1.012	.13073E+07	.77026E-02	.29106E+06	.28092E+05	.78614E-02	.14137E-02
0.978	1.006	0.906	0.929	1.272	.12925E+07	.79915E-02	.29762E+06	.56250E+05	.74697E-02	.28231E-02
0.980	0.987	1.033	0.979	0.899	.13107E+07	.76889E-02	.28428E+06	.37961E+05	.74049E-02	.19038E-02

Table B.18 Maximum load effect, Sag bend Hs 4 Tp 10

Random variable					Load effect					
σ_0	Mass	RAO	Stiff	Tp	Static Mom.	Static Curv.	Dynamic Mom.	Dyn. Mom. Std	Dynamic Curv.	Dyn. Curv. Std
1.032	1.024	0.847	0.990	0.955	.13080E+07	.76841E-02	.44822E+06	.27398E+05	.11665E-01	.12989E-02
1.004	0.992	1.030	0.961	1.073	.13191E+07	.78263E-02	.30590E+06	.26576E+05	.72501E-02	.12975E-02
0.992	0.990	1.031	0.971	0.569	.13033E+07	.77341E-02	.24562E+06	.35703E+05	.44389E-02	.17652E-02
0.951	0.980	1.101	1.143	1.104	.12645E+07	.76223E-02	.23636E+06	.65045E+04	.50209E-02	.33463E-03
1.038	0.987	1.061	0.890	0.830	.13256E+07	.77930E-02	.33858E+06	.30216E+05	.68336E-02	.14235E-02
0.955	1.009	1.046	1.071	1.032	.12958E+07	.79998E-02	.27080E+06	.16331E+05	.77726E-02	.83946E-03
1.011	0.996	0.935	1.100	1.066	.13098E+07	.77178E-02	.28956E+06	.43143E+05	.55890E-02	.20904E-02
1.023	0.992	0.999	0.997	0.948	.13232E+07	.77931E-02	.32018E+06	.37386E+05	.68315E-02	.17890E-02
0.992	1.000	0.864	1.032	0.643	.13019E+07	.77181E-02	.28850E+06	.47004E+05	.65183E-02	.23239E-02
0.920	1.027	1.045	1.062	0.904	.12608E+07	.78885E-02	.33518E+06	.16972E+05	.12786E-01	.20018E-02
1.046	0.983	0.862	1.028	1.245	.13273E+07	.77961E-02	.30824E+06	.35677E+05	.49559E-02	.16685E-02
0.958	1.014	1.021	0.882	0.957	.12822E+07	.77846E-02	.32726E+06	.50220E+05	.99032E-02	.25749E-02
1.008	1.018	0.887	1.145	1.258	.13054E+07	.76929E-02	.38078E+06	.53440E+05	.10072E-01	.25971E-02
0.970	0.967	1.027	0.938	1.251	.13074E+07	.79977E-02	.23016E+06	.22664E+05	.51517E-02	.11475E-02
0.965	0.997	0.869	1.050	1.071	.13024E+07	.79855E-02	.28392E+06	.22402E+05	.80425E-02	.11411E-02
0.988	1.006	0.879	1.088	1.145	.13129E+07	.78943E-02	.27630E+06	.41777E+05	.65615E-02	.20753E-02
0.979	0.993	1.108	0.825	1.191	.13100E+07	.79383E-02	.25198E+06	.34516E+05	.57641E-02	.17308E-02
1.026	1.017	0.994	0.966	0.860	.13082E+07	.76911E-02	.40292E+06	.49131E+05	.99441E-02	.23435E-02
1.006	0.990	0.946	0.865	0.649	.13197E+07	.78128E-02	.28016E+06	.26510E+05	.58840E-02	.12914E-02
0.993	1.012	0.858	1.016	0.946	.13012E+07	.76977E-02	.34708E+06	.41408E+05	.93069E-02	.20446E-02
1.009	1.014	0.941	1.182	1.195	.13189E+07	.77812E-02	.32384E+06	.37618E+05	.78148E-02	.18268E-02
1.007	1.002	0.943	0.807	0.947	.13193E+07	.77958E-02	.30782E+06	.20522E+05	.71338E-02	.99806E-03
0.906	1.007	1.047	1.082	1.312	.12661E+07	.81199E-02	.22316E+06	.25904E+05	.74093E-02	.14084E-02
0.979	0.990	0.995	0.969	0.925	.13102E+07	.79481E-02	.30686E+06	.26719E+05	.85727E-02	.13401E-02
0.993	0.996	0.970	1.053	1.275	.13160E+07	.78830E-02	.28466E+06	.21242E+05	.67504E-02	.10485E-02

PREVIOUS DR.ING. THESES

Department of Marine Structures

Kavlie, Dag	:	Optimization of Plane Elastic Grillages. 1967.
Hansen, Hans R.	:	Man-Machine Communication and Data-Storage Methods in Ship Structural Design. 1971.
Gisvold, Kaare M.	:	A Method for non-linear mixed-integer programming and its Application to Design Problems.
Lund, Sverre	:	Tanker Frame Optimalization by means of SUMT-Transformation and Behaviour Models. 1971.
Vinje, Tor	:	On Vibration of Spherical Shells Interacting with Fluid. 1972.
Lorentz, Jan D.	:	Tank Arrangement for Crude Oil Carriers in Accordance with the new Anti-Pollution Regulations. 1975.
Carlsen, Carl A.	:	Computer-Aided Design of Tanker Structures. 1975.
Larsen, Carl M.	:	Static and Dynamic Analysis of Offshore Pipelines during Installation. 1976.
Hatlestad, Brigt	:	The Finite Element Method used in a Fatigue Evaluation of Fixed Offshore Platforms. 1979.
Valsgård, Sverre	:	Finite Difference and Finite Element Method Applied to Non-Linear Analysis of Plated Structures. 1979.
Pettersen, Erik	:	Analysis and Design of Cellular Structures. 1979.
Nordsve, Nils T.	:	Finite Element Collapse Analysis of structural Members considering Imperfections and Stresses due to Fabrication. 1980.
Fylling, Ivar J.	:	Analysis of towline Forces in Ocean towing Systems. 1980.
Haver, Sverre	:	Analysis of Uncertainties related to the stochastic Modelling of Ocean Waves. 1980.
Odland, Jonas	:	On the Strength of welded Ring stiffened cylindrical Shells primarily subjected to axial Compression. 1981.
Engesvik, Knut	:	Analysis of Uncertainties in the fatigue Capacity of Welded Joints. 1982.
Eide, Oddvar Inge	:	On Cumulative Fatigue Damage in Steel Welded Joints. 1983.
Mo, Olav	:	Stochastic Time Domain Analysis of Slender Offshore Structures. 1983.
Amdahl, Jørgen	:	Energy absorption in Ship-platform impacts 1983.
Czujko, Jerzy	:	Collapse Analysis of Plates subjected to Biaxial Compression and Lateral Load. 1983.

Soares, C. Guedes	:	Probabilistic models for load effects in ship structures. 1984.
Mørch, Morten	:	Motions and mooring forces of semi submersibles as determined by full-scale measurements and theoretical analysis. 1984.
Engseth, Alf G.	:	Finite Element Collapse Analysis of Tubular Steel Offshore Structures. 1985.
Baadshaug, Ola	:	Systems Reliability Analysis of Jacket Platforms. 1985. (Confidential)
Hessen, Gunnar	:	Fracture Mechanics Analysis of Stiffened Tubular Members. 1986.
Taby, Jon	:	Ultimate and post-ultimate strength of dented tubular members. 1986.
Wessel, Heinz-J.	:	Fracture mechanics analysis of crack growth in plate girders. 1986.
Leira, Bernt Johan	:	Gaussian Vector-processes for Reliability Analysis involving Wave-induced Load Effects. 1987.
Xu JUN	:	Non-linear Dynamic Analysis of Space-framed Offshore Structures. 1988.
Guoyang Jiao	:	Reliability Analysis of Crack Growth under Random Loading considering Model Updating. 1989.
Olufsen, Arnt	:	Uncertainty and Reliability Analysis of Fixed Offshore Structures. 1989.
Wu Yu-Lin	:	System Reliability Analyses of Offshore Structures using improved Truss and Beam Models. 1989.
Farnes, Knut-Aril	:	Long-term Statistics of Response in Non-linear Marine Structures. 1990.
Sotberg, Torbjørn	:	Application of Reliability Methods for Safety Assessment of Submarine Pipelines. 1990.
Hoen, Christopher	:	System Identification of Structures Excited by Stochastic Load Processes. 1991.
Sødahl, Nils	:	Methods for Design and Analysis of Flexible Risers. 1991.
Haugen, Stein	:	Probabilistic Evaluation of Frequency of Collision between Ships and Offshore Platforms. 1991.
Ormberg, Harald	:	Non-linear Response Analysis of Floating Fish Farm Systems. 1991.
Marley, Mark J.	:	Time Variant Reliability Under Fatigue Degradation. 1991.
Bessason, Bjarni	:	Assessment of Earthquake Loading and Response of Seismically Isolated Bridges. 1992.
Sævik, Svein	:	On Stresses and Fatigue in Flexible Pipes. 1992.

Dalane, Jan Inge	:	System Reliability in Design and Maintenance of Fixed Offshore Structures. 1993.
Karunakaran, Daniel	:	Nonlinear Dynamic Response and Reliability Analysis of Drag-dominated Offshore Platforms. 1993.
Passano, Elizabeth	:	Efficient Analysis of Nonlinear Slender Marine Structures. 1994.
Bech, Sidsel M.	:	Experimental and Numerical Determination of Stiffness and Strength of GRP/PVC Sandwich Structures. 1994.
Hovde, Geir Olav	:	Fatigue and Overload Reliability of Offshore Structural Systems, Considering the Effect of Inspection and Repair. 1995.
Wang, Xiaozhi	:	Reliability Analysis of Production Ships with Emphasis on Load Combination and Ultimate Strength. 1995.
Hellan, Øyvind	:	Nonlinear Pushover and Cyclic Analyses in Ultimate Limit State Design and Reassessment of Tubular Steel Offshore Structures. 1995.
Hermundstad, Ole A.	:	Theoretical and Experimental Hydroelastic Analysis of High Speed Vessels. 1995.
Eknes, Monika Løland	:	Escalation Scenarios Initiated by Gas Explosions on Offshore Installations. 1996.

ISBN 82-471-0114-9
ISSN 0802-3271